UNIVERSIDADE DE LISBOA

INSTITUTO SUPERIOR TÉCNICO

Integrative platforms for downstream processing and detection of viral particles

Maria João Cardoso Jacinto

Supervisor: Doctor Maria Raquel Múrias dos Santos Aires Barros

Co-supervisors: Doctor Ana Margarida Nunes da Mata Pires de Azevedo

Doctor Richard C. Willson

Thesis approved in public session to obtain the PhD Degree in Bioengineering

Jury final classification: Pass with Distinction

2019

UNIVERSIDADE DE LISBOA

INSTITUTO SUPERIOR TÉCNICO

Integrative platforms for downstream processing and detection of viral particles

Maria João Cardoso Jacinto

Supervisor: Doctor Maria Raquel Múrias dos Santos Aires Barros

Co-supervisors: Doctor Ana Margarida Nunes da Mata Pires de Azevedo

Doctor Richard C. Willson

Thesis approved in public session to obtain the PhD Degree in Bioengineering

Jury final classification: Pass with Distinction

Jury

Chairperson: Doctor Duarte Miguel de França Teixeira dos Prazeres, Instituto Superior Técnico, Universidade de Lisboa

Members of the Committee:

Doctor José António Couto Teixeira, Escola de Engenharia, Universidade do Minho

Doctor Maria Raquel Múrias dos Santos Aires Barros, Instituto Superior Técnico, Universidade de Lisboa

Doctor Duarte Miguel de França Teixeira dos Prazeres, Instituto Superior Técnico, Universidade de Lisboa

Doctor Mara Guadalupe Freire Martins, Universidade de Aveiro

Doctor Isabel Maria Delgado Jana Marrucho Ferreira, Instituto Superior Técnico, Universidade de Lisboa

Funding Institution: Fundação para a Ciência e Tecnologia

2019

Quando nos despedimos,

chamaste-me atrás e desejaste "que tudo corra bem".

... Correu avô, correu tudo bem.

RESUMO

Os vírus são as formas biológicas mais abundantes na Terra. Estes produtos biológicos são principalmente conhecidos pela sua patogénese viral, processo onde um vírus infecta o seu hospedeiro-alvo, originando consequências moleculares e celulares. No entanto, partículas virais também podem ser encaradas como agentes biomédicos, nomeadamente partículas semelhantes a vírus (VLPs) - nanopartículas biológicas, expressas por sistemas de expressão recombinantes, compostas por proteínas estruturais virais que espontaneamente se aglomeraram na forma de partícula viral sem conter o material genómico viral. Devido à exposição repetitiva de epitopos, a aplicação mais direta de VLPs é o seu uso como vacinas contra o vírus do qual foram derivados, fornecendo uma alta resposta imunogénica. VLPs podem também ser sistemas de exposição de outros antígenos. Outra possibilidade são os bacteriófagos, também conhecidos como fagos, que se tratam de partículas virais que apenas infectam bactérias. Devido ao estreito leque de hospedeiros atacados por um bacteriófago específico (frequentemente composto por um subconjunto de estirpes de uma única espécie bacteriana), estas partículas virais têm sido consideradas como agentes antibacterianos. A sua possível aplicação direta em tecidos vivos, sem agredir o meio circundante mas apenas o seu hospedeiro alvo, assim como os seus modos de ação que não são afectados pelos mecanismos de resistência bacteriana aos antibióticos, demonstram a toxicidade seletiva do bacteriófago e o seu potencial como um agente biológico antibacteriano alternativo.

Nas últimas décadas, à medida que as partículas virais começaram a ser usadas como agentes biomédicos, os procedimentos de produção de vírus e partículas virais foram otimizados, levando a maiores rendimentos e volumes de produção. Assim, o processamento a jusante, onde a recuperação e purificação do produto biológico alvo das impurezas e outras partículas relacionadas com o vírus, como proteínas livres, partículas virais incompletas, etc., é alcançado, tem se tornado um factor importante na busca de um processo com alta produtividade e menor custo. Nesta tese foram desenvolvidos dois casos de estudo de purificação de partículas virais.
Como os sistemas aquosos de duas fases (ATPS) são uma técnica de purificação à base de água e, portanto, biocompatível pelas suas baixas tensões interfaciais, retenção da atividade biológica e potencial efeito estabilizador das proteínas por acção de alguns polímeros, foi estudado o desempenho desta técnica, tanto em '*batch*' em escala de mL como em contínuo à microescala,

para a recuperação de VLPs recombinantes do vírus da imunodeficiência humana (HIV) do sobrenadante de células do ovário de hamsters chineses (CHO).
Noutro caso de estudo de purificação, líquidos iónicos poliméricos (PILs) foram estudados tanto em estudos de adsorção/eluição como em modo de operação cromatográfica para o desenvolvimento de uma nova matriz de separação para purificação produtos biológicos, nomeadamente para o bacteriófago M13, que foi usado como modelo viral.

Em relação à detecção viral, os métodos tradicionais como microscopia eletrônica, ELISA e PCR apresentam algumas desvantagens significativas, como a necessidade de pessoal altamente treinado, a instrumentação dispendiosa, o tempo dispensado e a utilização de equipamentos de laboratório. Assim, tem sido considerado como um grande desafio a capacidade de criar ferramentas de diagnóstico com as mesmas características de desempenho e garantia de qualidade que métodos laboratoriais, mas num formato mais amigável ao utilizador final/paciente. Nesta tese foram desenvolvidos dois casos de estudo de detecção de partículas virais.
Nanopartículas magnéticas foram exploradas como ferramentas de multitarefas (captura e concentração do alvo a detectar, e repórter do teste) para atingir um baixo limite de detecção de um ensaio de fluxo lateral (LFA) para detecção de Norwalk.
Noutro caso de estudo de detecção viral, e ao reconhecer as propriedades intrínsecas do ATPS combinadas com a versatilidade, baixo custo e facilidade de uso e preparo, que podem ser escalonáveis pelo processamento paralelo por máquinas automáticas de manipulação de líquidos, foi desenvolvido o primeiro biosensor no qual os ATPS desempenham o papel principal, explorando a sua capacidade de mudar a partição de um repórter de afinidade quando a partícula viral a detectar está presente.

Palavras-chave: Virus; Partículas semelhantes a vírus (VLPs); Bacteriófago; Vírus da Imunodeficiência Humana (HIV); Bacteriófago M13; Vírus Norwalk; Sistemas Aquosos de Duas Fases (ATPS); Líquidos Iónicos Poliméricos (PILs); Ensaios de Fluxo Lateral (LFA); Partículas magnéticas

ABSTRACT

Viruses are the most abundant biological forms on Earth. These biological products are mainly known by its viral pathogenesis, which is the process where a biological virus infects its target host, leading to molecular and cellular level consequences. However, viral particles can also be faced as biomedical, namely Virus Like Particles (VLPs) - biological nanoparticles, expressed by recombinant expression systems, composed by viral structural proteins that spontaneously self-assemble into viral particle shape without containing the viral genomic material. Due to high density display of epitopes, the most direct application of VLPs is their use as vaccines against the virus from which they were derived, providing a high immunogenic response. VLPs can also be foreign antigen display systems. On another hand, bacteriophages, also commonly known as phages, are viral particles that only infect bacteria. Due to the bacteriophage's narrow host range (often comprising a subset of strains of a single bacterial specie), they have been considered as antibacterial agents. Its possible direct application to living tissues, without damaging the surrounding environment but only its target host, as well as its action modes not affected by bacterial resistance to antibiotics mechanisms, demonstrate the bacteriophage selective toxicity and its potential as a biological alternative antibacterial agent.

In the last decades, when viral particles have been starting to be used as biomedical agents, the virus and viral particles production procedures have been optimized, leading to higher yields and harvest volumes. Thus, the downstream processing, where the recovery and purification of the target biological product from impurities and other virus particle-related, as free proteins, incomplete viral particles, etc., is achieved, has becoming an important factor in the seeking for an overall high productivity and lower process cost. In this thesis, two viral particles purification case-studies were developed.

Since aqueous two-phase systems (ATPS) are water-based purification technique, and thus biocompatible by its low interfacial tensions, retention of biological activity and stabilizing effect on proteins by some polymers, it was studied the performance of this technique, both in batch mL scale and in continuous microscale, for the recovery of recombinant Human Immunodeficiency Virus (HIV) VLP from chinese hamster ovary (CHO) cell supernatant.

In another different work, polymeric ionic liquids (PILs) were also studied either in adsorption/elution studies or chromatographic operation mode as a novel separation matrix for biological products purification, namely for M13 bacteriophage, which was used as a viral model.

Concerning viral detection, traditional methods as electron microscopy, ELISA and PCR, present some important disadvantages as the need of highly-trained personnel, requires expensive instrumentation, and it is time and lab equipment consuming. Thus, it has been considered as a major challenge the ability to create diagnostic tools with the same performance and quality assurance characteristics as in laboratory-based methods but in a more patient/final user friendly format. In this thesis, two viral particles detection case-studies were developed.

Magnetic nanoparticles were explored as multi-tasking tools (target capture and concentration, and test reporter) for low limit of detection of a lateral flow assay (LFA) for Norwalk detection.

In another viral detection case study, by acknowledging the ATPS intrinsic properties combined with the versatility, environmentally-friendliness, low costs, ease to use and prepare which can even be scalable by parallel processing, it was developed the first biosensor in which the ATPS plays a primary role, by exploring its ability to switch the partition of an affinity reporter when the target viral particle is present.

Keywords: Viral particles; Virus Like Particles (VLPs); Bacteriophage; Human Immunodeficiency Virus (HIV); Bacteriophage M13; Norwalk virus; Aqueous Two-Phase Systems (ATPS); Polymeric Ionic Liquids (PILs); Lateral Flow Assays (LFA); Magnetic particles

ACKNOWLEDGEMENTS

O meu primeiro agradecimento vai para a professora Raquel Aires Barros, por ter sempre acreditado e lutado por mim, desde do dia zero. Levo desta viagem não só a forma como me guiou e incentivou ao longo deste percurso, mas também o seu exemplo enquanto mulher da ciência e da academia. Um obrigada à professora Ana Azevedo por todos os conselhos e sugestões num ambiente mais próximo do laboratório.

I would like to also thank to prof. Richard C. Willson for the nice and helpful reception in University of Houston for one year. I enjoyed every day of my 'texan' adventure. Your enthusiastic discussions about such diverse topics and passion for science and technology will always be inspiring for me. A special thank you for all Willson's lab members, namely Katerina for your dedicated and kind guiding since day one; Binh for being so helpful with the magnetic LFA work; Mary, Heather, Andrew, Bala, Hui, Ujwal for providing such a nice work environment; Stuti, Jin Su and Ahmad for so many funny moments; a special thank you to Gavin Garvey for being such a good friend since the beginning, a friendship that I intend to keep; e um obrigada ao 'tuga' João Trabuco por toda a ajuda desde da minha primeira aterragem a Houston até ao meu regresso definitivo em Lisboa.

Gostaria também de agradecer ao programa MIT Portugal por me ter aceite no programa e ter dado a oportunidade de explorar este desafio que foi o doutoramento, e a todos os colegas da turma de 2014 que tornaram a aventura do ano lectivo um desafio passado de forma divertida e descontraída. O meu sincero obrigado a todos os parceiros que ajudaram a melhorar este trabalho, nomeadamente ao prof. João Pedro Conde, Dra. Virginia Chu e Dr. Ruben Soares do INESC-MN, ao prof. João Gonçalves da Faculdade de Farmácia, e à prof. Isabel Marrucho e ao David Patinha do Centro de Química Estrutural.

Um sincero obrigado ao iBB por me ter recebido ao longo destes 5 anos, especialmente a todo o grupo de bioseparações. Todos os que se cruzaram comigo neste laboratório têm um bocadinho seu nesta tese (e são tantos que nem me vou arriscar a escrever nomes porque esquecer-me-ia de alguém de certeza). Obrigada ao Ricardo Pereira e à dona Rosa por serem incansáveis em nos dar as melhores condições para trabalhar. Um especial obrigado por cada 'picadito de Arturito' à Alexandra Wagner, Sara Rosa, Ana Rita Santos e Cláudia Alves. Tornaram os últimos dois anos muito mais fáceis e alegres. Obrigada também ao Rui Silva e Diogo Faria por tantas ideias e discussões científicas.

Faltam aqueles que provavelmente ainda hoje não percebem bem do que se trata esta tese, e ainda assim não duvidaram de mim nem um segundo.

Obrigada à equipa de futsal feminino do Técnico, que me deu ao longo de tantos anos momentos de descompressão das frustrações da ciência ao me deixarem fazer outra coisa que tanto gosto. Todas as vitórias (e também as derrotas), especialmente das competições universitárias, são parte bem definida da duração desta tese. Um especial obrigada à Leonor Burguete, Inês Pinto e Carolina Peixoto por todo o apoio e preocupação. Obrigada também às 'PPs' Inês Cabral, Ana Patrícia Barreiros e Margarida Pires por estarem sempre perto já há tantos anos.

Porque a base da minha bioengenharia já começou há mais de 10 anos, e deu-me mais do que alguma vez imaginei. Obrigada ao meu 'quorum sensing', nomeadamente à Inês Leite, Marilena Ornelas, Catarina Honório, Marcelo Ferreira, Guilherme Benedito, André Belo, João Sá, Nuno Araújo, Teresa Gouveia, Andreia Correia, André Fernandes, Dr. João Crispim e Ricardo Figueiredo; que continuem a acompanhar-me em todas as minhas caminhadas.

Um obrigada especial à família que escolhi. À Marta, ao Alan, à Inês, à 'avó' e à princesa Mariana. Porque sempre me tomaram por mais do que sou, e fizeram da presença possível um apoio incondicional.

Esta tese também é muito dos meus. Dos que estão ligados por sangue e para sempre. Obrigada Rita, Armando e primas Cuca e Margarida por cada sorriso espontâneo que me fizeram fazer sem notar e por todos os elogios exagerados. Obrigada avó Mila e avó Carmo, por todo o carinho desde sempre, e obrigada avô Américo por teres continuado a olhar por mim; vocês estarão sempre na base de tudo o que sou. À Lena, à Luisa, à Kika e aos pais: um simples 'obrigada' não chega. Vocês acreditaram e acreditam sempre mais em mim do que eu em mim própria, e isso vence qualquer coisa.

Por fim, um grande obrigado ao Francisco. Por tudo, não há outra forma de o dizer. Cada decepção, vitória, frustração e descoberta foi quase tão sentida por ti como por mim. Por todos os mimos, cuidados, atenções, 'piscinas' em modo contra-relógio para que eu atingisse todos os meus objectivos pessoais e profissionais. Não teria sido a mesma coisa sem ti, tenho a certeza.

As teses são assinadas a título individual, mas é um trabalho de grupo. E eu tive os melhores comigo.

“Success is not final, failure is not fatal, it is the courage to continue that counts.”

- *Winston Churchill*

ABBREVIATIONS LIST

AC	Affinity chromatography
AEC	Anion exchange chromatography
AI	Avian influenza
ATPE	Aqueous two phase extraction
ATPS	Aqueous two phase systems
BVDV	Bovine viral diarrhea vírus
CEC	Cation exchange chromatography
cGMP	current Good Manufacturing Practices
CHO	Chinese Hamster Ovary
CsCl	Caesium chloride
CTV	Citrus tristeza virus
DEAE	Diethylaminoethanol
DNA	Deoxyribonucleic acid
ds	Double-stranded
DSP	Downstream processing
DVB	Divinylbenzene
EBA	Expanded bed adsorption
EGDMA	Ethylene glycol dimethylacrylate
ELISA	Enzyme-linked immnunosorbent assay
FDA	Food and Drug Administration
GFP	Green fluorescence protein
HA	Influenza virus' hemagglutinin
HIC	Hydrophobic interaction chromatography
HIV	Human immunodeficiency virus
HPTFF	High performance tangential flow filtration
HPV	Human papillomavirus
HRP	Horseradish peroxidase
ICTV	International Committee on Taxonomy of Viruses
IEX	Ion-exchange chromatography

ILs	Ionic liquids
K	Partition coefficient
LFA	Lateral flow assay
LoD	Limit of detection
MMC	Multimodal chromatography
mRNA	Mensenger RNA
MW	Molecular weight
MWCO	Molecular weight cutoff (MWCO)
NEMS	Nanoelectromechanical systems
NTA	Nanoparticle tracking analysis
PCR	Polymerase chain reaction
PDMS	Polydimethylsiloxane
PEG	Polyethylene glycol
PGMEA	Propylene glycol monomethyl ether acetate
PILs	Poly(ionic liquids)
poly(VEIM-TFSI)	Poly (1–vinyl-3-ethyl imidazolium bis(trifluoromethylsulfonyl) imide)
Q	Quaternary ammonium
QDs	Quantum dots
qPCR	Quantitative PCR
RNA	Ribonucleic acid
SEC	Size exclusion chromatography
SEM	Scanning Electron Microscopy
SERS	Surface-enhanced Raman scattering
ss	Single-stranded
SXC	Steric-exclusion chromatography
TEM	Transmission Electron Microscopy
TLL	Tie-line length
UF	Ultrafiltration
VLPs	Virus Like Particles

INDEX

THESIS SCOPE AND OUTLINE

This thesis was developed in the framework of MIT Portugal program in bioengineering systems at Institute for Biotechnology and Bioengineering in Instituto Superior Técnico (Lisbon, Portugal), and in Prof. Willson's lab in University of Houston (Texas, USA). Also, it was combined different expertises from various collaborations as miniaturized approaches of INESC-MN (Lisbon, Portugal), the production and manipulation of virus particles of the Faculdade de Farmácia (University of Lisbon) Dr. João Gonçalves' laboratory, and the ionic liquids manufacturing by Dra. Isabel Marrucho's group in Instituto Superior Técnico.

The main goal of this work was to investigate and/or develop different purification and detection techniques for viral applications. This thesis is thus divided in six chapters.

Chapter I includes a general introduction where it is pointed out a generic background of viral particles, its double applications as pathogenic agents or biomedical instruments, and consequent need of early detection or process purification, respectively. Classic and alternative viral purification and detection techniques are also reported.

Chapter II presents a first purification case study, where recombinant human immunodeficiency virus-like particles were purified from a Chinese Hamster Ovary (CHO) cell supernantant by aqueous two-phase extraction. Batch mL scale separation and continuous microfluidic extraction were compared in terms of partition and protein purity analysis.

A second viral purification case study is described in Chapter III, where polymeric ionic liquids were developed as novel biological separation matrices, using M13 bacteriophage as viral model. Optimization tests with pre-purified M13 were followed by purification assays from *E. coli* supernatant, either in adsorption-elution and chromatographic operation mode.

Chapter IV and V describe two different viral detection case studies. Chapter IV report the development of an efficient system point-of-need analytical technology by simple and robust lateral flow assays (LFAs) using magnetic nanoparticles as reporters, in a fully integrated format, for Norwalk detection. The test sensitivity was increased by using an

electromagnetic field to externally manipulate the reporters position and its binding capacity, by the addition of a enzymatic signal enhancer and by using the magnetic particles' properties to perform a sample pre-concentration step.

Finally, in Chapter V it was explored aqueous two-phase systems, a conventional downstream technique, as a one-step detection platform. In this second viral purification case study, it was studied a aqueous two-phase system (ATPS) which would independently partition M13 bacteriophage, the viral model chosen, to a different phase of a fluorescence labelled anti-M13 reporter. The goal was to validate if, in the presence of the viral target, the labelled reporter would reflect a fluorescence shift from its ATPS rich-phase to the other where the viral particle is more abundant.

Chapter VI presents the final remarks of this thesis by summing up and concluding the main achievements of this work and its future challenges.

CHAPTER I – General introduction

Abstract This introductory chapter describes and discusses (1) the fundamental features of viral particles, in particular the viral particles used in this thesis, (2) the relevance of early and accurate diagnostic methods of viral pathogens for health safety and (3) the potential of viral particles as biomedical agents and its consequent need of purification as part of the bioproduction process. A primary focus will be directed to virus and viral particles in general, where virus-like particles and bacteriophages are mainly explored. Furthermore, an emphasis is placed on the viral detection techniques, namely classic applications and advances in detection methods, and on purification procedures, with detailed description of classic and novel purification techniques applied in each downstream processing step of a bioprocess. Examples of commercial viral detection kits as well as industrial downstream processes are also referenced in this chapter.

Keywords: Virus, Virus-like particles, Downstream processing, Viral detection

I.1. Viral particles

Viruses are the most abundant biological forms on Earth, with an estimated 10^{31} total viruses [1]. The majority of these viral particles infect microorganisms, including bacteria, archaea, and microeukaryotes, all of which are fundamental in the global fixation and cycling of basic elements such as carbon, nitrogen, and phosphorus. This fact suggests that viruses, too, play an important responsibility in the planet's biosphere [1].

a. Definition and characteristics

A virus is an infectious nanoparticle that can only reproduce by infecting a host cell. Since viruses depend on the host cell complex metabolic and biosynthetic machinery to replicate, its main function is to deliver its genome into the host cell so that the genome can then be expressed [2]. Thus, viruses are inert outside the host cell and consequently are not considered free-living. Still, viruses have some significant features in common with cells. For example, as cell-based life, viruses have genetic variation and can mutate to a new evolved form of the same virus.

Viruses differ in sizes, shapes and life cycles, but they all share key features, such as the presence of a nucleic acid genome – either deoxyribonucleic acid (DNA) or ribonucleic acid (RNA) – and a virus-coded symmetric protein coat protective shell (single or double layer), conventionally named as capsid [2]. The capsid is formed by multiple copies of one or a few different proteins with the purpose of protecting the nucleic acid genome from nucleases, and providing attachment conditions to specific receptors in the host cell [2, 3]. The enclosed genome in the viral capsid forms the so called nucleocapsid, and this basic infectious viral structure is entitled a virion [3]. Based on the repetitive capsid's protein structure, and since each capsid's constituent protein is encoded in a single gene present in the viral genome, viral particles can encode all the information necessary to build a large capsid structure in a small number of genes [3]. The virus genetic information can be simple and encoding only four proteins, or more complex encoding up to 100 or 200 proteins [3].

Multiple capsid protein subunits self-assembly in two elementary forms: filamentous (or helical) or icosahedral [2, 3]. The helical symmetry is a simple rod-shaped structure in which the capsid protein subunits and the virus genome are arranged in a helix to

protect the RNA or DNA within [2, 3]. The icosahedral symmetry is based on a solid object built of 20 identical faces in which the capsid protein subunits assemble into a *quasi-spherical* shell that covers the viral genome in the inside core [2, 3]. Some viruses also present a "hybrid" capsid shape between the previous described basic shapes, usually called head-tail. This structure consists in a conjugation of an icosahedral head connected to a rod tail.

Some viruses also present a lipid bilayer membrane, known as envelope, covering the symmetrically arranged nucleocapsid providing an additional protective coat [3]. The envelope is usually derived from the host cell membranes, which consists mainly in a phospholipid bilayer and a few types of virus-encoded membrane-associated glycoproteins [2, 3]. The formation of non-enveloped and enveloped viral particles is represented in Figure I-1.

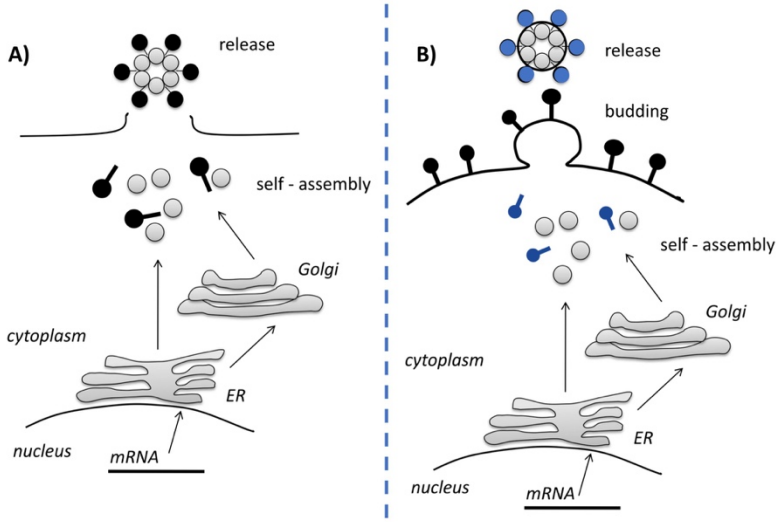

Figure I-1 - Schematic representation of the formation of non-enveloped (A) and enveloped (B) viral particles. Adapted from [4].

As viruses present different features, like shapes and target hosts, virus size distribution also ranges between small virus as *porcine circovirus* with 17 nm in diameter [5], and bigger virus as *megavirus* with 590 nm in diameter or *pandoravirus* with 1000 × 500 nm ovoid shape [6].

b. Virus evolution and classification

Viral origin and evolution are an essential part of epidemiology, since the high viral mutation rate is a major drawback for the development of successful vaccines and

antiviral drugs. Three main theories have been suggested to describe the origin of viruses [7]:

- The 'virus-first' hypothesis propose that virus are older that cells and have contributed to its evolution and rise. This theory is mainly justified since most of all viral genomes encode virus-specific sequences, not presenting cellular homologs and thus supporting a putative unique origin. On other hand, this theory neglects the viral need of a host to replicate.
- A different hypothesis states that viruses may have evolved from small cells that parasitized larger cells. Thus, this 'reduction' hypothesis claims that cells are older than viruses, and these infectious particles are reduced forms of parasitic organisms. This thesis is supported by the discovery of large virus, as *mimiviruses*, that present similar size and genomic features of parasitic bacteria. However, it still lacks explanation about the inexistence of similarities between small cellular parasites and viruses.
- A third theory, the 'escape' hypothesis, suggests that viruses are descendent of small pieces of genetic material of the host cells that escaped cell control and further evolved by horizontal gene transfer. However, this theory doesn't explain the complex viral capsids and why some structures are exclusively present in viruses and not in cells.

Darwin evolution is not a cell exclusive evolution route, since viruses evolve through changes in their genome, which will lead to new virus strains and the best adapted mutants will succeed. This phenomenon is more frequent in RNA viruses [8]. Some viruses, as influenza, can also "switch" their genomic information with other similar viruses that have infect the same host, leading to new and more virulent strains [9].

Since the viral origin is still not clear, it is hard to predict the consequent phylogenetic relationship between different viruses. Still, there are a lot of different ways to classify viruses based on similarities, such as the structural basis, replication properties, host range, etc. Nevertheless, viruses were first classified in the early 1960s based on Linnaeran hierarchichal system of phylum, class, order, family, genus and species. [10] Later, the International Committee on Taxonomy of Viruses (ICTV) was formed and developed the current classification system that is progressively updated with new discovered viruses. The taxonomic scheme is universal for all viruses and groups viral

particles according to their structure, genome, biology and phylogenetics [11]. The hierarchy of recognized viral particles is based in *order, family, sub-family, genus and species*. Currently, there are 8 *order*s, 122 *families*, 35 *subfamilies*, 735 *genus* and 4404 *species* [11].

The ICTV classification is usually used together with Baltimore classification system. David Baltimore developed a classification based on the genome type, and mode of replication and transcription in seven different groups [12]. Viruses are thus distinguished by their nucleic acid content (DNA or RNA), its conformation (single- or double-stranded, ss or ds), and consequent messenger RNA (mRNA) production process from their genome to produce their structural proteins and thus replicate [12] (Figure I-2):

- Group I: dsDNA. Most group I viruses enter in the host nucleus and require host cell polymerases and cellular transcription factors to replicate the viral genome and to synthesize mRNA (e.g. Adenoviruses). Poxvirus family is an exception: it replicates in the cytoplasm and makes their own enzymes for nucleic acid replication.
- Group II: ssDNA. Must enter in the host nucleus since it requires host cell polymerases. Form dsDNA as intermediate during replication which is then used in the transcription process by RNA polymerase (e.g. Inoviruses).
- Group III: dsRNA. Replicates in the cytoplasm. Contains RNA polymerase within the virion that enters in the cell along with the genomic RNA to synthesize mRNA. Complementary positive-sense RNA is synthesized by RNA polymerase and used as mRNA. Positive-sense RNA is also used as template to produce more negative-sense genome (e.g. Reoviruses).
- Group IV: ssRNA positive-sense. Replicates in the cytoplasm. Can be directly used as mRNA. Virus encodes a virus specific and RNA dependent RNA polymerase (RNA replicase) that will produce complementary negative-sense RNA that will be further used as template to make more positive-strand RNA (e.g. Caliciviruses).
- Group V: ssRNA negative-sense. Contains RNA polymerase within the virion that enters the cell along with the genomic RNA to synthesize mRNA/ssRNA positive-sense. The genome is transcribed by the viral polymerases into positive-sense

reciprocal. A positive-sense genome copy is then produced that serves as mRNA and as template to produce more negative-strand genome (e.g. Orthomyxoviruses).

- Group VI: ssRNA positive-sense that replicate through a DNA intermediate. Use virion reverse transcriptase to convert the positive-sense RNA into DNA. The mRNA and replication is formed using the DNA template created by host cell RNA polymerase. Formed dsDNA can be integrated into host cell chromosome. Reverse transcriptase and not being directly infectious is what differentiates group IV from group VI (e.g. Retroviruses).
- Group VII: dsDNA that replicate through a ssRNA intermediate. Requires reverse transcriptase for production of the DNA genome (e.g. Hepadnaviruses).

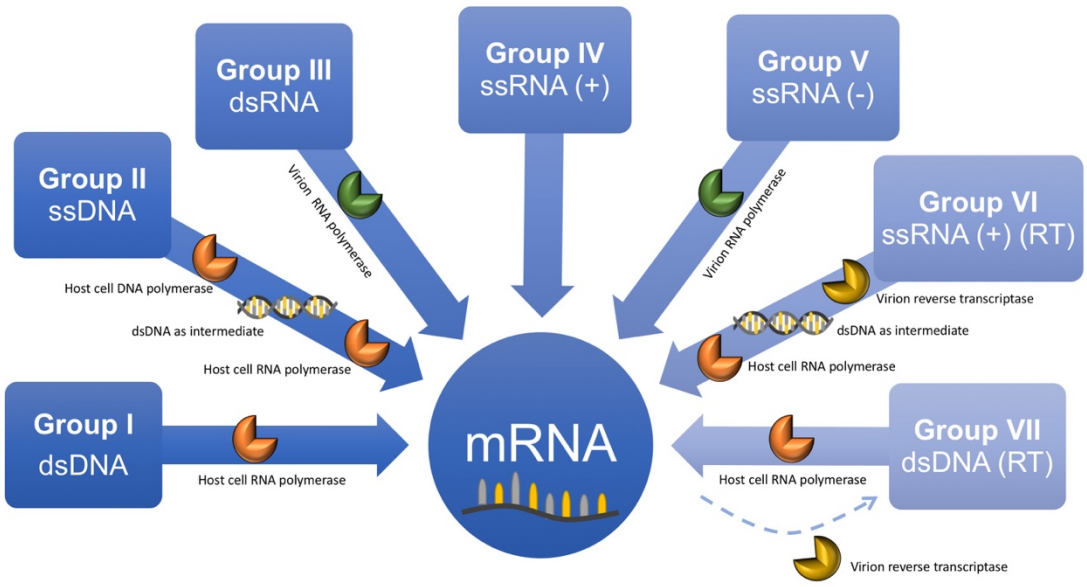

*Figure I-2 – **Baltimore classification for viruses**. The viruses are divided by genome configuration (DNA or RNA, single- or double-stranded) and the mechanism to produce mRNA for viral protein production in seven different groups.*

c. Virus as pathogenic threats

Viral pathogenesis is the process where a biological virus infects its target host, leading to molecular and cellular level consequences [13]. The viral contact and consequent infection might lead to simple and non-significant effects, or to cellular discernable effects and clinical disease (Figure I-3) [14].

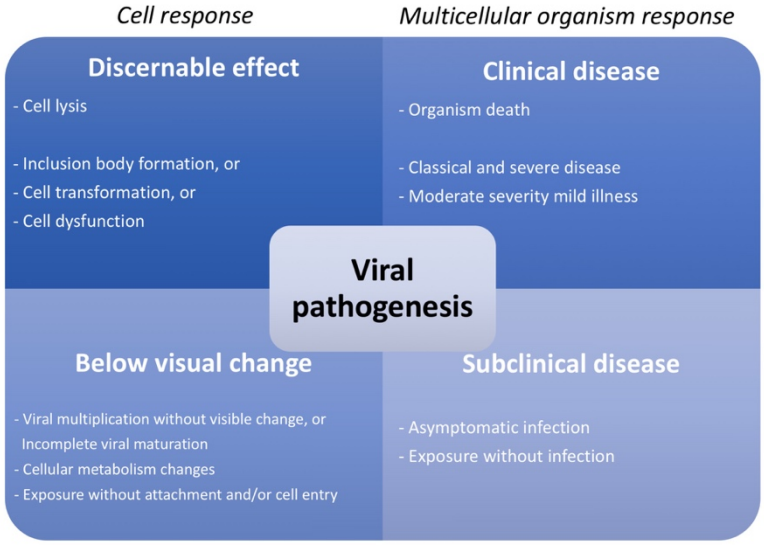

Figure I-3 - ***Viral pathogenesis consequences at cell and whole organism level****. Adapted from [14].*

Viral pathogenesis can present different infection profiles (Figure I-4). Acute infection is often followed by virus clearance, although viruses or virus' parts may endure and cause late problems [14]. Norovirus infection is one example of an acute infection profile. In latent infections there is an equilibrium between the virus and the host, where the virus might be active and infectious, or in a noninfectious occult form. Chronic infections appear to persist because the virus doesn't disrupt the essential functions of the cells or the organism can adapt and survive even with the viral infection consequences. The human immunodeficiency virus (HIV) is an example of a chronic viral infection since it attacks the human immune system, reducing the number of CD4+ T lymphocytes (T-cells), and the human body can't eliminate the virus, even with treatment. This makes it difficult for the body to respond to other infections and diseases.

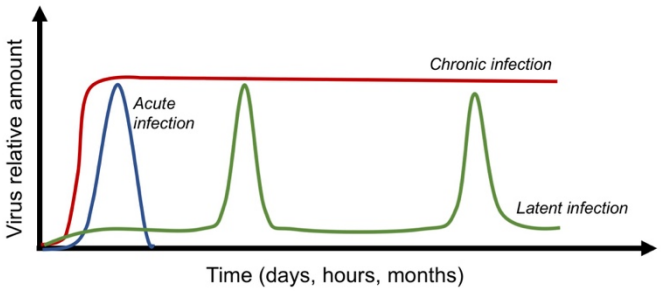

Figure I-4 – ***Possible virus infection patterns.***

In this work, we will focus on noroviruses and HIV as pathogen agent examples.

Noroviruses are a viral group of single-stranded positive-sense RNA (group IV in Baltimore classification), non-enveloped viruses that belong to the genus Norovirus within the family Caliciviridae [15] (Figure I-5). Norwalk virus was the first identified norovirus and it is named from an outbreak of 'winter vomiting disease' in 1968 at an elementary school in Norwalk, Ohio, USA [16]. The norovirus structure present 38 nm in diameter, constituted by 90 dimers of capsid protein (Figure I-5, left) assembled in a triangle shape. Each monomer (Figure I-5, right) is divided into an N-terminal arm region (Figure I-5, green) facing the virus interior, a shell domain (S-domain, Figure I-5 - yellow) that forms the continuous surface, and an external P-domain that derives from the S-domain. The P-domain is divided into two subdomains, P1 and P2 (Figure I-5, red and blue, respectively), in which the P2-subdomain is the most outer element of the virus structure.

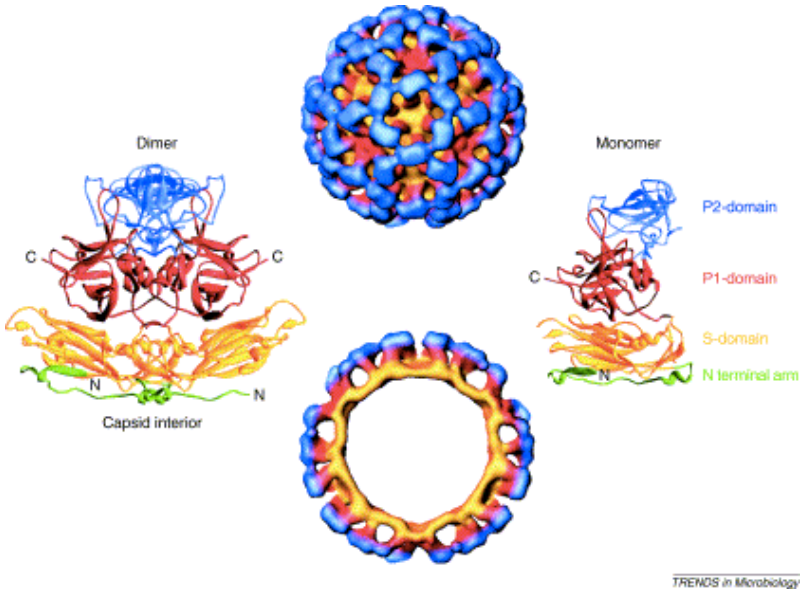

Figure I-5 - The Norwalk virus-like particle structure solved by cryo-electron microscopic reconstruction to 22 Å (surface representation in the top, and cross-section in the bottom) and by x-ray crystallography to 3.4 Å. Source: [15].

Norovirus are currently the major source of foodborne illness (58%), causing around 19-21 million disease cases, between 56 000-71 000 hospitalizations and 570-800 deaths per year in the United States [17, 18]. These viruses infect epithelium cells and perform acute infections, which the common symptoms are nausea, vomiting, abdominal cramps and watery diarrhea [19, 20]. The more usual environmental sites for contamination are crowded closed spaces like cruiser and military ships, long-term care facilities, restaurants, schools and hospitals [20-23]. The most common transmission routes are person-to-person (fecal-oral mode or inhalation of airborne droplets of vomitus) and

food-borne outbreaks [20, 23]. It is a highly contaminant pathogen, where the 50% human infectious dose is around 10^3 virions [19, 24]. The symptoms usually start 10–51 hours after exposure and illness lasts between 12 and 60 hours [15, 20], and the virus can still be present in the patient stool after 3 weeks [25]. These viruses are easily transmitted and are highly prevalent in the society due to their high stability in the ecosystem and their ability to release infectious virus particles from asymptomatic individuals, consequently delaying detection and diagnosis [15].

HIV is a bilayer enveloped retrovirus that belongs to the lentivirus subfamily, presenting a viral single-stranded positive-sense RNA that replicates through a DNA intermediate using a virion reverse transcriptase (group VI in Baltimore classification) [26, 27]. This virus presents a spherical shape with several spikes on its outer surface composed by the combination of two types viral envelope glycoproteins: external gp120 and transmembrane gp41 (Figure I-6) [26-28]. The underlying layer (called matrix) is constituted by several copies of p17 protein [27]. The viral core is constituted by a capsid, that contains the genetic material and it is formed by several copies of protein capsid p25, two strands of RNA molecules of about 9200 nucleotide bases and three enzymes (reverse transcriptase, integrase, and protease) - Figure I-6 [26, 27]. HIV genome presents three structural genes: *Env*, which encodes the viral envelope glycoproteins gp120 and gp41; *Gag*, which encodes for the matrix p17 and capsid p25 proteins; and *Pol*, for the viral enzymes reverse transcriptase, RNase, integrase and protease [27]. *Tat*, *Rev*, *Nef*, *Vif*, *Vpr*, *Vpx* and *Vpu* are the main regulatory genes [27].

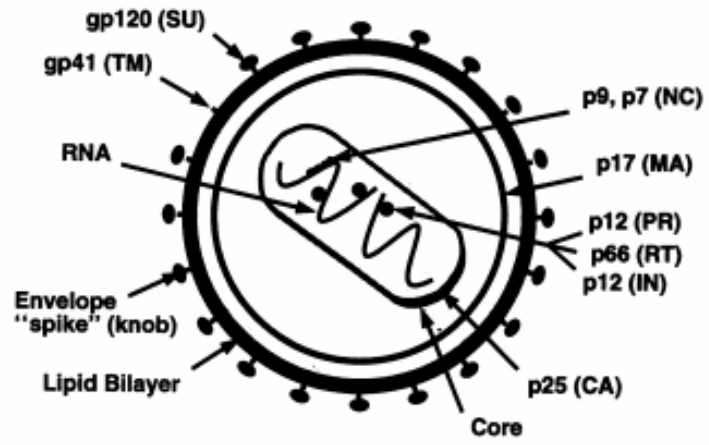

Figure I-6 - ***Structural representation of an HIV virus with viral proteins identified****. Surface (SU), transmembrane (TM), matrix (MA), capsid (CA) and nucleocapsid (NC) proteins are represented. integrase (IN), reverse transcriptase (RT), protease (PR) enzymes are also symbolized. Source: [28].*

HIV infection comprises a complex interaction between the virus, its regulatory genes and the host, combining the virus binding and entry, viral RNA replication and integration, virions processing and assembly, budding of the viruses from the host cell and maturation of new viral particles [27]. After entry into the host cell, HIV RNA is converted to DNA, by the viral reverse transcriptase, which is integrated into the host DNA by the viral integrase and becomes a provirus [26]. Then, the host cell produces messenger RNAs that will synthesize the new viral genetic material, proteins and enzymes. The viral protease converts long strands protein precursors into smaller proteins that compose the viral cores [27].

HIV was originally described more than 30 years ago and, since then, has become one of the most significant infectious diseases worldwide involving difficult challenges for the public health systems. At the end of 2010, it was estimated that 34 million people were living with the HIV worldwide [29]. Despite major reductions in 'new infections' rates, almost every regions of the world continue to experience high disease burden; as example, in Eastern Europe and Central Asia, the number of people living with HIV rose 250% from 2001 to 2010 [29].

d. Viral particles adapted as biomedical agents

i. Virus Like Particles (VLPs): vaccines, gene and drug delivery

Virus Like Particles (VLPs) are biological nanoparticles, expressed by recombinant expression systems (bacteria, insect, yeast or animal cells), composed by viral structural proteins that spontaneously self-assemble into viral particle shape without containing the viral genomic material [30]. Due to high density display of epitopes, the most direct application of VLPs is their use as vaccines against the virus from which they were derived, providing a high immunogenic response (ex: Human papillomavirus – HPV - VLP-based vaccines Gardasil by Merck and Cervarix® by GlaxoSmithKline).

Besides mimicking the structure of an infectious virus and thus enhancing the patient immunogenic response, VLPs can also be foreign antigen display systems (ex: malaria VLP-based vaccines candidates, which is composed by hepatitis B core VLP decorated with epitopes of *Plasmodium falciparum* circumsporozoite protein). Currently, there are several VLPs under clinical evaluations or development (Table I-1).

Another advantage of VLP-based vaccines is the production time consumption. The most critical example is the influenza vaccine, which new strains are selected, developed, produced and approved each year. Conventionally, influenza vaccines are prepared by the inoculation of embryonated chicken eggs with the selected virus strains, and the produced viruses are then harvested, chemically inactivated and purified. VLP-based vaccines are a faster, cheaper and safer alternative (Figure I-7), but they lack the optimum antigen selection for each year [4].

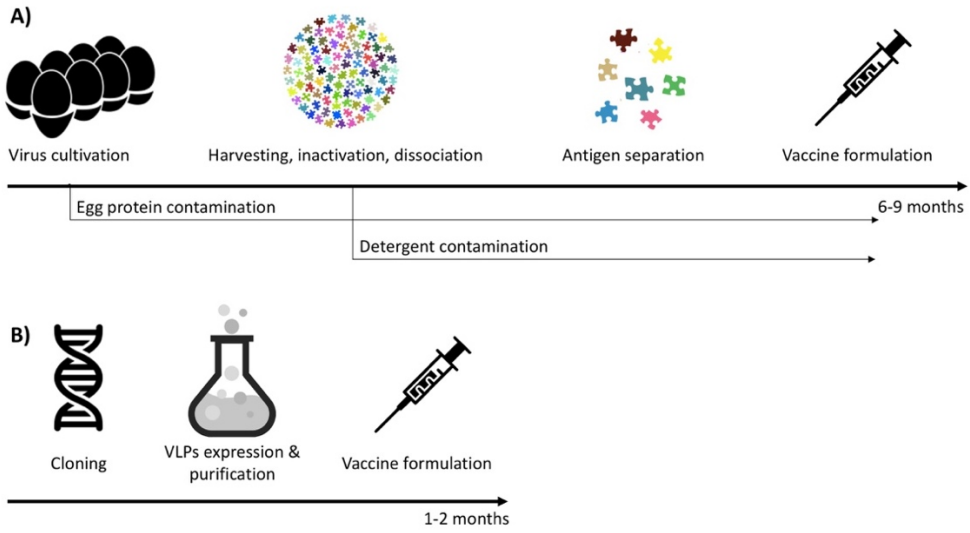

Figure I-7 - Comparison of vaccine production using traditional virus cultures (A) and VLPs (B) [4].

HIV and norovirus VLPs are thus options not only for developing vaccination, but also for antibody screening studies, and other works that require the same viral physical structural, as detection or purification studies.

VLPs can also include and carry nucleic acids or small molecules, leading to another use as carriers for drug, proteins and gene delivery to targeting cells, organs or tissues [31, 32]. Due to the basic profile of the polypeptide domains oriented toward the capsid interior, negatively charged nucleic acids and small molecules with appropriate charge, can be included within the VLP and create stable interactions [31]. Wu, Min *et al*. (2005) described the study of the uptake of MS2 bacteriophage VLPs and its use to deliver targeted antisense oligodeoxynucleotides, as p120 messenger RNAs, a biomarker overexpressed in myelogenous leukemia cells [33]. Virus-based nanoparticles have also been used for bio-medical imaging, as intravital and magnetic resonance imaging, and tumor targeting in vivo [34].

*Table I-1 - **Some examples of VLP-based human licensed vaccines or vaccine candidates in clinical trials.***

Target	Vaccine name / Clinical trial description	Expression system	Company/Institution	Status	Reference / NCT identifier*
Hepatitis B virus	Recombivax HB®	Yeast (*S. cerevisiae*)	Merck & Co. Inc.	Licensed	[35]
	GenHevac B®	Mammalian (Chinese hamster ovary cells)	Pasteur-Merieux Aventis	Licensed	[36]
Hepatitis E virus	Hecolin®, HEV 239	Bacteria (*E. coli*)	Xiamen Innovax Biotech Co., Ltd	Licensed	[37]
Malaria	Pfs25-CP VLP formulated with Alhydrogel®	Plant	-	Phase 1	NCT02013687
	ICC-1132	Bacteria (*E. coli*)	Apovia	Phase 1	NCT00587249, [38]
	RTS,S/AS01	Yeast (*S. cerevisiae*)	KEMRI-Wellcome Trust Collaborative Research Program; GlaxoSmithKline	Phase 3	NCT00872963
Human papillomaviruses (HPV)	Gardasil 9	Yeast (*S. cerevisiae*)	Merck & Co., Inc	Licensed	[39]
	Cervarix®	Insect (High Five™ cells)	GlaxoSmithKline	Licensed	[40]
	HPV 16/18	Bacteria (*E. coli*)	Xiamen Innovax Biotech Co., Ltd	Phase 3	NCT01735006
Influenza	Cadiflu-S	Insect	CPL Biologicals Pvt. Ltd	Licensed	[41]
	Flublok®	Insect cell line (expresSF+®)	Protein Sciences Corporation	Licensed	[42]
	Quadrivalent VLP Influenza Vaccine	Plant	Medicago	Phase 3	NCT03301051
HIV	HIV p17/p24:Ty-VLP	Yeast	National Institute of Allergy and Infectious Diseases (NIAID)	Phase 1	NCT00001053, [43]
Human parvovirus B19	VAI-VP705	Insect (Sf-9 cells)	Meridian Life Science, Inc.	Phase 2	NCT00379938, [44]
Norovirus	rNV VLP	-	Baylor College of Medicine	Phase 1	[45]
	Norovirus Bivalent Vaccine	-	Takeda	Phase 2	NCT01609257, [46]
Hypertension	CYT006-AngQß	-	Cytos Biotechnology AG	Phase 2	NCT00710372, [47]
Malignant melanoma	CYT004-MelQßG10	-	Cytos Biotechnology AG	Phase 2	NCT00651703
Alzheimer's disease	CAD106	-	Cytos Biotechnology, Novartis Pharmaceuticals	Phase 3	NCT02565511, [48]

*Bibliographic references or NCT identifiers (registered at https://clinicaltrials.gov) are provided.

ii. Bacteriophages

Bacteriophages, also commonly known as phages, are viral particles that only infect bacteria. Some of these virus are lysogenic, where the viral DNA is integrated in the bacterial genome and is replicated passively along with the host genome as the host cell divides without bacterial disruption. In the case of lytic phages, these viral particles disrupt bacterial metabolism and lead to bacterial cells lyse [49, 50]. The bacterial lysis promoted by lytic bacteriophages not only kills the bacterial cells, but also releases the produced bacteriophage particles into the surrounding environment to infect similar bacteria cells found nearby [49].

The discovery of bacteriophages and the consequent treat of bacterial infections (commonly called phage therapy) dates to the mid 1910s, after the discoveries of Frederick Twort, an English medically trained bacteriologist, [51] and Felix d'Hérelle [52]. Although Twort was the first to advance the hypothesis of bacterial killing virus [51], he didn't pursue this finding [50]. Thus, the discovery of bacteriophages is "officially" associated to Felix d'Hérelle, a microbiologist working at that time at the Institut Pasteur in Paris [52]. The discovery of bacteriophages by d'Hérelle is associated with an outbreak of dysentery among French troops, which at the time had no effective treatment [49, 50]. During his studies, d'Hérelle isolated *Shigella* strains from the patients and mixed with bacterium-free filtrates of patients' fecal samples. The inoculation of these mixtures in agar plates revealed the appearance of small, clear areas, which d'Hérelle called taches, and, later, plaques [50, 52]. D'Hérelle proposed that this phenomenon was caused by a virus able to parasitize bacteria, and thus he proposed the name 'bacteriophage' as a combination of 'bacteria' and 'phagein' (eater or devour, in Greek) [50, 52].

Due to the bacteriophage's narrow host range (often comprising a subset of strains of a single bacterial species), they have been considered as antibacterial agents, even before the discovery and first uses of antiseptics and antibiotics [49, 50, 53]. Their potential to be applied directly to living tissues, without damaging the surrounding environment but only its target host, demonstrate the bacteriophage selective toxicity and is the reason why bacteriophages are considered as a biological alternative antibacterial agent [49]. Also, bacteriophages antibacterial action modes tend to not be affected by bacterial

resistance to antibiotics mechanisms, which leads to a valuable ability of specific phages to impact bacterial infections [49].

There are different range of target hosts and mechanisms of production for different types of bacteriophages. Thus, bacteriophages are divided in three groups based on their production method profile:

- Lytic phages (bacterial cells are lysed and disrupted during viral replication) as T4;
- Lysogenic phages (bacterial cells produce all the viral constituents and the phage can cross the bacterial membrane without cell disruption), as M13;
- Temperate phages (the viral genomic information is integrated into the bacterial genome, and thus phage replicates through the natural bacteria cell cycle; it works in a lysogenic profile unless, in stressful conditions, when the phages are activated and act as lytic), as Lambda [54].

In this work, we will focus on M13 bacteriophages (group II in Baltimore classification) as a phage model. M13 is a long rod-like structure formed by a few proteins, namely pVIII, which covers the M13 filamentous body with over 2700 copies and it is responsible for 98% of the viral protein mass [55]. Additional proteins such as pIII, pVI, pVII and pIX constitute the M13 rod tops and play a co-constructive role of the phage coat [54]. The M13 structure and the pVIII 3D structure is presented in Figure I-8.

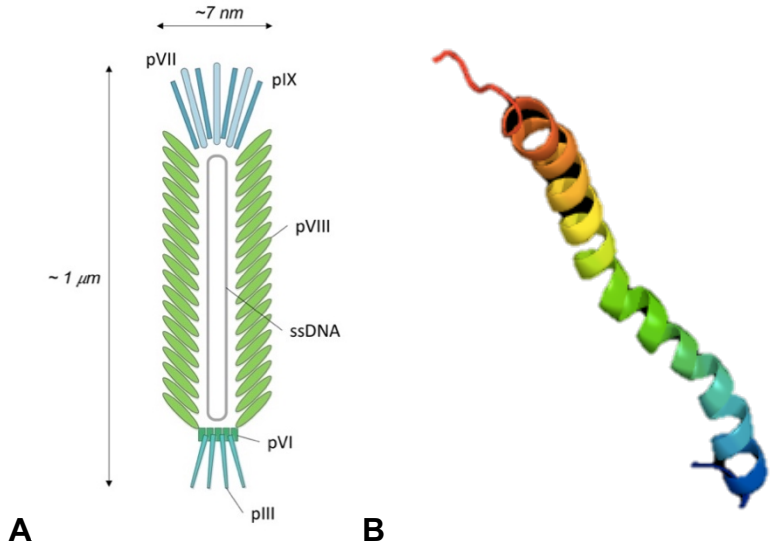

Figure I-8 – ***A) M13 simplified structure.*** *M13 ssDNA is enclosed by five capsid proteins. Minor capsid proteins are presence in low copies (3-8) at each end of the virus and include pIII and pVI, at one end, and pVII and pIX, at the other end. The major coat protein is the pVIII and there are around 2700 copies of this 7625 Da protein;* ***B) PVIII 3D structure prediction by PHYRE2 software (Protein Homology/16nalogy Recognition Engine v 2.0).*** *The pVIII protein is composed by 50 amino acids residues; the N-terminal contains several acidic residues and is exposed to the outside conferring a strong negative surface charge to the M13 bacteriophage. The pVIII surrounds the ssDNA in a 5-layer fashion.*

Phage display is an efficient tool for target discovery in pharmacology and study protein interactions. This technology is based on the insertion of randomized DNA sequences into specific sites of the phage genome, leading to the expression of varying fusion peptides on the surface of the phage [54]. This process corresponds to the construction of a phage display library. From the huge number of produced peptides, from which each phage expresses only one specific peptide according to the incorporated sequence, the relevant peptides are selected by affinity-based screening with the target analyte (a specific type of cell, a target protein, a toxin or a drug candidate of interest, etc) [54].

The filamentous phages are the main platform used in phage display applications, particularly the M13 bacteriophage. The filamentous bacteriophages long rod-like shape and its consequent high length to diameter ratio enhances their penetration into targeted cell by a higher number of ligand-receptor interactions [54].

A consequent application of phage display studies is its application into the construction of specific nanocarriers for the targeted delivery of therapeutic agents or diagnostic reporter molecules [54]. One possible example is the use of a modified M13 nanoparticle with:

- pIII protein fused to a cancer cells targeting ligand, the secreted protein, acidic and rich in cysteine – SPARC - binding peptide – SBP;
- pVIII protein conjugated with doxorubicin, a potent chemotherapeutic used extensively in the clinic, to generate a target treatment in vitro;
- pIX protein biotinylated to bind with streptavidin-coated AlexaFluor 488nm dye.

for a simultaneous cancer drug-delivery and imaging vector [56].

Filamentous phages are also potentially high immunogenic due to the repeated structure of the coat proteins and their relatively large size. Scala, G. *et al*. have shown a pioneering study for the production of vaccines against HIV-1 by fusing epitopes of gp120 and gp41 of HIV to pVIII N-terminal in the surface of M13 [57]. Antibody response against amyloid-ß 42 from Alzheimer's disease have been generated by using M13 phages fused with an mimotope peptide of interest [58].

I.2. Detection methods for diagnostic & control

a. Classic detection methods of viral particles

The first detection method applied for the detection of viral particles was **electron microscopy** for differential diagnosis since the late 40s [59, 60]. Electron microscopy uses a beam accelerated electrons as source of illumination instead of rays of light [61]. The wavelength of an electron is several orders of magnitude shorter than visible light photons, leading to a much higher resolving power and a higher limit of detection (LoD) [61]. The first electron microscope was built by Ernst Ruska and Max Knoll in 1931 [62]. The most common electron microscopy techniques are the original form of electron microscopy, Transmission Electron Microscopy (TEM) - where electrons of the high voltage beam form the image of the analyte -, and Scanning Electron Microscopy (SEM), which produces image by detecting low energy secondary electrons emitted from the surface of the analyte due to excitation by the electron beam [61, 63]. In a TEM analysis, some electrons interact with atoms of the specimen, being absorbed or scattered, while others are transmitted through the specimen with no interaction. The electrons that reach the objective lens will form an image with bright areas (which reveal areas where the electrons passed through the sample), and black and shades of gray areas (that represent denser areas or areas that bound heavy metal ions during specimen preparation, and that will absorb or deflect electrons) (Figure I-9a) [63]. In SEM analysis, the focused electron beam is scanned from point to point across the specimen surface, and doesn't pass through the sample as in TEM (Figure I-9b). In order to perform SEM, the sample has to be previously coated with metal atoms in order to interact with the electron beam and thus produce reflected electrons and newly emitted secondary electrons [63].

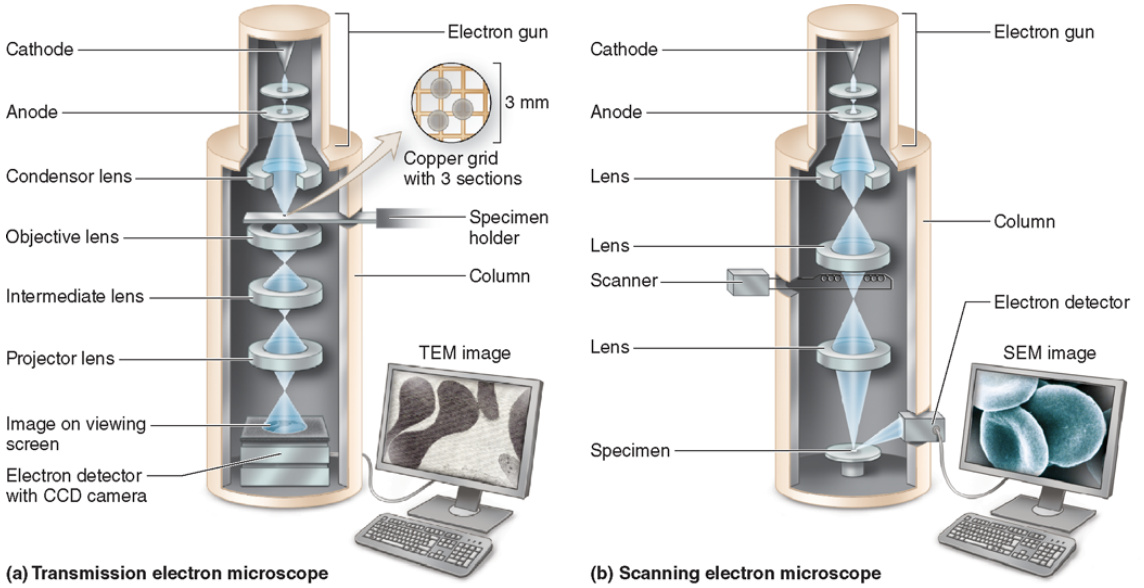

Figure I-9 – Schematic view of the major components of a (a) transmission electron microscope, and a (b) scanning transmission microscope. Source: [63].

With the introduction of negative staining in the late 1950s [64], and the increased availability of electron microscopes, this technique revealed to be essential in characterization of new isolates in cell cultures and clinical samples [65]. This method relies on visual identification of size and particle morphology information which, combined with the distinct morphology of different viral families and coupled with clinical information, is usually enough to set a provisional diagnosis and consequent treatment before other analytical results [65]. However, the main disadvantage is the lack of ability to screen a lot of samples in a large scale due to equipment requirements, time consumption and the need of trained human resources. Also, it is difficult to distinct virus with similar morphologies and/or from the same family or genus. Thus, immunologic and molecular methods were developed as an alternative and/or complementary solution.

Another method of detection commonly used is the **enzyme-linked immnunosorbent assay (ELISA),** with the first publication directed to the detection of viral particles dating back to the late 70s [66-68]. The introduction of this method revolutionized virus diagnosis and the increase use of monoclonal antibodies, improved the assay sensitivity and specificity, as well as it simplified detection and shortened the time required to reach conclusive results [69]. Besides, due to its speed, easy use and straightforward

result interpretation, ELISA is considered a high-throughput testing tool [69]. Briefly, in an ELISA an antigen must be immobilized and then complexed with a specific antibody that is linked to an enzyme. The detection of the formed complex is achieved by assessing the conjugated enzyme activity with a substrate to produce a measurable product [70]. To achieve the antigen – reporter complex, ELISAs can be performed in three different formats (Figure I-10): direct assay (antigen directly adsorbs to the assay plate and it is detected by a labeled primary antibody), indirect assay (antigen directly adsorbs to the assay plate and it is detected by a labeled secondary antibody), or "sandwich" assay (antigen is immobilized by two primary antibodies – the capture antibody, that has been attached to the plate, and the detection antibody - , and is detected by the labelled detection antibody – sandwich direct ELISA - or by a labeled secondary antibody – sandwich indirect ELISA) [70, 71].

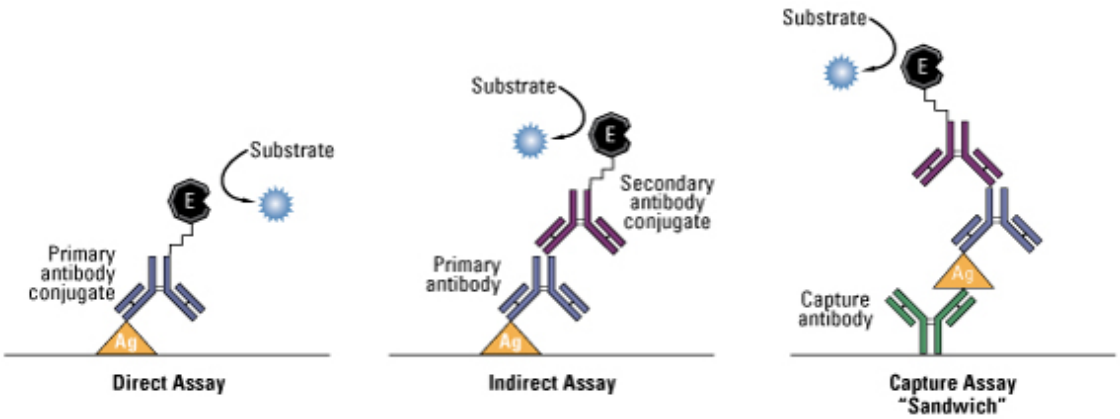

Figure I-10 – ***Common ELISA formats: direct, indirect and "sandwich" assays****. Source: [70].*

It is also possible to detect an antigen in ELISA by measuring the ability of the substance of interest in a pre-titrated system [71]. To do that, it is used a known amount of labeled purified antigen instead of the detection antibody, and it is detect the antigen concentration present in the sample by competition with the labeled antigen for binding to the capture antibody. In a 'competitive ELISA', a decrease in signal from the purified antigen indicates the presence of the antigen in the analyzed samples. However, this ELISA format is more commonly used for small antigens and with only one epitope [70]. Although direct ELISAs have as main advantages the elimination of cross-reactivity of the secondary antibody and the reduction of time consumption since only one antibody is used, the utilization of labeled primary antibodies for each ELISA system is expensive and restrictive. On another hand, an indirect ELISA detection is more sensitive due to

the several epitopes of the primary antibody that can be recognized by the secondary detection antibody, and it is possible to use a wide variety of labeled secondary antibodies [70]. Still, considering ELISA disadvantages in general, it is important to highlight the requirement of high-quality antiserum to permit sensitive and specific detections, which limits not only the detection of a not well known virus, but also the distinction of virus strains [69].

After ELISA, **polymerase chain reaction (PCR)** became a commonly known molecular method for viral detection due to its high specificity and LoD. The detection of Norwalk viral particles is one of many possible examples [72, 73]. PCR can be used as a target amplification method for the detection of viruses by their genetic information in cell cultures or clinical specimens [74]. PCR method relies on the production of multiple copies of a genomic sequence of interest. To do that, PCR involves the use of heat (~ 95°C) to denature the two DNA strands of the analyte, and, when the temperature cools to about 60°C, two short oligonucleotide primers complementary to nucleic acid sequences of the target DNA (15-30 bases) bind to the denatured strands (annealing) - Figure I-11. Then, the hybridized primers act as a substrate for a thermostable DNA polymerase to extend the primer, one base at a time, according to the gene sequence of the target DNA (Figure I-11) [74, 75]. This method also works for RNA samples.

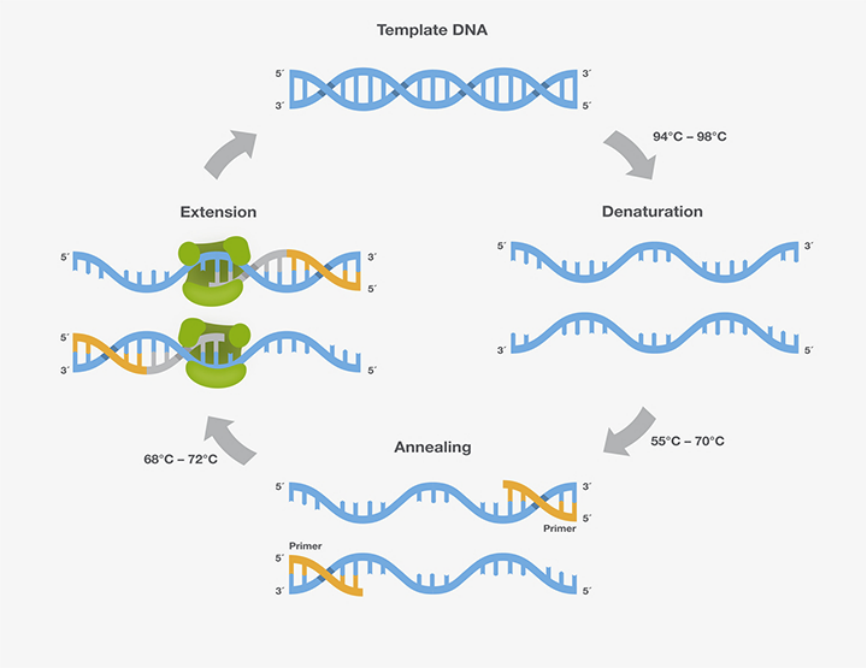

Figure I-11 - **Illustration of the main steps in PCR**: denaturation, annealing, extension to amplified target sequence from a template DNA. Source: [76].

However, being PCR is an extremely precise laboratory technique, a really low quantity of contaminating nucleic acids can produce false-positive results with non-specific amplified DNA [74]. Also, mutations in the primer target region and the lack of ability to identify subviral components (e.g. empty virus) might lead to false-negative results [65]. Besides, classical PCR only provides a qualitative approach based on the target DNA size, detected by electrophoresis of the nucleic acids in the presence of ethidium bromide and visual analysis of the resulting bands after UV light irradiation [75]. To correct this problem, real-time quantitative PCR (qPCR) provides a quantitative analysis, based on classical PCR principles, in real-time. This method monitors the accumulation of amplified DNA target sequence in real time by labelling of primers, probes or amplified chains with fluorogenic molecules [75]. Although qPCR is faster compared to classic PCR due to reduced cycle times, post-detection procedures and the use of fluorogenic labels for sensitive emission detection, it presents as main disadvantages the inability to monitor the amplified size (without opening the system), the incompatibility of some platforms with some fluorogenic chemistries and the high start-up expense [75].

Still, immunologic tests and nucleic acid amplification techniques can only identify previously identified agents since specific antibodies or primers may not currently exist for a complete testing [65]. Besides, electron microscopy, ELISA and PCR detection methods present some disadvantages as they require highly-trained personnel and expensive instrumentation, and are time and lab equipment consuming. Thus, it has been considered as a major challenge the ability to create diagnostic tools with the same performance and quality assurance characteristics as in laboratory-based methods but in a more patient/final user friendly format [69].

In order to achieve a simpler and more user friendly diagnostic tool, **lateral flow assays (LFAs)** have been developed as fast, inexpensive and simple point-of-care diagnostic tools which have been used in the detection of a variety of targets such as proteins, pathogens, drugs, and hormones; the human chorionic gonadotropin pregnancy hormone home test is probably the best-known application of the LFA technology [77]. LFAs have also been used in the detection of various viral particles, such as plant viruses, rotaviruses, dengue virus, noroviruses and HIV detections [78-84].

In LFA, a sample wicks by capillary action along a porous chromatographic membrane, composed of nitrocellulose. Immobilized analyte-specific recognition elements, e.g. antibodies or DNA/RNA probes, form analyte detection 'test lines'. Reporter particles bearing capture antibodies are analyte-bridged to the membrane at the test line to produce a visible line indicating a positive result. Excess reporter particles are directly captured at the 'control line' to produce a visible line that confirms the proper flow of the liquid through the membrane (Figure I-12) [77, 85]. Apart from colloidal gold, other particles such as colored latex particles, carbon nanoparticles [86], phosphors [87], viral particles [81, 88, 89] or magnetic particles (read by optical analysis or magnetic intensity in test line) [90-99] can be used as reporters.

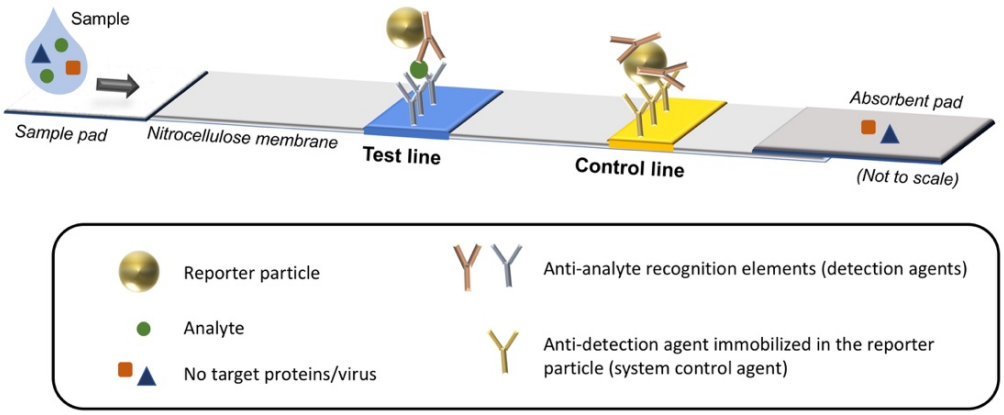

*Figure I-12 – **General lateral flow assay scheme**. In this general example, detection and system control agents are represented in the shape on antibodies; However, it could have been used other recognition elements, as DNA/RNA probes.*

b. Novel methods for the detection of viral particles

Although PCR is a powerful diagnosis technique, the detection of amplified products has some disadvantages as the use of toxic or mutagenic stains, as silver nitrate or ethidium bromide. Also, non-specific amplified DNA can produce a false-positive result. To correct this, several protocols of combined PCR and ELISA for the detection of viruses have been described [100-103]. In this integrated target and signal amplification assay, the amplified target sequence PCR product bounds to a DNA probe immobilized in a 96-well plate and this bond is after detected spectrophotometrically. This approach promotes an improve in sensitivity and specificity, namely some **PCR-ELISAs** were about two orders of magnitude more sensitive than detection by PCR and agarose gel electrophoresis [101].

There is also the possibility to perform a simpler format of an immunoassay called **particle immunoagglutination assay**, also known as particle immunoassay [104, 105]. In this test, antibodies to a given target are conjugated to micro or nanoparticles and then mixed with the sample fluid. If the antigen is present, the particles form larger aggregates due to antibody-antigen interactions (Figure I-13). Particle immunoagglutination assays provide a highly sensitive antibody-antigen binding efficiency and a decreased assay time due to a larger reaction surface area compared to an ELISA assay [104]. Thus, these assays can be performed with complex samples, such as blood, saliva or urine, which contain interfering proteins, cells and lipids [104].

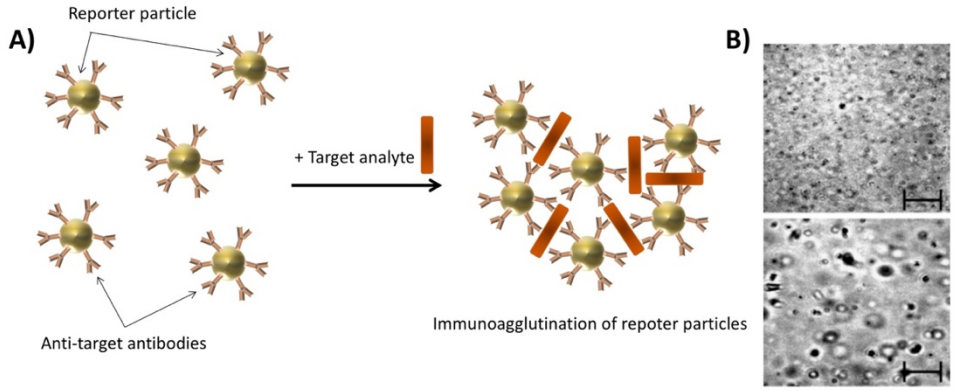

Figure I-13 - A) Particle immunoagglutination assay schematic. B) Bovine viral diarrhea vírus (BVDV) induced particle immunoagglutination of 510 nm particles, top: PBS negative control, bottom: 10^7 # BVDV mL-1. Scale bars represent 50 µm [106].

Since a relatively high concentration of target analyte is required for the immunoagglutination phenomenon to occur and to be optically detected, monitoring the agglutination of the particles via light scattering have been demonstrated to increase the LoD of the test. Thus, simple immunoagglutination assays have been performed in micro devices, integrating optics onto lab-on-a-chip devices. Heinze *et al.* detected different viral particles, such as BVDV in diluted tissue culture media and fetal calf serum, reaching a LoD two order of magnitude lower than a qPCR (Table I-2) [106], or avian influenza (AI) in real chicken feces, with 1 pg/mL LoD for AI antigens in both buffer and real biological matrix (Table I-2) [107]. The performance of immunoagglutination in microfluidic devices present as main advantages a high control over mixing parameters, improving reproducibility and signal-to-noise ratio. Also, potential automated fluid handling reduces user handling and consequent operator-related error [104].

Microfluidic devices can also perform immunological tests for viral detection in an integrated format with low sample, reagent and power consumption, short reaction time, portability and potential parallel operation [108, 109]. A lot of different examples of microfluidic biosensors have been described. For example, Ymeti *et al.* reported a multiplexed microfluidic biosensor integrated with optical Young Interferometer sensor for the detection of herpes simplex virus type 1 (Figure I-14, Table I-2) [110]. In a different format, Zaytseva *et al*. developed a microfluidic biosensor based on the hybridization of reporter and capture DNA probes with the Dengue viral genomic RNA, and liposomes that encapsulate a fluorescent dye for signal amplification. Additionally, the authors used of a permanent magnet located on the outside of the device to easily manipulate the 'capture magnetic beads' location inside the microchannel [111]. It has also been described an integrated microfluidic device with microbead array for the detection and genotyping of hepatitis B virus DNA (Table I-2) [112].

The combination of microfluidic devices with qPCR has also been reported. It is possible to perform the qPCR assay either directly from pre-extracted viral RNA from real samples (Table I-2) [113], or by first concentrating the target virus using antibodies-conjugated superparamagnetic beads, and then proceeding to the viral RNA extraction and following nucleic acid amplification process in a micro-qPCR biosensor (Table I-2) [114].

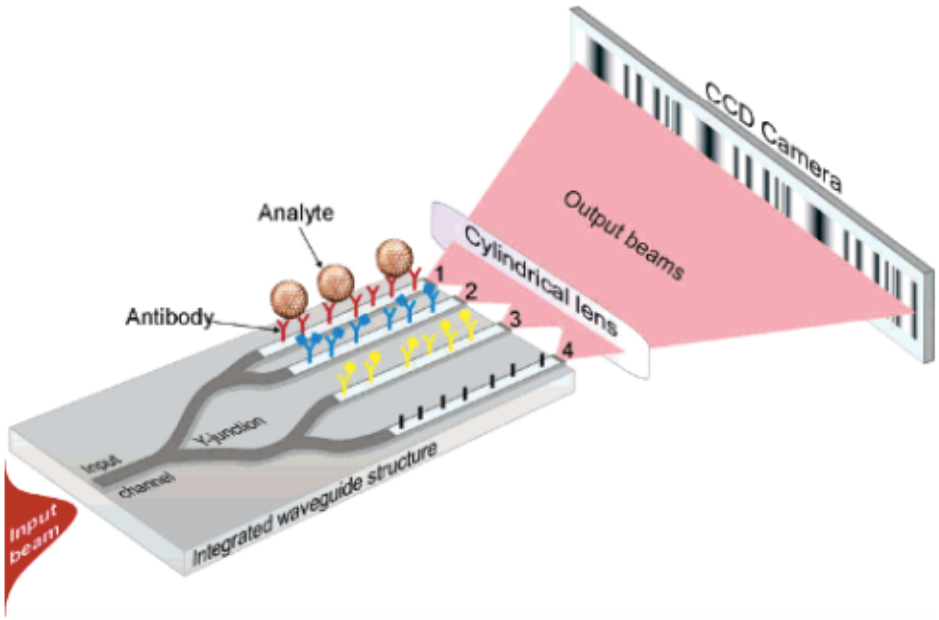

Figure I-14 – Representation of the four-channel microfluidic device integrated with an optical Young Interferometer sensor (not on scale): 1, 2 and 3 represent the measuring channels; channel 4 is the reference channel. Source: [110]

Nanoelectromechanical systems (NEMS) have also been considered as new and highly sensitive lab-on-a-chip biosensors of different biomolecules, such as DNA [115, 116], cells [117, 118] and virus [119, 120]. NEMS can be used as mass-based sensors, where the adsorption of target analytes to pre-treated surfaces induce mechanical stress and consequent cantilever bending. This mechanical signal is then transduced into either an optical or electrical signal [115, 116]. On another hand, biological analytes, such as baculovirus (Figure I-15) or vaccinia virus, can also be detected by the dynamic interrogation utilizing resonant mechanical sensors. In this case, the additional mass load lead to a change of the oscillator resonant frequency (Table I-2) [119, 120].

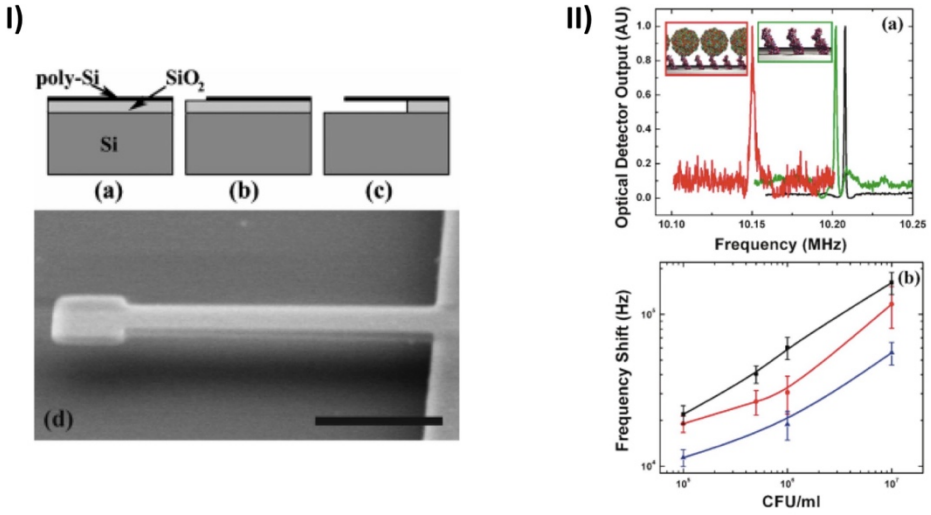

Figure I-15 – I) Fabrication sequence of the nanomechanical oscillators. (a) 1 µm thermal oxidation and low pressure chemical vapor deposition of the polycrystalline silicon device layer; (b) lithographic definition of the oscillator; (c) sacrificial silicon dioxide is removed in hydrofluoric acid; and (d) scanning electron micrographs of released cantilever oscillators with length 6 µm, width 0.5 µm, thickness 150 nm, with a 1 µm x 1 µm paddle. Scale bar corresponds to 2 mm. II) Frequency spectra and sensitivity of the nanoelectromechanical cantilevers. (a) Measured frequency spectra of as fabricated length 6 µm oscillator (black), with additional antibody (green) and bacullovirus (red) mass loading. (b) Frequency shift as a function of the baculovirus concentration for 6-µm (black), 8-µm (red), and 10-µm (blue) long cantilevers. Source: [119]

Magnetic nanoparticles are also very used in immunoassays for the concentration and detection of viral particles [121-123]. Magnetic beads are highly biocompatible and present great spatial controllability; also, their magnetic susceptibility make them an extraordinary tool for easy separation and enrichment of bioproducts by applying an external magnetic field, leading to high specificity and reduction of assay duration [121]. Due to the high versatility of magnetic particles, these beads have been used in different assay formats. It has been reported a sensing methodology that combines magnetic

separation of large size magnetic beads (250 nm in diameter, MB_{250}) from small size magnetic beads (30 nm in diameter, MB_{30}), and magnetic relaxation switching for one-step detection of Newcastle disease virus (Table I-2) [123]. In this work, both size magnetic particles were conjugated with anti-Newcastle disease virus antibodies, leading to a sandwich immunocomplex (MB_{250}-virus-MB_{30}) in the presence of the target virus. The immunocomplex is rapidly removed by magnetic separation due to MB_{250}'s high saturation magnetization and, since MB_{30} is employed in excess, the amount of unreacted MB_{30} is measured to inversely correlate with the amount of detected target. The transverse relaxation time of water molecules around the small magnetic beads is thus the signal readout of the immunoassay [123]. Oh, S. *et al*. described a sensitive colorimetric assay for influenza A monitorization. In this work, the authors have used silica-shelled magnetic nanobeads for easy target separation, and enzyme-like activity of gold nanozymes for signal amplification. The assay can detect influenza A virus up to fentogram per mL (Table I-2) [121].

In a different format, Chen, H.W. and co-workers used erythrocyte membrane cloaked nanoparticles with magnetic functionalities (RBC-mNP)) for influenza virus targeting and isolation through magnetic extraction [122]. Viral samples enriched by this approach led to significantly enhanced virus detection by different quantification methods, such as LFA (Figure I-16) [122].

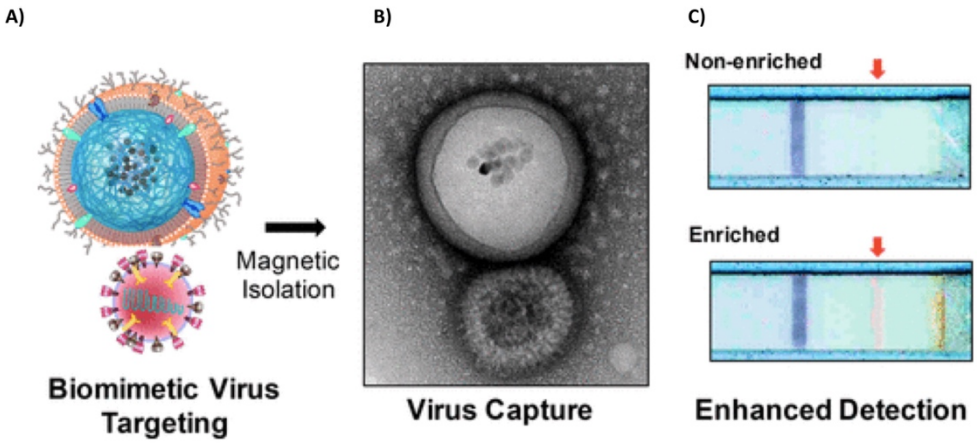

Figure I-16 – A) Schematic illustration of erythrocyte membrane cloaked magnetic nanoparticles (RBC-mNP, top structure) for influenza virus (bottom structure) isolation. B) TEM images of captured virus samples show clusters of RBC-mNP (top structure) and influenza viruses (bottom structure). C) A strip-based rapid flu testing shows that sample enrichment by RBC-mNP improves virus detection as evidenced by the enhanced signal (red arrow). The presence of the blue line indicates a valid LFA (control line). Adapted from: [122].

The development of different biosensors using nanotechnology has also led to the development of new reporter nanoparticles. In particular, **quantum dots** (QDs) are innovative size-tunable and semiconductor nanocrystals with excellent optical properties [124, 125]. Typically, QDs are nanoparticles formed by a semiconductor metal composite arranged in a spherical crystalline core and covered with a different metal alloy shell [126]. When exposed to the appropriate light wavelength range, the excitation of an electron within the core occurs. Since the exciton Bohr radius is bigger than the QD core diameter, the excited electron is confined within the nanocrystal, leading to quantum confinement. When the electron returns to its ground state, the QD emits a photon of light with a defined wavelength, which is dependent on the QD material and diameter (Figure I-17). Thus, the size, shape, and core and shell composition controls the discrete energy levels that the excited state electron can accomplish within it [126]. Therefore, QDs present broad adsorption and narrow emission spectrums, which enables simultaneous excitation of multiple fluorescent colors for multicolor applications [125].

When building close-packed solids of these semiconductor or metal nanocrystals, electronic and optical properties of materials on a nanometer scale can be engineered [127]. Besides, QDs are recognized for better brightness and photostability (more resistant to photobleaching) compared to traditional fluorescent dyes [124].

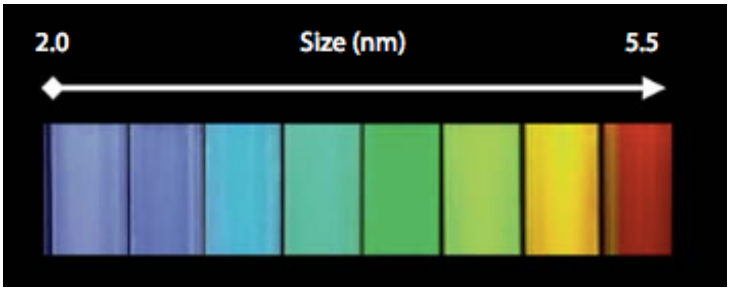

*Figure I-17 – **The relationship between size and color of cadmium selenide quantum dots**. Source: [128]*

QDs have been applied in different formats for virus detection [125, 129, 130]. Adegoke, O. *et al*. reported the detection of norovirus genogroup II detection by norovirus RNA hybridization with a QD-conjugated molecular beacon probe [129]. In the absence of the target norovirus RNA, the QD and the molecular beacon quencher molecule are close and thus the QD emission is extinguished. However, in the presence of the target RNA, the DNA/RNA hybridization leads to a nucleic acid stretching and consequent separation of the QD reporter from the quencher molecule. This effect creates a

fluorescent signal proportional to the norovirus RNA concentration present in the sample, with a LoD of 8.2 norovirus RNA copies/mL in human serum (Table I-2) [129]. In a different format, Shen, W. and Gao, Z. created a quantum dot based platform for detection and serotyping of Dengue viruses in one step [130]. In this work, it was combined four different hybrid quantum dots with specific DNA capture probes (one for each dengue serotype) with magnetic particles to separate the bound capture probes from the unbound ones. In the presence of a Dengue serotype RNA, heteroduplexes with the correspondent capture probe will be formed that will be consequently cleaved off the magnetic particle by a duplex-specific nuclease. This will lead to the releasing of the specific serotype QD to the solution and, when a permanent magnet is applied and the unreacted/uncleaved QDs are removed, the free QDs in solution will reveal the color of the detected dengue serotype [130]. QDs can also be used in an indirect report mode, as in QD-based fluorescence resonance energy transfer (FRET) sensor for human papillomavirus or *citrus tristeza virus* [131, 132]. As example, in Shamsipur, M. *et al.* work it is explored the hybridization of a complementary dye-labelled DNA probe with a QD-DNA conjugate and the target nucleic acid sequence. The complete hybridization leads to a different signal readout from the QD emission, since the QD emission is used as the dye (present in the capture DNA probe) adsorption energy. Thus, QD is responsible to sensitize dye FRET signals as a readout for labelled nucleic acid detection. This biosensor achieved 0.2 nM as detection limit for human papillomavirus (Table I-2) [131].

In the optics of the final consumer - the patient who needs a diagnostic or wants to follow up a certain biomarker - a biosensor is as better as the fast, non-invasive, friendly user, cheap and sensitive as it can be. Thus, improvements in point-of-care LFAs tests have been explored considering their simpler operation mode, not only for patient direct use but also to speed up medical/hospital diagnostic burden.

One possible approach to reach better LoD is to pre-concentrate the target analyte from the sample matrix prior to the detection test. Mashayekhi, F. *et al.* enhanced the LoD of a M13 bacteriophage LFA test by using an aqueous two-phase micellar system [133]. The authors investigated a nonionic surfactant (Triton X-114) to create two coexisting micellar phases and concentrate M13 in the top, micelle-poor phase prior to apply in a

conventional LFA format. The preceding concentration step improved the test LoD by tenfold (Figure I-18, Table I-2).

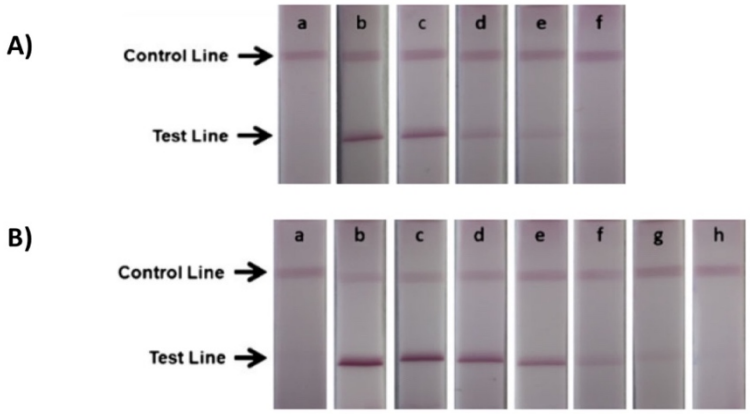

Figure I-18 – LFA used to detect M13 without (A) and with (B) prior micellar concentration step. A negative control (M13 absence) is shown in (a) strips. The remaining LFA strips were incubated with (b) $1x10^{10}$, (c) $5x10^{9}$, (d) $1x10^{9}$, (e) $5x10^{8}$, (f) $1x10^{8}$, (g) $5x10^{7}$ and (h) $1x10^{7}$. Adapted from: [133]

In a different format, Doering, W. E. *et al.* used surface-enhanced Raman scattering (SERS) tags in a LFA kit for the detection of influenza A, influenza B and respiratory syncytial virus [134]. Briefly, SERS occurs when a molecule is very close to a metallic surface and the metal's energy release after photons incidence enhances the occurrence of Raman effect in that molecule, and consequent its Raman signal improves by at least 10^6 times [134, 135]. Therefore, the authors used SERS nanotags (Nanoplex biotags), composed by Ag or Au nanoparticle with a label molecule on its surface, thereby creating the respective label's SERS spectrum to be further detected. A biomolecule recognition element, like an antibody, was also added so it can recognize and detect the viral target. Although Nanoplex biotags could also be used as visual reporters, as the traditional Au nanoparticles in LFAs, the use of a Raman spectrometer in the test line allows its quantification and the use of multiple tag signatures to run multiplexed test. A multiplexed LFA for influenza A, influenza B and respiratory syncytial virus was developed using Nanoplex biotags with three different Raman signatures (one different recognition antibody for each Raman signature) and the corresponding capture antibodies were striped onto a single test line. When the test was performed for one of the targets, the background levels of the other two viruses in study were very low and didn't affect the influenza A test performance. LoD were comparable to commercially available tests [134].

Table I-2 - Limit of detection of different novel virus detection methods.

	Method	Target	Limit of Detection	Reference
PCR-ELISA	**qPCR-ELISA**	Rabies-related viruses	2 x 10^{-5} $TCID_{50}$*/mL of a genotype 1 strain	[103]
Particle immunoagglutination assay	**Microfluidic immunosensor**	Bovine viral diarrhea virus	10 $TCID_{50}$*/mL vs 10^{3} $TCID_{50}$*/mL in traditional qPCR	[106]
		Avian influenza (AI) H3N2	1 pg of AI antigens/mL in clean buffer and real chicken feces matrix	[107]
Microfluidic devices	**Multiplexed antibody-based sensor integrated with optical Young interferometer**	Herpes simplex virus type 1	850 particles/mL	[110]
	Microbead arrays using QD as labels	Hepatitis B virus	1 x 10^{3} DNA copies/mL in clinical serum samples	[112]
	Integrated micro-qPCR	Rotavirus	3.6 x 10^{4} RNA copies/µL from human stool specimens	[113]
	Micro-qPCR biosensor integrated with antibody-conjugated magnetic beads	Dengue virus serotype 2 Enterovirus 71	10^{2} Dengue virus serotype 2 particles/mL (same as traditional RNA extraction kit + qPCR)	[114]
Nanoelectromechanical systems (NEMS)	**Antibody-coated resonating mechanical cantilever**	Baculovirus	Distinguish between 10^{5} and 10^{7} particles/mL	[119]
	Microresonator sensor with nanoscale thickness	Vaccinia virus	Single vaccinia virus particle = 9.5 fg	[120]
Magnetic particles	**Magnetic nano(e)zyme-linked immunosorbent assay**	Influenza virus A (H1N1)	5.0 x 10^{-12} g/mL by human eye 4.42 x 10^{-14} g/mL by microplate reader 2.5 particles/mL in clinical human serum samples vs 5,000 particles/mL for commercial kit, 1,000 particles/mL in traditional ELISA	[121]
	Magnetic separation and magnetic relaxation switching	Newcastle disease virus	10^{2} particles/mL	[123]
Quantum dots	**Quantum dot-conjugated molecular beacon probe**	Norovirus genogroup II	8.2 norovirus RNA copies/mL in human serum 9.3 norovirus RNA copies/mL in buffer	[129]
	Quantum dot FRET-genosensor	Human papillomavirus (HPV)	0.2 nM of HPV 22-mer oligonucleotides sequence	[131]
	Quantum dot FRET	Citrus tristeza virus (CTV)	0.13 µg CTV coat protein/mL, 93% sensitivity, 94% specificity (20x better than ELISA)	[132]
LFA improvements	**Target concentration using prior aqueous two-phase micellar system**	M13 bacteriophage	5 x 10^{7} particles/mL with prior target concentration vs 5 x 10^{8} particles/mL without prior concentration step	[133]

*$TCID_{50}$ – virus titer, 50% tissue culture infective dose

I.3. Purification methods for viral bioproducts

As with another biological therapeutic molecules, the use of viral particles as biomedical agents require their production and consequent purification to meet regulatory requirements. The production procedures of virus and viral particles have been optimized in the last decades, leading to higher yields and harvest volumes. The following operation step is the downstream processing (DSP), where the recovery and purification of the target biological product from impurities is achieved. Impurities can range from process-related (as cell culture reagents and additives like antibodies), to purification process-related (as ligands leachables), or even cell substrate-related (as host cell proteins or nucleic acid). It might also be necessary to separate the target viral product from other virus particle-related, as free proteins, incomplete viral particles, etc. Thus, the purification operation step is becoming an important factor in the seeking for an overall high productivity and lower process cost [136].

Due to the complex structure and properties of virus and viral particles (shape, size, surface composition and structure) and the generated impurities in viral production process, the DSP is usually achieved by a combination of different unit operations (Figure I-19) [136, 137].

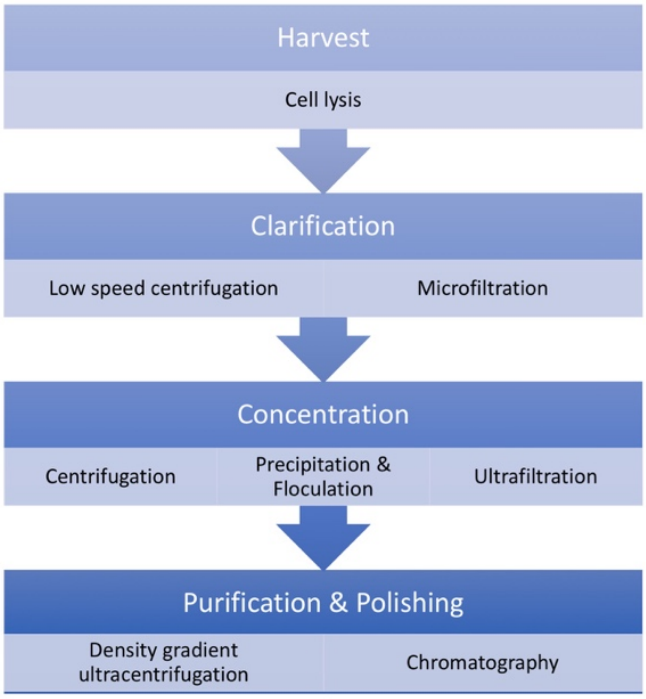

*Figure I-19 – **Standard flow chart for the DSP of virus and viral particles.** Traditional unit operations for each downstream step are indicated.*

a. Clarification

Clarification, the first downstream step, has as main function the removal of producer cells, cell debris and large aggregates (product- or process-related) from crude supernatant, while maintaining the quality of the bioproduct. At small/lab scale, this step is usually performed by a first **low speed centrifugation**, to avoid membrane clogging, and following **microfiltration** (dead-end or tangential flow filtration) [137]. For larger working volumes, a single membrane filtration step is preferred, although fast clogging and consequent virus rejection and reduction of the membrane actual pore size can occur [138]. Microfiltration membranes present a pore size range between 0.1 to 10 µm and can work as depth (solids are retained across the filter depth) or "classic" filters (solids are retained at its surface). The careful choice of the filter, regarding pore size and filter material, as well as its operating parameters, as flow rate and pressure drop, it is key to avoid viral particles loss/damaging, mainly by mechanical disruption, and retain solid impurities [136, 137]. Microfiltration has been widely used in different viral products, such as rotavirus like particles [139], human influenza A virus [140], recombinant baculoviruses [141], or adenoviruses [142].

In order to avoid fast membrane clogging, there is the possibility to filter the crude supernatant through a sequence of decreasing pore size membranes, and thus achieve an efficient clarification with minimum virus loss; the use of a 3 µm depth filter followed by another with 0.65 µm pore size in an initial clarification step for recombinant baculoviruses is one possible example [141].

b. Concentration

Centrifugation

It is possible to concentrate the virus titer after an initial clarification by centrifugation. This method can pellet viral particles when applied by several hours or even days. As example, retrovirus have been concentrated the over 100-fold in small volumes of resuspension buffer, recovering between 80 and 97% of the infectious particles when using between 6000 and 7277 *g* for 16 to 24 hours [143, 144]. However, this technique might promote loss of active particles due to shear stress or extended processing time [138]. Another drawbacks related with centrifugation are the high capital investment

required at large-scale and scalability problems, since the shear stress conditions experienced by the fluid are hard to calculate and mimic in scale-down optimization experiments [137].

Precipitation & Flocculation

Biological products precipitation is a widely used downstream technique to concentrate the target product and to remove unwanted contaminants. Precipitation is based on the decrease of the product solubility and alteration of the solvation potential of the solvent after the addition of a precipitation agent. The most traditional process is the 'salting out' of proteins through the addition of a salt, as ammonium sulfate. The use of non-ionic polymers, as polyethylene glycol (PEG), divalent or multivalent cations, as calcium ions and spermidine, have demonstrated to offer selectivity and it have been used to precipitate M13 bacteriophage with recoveries over 91% [145]. Isoelectric precipitation has also been used for M13 selective precipitation, where the net charge of the bacteriophage is neutralized and phage-phage mutual repulsion is reduced to minimum. This revealed to be an efficient method to separate the viral particle from contaminants based on its isoelectric points, where up to 99% recoveries were achieved with no denaturation [145, 146]. Viral precipitation is also commonly used as one of the initial purification processes in a multi-step viral particles downstream scheme [147, 148].

On another hand, in case of intracellular viral particles production process the first downstream step of the purification includes cell lysis (harvesting). Although cell lysis releases the viral particles to the cell lysate solution, it also releases unwanted host cell DNA and proteins. When present in the medium, host cell DNA increases the solution viscosity and its concentration needs to be controlled due to regulatory requirements depending on the type of product, production host, etc. [137]. Thus, precipitation of host cell DNA has been reported as an alternative to the use of nuclease treatments or chromatographic steps to enhance further virus purification. Cationic detergents, namely domiphen bromide, were used to selectively precipitate DNA from adenovirus-containing cell lysate, where up to 90% PER.C6 cell DNA precipitated at a certain detergent concentration and 90% of adenovirus recovery was also achieved [149]. In a cell culture-derived influenza vaccine production, polyethyleneimine was used to precipitate 85% host cell DNA, which was further removed by depth filtration, with 86%

influenza virions recovery. This study was based on full factorial design and revealed to be inexpensive, easy scalable and suitable for high cell density processes [150].

Ultrafiltration

Ultrafiltration (UF) is a key concentration method in large-scale downstream of virus due to its capacity to process large volumes in a few hours [138]. UF membranes are selected to enrich or maintain viral particles in the retentate effluent, while water and small-molecular-weight impurities are removed in the permeate [136-138]. Thus, this technique presents itself as very important in the downstream process since it not only allows obtaining high volumetric concentration, reducing the handled volume of further purification steps, but it also provides the opportunity to perform a buffer exchange to obtain a higher virus titer in the proper formulation buffer (diafiltration) [136, 137]. UF molecular weight cutoff (MWCO) can range between 0.5 and 1000 kDa, but 50 to 500 kDa UF membranes are most often employed for viral particles retention. In order to keep viral particles in the retentate, the MWCO has to be significantly smaller than the virus particle size, since the MWCO is defined as the minimum molecular weight at which 90% of the product is retained. However, if the MWCO is too small, the permeate flux is reduced and consequent longer filtration times, higher transmembrane pressure and decreased ability to remove contaminants are achieved. On another hand, membrane fouling can often be greater for larger pore size membranes, where cell and virus debris can enter the pores and be trapped in constricted channels. It is important to consider appropriate transmembrane pressure and retentate flux for low wall shear rate during filtration, particularly in active virus particles productions [136].

Different viral products have been concentrated by ultrafiltration modules, namely by using polysulfone [142, 151], regenerated cellulose [152] or polyethersulfone [153, 154] UF membranes, in flat sheet (cassettes) [152-154] or hollow fiber [142, 151] membrane geometries. All these approaches reached above 90% recovery yield for adenovirus [142], influenza virus [153, 154] or retrovirus [151, 152].

c. Purification

Density gradient ultracentrifugation

Density gradient centrifugation, either with sucrose, cesium chloride (CsCl) or iododixanol, is the most common method for the purification of small amounts of viral particles. This method is based on the separation of particles according to their difference in density, leading to the possibility to separate viral particles from defective viral forms, as viral debris or empty capsids, and/or cell membrane vesicles, in a highly purified band [137, 138]. It can be executed a rate-zonal separation, which is based not only on the particles density but also on its size – it is based on the sedimentation coefficient. Different viral particles have been purified using density gradient ultracentrifugation, such as adenovirus [155, 156], plant virus [157], hepatitis C virus [158], retrovirus [159, 160] or rotavirus [161].

However, from an operational point of view, this technique reveals to be very laborious and hard to scale up due to the high equipment investment needed, CsCl cytotoxicity and sucrose viscosity followed by an indispensable extensive dialysis, and loss of surface structures and consequent loss of infectivity [137, 138].

Chromatography

Easy scalable chromatographic separation techniques have been strongly encouraged for large-scale viral particles downstream processing. The chromatographic separation is driven by different interaction of the viral particles and process impurities with the chromatographic stationary phase. Those interactions can be based on the physicochemical properties of the outer particle surface, particle's electrostatic properties or hydrodynamic volume [136]. There are two possible operation modes: Positive/bind-elute operation mode, where viral particles are adsorbed to the chromatographic stationary phase while most of the impurities remain in the mobile phase and are collected in the flow-through pool; or negative-mode operation, where the contaminants are adsorbed to the stationary phase and the viral particles flow-through the column unretained – this operation mode is usually used for the final polishing.

One of the most important features of a chromatographic procedure is the physical structure of the stationary phase, as **packed beads**, **monoliths** or **membrane adsorbers**.

Packed beads are the most traditional example of stationary phases, where the matrix is composed by resins (beads) packed into a column. Beads can be spherical or non-spherical shaped and can also be designed as nonporous or porous, which enable a better access of molecules and increase the accessible surface area. However, since most viral particles range from 30 to 300 nm and conventional porous beads pores sizes vary generally between 10 and 100 nm [162], large viral particles can't easily diffuse into the pores of most commercial resins. Although packed beads have been used for the purification of different virus, as adenovirus [163, 164], retroviruses [165], poliovirus [166], bacteriophages MS-2, PRD-1 [167], M13 [168] or T4 [169], the limited flow rate forced by the balance between pressure drop and mass transfer resistance, and the low dynamic binding capacity mainly for large viruses, represent the two main disadvantages.

On another hand, convective chromatographic mediums present great improvements in capacity, resolution, recovery and shorter operation time, as well as low pressure drop and little compression or channeling.

Monoliths are a fixed continuous stationary phase with highly interconnected macropores through which the biomolecules are transported by mainly convective flux. These structures, which are commonly composed by silica, polymethacrylate, polyacrylamide, polystyrene or even cellulose presenting channel diameters ranging from few nm up to 2 µm, are being commercialized by several companies as BIA Separations, Bio-Rad, Merck and Isco [170]. Bacteriophages [171-173], influenza [174], lentivirus [175], baculovirus [176], retrovirus [177] and canine adenovirus [178] purifications are a few examples of virus purified by monoliths-based processes.

Membrane adsorbers have a similar purpose to monoliths, but in the format of conventional filtration modules. Membrane chromatography uses microporous membranes, usually in multiple layers, that contain functional ligands attached to the internal pore surface throughout the membrane structure. For membrane chromatography, binding sites are located along convective pores rather than inside long diffusive pores [179]. Accordingly, mass transfer of biomolecules to binding sites depends on convection instead of diffusion, and binding capacities of membrane chromatography are largely independent of flow-rate. These membranes consist in a polymeric substrate, as polyamine, sulfone or cellulose, to which a functional ligand is

chemically coupled, as in conventional chromatography resins. Furthermore, membranes are often used as disposable units, supporting the current efforts in the pharmaceutical industry to reduce costs for validation procedures and lengthy cleaning [136, 137]. Retrovirus [180], active Vaccinia virus particles [181] and adenovirus [142, 182] have been used in some examples of purification processes based on membrane technology.

Another important feature to consider is the surface chemistry of the stationary phase and consequent chromatographic operation mode. **Size exclusion chromatography (SEC)**, **ion-exchange chromatography (IEC)**, **hydrophobic interaction chromatography (HIC)**, **affinity chromatography (AC)**, or **multimodal chromatography (MMC)** can be considered for viral particles purification. The action principle is thus dependent on the viral particle features, as well as the remain impurities, to reach the best separation possible.

SEC can only be achieved by bead-based porous media, but not by membrane adsorbers or monoliths. This separation is based on the difference in molecular size between the target viral particle and the remaining impurities; the viral particles are excluded from the porous matrix, and thus are generally recovered in the column void volume, whereas bulk proteins and small molecular contaminants elute through the porous matrix at different rates. The SEC operational conditions are gentle and don't require any buffer change, allowing to maintain infectivity and immunogenicity. SEC has been used for the purification of influenza [183], adenovirus [184] and poliovirus [185], for example. However, the limited capacity, product dilution and poor pressure resistance of the matrix are some of the disadvantages of this type of chromatography, leading to some replacement by UF [136, 137].

The purification of viral particles by **IEC** is traditionally operated in positive/ bind-elute operation mode, where viral particles adsorb to the chromatographic medium while most of the impurities are collected in the flow-through pool. Viral particles are then desorbed by an increasing ionic strength and/or pH change to lead to an unfavorable overall charge of the virus surface, where it won't bind anymore to the stationary phase, and exchange with another ion more suitable to bind to the column at those conditions. Depending on the overall isoelectric point of the target viral particles, cation (CEC) or anion exchange chromatography (AEC) matrixes are used. Diethylaminoethanol (DEAE)

and quaternary ammonium (Q) are probably the most used ligands for viral AEC [142, 164, 165, 168, 171-173, 175, 176, 178, 180, 182]. CEC can also be used for viral particles purification by using sulfonic acid chemistry, as for influenza [174] and adenovirus [163]. On another hand, **HIC** has been rarely used for viral particles purification due to the use of high salt concentrations for viral adsorption, which can affect the virus integrity, transfection efficiency and immunogenicity [136]. Still, ether, poly-propylene glycol, phenyl, butyl and hexyl HIC ligands have been used to remove residual DNA after AC for purification of active Vaccinia virus particles [181]; as well as butyl ligands for adenovirus purification [163].

AC is based on the specific and reversible adsorption and subsequent recovery of the active target viral particle to a ligand that will bind to a component of the virus capsid. These ligands can be immobilized metal ion (as zinc for adenovirus [186]), peptides (as heparin for active Vaccinia virus particles [181], glutathione for T4 bacteriophage [169, 181]), biotin streptavidin systems (for biotinylated retroviruses [177]) or specific recognizing agents, as antibodies for poliovirus [166] or DNA aptamers for vaccinia virus [187]. However, AC is expensive for large-scale production processes due to the large cost for the purification and immobilization of the ligand; still, it has been extensively used at laboratory scale.

Finally, **MMC** or mixed-mode chromatography exploits a multimodal functionality using various target-matrix interaction, such as ionic, hydrogen bonding and/or hydrophobic interactions. A traditional MMC media is hydroxyapatite, which supports metal affinity interactions through its calcium groups, and cation exchange interactions through its phosphate groups. This type of chromatography interaction has been used for adenovirus [164], papillomavirus [188] or Moloney murine leukemia viruses [189], for example.

d. Non-classic purification methods

Aqueous two-phase extraction

Aqueous two-phase extraction is a promising alternative to traditional downstream techniques to achieve clarification and concentration in just one step. This liquid-liquid extraction technique is based on aqueous two-phase systems (ATPSs) that are formed when two immiscible compounds, such as two polymers or a polymer and a salt, are

mixed in an aqueous solution above a certain critical concentration (described by the system binodal curve), and spontaneously separate into two immiscible phases (Figure I-20). These systems provide a biocompatible environment since they have a high water content, low interfacial tensions and some polymers also have a protein stabilizing effect [190], resulting in an efficient separation without denaturation or loss of biological activity. These systems have already been successfully applied to the separation of proteins from cell debris or to the purification of a target bioproduct from a crude feedstock, including, viruses [191-194] and VLPs [195, 196].

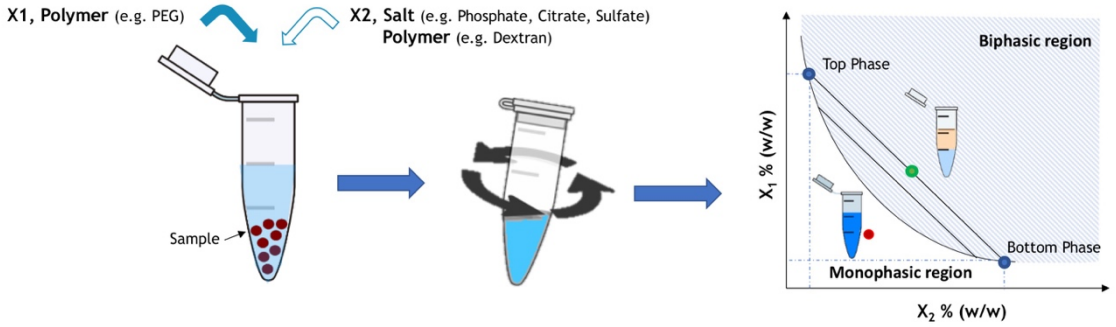

*Figure I-20 – **Schematic representation of ATPS formation**. ATPS forms when components (X1 and X2, as two polymers or one polymer and a salt) are mixed in an aqueous solution above their critical solubility concentrations, i.e. when the system composition is described in the biphasic region of that equilibrium. The mixture will then separate into two immiscible phases, where the light phase (top phase) is rich in component X1 and the heavy phase (bottom phase) is rich in the second system component X2. Each phase composition is described by the correspondent system tie-line.*

ATPS has been explored for virus recovery, namely for adenovirus recovery using PEG 300-phosphate system yielding 90% recovery [192], or with a PEG8000 - ammonium sulfate system reaching up to 97% recovery [191]. M13 has also been used in aqueous two-phase extraction studies, where a PEG-potassium phosphate system recovered M13 viral particles from crude broth to the system top phase with 83% recovery yield and 18.2 purification fold [193].

The purification of VLPs using ATPS was first reported in 1989 for the concentration and purification of the outer envelope protein gp70 of the feline leukemia virus and the gag protein p27 using dextran-sulfate and polyvinyl alcohol, where both proteins were more than 40-fold purified [197]. More recently, intracellular and extracellular double-layered rotavirus-like particles from insect cell culture were separated using PEG-phosphate systems with an overall recovery of 85% and a purity increase of 30–55 times comparing to the initial medium has also been described [195]. An initial extraction of a recombinant viral coat protein from cytoplasm of *E. coli* using a PEG-phosphate system with a high

partition to the top phase [198], and an initial extraction step of B19 particles to the bottom phase of PEG 1000 – magnesium sulfate system with a yield around 90%, while removing cell debris and 31% of total protein to the system's top phase, interface and sediment [196], were also described.

High performance tangential flow filtration (HPTFF) is an emerging technology that can combine protein purification, concentration and buffer exchange in a single step. In HPTFF, high selectivity is achieved by operating in the pressure-dependent regime, which minimizes fouling and exploits the effects of concentration polarization. Also, part of the permeate is recirculated in co-current to the feed on the permeate side of the module using a recirculation pump, leading to a more constant local transmembrane pressure and consequent improved selectivity (Figure I-21). Parvovirus, as a small virus model, has been studied for its purification using 30, 50 and 100 kDa flat-sheet filtration membranes in HPTFF operation mode; more than 90% recovery and up to 10-fold concentration has been achieved [199-201].

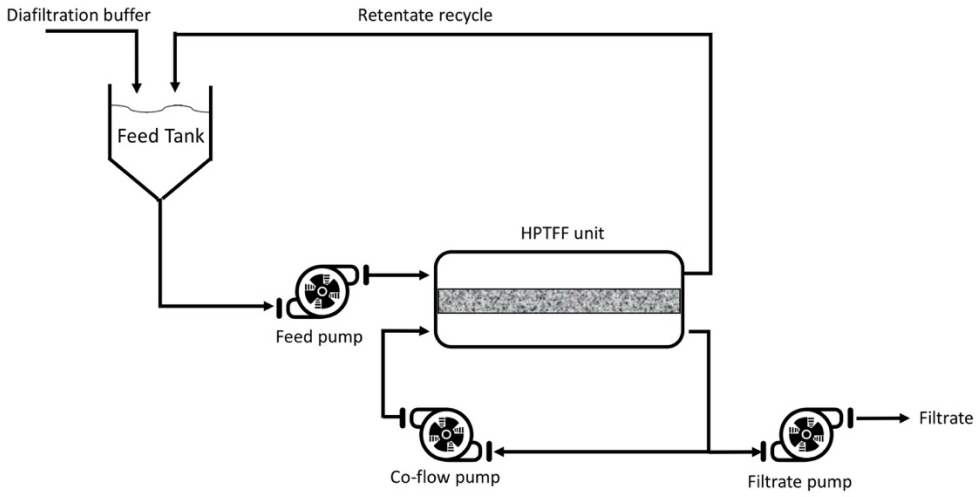

Figure I-21 – ***Schematic representation of a filtration set-up used for HPTFF.***

Recent advances are based on electrostatic interactions between bioproducts and charged membranes, where a positively charged membrane will provide a much greater retention of a positively charged bioproduct than a negatively charged or neutral membrane, and vice-versa [202, 203]. It is also possible to significantly improve the system performance through a careful study of buffer pH and ionic strength to maximize differences in the effective volume of the product and impurities. With these

modifications, HPTFF performance is governed by membrane properties, such as pore size, and surface charge-density, and process parameters, such as filtrate flow-rate, load pH and ionic strength [203]. It is expected that new studies exploring these features for viral purification will be explored in the next few years.

There have also been developments in chromatographic operations.

Steric-exclusion chromatography (SXC) is a new chromatographic method where adsorption is achieved by no chemical interaction between a non-reactive hydrophilic solid phase and the target biomolecule. Here, the target biomolecule adsorb to the solid phase by their mutual steric exclusion of a promoter substance, as PEG (Figure I-22). Thus, the hydrophilic solid phase works as a 'nucleation center' on which biomolecules interact instead of forming precipitates. Elution is achieved by reducing the PEG concentration [204, 205].

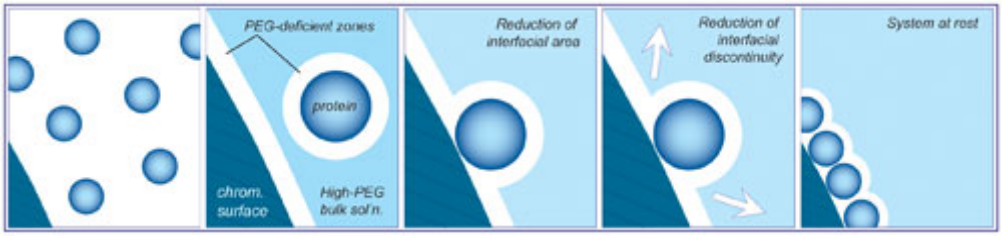

*Figure I-22 - **Fundamentals of SXC**. When proteins suspended in an aqueous buffer and a non-reactive hydrophilic chromatography surface (first panel) meet high concentrations of PEG, there is the formation of PEG-deficient zones created by steric exclusion of PEG from the proteins and surface hydrophilic surfaces (second panel). Then, there is a reduction of interfacial area between the high-PEG bulk solvent and the PEG-deficient zones (third panel). Excess water is released to the bulk solvent (fourth panel), reducing the bulk PEG concentration, which reduces the discontinuity between the high-PEG bulk solvent and PEG-deficient zones, further reducing free energy in the system. The system finally reaches an equilibrium with proteins eliminated from the bulk solvent. Source: [205]*

Bacteriophage M13K07 was purified from *E. coli* broth by SXC on a hydrophilic OH monolith [204]. These SXC application reached a dynamic binding capacity near of 10^{13} particles per mL (1000 times higher than a traditional chromatographic media), 99.8% and 93% reduction of host cell proteins and DNA, respectively, and more than 90% viral recovery with full infectivity in a rapid single step [204]. Cell culture-derived influenza A has also been purified using SXC with more than 95% recovery and 99.7% and 92.4% depletion of host cell DNA and proteins, respectively [206].

The SXC selectivity is generally achieved by the biomolecule hydrodynamic size and by the PEG size and concentration used. This operation technique can be applied to other viruses or large biomolecules, and thus it can be faced as an alternative to SEC application. Still, there are two fundamental differences: in SXC, larger particles are

strongly retained (the opposite of SEC procedures); also, SXC only uses monolith and fluidized chromatographic formats due to the high PEG viscosity driven pressure, whereas SEC is still limited to packed-bed configurations [137].

Concerning chromatographic bed format improvements, **expanded bed adsorption (EBA)** involves the novel use of adsorbent particles dispersed in a liquid medium, which could be used for direct product recovery from crude feedstocks, potentially replacing the clarification and capture steps. The simplest example is batch chromatography, where the fluidized bed expansion is controlled by the upward flow of the mobile phase. This highly engineered up-flow columns maintain the particles in an evenly dispersed state throughout equilibration, sample application, and washing. Once the unclarified feedstock is introduced within the column of the fluidized adsorbent, cells and cell debris pass unhindered through the interstitial voids created in the expanded bed and ultimately escape through the top of the column. The target adsorption onto the chromatographic media takes place in this stage. Elution, cleaning, and sanitization can be performed in packed bed mode (Figure I-23). [207]

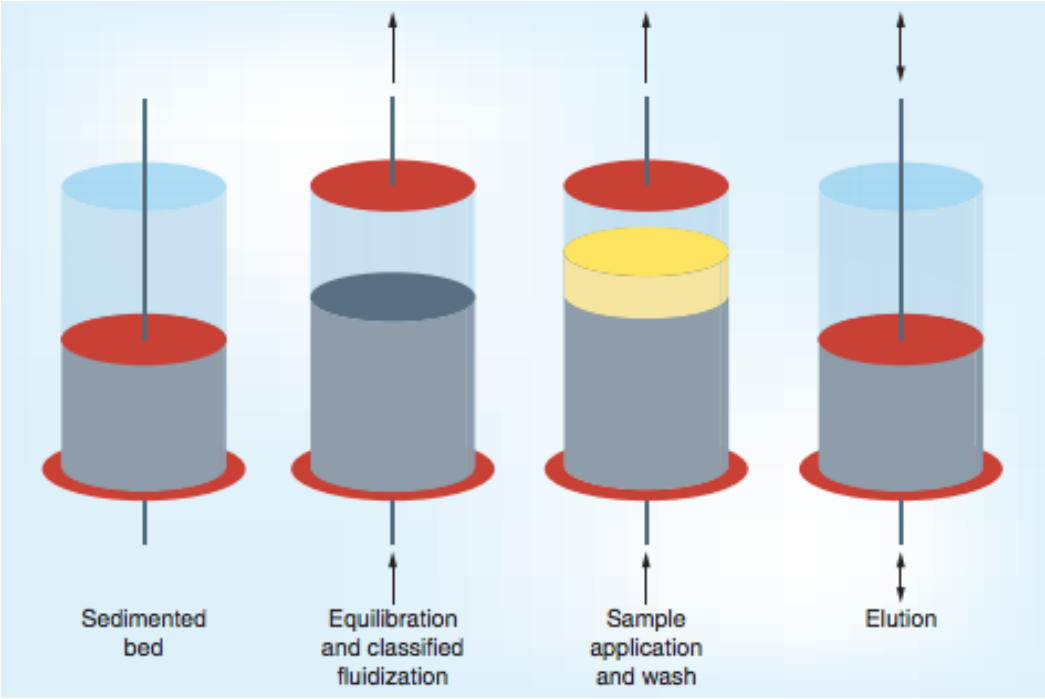

*Figure I-23 – **Schematic representation of EBA chromatography working principle.** Source: [207]*

The first generation of EBA adsorbents (Streamline, GE Healthcare) have been used for different viral purifications, as adenovirus [208]. It has also been used for M13

purification, where 82.9% of the bacteriophages were recovered in a fast single step [209].

However, technical limitations in first generation materials stopped a broader implementation. Since the density of the chromatography particles was partially overlapped with the density of cells and debris that were intended to pass through, this led to unfavorable biomass-adsorbent interaction and improper bed fluidization, and consequent process failure. A second generation systems (Rhobust™, DSM) have overcome these physical limitations and led to significant improvements [207]. A rotating arm at the inlet port achieves effective flow distribution. Also, the use of high-density tungsten carbide-cored beads coated with cross-linked agarose (with several types of functionalities available) increase the density differential between cells and chromatography particles, and allow faster flow (up to 500 cm/h) rates that achieve more efficient flow of debris through the system [210, 211]. It is expected that these new EBA mediums will be applied for processing viral particles in a near future.

Although most chromatographic methods explore a positive/bind-elute operation mode, where viral particles adsorb to the chromatographic medium while most of the impurities are collected in the flowthrough pool, it is also possible to explore negative/flow-through mode operations. In a negative mode operation, the contaminants adsorb to the matrix and the viral particles flow through. GE Healthcare has launched a new chromatographic stationary phase, **Capto Core 700**, for negative operation mode to achieve intermediate purification and polishing, instead of traditional final flow-through mode for polishing process. Capto Core 700 is a resin composed of an active core, functionalized with multimodal binding ligands, and an inactive porous shell. This design excludes larger molecules from entering the core and are thus collected in the flow-through pool (Figure I-24).

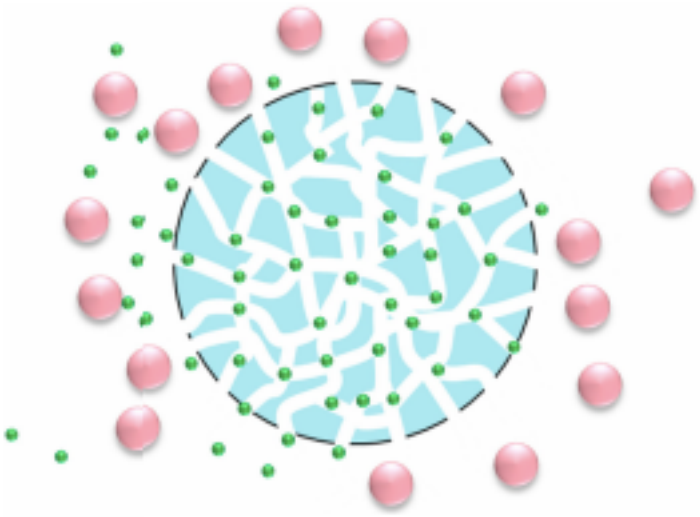

Figure I-24 – ***Schematic cross-sectional view of a Capto Core 700 particle.*** *Small impurities (green) can enter the core and interact with the ligand. Larger biomolecules (pink) can't pass through the porous shell and will thus pass through the column unretained. Source: [212]*

It has already been reported the decreasing ovalbumin into regulatory requirements and 69% viral recovery in an UF/DF plus Capto Core 700 downstream process for influenza A vaccine, which is still produced with allantoic fluid from fertilized chicken eggs [212]. In a different example, Fernandes *et al.*, used a core bead prototype chromatography as polishing step to bind fragmented host cell DNA and host cell impurities by ion-exchange and hydrophobic interaction while recovering 86% of canine adenovirus through the flow-through [178].

I.4. Commercial viral detection kits and industrial purification examples

Detection - Commercial examples of viral detection assays

The most common 'final user' / 'home test' detection kits are LFA tests. All the following described examples work in a similar operation mode; still, the reporter agents used might differ. These immunochromatographic tests use the patient sample incubated with a 'sample buffer' to allow the migration along the strip.

All influenza detection kits seek to detect the viral nucleoproteins. SAS™ FluAlert Influenza A&B (SAS Institute, USA) is one of the most used influenza detection kits. This test presents 76% sensitivity and 98% specificity for Influenza A and 90.5% sensitivity and 100% specificity for influenza B using gold nanoparticles as reporters [213]. TRUFLU® (Meridian Bioscience, Inc., USA), Remel Xpect® Flu A&B (Thermos Fisher Scientific, Canada), Quickvue Influenza A + B test (Quidel Corp., USA - Figure I-25) are other influenza 'home detection kits' that also use color particles as reporters. As example, a 'QuickVue Influenza A + B test' kit with 25 tests cost around 450 USD [214].

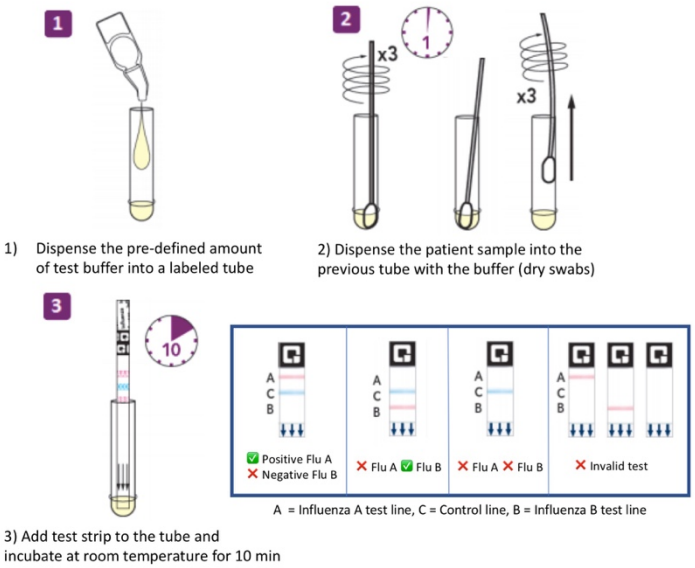

*Figure I-25 – **'Quick Vue Influenza A + B' schematic test procedure for nasal/nasopharyngeal swab sample application.** Adapted from [215].*

In a different read-out format, the 3M™ Rapid Detection Flu A+B Test (Response Biomedical Corp. for 3M Healthcare, USA) uses the 3M™Rapid Detection Reader for the differential determination of Influenza A and Influenza B in nasal wash/aspirate,

nasopharyngeal aspirate, and nasopharyngeal swab samples by using fluorescent-dyed particles conjugated to specific antibodies. The reader devices measures the amount of fluorescence emitted by the complexes at the two detection zones (Influenza A and Influenza B) and compares it to pre-defined threshold limits to determine a positive or negative result for Influenza A and Influenza B in the tested sample [216].

The 'OraQuick In-Home HIV Test' (OraSure Technologies, Inc., Bethlehem, PA) was approved by Food and Drug Administration (FDA) in 2002 for HIV-1 and HIV-2 diagnosis through the detection of anti-gp41 domain antibodies present in the sample [217]. This home test comes with a test stick and a tube with a testing solution. The test stick is used to swab the gums to get a sample of oral fluids. The test stick is inserted into the test tube and it should be incubated for 20 minutes to complete the results (Figure I-26). A single test can be acquired online and in several retailers for approximately 60 USD [218].

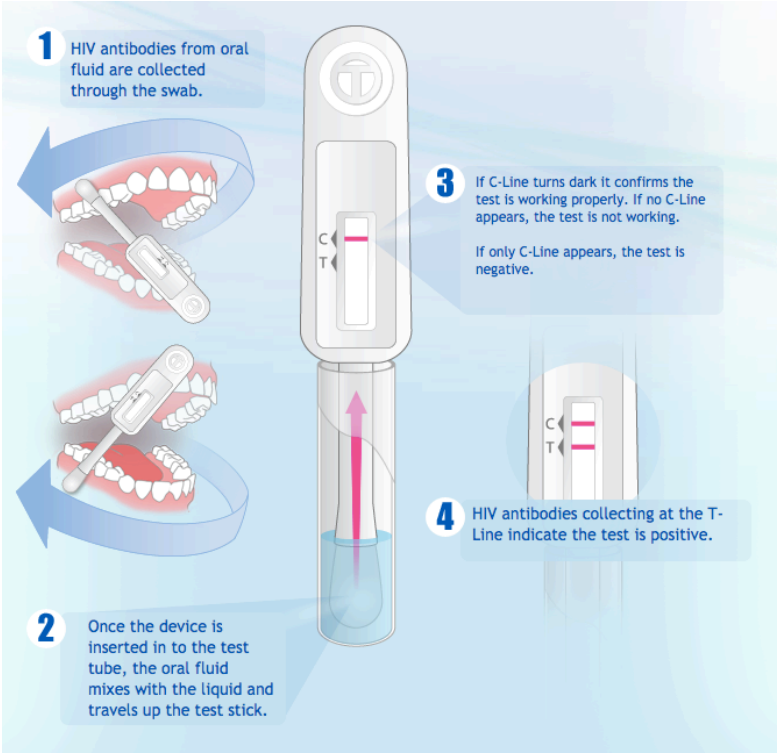

*Figure I-26 – **OraQuick test procedure** [219].*

On another hand, Alere Determine™ HIV-1/2 Ag/Ab Combo (Abbott Laboratories, Abbott Park, IL) is the first and only FDA approved test that simultaneously and separately detects HIV-1/2 antibodies and free HIV-1 p24 antigen on a single test strip

[220]. However, although this is a LFA test, this kit is only used for trained personal in healthcare establishments since it requires laboratory material.

The most studied test for norovirus detection is the lab-commercial RIDA®QUICK Norovirus (R-Biopharm, Germany - Figure I-27), which provides a yes/no response for genogroups 1 (GI) and 2 (GII) in stool samples with high sensitivity (64-83% in published works, or 92% according to the manufacturer) and 97-100% specificity [221-226]. However, it is only reported the limit of detection LoD for genogroup GII.17 ($6.54x10^6$ copies/g of stool [223]). The test uses biotinylated anti-norovirus antibodies and gold-labeled anti-norovirus antibodies; when target noroviruses are present in the sample, it is formed a complex with both kinds of antibodies and start flowing through the strip. A streptavidin test line captures the gold-labeled migrating complexes via the biotinylated anti-norovirus antibodies. Unbound gold-labeled antibodies are bound later at the control line, assuring that the test was performed correctly.

*Figure I-27 - **RIDA®QUICK Norovirus** [226].*

It has also been reported a LoD for the commercial SD BIOLINE norovirus of $1.7x10^7$ and $9.5x10^7$ copies/g of feces for GII.3 and GII.4, respectively [227], and $4.48x10^6$ copies/mL in stool samples [228]. This test is documented with 84.1% sensitivity and 96.1% specificity, according to the manufacturer [229].

However, these testes are still only used as an aid in the diagnosis of acute gastroenteritis in health care institutions. Also, the main drawback of traditional LFAs

using color latex or gold nanoparticles is the high LoD, which reveals as an opportunity for new reporters and approaches.

Large scale viral purification

One of the most described large scale example is the production of inactivated poliovirus vaccine [230, 231]. The viral particles are produced in thousand liters cultures of Vero cells and subsequent 0.22 µm filtration for cell debris removal, concentration by ultrafiltration and Sepharose 6B CL and DEAE-Sephadex chromatography for final polishing. The viruses are then inactivated by formaldehyde incubation [230, 231]. The overall process recovery reaches 50 to 60%, where 1,000 L of poliovirus cultures generate 10^6 vaccine doses [230].

Another classic example is the influenza vaccine production. This vaccine has a unique annual plan since, in every February, the World Health Organization (WHO) Global Influenza Surveillance and Response System provides to the manufacturers a list of potentially more common influenza strain in the next 'flu season', and the vaccines must be ready to shipment according to FDA regulatory requirements before the following winter [232]. This process is focused on the production of influenza virus' hemagglutinin (HA) protein, which its use in immunization will produce antibody to HA to neutralize a similar virus on a future infection [233]. Most of these vaccines are produced by growing the target influenza virus strain in fertile chicken eggs for several days. This manufacturing process has been used for more than 70 years and it is used to produce both inactivated (commonly called "the flu shot") and live attenuated vaccines (usually called "nasal spray") [232]. The standard purification process is based on density gradient centrifugation, followed by optional virus inactivation (depending on the type of final product), detergent treatment, diafiltration and sterile filtration to remove most of the egg and influenza proteins other than the HA protein, where up to 80% HA recovery is achieved [234].

New production methods are being developed to replace the chicken-egg based classic process, such as the use of mammalian or insect cell lines [232, 233]. It has also been described the production of recombinant subunit HA vaccines targeting H1N1 and H5N1 influenza using 50 kg of plant biomass under current Good Manufacturing Practice

regulations (cGMP). For its purification, it was used a downstream process with centrifugation and microfiltration for clarification, followed by purification using a three-chromatography sequence composed by AC, HC, AEC, and UF and diafiltration before aliquoted to be stored at -70°C [235].

Every process development aims to reduce plant size for maximum productivity with lower costs as possible. To do that, biopharmaceutical industry have been presenting some innovative trends in the last decades [137]. The proper process understanding and characterization has become more and more necessary and used. A common approach is the use of simulation software, such as Intelligen SuperPro Designer, Aspen Batch Plus and BioSolve, for cost of goods estimation and model most the process features, including material and energy balances, scheduling, etc. Although the simulation software is still limited to accurately predict unit operation scale-up and perform a perfect bioprocess optimization, as shown in a simulation for a vaccine manufacturing process under development at Merck & Company [236], it can effectively analyze the economics of a murine polyomavirus VLP vaccine production [237].

The modeling of single unit operation has also became a more common optimization approach, as in the separation of influenza virus from host-cell protein [238]. However, model-based global process optimization with several unit operations has not been attempted so far [137].

For process understanding, it is also common to use Design of Experiments (DoE), which relies on the fitting of multivariate data to an empirical function. This tool provides information about the system, as maximum, minimum and trends of different parameters. The studies of adenovirus [182] and baculovirus [239] adsorption/desorption for different ligand density and salt concentration are a few examples. However, factorial designs with levels higher than two require a large number of experiments to be performed, which has been solved through high-throughput screening techniques, and it doesn't provide fundamental information about the interactions observed [137].

Concerning more practical approaches for process optimization, the use of disposable technologies has become very appealing in the recent years. As an example, a new

facility for insect cell production for influenza VLP is estimated would cost one-twelfth of a mammalian cell-culture facility at 50 million doses per year [233]. This cost reduction is not only due to the 7 to 10 times higher HA production yield than traditional methods, but also due to the use of disposable technologies. The use of flexible tubing, disposable filters and chromatographic columns avoids the use of increasing cost of stainless steel and the need for clean-in-place and sterilize-in-place equipment. Consequently, this approach also requires much less labor [233]. As proof-of-concept, Novavax has built a fully disposable facility for H5N1 vaccine which, at current yields, can produce up to 30 million doses in 6 months. The processes uses two 200-L Xcellerex wave bioreactor for seed preparation and 1,000-L Xcellerex bioreactor for VLP production [233]. Still, the scale limitation, mainly in the downstream processing technologies, remains as the main disadvantage of current single-use systems.

Continuous downstream processing for biological products has been considered in the last few years in order to achieve reduced footprint and cost while increasing the process productivity and flexibility. However, since a continuous process definition is hard to achieve, its optimization in scale-down requires more material than a batch approach, and the general batchwise purification of some biological products has not encountered any limits of scability, the industrial application is reluctant to change and follow a continuous approach. Studies concerning continuous downstream processing of viral particles has rarely been explored. Still, for example, the quasi-continuous purification of adenovirus using two SEC columns presented an increase of recovery yield from 57% in a batch approach to 86%, with 90% clearance for DNA and host cell proteins [240]. It is expected that more continuous approaches for viral particles purification will be reported in the upcoming years.

I.5. References

1. Weitz, J.S. and S.W. Wilhelm, *Ocean viruses and their effects on microbial communities and biogeochemical cycles.* F1000 Biol Rep, 2012. **4**: p. 17.
2. Gelderblom, H.R., *Structure and Classification of Viruses*, in *Medical Microbiology*, S. Baron, Editor. 1996, The University of Texas Medical Branch at Galveston: Galveston, Texas, USA.
3. Lodish , H., et al., *Viruses: Structure, Function, and Uses*, in *Molecular Cell Biology*, W.H. Freeman, Editor. 2000: New York.
4. Naskalska, A. and K. Pyrć, *Virus Like Particles as Immunogens and Universal Nanocarriers.* Pol J Microbiol, 2015. **64**(1): p. 3-13.
5. Ellis, J., *Porcine circovirus: a historical perspective.* Vet Pathol, 2014. **51**(2): p. 315-27.
6. Aherfi, S., et al., *Giant Viruses of Amoebas: An Update.* Front Microbiol, 2016. **7**: p. 349.
7. Nasir, A., K.M. Kim, and G. Caetano-Anollés, *Viral evolution.* Mobile Genetic Elements, 2012. **2**(5): p. 247-252.
8. Domingo, E., et al., *Basic concepts in RNA virus evolution.* FASEB J, 1996. **10**(8): p. 859-64.
9. Chen, J. and Y.M. Deng, *Influenza virus antigenic variation, host antibody production and new approach to control epidemics.* Virol J, 2009. **6**: p. 30.
10. LWOFF, A., R. HORNE, and P. TOURNIER, *A system of viruses.* Cold Spring Harb Symp Quant Biol, 1962. **27**: p. 51-5.
11. International Committee on Taxonomy of, V. and A. King, *Virus taxonomy : ninth report of the International Committee on Taxonomy of Viruses*. 2011, Oxford: Elsevier.
12. Baltimore, D., *The strategy of RNA viruses.* Harvey Lect, 1974. **70 Series**: p. 57-74.
13. Nathanson, N., *Viral pathogenesis*. 1997, Philadelphia, Pa.: Lippincott-Raven.
14. Ackermann, H.-W., L. Berthiaume, and M. Tremblay, *Viral pathogenesis in diagrams*. 2000, Boca Raton, FL: CRC Press.
15. Hutson, A.M., R.L. Atmar, and M.K. Estes, *Norovirus disease: changing epidemiology and host susceptibility factors.* Trends Microbiol, 2004. **12**(6): p. 279-87.
16. Adler, J.L. and R. Zickl, *Winter vomiting disease.* J Infect Dis, 1969. **119**(6): p. 668-73.
17. Scallan, E., et al., *Foodborne illness acquired in the United States--major pathogens.* Emerg Infect Dis, 2011. **17**(1): p. 7-15.
18. Hall, A.J., et al., *Norovirus disease in the United States.* Emerg Infect Dis, 2013. **19**(8): p. 1198-205.
19. Atmar, R.L., et al., *Determination of the 50% human infectious dose for Norwalk virus.* J Infect Dis, 2014. **209**(7): p. 1016-22.
20. Glass, R.I., U.D. Parashar, and M.K. Estes, *Norovirus gastroenteritis.* N Engl J Med, 2009. **361**(18): p. 1776-85.

21. Rhinehart, E., et al., *Frequency of outbreak investigations in US hospitals: results of a national survey of infection preventionists.* Am J Infect Control, 2012. **40**(1): p. 2-8.
22. Riddle, M.S., et al., *Epidemic infectious gastrointestinal illness aboard U.S. Navy ships deployed to the Middle East during peacetime operations--2000-2001.* BMC Gastroenterol, 2006. **6**: p. 9.
23. Vega, E., et al., *Genotypic and epidemiologic trends of norovirus outbreaks in the United States, 2009 to 2013.* J Clin Microbiol, 2014. **52**(1): p. 147-55.
24. Teunis, P.F., et al., *Norwalk virus: how infectious is it?* J Med Virol, 2008. **80**(8): p. 1468-76.
25. Rockx, B., et al., *Natural history of human calicivirus infection: a prospective cohort study.* Clin Infect Dis, 2002. **35**(3): p. 246-53.
26. Hutchinson, J., *The biology and evolution of HIV.* Annual Review of Anthropology, 2001. **30**: p. 85-108.
27. Younai, F.S., *Thirty years of the human immunodeficiency virus epidemic and beyond.* Int J Oral Sci, 2013. **5**(4): p. 191-9.
28. Levy, J.A., *Pathogenesis of human immunodeficiency virus infection.* Microbiol Rev, 1993. **57**(1): p. 183-289.
29. Joint United Nations Programme on HIV/AIDS., *UNAIDS World AIDS day report 2011*. 2011, Geneva: UNAIDS. 48 p.
30. Roldão, A., et al., *Virus-like particles in vaccine development.* Expert Rev Vaccines, 2010. **9**(10): p. 1149-76.
31. Garcea, R.L. and L. Gissmann, *Virus-like particles as vaccines and vessels for the delivery of small molecules.* Curr Opin Biotechnol, 2004. **15**(6): p. 513-7.
32. Ma, Y., R.J. Nolte, and J.J. Cornelissen, *Virus-based nanocarriers for drug delivery.* Adv Drug Deliv Rev, 2012. **64**(9): p. 811-25.
33. Wu, M., et al., *Delivery of antisense oligonucleotides to leukemia cells by RNA bacteriophage capsids.* Nanomedicine, 2005. **1**(1): p. 67-76.
34. Manchester, M. and P. Singh, *Virus-based nanoparticles (VNPs): platform technologies for diagnostic imaging.* Adv Drug Deliv Rev, 2006. **58**(14): p. 1505-22.
35. Control, C.f.D., *Recommendations of the immunization Practices Advisory Committee Update on Hapetitis B Prevention.* Morbid. Mortal. Week. Rep, 1987. **36**(23).
36. Girard, M., *The Pasteur Institute's contributions to the field of virology.* Annual Reviews in Microbiology, 1988. **42**: p. 745-763.
37. Proffitt, A., *First HEV vaccine approved.* Nature Biotechnology, 2012. **30**: p. 300.
38. Gregson, A.L., et al., *Phase I trial of an alhydrogel adjuvanted hepatitis B core virus-like particle containing epitopes of Plasmodium falciparum circumsporozoite protein.* PLoS One, 2008. **3**(2): p. e1556.
39. Printz, C., *FDA approves Gardasil 9 for more types of HPV.* Cancer, 2015. **121**(8): p. 1156-7.
40. Monie, A., et al., *Cervarix: a vaccine for the prevention of HPV 16, 18-associated cervical cancer.* Biologics, 2008. **2**(1): p. 97-105.
41. Ltd, C.P., *CPL Biologicals launches Cadiflu-S, World's first virus like particle (VLP) vaccine for seasonal influenza*. 2016: Ahmedabad.

42. Cox, M.M. and Y. Hashimoto, *A fast track influenza virus vaccine produced in insect cells.* J Invertebr Pathol, 2011. **107 Suppl**: p. S31-41.
43. Weber, J., et al., *Immunogenicity of the yeast recombinant p17/p24:Ty virus-like particles (p24-VLP) in healthy volunteers.* Vaccine, 1995. **13**(9): p. 831-4.
44. Bernstein, D.I., et al., *Safety and immunogenicity of a candidate parvovirus B19 vaccine.* Vaccine, 2011. **29**(43): p. 7357-63.
45. Ball, J.M., et al., *Recombinant Norwalk virus-like particles given orally to volunteers: phase I study.* Gastroenterology, 1999. **117**(1): p. 40-8.
46. Bernstein, D.I., et al., *Norovirus vaccine against experimental human GII.4 virus illness: a challenge study in healthy adults.* J Infect Dis, 2015. **211**(6): p. 870-8.
47. Tissot, A.C., et al., *Effect of immunisation against angiotensin II with CYT006-AngQb on ambulatory blood pressure: a double-blind, randomised, placebo-controlled phase IIa study.* Lancet, 2008. **371**(9615): p. 821-7.
48. Chackerian, B., *Virus-like particle based vaccines for Alzheimer disease.* Hum Vaccin, 2010. **6**(11): p. 926-30.
49. Chan, B.K., S.T. Abedon, and C. Loc-Carrillo, *Phage cocktails and the future of phage therapy.* Future Microbiol, 2013. **8**(6): p. 769-83.
50. Sulakvelidze, A., Z. Alavidze, and J.G. Morris, *Bacteriophage therapy.* Antimicrob Agents Chemother, 2001. **45**(3): p. 649-59.
51. Twort, F.W., *An investigation on the nature of ultra-microscopic viruses.* The Lancet, 1915. **186**(4814): p. 1241–1243.
52. D'Hérelle, F., *On an invisible microbe antagonistic to dysentery bacilli.* C.R. Acad. Sci. Paris, 1917. **165**: p. 373–375.
53. Hyman, P. and S.T. Abedon, *Bacteriophage host range and bacterial resistance.* Adv Appl Microbiol, 2010. **70**: p. 217-48.
54. Karimi, M., et al., *Bacteriophages and phage-inspired nanocarriers for targeted delivery of therapeutic cargos.* Adv Drug Deliv Rev, 2016. **106**(Pt A): p. 45-62.
55. Rasched, I. and E. Oberer, *Ff coliphages: structural and functional relationships.* Microbiol Rev, 1986. **50**(4): p. 401-27.
56. Ghosh, D., et al., *Refactored M13 bacteriophage as a platform for tumor cell imaging and drug delivery.* ACS Synth Biol, 2012. **1**(12): p. 576-582.
57. Scala, G., et al., *Selection of HIV-specific immunogenic epitopes by screening random peptide libraries with HIV-1-positive sera.* J Immunol, 1999. **162**(10): p. 6155-61.
58. Tanaka, K., et al., *A mimotope peptide of Aβ42 fibril-specific antibodies with Aβ42 fibrillation inhibitory activity induces anti-Aβ42 conformer antibody response by a displayed form on an M13 phage in mice.* J Neuroimmunol, 2011. **236**(1-2): p. 27-38.
59. VAN ROOYEN, C.E. and G.D. SCOTT, *Smallpox diagnosis with special reference to electron microscopy.* Can J Public Health, 1948. **39**(12): p. 467-77.
60. Nagler, F.P. and G. Rake, *The Use of the Electron Microscope in Diagnosis of Variola, Vaccinia, and Varicella.* J Bacteriol, 1948. **55**(1): p. 45-51.
61. Bozzola, J.J. and L.D. Russell, *Electron microscopy : principles and techniques for biologists*. [2nd ed.] ed. 1998, Boston: Jones and Bartlett.
62. Ruska, E. *Ernst Ruska - Biographical*. 1986 [cited 2018 23-04-2018].
63. Mescher, A.L., *Histology & Its Methods of Study*, in *Junqueira's Basic Histology: Text & Atlas*, McGraw-Hill, Editor. 2013: New York.

64. BRENNER, S. and R.W. HORNE, *A negative staining method for high resolution electron microscopy of viruses.* Biochim Biophys Acta, 1959. **34**: p. 103-10.
65. Hazelton, P.R. and H.R. Gelderblom, *Electron microscopy for rapid diagnosis of infectious agents in emergent situations.* Emerg Infect Dis, 2003. **9**(3): p. 294-303.
66. Van Regenmortel, M.H.V. and J. Burckard, *Detection of a wide spectrum of tobacco mosaic virus strains by indirect enzyme-linked immunosorbent assays (ELISA).* Virology, 1980. **106**(2): p. 327-334.
67. Voller, A., et al., *The Detection of Viruses by Enzyme-Linked Immunosorbent Assay (ELISA).* Journal of General Virology, 1976. **33**(1): p. 165.
68. Clark, M.F. and A.N. Adams, *Characteristics of the microplate method of enzyme-linked immunosorbent assay for the detection of plant viruses.* J Gen Virol, 1977. **34**(3): p. 475-83.
69. Boonham, N., et al., *Methods in virus diagnostics: from ELISA to next generation sequencing.* Virus Res, 2014. **186**: p. 20-31.
70. Scientific, T.F. *Overview of ELISA*. 27-04-2018].
71. Crowther, J.R., *The ELISA guidebook*. 2nd ed. ed. 2009, Totowa, N.J.: Humana ; [London : Springer, distributor].
72. Jiang, X., et al., *Detection of Norwalk virus in stool by polymerase chain reaction.* J Clin Microbiol, 1992. **30**(10): p. 2529-34.
73. Atmar, R.L., et al., *Detection of Norwalk virus and hepatitis A virus in shellfish tissues with the PCR.* Appl Environ Microbiol, 1995. **61**(8): p. 3014-8.
74. Wiedbrauk, D.L., *Molecular Methods for Virus Detection.* Laboratory Medicine, 1992. **23**(11): p. 737 - 742.
75. Mackay, I.M., K.E. Arden, and A. Nitsche, *Real-time PCR in virology.* Nucleic Acids Res, 2002. **30**(6): p. 1292-305.
76. Scientific, T.F. *PCR Cycling Parameters—Six Key Considerations for Success*. 26-04-2018].
77. Posthuma-Trumpie, G.A., J. Korf, and A. van Amerongen, *Lateral flow (immuno)assay: its strengths, weaknesses, opportunities and threats. A literature survey.* Anal Bioanal Chem, 2009. **393**(2): p. 569-82.
78. Al-Yousif, Y., et al., *Development, evaluation, and application of lateral-flow immunoassay (immunochromatography) for detection of rotavirus in bovine fecal samples.* Clin Diagn Lab Immunol, 2002. **9**(3): p. 723-5.
79. Kusano, N., et al., *Immunochromatographic assay for simple and rapid detection of Satsuma dwarf virus and related viruses using monoclonal antibodies.* Journal of General Plant Pathology, 2007. **73**(1): p. 66-71.
80. Danks, C. and I. Barker, *On-site detection of plant pathogens using lateral-flow devices*.* EPPO Bulletin, 2008. **30**(3-4): p. 421-426.
81. Hagström, A.E., et al., *Sensitive detection of norovirus using phage nanoparticle reporters in lateral-flow assay.* PLoS One, 2015. **10**(5): p. e0126571.
82. Vyas, K., et al., *Comparison of five commercially available immunochromatographic tests for the detection of norovirus in faecal specimens.* J Hosp Infect, 2015. **91**(2): p. 176-8.
83. Rohrman, B.A., et al., *A lateral flow assay for quantitative detection of amplified HIV-1 RNA.* PLoS One, 2012. **7**(9): p. e45611.

84. Zaytseva, N.V., et al., *Multi-analyte single-membrane biosensor for the serotype-specific detection of Dengue virus.* Anal Bioanal Chem, 2004. **380**(1): p. 46-53.
85. O'Farrell, B., *Evolution in lateral flow-based immunoassay systems*, in *Lateral Flow Immunoassay*, R. Wong and H. Tse, Editors. 2009, Humana Press: New York. p. 1-33.
86. Posthuma-Trumpie, G.A., et al., *Amorphous carbon nanoparticles: a versatile label for rapid diagnostic (immuno)assays.* Anal Bioanal Chem, 2012. **402**(2): p. 593-600.
87. Paterson, A.S., et al., *Persistent luminescence strontium aluminate nanoparticles as reporters in lateral flow assays.* Anal Chem, 2014. **86**(19): p. 9481-8.
88. Adhikari, M., et al., *Functionalized viral nanoparticles as ultrasensitive reporters in lateral-flow assays.* Analyst, 2013. **138**(19): p. 5584-7.
89. Adhikari, M., et al., *Aptamer-Phage Reporters for Ultrasensitive Lateral Flow Assays.* Anal Chem, 2015. **87**(23): p. 11660-5.
90. Liu, C., et al., *Lateral flow immunochromatographic assay for sensitive pesticide detection by using Fe3O4 nanoparticle aggregates as color reagents.* Anal Chem, 2011. **83**(17): p. 6778-84.
91. Tang, D., et al., *Magnetic nanogold microspheres-based lateral-flow immunodipstick for rapid detection of aflatoxin B2 in food.* Biosens Bioelectron, 2009. **25**(2): p. 514-8.
92. Granade, T.C., et al., *Rapid detection and differentiation of antibodies to HIV-1 and HIV-2 using multivalent antigens and magnetic immunochromatography testing.* Clin Vaccine Immunol, 2010. **17**(6): p. 1034-9.
93. Workman, S., et al., *Rapid detection of HIV-1 p24 antigen using magnetic immuno-chromatography (MICT).* J Virol Methods, 2009. **160**(1-2): p. 14-21.
94. Handali, S., et al., *Development and evaluation of a magnetic immunochromatographic test to detect Taenia solium, which causes taeniasis and neurocysticercosis in humans.* Clin Vaccine Immunol, 2010. **17**(4): p. 631-7.
95. Xu, Q., et al., *Development of lateral flow immunoassay system based on superparamagnetic nanbeads as labels for rapid quantitative detection of cardiac troponin I.* Materials Science and Engineering C, 2009. **29**: p. 702-707.
96. Taton, K., et al., *Lateral flow immunoassay using magnetoresistive sensors.* Journal of Magnetism and Magnetic Materials, 2009. **321**: p. 1679-1682.
97. Wang, D.B., et al., *Rapid detection of Bacillus anthracis spores using a super-paramagnetic lateral-flow immunological detection system.* Biosens Bioelectron, 2013. **42**: p. 661-7.
98. Wang, Y., et al., *Study of superparamagnetic nanoparticles as labels in the quantitative lateral flow immunoassay.* Materials Science and Engineering C, 2009. **29**: p. 714-718.
99. Marquina, C., et al., *GMR sensors and magnetic nanoparticles for immuno-chromatographic assays.* Journal of Magnetism and Magnetic Materials, 2012. **324**: p. 3495-3498.
100. Chang, G.J., et al., *An integrated target sequence and signal amplification assay, reverse transcriptase-PCR-enzyme-linked immunosorbent assay, to detect and characterize flaviviruses.* J Clin Microbiol, 1994. **32**(2): p. 477-83.

101. Munch, M., et al., *Detection and subtyping (H5 and H7) of avian type A influenza virus by reverse transcription-PCR and PCR-ELISA.* Arch Virol, 2001. **146**(1): p. 87-97.
102. Menzel, W., V. Zahn, and E. Maiss, *Multiplex RT-PCR-ELISA compared with bioassay for the detection of four apple viruses.* J Virol Methods, 2003. **110**(2): p. 153-7.
103. Whitby, J.E., et al., *Rapid detection of rabies and rabies-related viruses by RT-PCR and enzyme-linked immunosorbent assay.* J Virol Methods, 1997. **69**(1-2): p. 63-72.
104. Fronczek, C.F. and J.-Y. Yoon, *Detection of Foodborne Pathogens Using Biosensors*, in *Antimicrobial Food Packaging*, J. Barros-Velazquez, Editor. 2016, Elsevier Science. p. 153 - 166.
105. Yoon, J.Y. and B. Kim, *Lab-on-a-chip pathogen sensors for food safety.* Sensors (Basel), 2012. **12**(8): p. 10713-41.
106. Heinze, B.C., et al., *Microfluidic immunosensor for rapid and sensitive detection of bovine viral diarrhea virus.* Sensors and Actuators B: Chemical, 2009. **138**(2): p. 491-496.
107. Heinze, B.C., et al., *Microfluidic immunosensor with integrated liquid core waveguides for sensitive Mie scattering detection of avian influenza antigens in a real biological matrix.* Analytical and Bioanalytical Chemistry, 2010. **398**(6): p. 2693-2700.
108. Stone, H.A. and S. Kim, *Microfluidics: Basic issues, applications, and challenges.* AIChE Journal, 2004. **47**(6): p. 1250-1254.
109. Beebe, D.J., G.A. Mensing, and G.M. Walker, *Physics and Applications of Microfluidics in Biology.* Annual Review of Biomedical Engineering, 2002. **4**(1): p. 261-286.
110. Ymeti, A., et al., *Fast, ultrasensitive virus detection using a Young interferometer sensor.* Nano Lett, 2007. **7**(2): p. 394-7.
111. Zaytseva, N.V., et al., *Development of a microfluidic biosensor module for pathogen detection.* Lab Chip, 2005. **5**(8): p. 805-11.
112. Zhang, H., et al., *A microfluidic device with microbead array for sensitive virus detection and genotyping using quantum dots as fluorescence labels.* Biosens Bioelectron, 2010. **25**(11): p. 2402-7.
113. Li, Y., C. Zhang, and D. Xing, *Integrated microfluidic reverse transcription-polymerase chain reaction for rapid detection of food- or waterborne pathogenic rotavirus.* Analytical Biochemistry, 2011. **415**(2): p. 87-96.
114. Lien, K.-Y., et al., *Integrated reverse transcription polymerase chain reaction systems for virus detection.* Biosensors and Bioelectronics, 2007. **22**(8): p. 1739-1748.
115. Fritz, J., et al., *Translating biomolecular recognition into nanomechanics.* Science, 2000. **288**(5464): p. 316-8.
116. Wu, G., et al., *Origin of nanomechanical cantilever motion generated from biomolecular interactions.* Proc Natl Acad Sci U S A, 2001. **98**(4): p. 1560-4.
117. Ilic, B., et al., *Single cell detection with micromechanical oscillators.* Journal of Vacuum Science & Technology B: Microelectronics and Nanometer Structures Processing, Measurement, and Phenomena, 2001. **19**(6): p. 2825-2828.

118. Ilic, B., et al., *Mechanical resonant immunospecific biological detector.* Applied Physics Letters, 2000. **77**(3): p. 450-452.
119. Ilic , B., Y. Yang , and H.G. Craighead *Virus detection using nanoelectromechanical devices.* Applied Physics Letters, 2004. **85**(13): p. 2604 - 2606.
120. Gupta, A., D. Akin, and R. Bashir, *Single virus particle mass detection using microresonators with nanoscale thickness.* Applied Physics Letters, 2004. **84**(11): p. 1976-1978.
121. Oh, S., et al., *Magnetic Nanozyme-Linked Immunosorbent Assay for Ultrasensitive Influenza A Virus Detection.* ACS Appl Mater Interfaces, 2018.
122. Chen, H.W., et al., *Targeting and Enrichment of Viral Pathogen by Cell Membrane Cloaked Magnetic Nanoparticles for Enhanced Detection.* ACS Appl Mater Interfaces, 2017. **9**(46): p. 39953-39961.
123. Chen, Y., et al., *One-step detection of pathogens and viruses: combining magnetic relaxation switching and magnetic separation.* ACS Nano, 2015. **9**(3): p. 3184-91.
124. Algar, W.R., A.J. Tavares, and U.J. Krull, *Beyond labels: a review of the application of quantum dots as integrated components of assays, bioprobes, and biosensors utilizing optical transduction.* Anal Chim Acta, 2010. **673**(1): p. 1-25.
125. Hong, S. and C. Lee, *The Current Status and Future Outlook of Quantum Dot-Based Biosensors for Plant Virus Detection.* Plant Pathol J, 2018. **34**(2): p. 85-92.
126. Hermanson, G.T., *Bioconjugate techniques*. 2nd ed. ed. 2008, London: Academic.
127. Murray, C.B., C.R. Kagan, and M.G. Bawendi, *Synthesis and Characterization of Monodisperse Nanocrystals and Close-Packed Nanocrystal Assemblies.* Annual Review of Materials Science, 2000. **30**(1): p. 545-610.
128. Moghimi, S.M., et al., *Particulate systems for targeting of macrophages: basic and therapeutic concepts.* J Innate Immun, 2012. **4**(5-6): p. 509-28.
129. Adegoke, O., et al., *An ultrasensitive SiO2-encapsulated alloyed CdZnSeS quantum dot-molecular beacon nanobiosensor for norovirus.* Biosens Bioelectron, 2016. **86**: p. 135-142.
130. Shen, W. and Z. Gao, *Quantum dots and duplex-specific nuclease enabled ultrasensitive detection and serotyping of Dengue viruses in one step in a single tube.* Biosensors and Bioelectronics, 2015. **65**: p. 327-332.
131. Shamsipur, M., et al., *A highly sensitive quantum dots-DNA nanobiosensor based on fluorescence resonance energy transfer for rapid detection of nanomolar amounts of human papillomavirus 18.* J Pharm Biomed Anal, 2017. **136**: p. 140-147.
132. Shojaei, T.R., et al., *Detection of Citrus tristeza virus by using fluorescence resonance energy transfer-based biosensor.* Spectrochim Acta A Mol Biomol Spectrosc, 2016. **169**: p. 216-22.
133. Mashayekhi, F., et al., *Enhancing the lateral-flow immunoassay for viral detection using an aqueous two-phase micellar system.* Anal Bioanal Chem, 2010. **398**(7-8): p. 2955-61.
134. Doering, W.E., et al., *SERS as a Foundation for Nanoscale, Optically Detected Biological Labels.* Advanced Materials, 2007. **19**(20): p. 3100-3108.
135. Moskovits, M., *Surface-enhanced spectroscopy.* Reviews of Modern Physics, 1985. **57**(3): p. 783-826.

136. Wolf, M.W. and U. Reichl, *Downstream processing of cell culture-derived virus particles.* Expert Rev Vaccines, 2011. **10**(10): p. 1451-75.
137. Nestola, P., et al., *Improved virus purification processes for vaccines and gene therapy.* Biotechnol Bioeng, 2015. **112**(5): p. 843-57.
138. Segura, M.M., A. Kamen, and A. Garnier, *Downstream processing of oncoretroviral and lentiviral gene therapy vectors.* Biotechnol Adv, 2006. **24**(3): p. 321-37.
139. Peixoto, C., et al., *Downstream processing of triple layered rotavirus like particles.* J Biotechnol, 2007. **127**(3): p. 452-61.
140. Kalbfuss, B., et al., *Harvesting and concentration of human influenza A virus produced in serum-free mammalian cell culture for the production of vaccines.* Biotechnology and Bioengineering, 2006. **97**(1): p. 73-85.
141. Vicente, T., et al., *Purification of recombinant baculoviruses for gene therapy using membrane processes.* Gene Ther, 2009. **16**(6): p. 766-75.
142. Peixoto, C., et al., *Towards purification of adenoviral vectors based on membrane technology.* Biotechnology Progress, 2008. **24**(6): p. 1290-1296.
143. Bowles, N.E., et al., *A simple and efficient method for the concentration and purification of recombinant retrovirus for increased hepatocyte transduction in vivo.* Hum Gene Ther, 1996. **7**(14): p. 1735-42.
144. Neff, T., et al., *Efficient gene transfer to hematopoietic repopulating cells using concentrated RD114-pseudotype vectors produced by human packaging cells.* Mol Ther, 2004. **9**(2): p. 157-9.
145. Branston, S., et al., *Precipitation of filamentous bacteriophages for their selective recovery in primary purification.* Biotechnol Prog, 2012. **28**(1): p. 129-36.
146. Dong, D., et al., *A simple and rapid method to isolate purer M13 phage by isoelectric precipitation.* Appl Microbiol Biotechnol, 2013. **97**(18): p. 8023-9.
147. Ro, H.S., et al., *Isolation of a novel mycovirus OMIV in Pleurotus ostreatus and its detection using a triple antibody sandwich-ELISA.* J Virol Methods, 2006. **138**(1-2): p. 24-9.
148. Loa, C.C., et al., *Purification of turkey coronavirus by Sephacryl size-exclusion chromatography.* J Virol Methods, 2002. **104**(2): p. 187-94.
149. Goerke, A.R., et al., *Development of a novel adenovirus purification process utilizing selective precipitation of cellular DNA.* Biotechnol Bioeng, 2005. **91**(1): p. 12-21.
150. Kröber, T., et al., *DNA Depletion by Precipitation in the Purification of Cell Culture-Derived Influenza Vaccines.* Chemical Engineering & Technology, 2010. **33**(6): p. 941-959.
151. Rodrigues, T., et al., *Scaleable purification process for gene therapy retroviral vectors.* The Journal of Gene Medicine, 2007. **9**(4): p. 233-243.
152. Kotani, H., et al., *Improved methods of retroviral vector transduction and production for gene therapy.* Hum Gene Ther, 1994. **5**(1): p. 19-28.
153. Nayak, D.P., S. Lehmann, and U. Reichl, *Downstream processing of MDCK cell-derived equine influenza virus.* J Chromatogr B Analyt Technol Biomed Life Sci, 2005. **823**(2): p. 75-81.
154. Wickramasinghe, S.R., et al., *Tangential flow microfiltration and ultrafiltration for human influenza A virus concentration and purification.* Biotechnol Bioeng, 2005. **92**(2): p. 199-208.

155. Burova, E. and E. Ioffe, *Chromatographic purification of recombinant adenoviral and adeno-associated viral vectors: methods and implications.* Gene Ther, 2005. **12 Suppl 1**: p. S5-17.
156. Yamada, K., et al., *Adenovirus vector production using low-multiplicity infection of 293 cells.* Cytotechnology, 2009. **59**(3): p. 153-60.
157. Ali, A. and M.J. Roossinck, *Rapid and efficient purification of Cowpea chlorotic mottle virus by sucrose cushion ultracentrifugation.* J Virol Methods, 2007. **141**(1): p. 84-6.
158. Guo, J., et al., *Construction of the Vero cell culture system that can produce infectious HCV particles.* Mol Biol Rep, 2009. **36**(1): p. 111-20.
159. Segura, M.M., A. Garnier, and A. Kamen, *Purification and characterization of retrovirus vector particles by rate zonal ultracentrifugation.* J Virol Methods, 2006. **133**(1): p. 82-91.
160. Reiser, J., *Production and concentration of pseudotyped HIV-1-based gene transfer vectors.* Gene Therapy, 2000. **7**: p. 910.
161. Villegas, G.A., et al., *A rapid method to produce high yields of purified rotavirus particles.* J Virol Methods, 2002. **104**(1): p. 9-19.
162. Jungbauer, A. and R. Hahn, *Polymethacrylate monoliths for preparative and industrial separation of biomolecular assemblies.* J Chromatogr A, 2008. **1184**(1-2): p. 62-79.
163. Chahal, P.S., M.G. Aucoin, and A. Kamen, *Primary recovery and chromatographic purification of adeno-associated virus type 2 produced by baculovirus/insect cell system.* J Virol Methods, 2007. **139**(1): p. 61-70.
164. Konz, J.O., et al., *Development of a purification process for adenovirus: controlling virus aggregation to improve the clearance of host cell DNA.* Biotechnol Prog, 2005. **21**(2): p. 466-72.
165. Rodrigues, T., et al., *Screening anion-exchange chromatographic matrices for isolation of onco-retroviral vectors.* J Chromatogr B Analyt Technol Biomed Life Sci, 2006. **837**(1-2): p. 59-68.
166. Cameron-Smith, R. and C. Harbour, *Removal of poliovirus type 1 from a protein mixture using an immunoaffinity chromatography column.* Biomed Chromatogr, 2001. **15**(7): p. 471-83.
167. Chen, Z., et al., *Capture and release of viruses using amino-functionalized silica particles.* Analytica Chimica Acta, 2006. **569**(1): p. 76-82.
168. Monjezi, R., et al., *Purification of bacteriophage M13 by anion exchange chromatography.* J Chromatogr B Analyt Technol Biomed Life Sci, 2010. **878**(21): p. 1855-9.
169. Ceglarek, I., et al., *A novel approach for separating bacteriophages from other bacteriophages using affinity chromatography and phage display.* Sci Rep, 2013. **3**: p. 3220.
170. Jungbauer, A. and R. Hahn, *Monoliths for fast bioseparation and bioconversion and their applications in biotechnology.* J Sep Sci, 2004. **27**(10-11): p. 767-78.
171. Kramberger, P., et al., *Purification of the Staphylococcus aureus bacteriophages VDX-10 on methacrylate monoliths.* J Virol Methods, 2010. **166**(1-2): p. 60-4.
172. Adriaenssens, E.M., et al., *CIM(®) monolithic anion-exchange chromatography as a useful alternative to CsCl gradient purification of bacteriophage particles.* Virology, 2012. **434**(2): p. 265-70.

173. Oksanen, H.M., A. Domanska, and D.H. Bamford, *Monolithic ion exchange chromatographic methods for virus purification.* Virology, 2012. **434**(2): p. 271-7.
174. Banjac, M., et al., *Purification of Vero cell derived live replication deficient influenza A and B virus by ion exchange monolith chromatography.* Vaccine, 2014. **32**(21): p. 2487-2492.
175. Bandeira, V., et al., *Downstream processing of lentiviral vectors: releasing bottlenecks.* Hum Gene Ther Methods, 2012. **23**(4): p. 255-63.
176. Gerster, P., et al., *Purification of infective baculoviruses by monoliths.* J Chromatogr A, 2013. **1290**: p. 36-45.
177. Williams, S.L., M.E. Eccleston, and N.K. Slater, *Affinity capture of a biotinylated retrovirus on macroporous monolithic adsorbents: towards a rapid single-step purification process.* Biotechnol Bioeng, 2005. **89**(7): p. 783-7.
178. Fernandes, P., et al., *Bioprocess development for canine adenovirus type 2 vectors.* Gene Ther, 2013. **20**(4): p. 353-60.
179. Knudsen, H.L., et al., *Membrane ion-exchange chromatography for process-scale antibody purification.* Journal of Chromatography A, 2001. **907**(1): p. 145-154.
180. McNally, D.J., et al., *Optimised concentration and purification of retroviruses using membrane chromatography.* J Chromatogr A, 2014. **1340**: p. 24-32.
181. Wolff, M.W., et al., *Purification of cell culture-derived modified vaccinia ankara virus by pseudo-affinity membrane adsorbers and hydrophobic interaction chromatography.* Biotechnol Bioeng, 2010. **107**(2): p. 312-20.
182. Nestola, P., et al., *Impact of grafting on the design of new membrane adsorbers for adenovirus purification.* J Biotechnol, 2014. **181**: p. 1-11.
183. Kalbfuss, B., et al., *Purification of cell culture-derived human influenza A virus by size-exclusion and anion-exchange chromatography.* Biotechnol Bioeng, 2007. **96**(5): p. 932-44.
184. Eglon, M.N., et al., *Purification of adenoviral vectors by combined anion exchange and gel filtration chromatography.* J Gene Med, 2009. **11**(11): p. 978-89.
185. Thomassen, Y.E., et al., *Scale-down of the inactivated polio vaccine production process.* Biotechnol Bioeng, 2013. **110**(5): p. 1354-65.
186. Lee, D.S., B.M. Kim, and D.W. Seol, *Improved purification of recombinant adenoviral vector by metal affinity membrane chromatography.* Biochem Biophys Res Commun, 2009. **378**(3): p. 640-4.
187. Nitsche, A., et al., *One-step selection of Vaccinia virus-binding DNA aptamers by MonoLEX.* BMC Biotechnol, 2007. **7**: p. 48.
188. Baek, J.O., et al., *Production and purification of human papillomavirus type 33 L1 virus-like particles from Spodoptera frugiperda 9 cells using two-step column chromatography.* Protein Expr Purif, 2011. **75**(2): p. 211-7.
189. Kuiper, M., et al., *Purification of a functional gene therapy vector derived from Moloney murine leukaemia virus using membrane filtration and ceramic hydroxyapatite chromatography.* Biotechnol Bioeng, 2002. **80**(4): p. 445-53.
190. Asenjo, J.A. and B.A. Andrews, *Aqueous two-phase systems for protein separation: phase separation and applications.* J Chromatogr A, 2012. **1238**: p. 1-10.

191. Guo, P., et al., *Rapid and simplified purification of recombinant adeno-associated virus.* J Virol Methods, 2012. **183**(2): p. 139-46.
192. Negrete, A., T.C. Ling, and A. Lyddiatt, *Production of adenoviral vectors and its recovery.* Process Biochemistry, 2007. **42**(7): p. 1107-1113.
193. González-Mora, A., et al., *Recovery and Primary purification of Bacteriophage M13 Using Aqueous Two-Phase Systems.* Journal of ChemicalTechnology and Biotechnology, 2017.
194. Negrete, A., T.C. Ling, and A. Lyddiatt, *Aqueous two-phase recovery of bio-nanoparticles: a miniaturization study for the recovery of bacteriophage T4.* J Chromatogr B Analyt Technol Biomed Life Sci, 2007. **854**(1-2): p. 13-9.
195. Benavides, J., et al., *Rotavirus-like particles primary recovery from insect cells in aqueous two-phase systems.* J Chromatogr B Analyt Technol Biomed Life Sci, 2006. **842**(1): p. 48-57.
196. Luechau, F., T.C. Ling, and A. Lyddiatt, *Recovery of B19 virus-like particles by aqueous two-phase systems.* Food and Bioproducts Processing, 2011. **89**(4): p. 322-327.
197. Hammar, L., et al., *Concentration and purification of feline leukaemia virus (FeLV) and its outer envelope protein gp70 by aqueous two-phase systems.* J Virol Methods, 1989. **24**(1-2): p. 91-101.
198. Rito-Palomares, M. and A.P.J. Middelberg, *Aqueous two-phase systems for the recovery of a recombinant viral coat protein from Escherichia coli.* Journal of Chemical Technology and Biotechnology, 2002. **77**(9): p. 1025-1029.
199. Grzenia, D.L., J.O. Carlson, and S.R. Wickramasinghe, *Tangential flow filtration for virus purification.* Journal of Membrane Science, 2008. **321**(2): p. 373-380.
200. Grzenia, D.L., S.R. Wickramasinghe, and J.O. Carlson, *Ultrafiltration of Parvovirus.* Separation Science and Technology, 2007. **42**(11): p. 2387-2403.
201. Hensgen, M.I., et al., *Purification of Minute Virus of Mice using high performance tangential flow filtration.* Desalination, 2010. **250**(3): p. 1121-1124.
202. van Reis, R., et al., *High-performance tangential flow filtration using charged membranes.* Journal of Membrane Science, 1999. **159**(1): p. 133-142.
203. van Reis, R. and A. Zydney, *Bioprocess membrane technology.* Journal of Membrane Science, 2007. **297**(1): p. 16-50.
204. Lee, J., et al., *Principles and applications of steric exclusion chromatography.* J Chromatogr A, 2012. **1270**: p. 162-70.
205. Gagnon, P. *Steric Exclusion Chromatography*. 2013 [cited 2018 02/08/2018].
206. Marichal-Gallardo, P., et al., *Steric exclusion chromatography for purification of cell culture-derived influenza A virus using regenerated cellulose membranes and polyethylene glycol.* J Chromatogr A, 2017. **1483**: p. 110-119.
207. D'Souza, R.N., et al., *Emerging technologies for the integration and intensification of downstream bioprocesses.* Pharmaceutical Bioprocessing, 2013. **1**(5): p. 423 - 440.
208. Peixoto, C., et al., *Purification of adenoviral vectors using expanded bed chromatography.* J Virol Methods, 2006. **132**(1-2): p. 121-6.
209. Ling, T.C., et al., *Purification of filamentous bacteriophage M13 by expanded bed anion exchange chromatography.* J Microbiol, 2004. **42**(3): p. 228-32.

210. Arpanaei, A., et al., *Critical evaluation and comparison of fluid distribution systems for industrial scale expanded bed adsorption chromatography columns.* J Chromatogr A, 2008. **1198-1199**: p. 131-9.
211. Xia, H.-F., D.-Q. Lin, and S.-J. Yao, *Chromatographic performance of macroporous cellulose–tungsten carbide composite beads as anion-exchanger for expanded bed adsorption at high fluid velocity.* Journal of Chromatography A, 2008. **1195**(1): p. 60-66.
212. Blom, H., et al., *Efficient chromatographic reduction of ovalbumin for egg-based influenza virus purification.* Vaccine, 2014. **32**(30): p. 3721-4.
213. Scientific, S. *FluAlert A&B*. 2013 [cited 2018 11/08/2018].
214. Corporation, Q. *QuickVue Influenza A+B Test*. [cited 2018 11/08/2018].
215. Corporation, Q., *'QuickVue Influenza A+B Test' procedure card*, Q. Corporation, Editor., Quidel Corporation. p. 1.
216. Care, M.H., *'3M™ Rapid Detection Flu A+B Test' brochure*, M.H. Care, Editor. 2009, 3M Health Care. p. 1 - 16.
217. OraSure Technologies, I., *First and Only In-Home Rapid Oral HIV Test Now Available to Consumers Across the U.S.*, in *A Major Breakthrough in the Fight Against HIV – the OraQuick® In-Home HIV Test Now Can Be Purchased at Retailers Nationwide and Online*. 2012, OraSure Technologies, Inc.
218. OraSure Technologies, I. *Where to Buy*. 2016 [cited 2018 11/08/2018].
219. OraSure Technologies, I. *How Oral Testing Works*. 2016 [cited 2018 11/08/2018].
220. Alere, *Alere Determine™ HIV-1/2 Ag/Ab Combo*, Alere, Editor. 2017, Alere. p. 1 - 2.
221. Geginat, G., D. Kaiser, and S. Schrempf, *Evaluation of third-generation ELISA and a rapid immunochromatographic assay for the detection of norovirus infection in fecal samples from inpatients of a German tertiary care hospital.* Eur J Clin Microbiol Infect Dis, 2012. **31**(5): p. 733-7.
222. Ambert-Balay, K. and P. Pothier, *Evaluation of 4 immunochromatographic tests for rapid detection of norovirus in faecal samples.* J Clin Virol, 2013. **56**(3): p. 194-8.
223. Théry, L., et al., *Evaluation of immunochromatographic tests for the rapid detection of the emerging GII.17 norovirus in stool samples, January 2016.* Euro Surveill, 2016. **21**(4).
224. Bruggink, L.D., et al., *Evaluation of the RIDA(®)QUICK immunochromatographic norovirus detection assay using specimens from Australian gastroenteritis incidents.* J Virol Methods, 2011. **173**(1): p. 121-6.
225. Battaglioli, G., et al., *Evaluation of the RIDAQuick norovirus immunochromatographic test kit.* J Clin Virol, 2012. **53**(3): p. 262-4.
226. AG, R.-B. *RIDA®QUICK Norovirus*. [cited 2018 11/08/2018].
227. Park, K.S., et al., *Evaluation of a new immunochromatographic assay kit for the rapid detection of norovirus in fecal specimens.* Ann Lab Med, 2012. **32**(1): p. 79-81.
228. Kim, H.S., et al., *Evaluation of the SD Bioline Norovirus rapid immunochromatography test using fecal specimens from Korean gastroenteritis patients.* J Virol Methods, 2012. **186**(1-2): p. 94-8.
229. Abbott. *SD BIOLINE Norovirus*. 2018 [cited 2018 11/08/2018].

230. van Wezel, A.L., et al., *Inactivated poliovirus vaccine: current production methods and new developments.* Rev Infect Dis, 1984. **6 Suppl 2**: p. S335-40.
231. Montagnon, B.J., B. Fanget, and J.C. Vincent-Falquet, *Industrial-scale production of inactivated poliovirus vaccine prepared by culture of Vero cells on microcarrier.* Rev Infect Dis, 1984. **6 Suppl 2**: p. S341-4.
232. Prevention, C.f.D.C.a. *How Influenza (Flu) Vaccines Are Made*. 2018 [cited 2018 27/08/2018].
233. Robinson, J.M., *An Alternative to the Scale-up and Distribution of Pandemic Influenza Vaccine.* BioPharm International, 2009. **2009**(1): p. 4.
234. Kon, T.C., et al., *Influenza Vaccine Manufacturing: Effect of Inactivation, Splitting and Site of Manufacturing. Comparison of Influenza Vaccine Production Processes.* PLoS One, 2016. **11**(3): p. e0150700.
235. Shoji, Y., et al., *Plant-based rapid production of recombinant subunit hemagglutinin vaccines targeting H1N1 and H5N1 influenza.* Hum Vaccin, 2011. **7 Suppl**: p. 41-50.
236. Shanklin, T., et al., *Selection of bioprocess simulation software for industrial applications.* Biotechnol Bioeng, 2001. **72**(4): p. 483-9.
237. Chuan, Y.P., et al., *The economics of virus-like particle and capsomere vaccines.* Biochemical Engineering Journal, 2014. **90**: p. 255-263.
238. Kalbfuss, B., et al., *Size-exclusion chromatography as a linear transfer system: purification of human influenza virus as an example.* J Chromatogr B Analyt Technol Biomed Life Sci, 2008. **873**(1): p. 102-12.
239. Vicente, T., et al., *Impact of ligand density on the optimization of ion-exchange membrane chromatography for viral vector purification.* Biotechnol Bioeng, 2011. **108**(6): p. 1347-59.
240. Nestola, P., et al., *Adenovirus purification by two-column, size-exclusion, simulated countercurrent chromatography.* J Chromatogr A, 2014. **1347**: p. 111-21.

CHAPTER II – Viral purification case study I: Optimization and Miniaturization of Aqueous Two-Phase Systems for the Purification of Recombinant Human Immunodeficiency Virus-Like Particles from a CHO Cell Supernatant

Abstract Virus-like particles (VLPs) are promising candidates for a new generation of biopharmaceuticals, with a high impact in gene therapy, vaccination and also in the construction of delivery vehicles. Despite the growing interest in these particles, their production is currently limited by the low capacities and throughputs of classical downstream processing technologies. In this work, aqueous two-phase extraction (ATPE) conditions for the purification of a HIV VLP were screened and optimized in mL scale batch conditions. PEG–salt (potassium phosphate, ammonium sulfate and trisodium citrate) and polymer–polymer (PEG–dextran) systems were investigated, among which the PEG–ammonium sulfate system demonstrated the higher partition coefficient (K = 4.4). This parameter was then compared with the obtained in a continuous microfluidic setting, performed by flowing both immiscible phases through a 100 width × 20 μm wide microchannel. The batch optimization results showed good agreement with the continuous miniaturized extraction, both in terms of K (K = 3.9 in microfluidic scale) and protein purity. These novel findings show that PEG–ammonium sulfate ATPE is a promising system for primary HIV-VLP recovery and demonstrate the potential of a miniaturized ATPE for massive parallelization (scale-out) at the preparative scale or integrated in analytical miniaturized systems.

Keywords: Virus-like particles, Downstream processing, Aqueous two-phase extraction, PEG–ammonium sulfate, Microfluidics

This chapter has been published as: Jacinto, M.J., Soares, R.R.G., Azevedo, A.M., Chu, V., Tover, A., Conde, J.P. and Aires-Barros, M.R., Optimization and miniaturization of aqueous two phase systems for the purification of recombinant human immunodeficiency virus-like particles from a CHO cell supernatant, Separation and Purification Technology, 2015, 154, 27-35

II.1. Introduction

VLPs are macromolecular structures resulting from the expression of viral proteins which spontaneously reassemble into the viral form without the nucleic acid content [1]. These particles cannot self-replicate, and thus they may serve as potential immunogens for vaccination. Furthermore, the structural proteins of VLPs are repetitive and present a high density display of epitopes leading to stronger and more effective immune responses [2]. VLPs can also be used as gene or biomolecule delivery tools [3]. However, there are still barriers to achieving high recovery efficiencies and maintaining the product quality after the downstream processing. The separation techniques currently used for purification of VLPs take advantage of the relatively large size of the particles and are based on gradient ultracentrifugation, ultrafiltration, precipitation or SEC [4]. However, all these methods share general drawbacks and are in general labor-intensive, time-consuming and not easily amenable to scaling-up [5]. In particular, sucrose and cesium chloride density-gradient ultracentrifugation provided low yields, retained impurities and is very difficult to implement at an industrial scale [6, 7]; precipitation with PEG, ammonium sulfate or calcium phosphate has a low selectivity towards VLPs [5, 8]; and traditional membrane-based tangential flow filtration techniques, such as ultrafiltration and microfiltration, suffer from membrane fouling issues and the retention and co-concentration of large molecular weight contaminants [5, 9].

ATPS are a promising alternative to address these challenges. ATPSs are formed when two immiscible compounds, such as two polymers or a polymer and a salt are mixed in an aqueous solution above a certain critical concentration, and spontaneously separate into two immiscible phases. These systems provide a biocompatible environment since they have a high water content, low interfacial tensions and some polymers also have a protein stabilizing effect [10], resulting in an efficient separation without denaturation or loss of biological activity. These systems have already been successfully applied to the separation of proteins from cell debris or to the purification of a target bioproduct from a crude feedstock [11, 12], including antibodies [12], viruses [13], intact cells [14], VLPs [15, 16], inclusion bodies [17], and plasmid DNA (pDNA) [18].

The separation effect arises from the differences in the physicochemical properties of the immiscible phases. Different solutes may have different affinities for the top and bottom phases. This behavior is often evaluated by the partition coefficient (*K*), defined in Equation 1.

$$K = \frac{C_T}{C_B} \qquad \text{Equation 1}$$

C_T and C_B are the equilibrium concentrations of the solute in the top and bottom phases, respectively.

The partition coefficient of a certain solute in ATPS depends on multiple factors either extrinsic to the target molecule such as (i) polymer molecular weights/size, (ii) concentration of the phase forming components, (iii) ionic strength, (iv) pH or (v) the use of an additional salt, such as NaCl, reported to promote the salting out effect of the desired protein to the top phase [19, 20] or intrinsic to the target molecule, such as the (vi) size of the target molecule, its (vii) hydrophobicity or its (viii) isoelectric point, which is related to the global charge at a given pH.

The purification of VLPs using ATPS was first reported in 1989 for the concentration and purification of the outer envelope protein gp70 of the feline leukemia virus and the gag protein p27 using dextran-sulfate and polyvinyl alcohol, and where the two proteins were more than 40-fold purified [21]. Also, the bovine leukemia virus outer envelope protein gp51 achieved 15-fold purification in the system bottom phase using a dextran-PEG system [22]. The infectivity titer in an dextran-PEG aqueous two-phase extraction (ATPE) of HIV-1 was retained in the interphase to about 48%, as measured by infectivity [23]. More recently, intracellular and extracellular double-layered rotavirus-like particles from insect cell culture were separated using PEG-phosphate systems with an overall recovery of 85% and a purity increase of 30–55 times comparing to the initial medium has also been described [15]. An initial extraction of a recombinant viral coat protein from cytoplasm of *E. coli* using PEG-phosphate system with a ln $K > 2.5$ [24], and an initial extraction step of B19 particles to the bottom phase of PEG 1000 – magnesium sulfate system with a yield around 90%, while removing cell debris and 31% of total protein to the system's top phase, interface and sediment [16], were also described.

Miniaturized techniques taking advantage of soft-lithography processes and microfluidics have recently emerged as effective tools for expediting bioprocess design in ATPE [25]. These miniaturized processes are based on a number of parallel streams of immiscible phases flowing in continuous in a microchannel under a laminar flow regime. They are cost-effective since a large number of variables can be evaluated in parallel, reducing the sample/reagent volumes required, and promote lab-scale process similar to the continuous large-scale processes. Such technique has been applied to the purification of biomolecules such as monoclonal antibodies [26], bovine serum albumin [27], membrane proteins from crude cell extract [28], and recombinant proteins from a cell lysate [29]. The main advantages of this design are (i) the possibility of adjusting the length and width of the separation channel in order to speed up the corresponding purification and separation process by decreasing diffusion times; (ii) the simple operation; (iii) the very low amount of required reagents, of the order of 1-100 µL; and (iv) the absence of major manual preparation steps [25].

The goal of this study is to perform the screening and optimization of ATPE conditions for the extraction and purification of a Human Immunodeficiency Virus (HIV) VLP produced in Chinese Hamster Ovary (CHO) cell cultures with a covalent bond to a green fluorescence protein (GFP) tag (HIV-GFP VLP) using different polymer-salt and polymer-polymer ATPS and to compare the obtained partition and purity results to a miniaturized continuous microfluidic approach.

II.2. Materials and methods

a. Chemicals and biologicals

PEG with molecular weights of 1 000, 1 500, 2 000, 3 350, 6 000, 8 000, 10 000 and 20 000 Da, dextran with molecular weights of 40 000, 100 000, 162 000, 298 000 and 500 000 Da, potassium phosphate monobasic anhydrous, potassium phosphate dibasic anhydrous, sodium phosphate monobasic anhydrous, sodium chloride (NaCl), ammonium sulfate, citric acid, trisodium citrate dehydrate, glycine and propylene glycol monomethyl ether acetate (PGMEA) 99.5% were purchased from Sigma-Aldrich. SU-8 negative photoresist 2015 formulation was purchased from Microchem. Polydimethylsiloxane (PDMS) was purchased from Dow-Corning (Midland, MI, USA) as a Sylgard 184 silicon elastomer kit.

CHO cell medium supernatant expressing HIV–GFP VLP (pH 7.6) was formulated and provided by Icosagen® (Tartumaa, Estonia). The culture medium comprised a mixture of CDCHO and 293SFM Life Technologies commercial serum-free mediums, supplemented with GlutaMAX™.

b. ATPS preparation in batch conditions

Stock solutions of PEG 50% (w/w), dextran 25% (w/w), potassium phosphate, ammonium sulfate and trisodium citrate 40% (w/w) were prepared using ultrapure water, obtained from a MilliQ purification system from Millipore (Billerica, MA, USA). ATPS were prepared by weighting the appropriated mass amounts of the phase forming components (PEG, dextran and salt stock solutions), sodium chloride, supernatant sample and MilliQ water to a total final system mass of 1.5 g, in order to achieve the desired final mass fractions of each component (% w/w).

The components concentrations in the system final composition were screened in order to optimize the partition coefficient for HIV-GFP VLPs: between 8 and 29 % (w/w) for PEG, 14 to 16.5 % (w/w) for dextran, 10 to 14 % (w/w) for potassium phosphate, 12.5 to 14.5 % (w/w) for ammonium sulfate, 12 to 15 % (w/w) for trisodium citrate, 0 to 6 % for sodium chloride, and between 15 and 30% (w/w) for CHO supernatant containing HIV-GFP VLPs.

All system components were thoroughly mixed in a vortex mixer (Ika, Staufen, Germany) and centrifuged at 4000 g for 5 min at room temperature in a fixed angle rotor centrifuge (Eppendorf, Hamburg, Germany), assuring total phase separation. The volumes of top and bottom phases were measured and samples from both phases were taken for protein analysis and/or fluorescence measurements.

c. Microchannel fabrication

The microfluidic device was fabricated using standard soft lithography methodologies similar to those used by Soares and co-workers [30]. In summary, the microchannel was designed in AutoCAD 2013 software. The pattern was transferred to a hard mask by the photolithographic patterning and subsequent wet chemical etching of a 200 nm aluminum film deposited on a glass substrate using a Nordiko 7000 magnetron sputtering system. SU-8 2015 negative photoresist was spin-coated onto a clean silicon substrate to a final average thickness of 20 µm. The hard mask was placed over the SU-8 after 4 min of pre-exposure bake at 95°C on a hotplate, and exposed to UV light. After exposure, a post-exposure bake at 95°C for 5 min was performed. The SU-8 was developed by submerging the substrate in PGMEA for 2 min and subsequently rinsing with isopropanol. The substrate was then subjected to a final hard bake step at 150°C for 15 min. PDMS, previously mixed at a ratio of 1:10 parts reticulating agent and degassed in a vacuum chamber, was poured over the SU-8 mold and left to reticulate in an oven at 70°C for 75-90 minutes. PDMS membranes (500-1000 µm thick) were prepared by pouring PDMS over a silicon wafer and prepared under the same conditions as the PDMS structures. The structure was peeled off from the mold and holes were punched with a blunt 20-ga needle (Instech Solomon, Plymouth Meeting, PA, USA) through the inlets and outlets of the structure. To seal the channels, a PDMS membrane and the PDMS device containing the microfluidic structures were oxidized using a hand-held corona discharge device for 60 seconds, keeping a distance of about 0.5 cm between the device and the surfaces to be treated. After oxidation, the membrane was placed over the channel side of the PDMS and the structure was baked on hot plate at 130°C for 5 minutes. The sealed channels were left undisturbed for at least 24 hours before usage.

d. Liquid handling in microfluidics

The two aqueous immiscible solutions (the PEG-rich phase and salt- or dextran-rich phase, depending on the system) were pumped using syringe pumps (New Era Pump Systems, Inc., NE-300 model) and flowed continuously through a microfluidic structure with two inlets and three outlets. The inlet channels were 50 µm wide and 20 µm high (W x H) and converged on a main channel with W = 100 µm. Polyethylene tubing (BTPE-90) was acquired from Instech Solomon and 1 mL syringes were purchased from CODAN (Lensahn, Germany).

According to the description in section 'II.2.b.', each optimized ATPS was first prepared in microtubes at the desired final polymer and salt concentrations, using MilliQ water instead of the HIV-GFP VLP supernatant loading mass (henceforth called blank system). For example, for the '20% PEG 3 350 – 14% Potassium phosphate pH 8 – 20% Loading' system, it was weighted 0.6 g of PEG 3 350 50% (w/w) (to obtain 20% of 1.5 g in PEG 3350), 0.525 g of potassium phosphate 40% (w/w) (14% of 1.5 g in potassium phosphate) and 0.375 g of MilliQ water (1.5 – 0.6 – 0.525 g = 0.375 g added to achieve a final system weight of 1.5 g). The phases of the blank system were allowed to separate and optimized amount of supernatant loading mass for each assay was then added to the blank bottom phase. For the given example, 0.2 g of CHO supernatant was mixed with 0.8 g of blank system's bottom phase (20% loading). All optimized systems were prepared according to this method. Both phases were further loaded in each of the two inlets of the microfluidic structure. It is important to highlight that removing a certain mass fraction of water in the batch system composition in order to compensate the further medium supernatant loading in the system bottom phase did not reveal as a viable alternative to match the optimized conditions at batch scale. The significantly higher concentration of both phase forming compounds would induce precipitation at the optimized loading concentration in batch conditions.

The microchannel was monitored using a Leica (Solms, Germany) DMLM fluorescence microscope coupled to a digital camera (DFC300FX). A band pass filter for excitation between 450 and 490 nm and long pass emission above 515 nm was used to monitor the HIV-GFP VLP partition experiments in real time (henceforth referred to as blue filter). The fluorescence values were measured with ImageJ software from the National

Institutes of Health (Bethesda, MD, USA) and averaged after subtracting the background value.

e. Analytical Methods

i. Protein Gel Electrophoresis, SDS-PAGE

Samples were diluted in Bio-Rad (Hercules, CA, USA) 4x loading buffer (277.8 mM Tris-HCl, pH 6.8, 4.4% LDS, 44.4% (w/v) glycerol, 0.02% bromophenol blue) and denatured in reducing conditions with 100 mM dithiothreitol at 100ºC for 5-10 min. Samples were applied in a gradient 4-20% acrylamide gel purchased from Bio-Rad and run at 90 mV for 1.5 hours using a running buffer containing 192 mM glycine, 25 mM Tris and 0.1% SDS, pH 8.3. Each gel was loaded with a Precision Plus Protein Dual-color standard from Bio-Rad. Gels were stained with Coomassie Brilliant Blue R-250 (Pharmacia, Uppsala, Sweden) for 1 hour. Gels were then destained by immersion in 30% (v/v) ethanol and 10% (v/v) acetic acid for 1.5 hours. Silver staining was performed whenever higher sensitivity was required using a Bio-Rad silver staining kit. Images were acquired with a GS-800 calibrated densitometer from Bio-Rad.

ii. Fluorimetric measurement

For the quantification of the HIV-GFP VLPs present in cell culture supernatant and in both phases in the batch ATPE optimization, the GFP fluorescence was measured with an excitation wavelength of 485 nm and emission of 506 nm on a Varian (Palo Alto, CA, USA) Cary Eclipse plate reader spectrofluorimeter. The excitation and emission slits were set at 5 nm. The readings were averaged from five consecutive readings with a 0.5 s interval in white polystyrene Corning® (Corning, NY, USA) 96 well plates.

iii. Nanoparticle Tracking Analysis (NTA)

NTA measurements were performed with a NanoSight LM10-HS (NanoSight, Amesbury, United Kingdom). The NTA 2.0 Build 127 software was used for film capturing and analyzing the samples. The samples were filmed for 60 s with manual shutter and gain adjustments in order to follow particle movement velocity in the sample. Using the properties of both light scattering and Brownian motion, the software used the Stokes-Einstein equation to calculate particles size distribution. The mean, mode and standard deviation of particle size, as well as correlation between particle size and its light scattered intensity is also provided by the software. The samples were injected into the

sample chamber with sterile syringes until the liquid reached the chamber outlet. Five measurements were performed for each sample. For each measurement, a new sample was added to the chamber. All measurements were performed at room temperature.

II.3. Results and Discussion

a. Optimization of HIV-GFP VLPs partition in batch ATPE conditions

The partition behavior of HIV-GFP VLPs was first evaluated at the mL scale by studying the influence of several parameters on their partitioning in ATPS: molecular weight of polymers (MW), tie-line length (TLL – directly related to the concentration of the phase forming components in the system), pH, sample load and the addition of a neutral salt. These parameters were evaluated for PEG-potassium phosphate, PEG-trisodium citrate, PEG-ammonium sulfate and PEG-dextran ATPSs. For each ATPS, the separation could be evaluated via simple fluorescence measurements since the Gag protein of these VLPs is covalently attached to GFP. Gag protein is a precursor of several structural proteins in the HIV VLP structure, as matrix and capsid. Since a VLP doesn't present any genomic information, these HIV VLPs don't present capsid structure, leading to an excess of Gag entrapped inside the VLP structure. The fluorescence intensity was directly proportional to the concentration of the VLPs, within the tested concentration range (Figure SII-1), which allowed us to calculate the K values as the ratio of the absolute fluorescence intensities between each phases, as performed in previous ATPE studies using GFP [30, 31].

After optimizing the partition coefficient for HIV-GFP VLPs for each of the ATPSs described above (Supplementary information, Figure SII-2to 5), the conditions that maximize the K values were extrapolated and are summarized on Table II-1. It is also important to highlight that due to the high salt and polymer concentrations, supernatant loading values higher than 20% (w/w) lead to precipitation effects. The NaCl concentrations are not specified on Table II-1 since it was observed that salt addition resulted in no significant improvements on HIV-GFP VLP extraction, for any of the systems tested.

*Table II-1 - **HIV-GFP VLPs partition in optimized PEG-potassium phosphate, PEG-dextran, PEG-trisodium citrate and PEG-ammonium sulfate**. The fluorescence of the initial sample was 54.6 AU. For all K calculations, the fluorescence value of the culture medium (8.0 AU) was subtracted from the fluorescence values of each ATPS phase, in order to eliminate any non-specific (not related with the HIV-GFP VLPs) fluorescence from the culture media.*

ATPS Composition	**Fluorescence (AU)**		***K***
	Top Phase	**Bottom Phase**	
20% PEG 3 350 – 14% Potassium phosphate pH 8 – 20% Loading	42.7	21.4	2.6
9% PEG 1 500 – 15% Dextran 100 000 – 20% Loading (pH 7)	28.7	39.8	0.7
27.5% PEG 1 500 – 15% Trisodium citrate pH 7.5 – 20% Loading	38.0	18.3	2.9
29% PEG 1 500 – 14,5% Ammonium sulfate – 15% Loading (pH 7.7)	41.4	15.7	4.4

The obtained partition results show that polymer-salt systems provide a significantly higher selectivity for the polymer rich phase highlighted by the higher K values, which contrasts with the results obtained for the PEG-dextran polymer-polymer system which provides a very low selectivity with a K closer to unity. Interestingly, in the latter polymer-polymer system the partition behavior of the VLPs seems to be mostly independent of the five tested parameters (TLL, PEG MW, Dextran MW, Loading percentage and NaCl concentration) providing K values concentrated in a narrow range between 0.5 and 0.8 (Supplementary information Figure SII-3). In contrast, for all polymer-salt systems tested there is a clear positive effect on the K values due to an increase in both the pH and the TLL of the system (Supplementary information Figure SII-2, Figure SII-4 and Figure SII-5). The observed correlation of an increasing TLL inducing an increase in the measured partition coefficients is widely reported in the literature and is due to the increasing differences in the chemical properties of each phase with an increase in the TLL [32]. On the other hand, the effect of the pH may be related with the increasingly negative charge of the HIV VLP provided by the major surface protein gp120 (isoelectric point of 6.8 [33]) in the pH range of 7-8. Thus, an increase in the negative charge may induce a progressively stronger exclusion from the phosphate, citrate or sulfate anion rich bottom phases.

Comparing all the polymer-salt systems tested it was also observed that the PEG-ammonium sulfate system was the one that provided more pronounced K values. This can be justified by the stronger salting out effect provided by sulfate anions in comparison to phosphate or citrate anions according to the Hoffmeister series. Therefore, the PEG-ammonium sulfate system was chosen as the most promising system for further testing due to the relatively high K of 4.4 (Table II-1).

b. Evaluation of HIV-GFP VLP structural integrity after partition in a PEG-ammonium sulfate ATPS

A nanoparticle tracking analysis (NTA) Nanosight technique was used to detect and measure the distribution of particle sizes and respective concentrations in the initial supernatant and both phases of the optimized PEG-ammonium sulfate ATPS after partition.

To perform the measurements of size distribution mean, mode and standard deviation of particle size and correspondent relative intensity distribution (Figure II-1), it was necessary to use a sample with 10^7 to 10^9 particles/mL, in order to allow the software (NTA 2.0 Build 127 from Malvern Instruments) to provide significant data above the background, which corresponds to a 100x dilution of the supernatant [34]. Since the ATPE provides different particle concentration in the top and bottom phases, the degree of dilution was different for each sample.

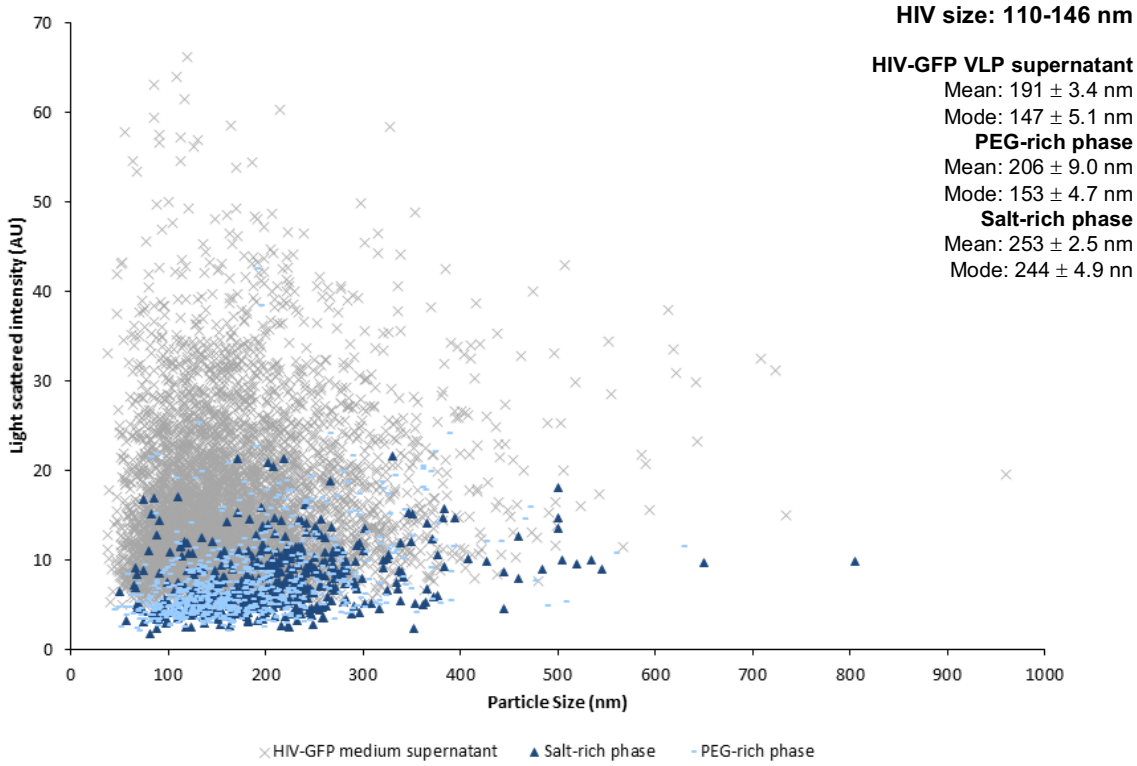

Figure II-1 - ***Correlation between particle size and light scattered intensity for HIV-GFP VLPs before and after ATPE in PEG-ammonium sulfate system****. HIV-GFP VLP supernatant with a dilution of 1:100; PEG-ammonium sulfate PEG-rich phase with a dilution of 1:20; PEG-ammonium sulfate salt-rich phase with a dilution of 1:10.*

Based on the analysis provided by the NTA Nanosight it is possible to obtain the mode, and thus, the particle size (or size range) most commonly found in each sample analysis. The presence of particles of a wide range of sizes was expected since the culture medium may contain cell debris and protein aggregates, in addition to the recombinant HIV-GFP VLPs (Figure II-1). The result obtained for the cell culture medium supernatant was 147 ± 5.1 nm for particle size mode, which is in accordance with the size estimated for HIV, ranging between 110 and 146 nm [35]. A similar value was obtained as mode in the ATPS PEG-rich phase 153 ± 4.7 nm, indicating that this result is in accordance with the results obtained in the previous section 'II.3.a.' showing that the HIV-GFP VLPs partition mainly to the PEG-rich phase. The results also suggest, given the similar mode in the supernatant and the PEG-rich phase that the VLPs are able to maintain their structural integrity and self-assembly properties after separation. In the salt-rich phase the particle size mode is 244 ± 4.9 nm (Figure II-1) which suggests that the larger particles i.e. cell debris and protein aggregates partitioned mainly to the salt-rich phase.

c. Evaluation of HIV-GFP VLP partition in a continuous microfluidic ATPE

Aiming at establishing a comparison between a batch and a miniaturized continuous approach to evaluate the ATPE of VLPs, a simple microchannel design, with two inlets, a main separation channel and three outlets was designed and fabricated using PDMS soft lithography (Figure II-2). Since the flow regime in microfluidics is laminar, this approach allows for both solutions to flow parallel to each other [25] along the 22 cm long separation channel. The small dimensions provide very fast diffusion times across the 100 µm channel width and a continuous partition under laminar flow conditions, which can be monitored on-line under a fluorescence microscope with negligible photo bleaching effects as the solution was being continuously renewed (liquid residence time of at most 0.5 s under the focal point of the objective).

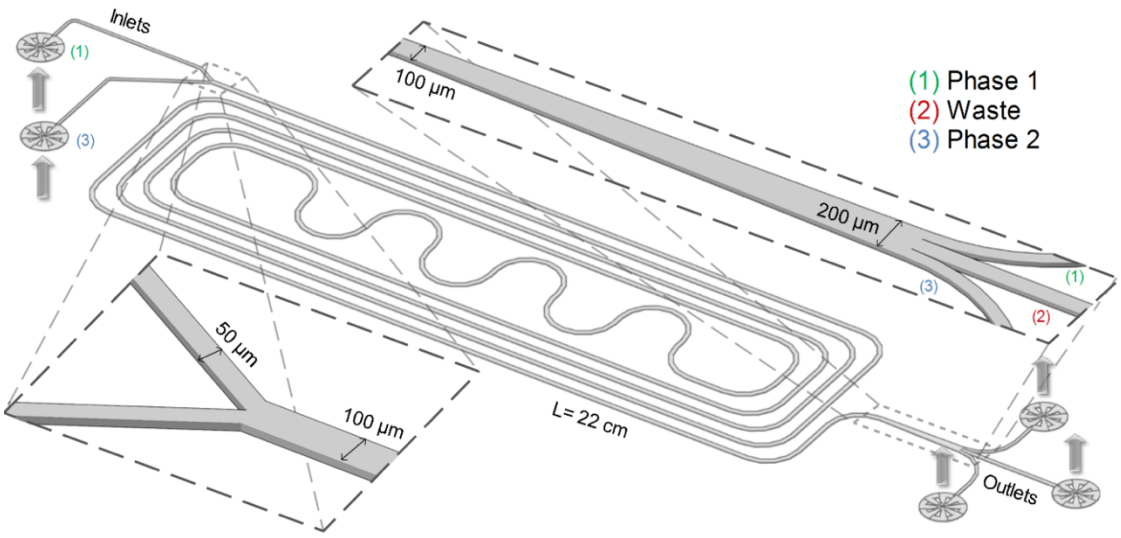

*Figure II-2 - **Schematics of the microchannel used for the miniaturized ATPE experiments**. The height of the microchannel is 20 µm throughout the entire structure. The whole structure presented 4 cm of length and 3 cm wide.*

In order to miniaturize the optimized batch systems, the optimal compositions for each system previously tested (section a; Table II-1) were also evaluated in a continuous flow microfluidic device in order to establish a comparison between the K values obtained using both separation conditions. Flow-rates of 0.1 µL/min for the PEG-rich phase and 1 µL/min for the salt-rich phase were used for the PEG-potassium phosphate system; 1

µL/min for both PEG-dextran phases; 0.5 µL/min for PEG-rich phase and 0.8 µL/min for the salt-rich phase for the PEG-trisodium citrate system; and 0.3 µL/min for the PEG-rich phase and 1 µL/min for the salt-rich phase for the PEG-ammonium sulfate system. These flow rate values were optimized in order to obtain a stable interface between both immiscible phases throughout the entire length of the separation channel.

The diffusion profile for VLP partition along the microchannel using the optimized PEG-trisodium citrate system is shown in Figure II-3. Multiple images were acquired under the fluorescence microscope at increasing lengths (L) in order to monitor the partition of the GFP labeled VLPs across the channel. It was possible to observe that while the HIV-GFP VLPs are mostly concentrated in the salt rich phase in the beginning of the separation channel, after 11 cm the VLPs have already partitioned mostly to the polymer-rich phase. In the second half of the channel, from 11 to 22 cm, only a slight change in the profile could be observed. Analyzing the slope of fluorescence intensity profile at the interface after the full length of the separation channel (L = 22 cm in Figure II-3), a K value of 2.7 was obtained by dividing the maximum fluorescence emission intensity obtained for the PEG-rich phase (blue circle in Figure II-3) by the minimum fluorescence emission intensity obtained for the salt-rich phase (orange circle in Figure II-3). This result is comparable to that obtained in the batch extraction at mL scale. The noise observed in the profile on each side of the interface is related with VLP adsorption and/or aggregation on the walls of the microchannel taking in account the highly hydrophobic nature of PDMS and its high tendency to non-specifically adsorb biomolecules.

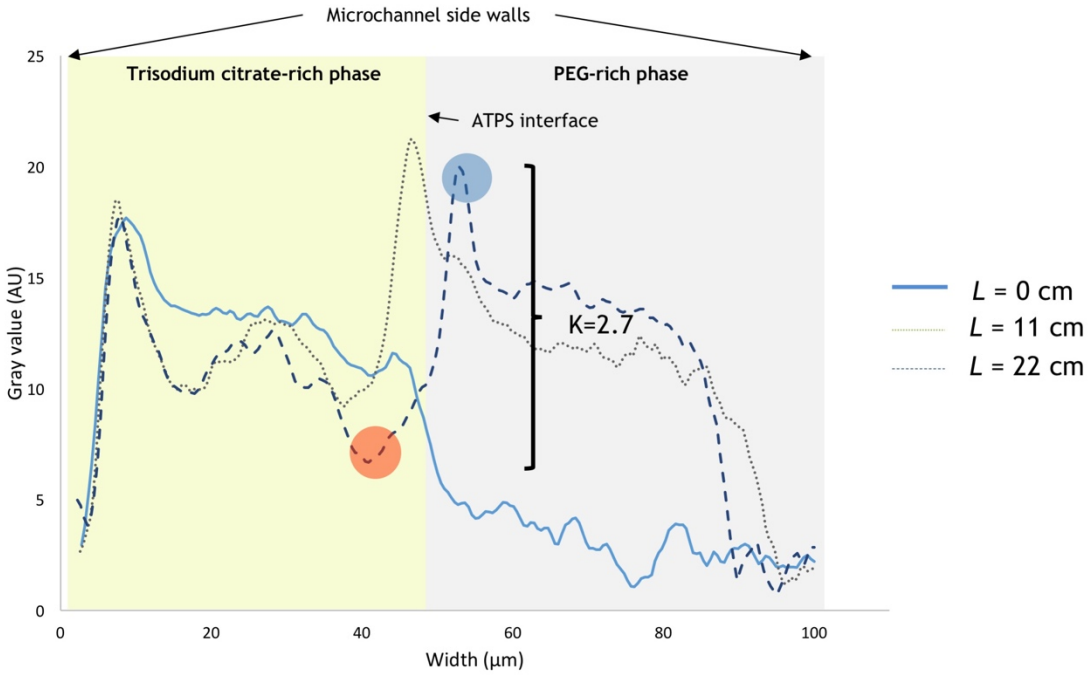

Figure II-3 - ***Fluorescence intensity profile across the width of the microchannel at L=0 (solid profile), L=11 (dashed profile) and L=22 cm (dotted profile) from the inlet during VLPs extraction in the optimized PEG-trisodium citrate system at mL scale****. The represented profiles correspond to a fit using a 7-point moving average. The blue and orange circles highlight the maximum and minimum fluorescence intensity values used to calculate the K value.*

Figure II- 4 shows images acquired at the entrance and exit of the separation channel, in order to evaluate and compare the partition behavior and K values obtained for each of the systems optimized at batch scale. It is possible to visualize in some of the images the adsorption/ aggregation effect on the walls of the microchannel reported above.

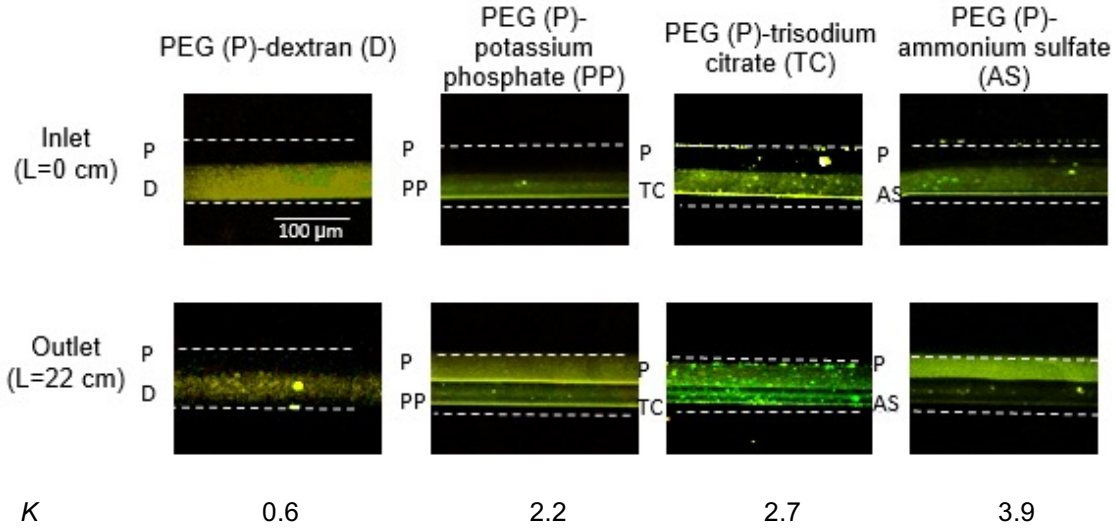

Figure II- 4 - ***HIV-GFP VLP partition in microfluidics for the system compositions optimized in batch conditions****. Fluorescence images of the microchannel inlet (top images) and outlet (bottom images). The dextran- and salt-rich phase containing HIV-GFP VLP was introduced through the bottom inlet and the PEG-rich phase was introduced through the top inlets. A flow rate of 0.1 µL/min for the PEG-rich phase and 1 µL/min for the salt-rich phase for the PEG-potassium phosphate system; 1 µL/min for both PEG-dextran phases; 0.5 µL/min for PEG-rich phase and 0.8 µL/min for the salt-rich phase for the PEG-trisodium citrate system; and 0.3 µL/min for the PEG-rich phase and 1 µL/min for the salt-rich phase for the PEG-ammonium sulfate system were used. The microchannel boundaries are indicated with a dashed white line. The loading concentrations used were the same as shown in Table II-1. The acquired fluorescence images were contrast enhanced for visualization purposes*

Overall, a good agreement between the batch and continuous miniaturized approaches was obtained in the K values. The slight decrease in K observed for all systems in the miniaturized extraction as compared to the batch extraction is expected and is related to the lower concentration of both phase forming compounds in the final system. This lower concentration arises from the selected approach of adding the supernatant loading to the bottom phase of the blank system with the final composition optimized in mL scale, which results in a lowering of the TLL. Thus, it is important to highlight that in this approach to a continuous miniaturized VLP partition, the phase separation of the immiscible phases is performed beforehand and the partition of the target analyte is achieved only by diffusion between the bottom and the PEG-rich phase interface, in contrast with a full microdroplet dispersion achieved by convection in batch mode of operation. Such intrinsic differences provide a challenge towards potential applications such as the high throughput screening of partition conditions.

d. Evaluation of HIV-GFP VLP purity after a continuous microfluidic ATPE processing

In order to evaluate and compare total protein extraction and VLP purity in both batch and miniaturized continuous extraction platforms, the system with the most promising partition results, PEG-ammonium sulfate, was selected. To perform this analysis, both phases from the batch and miniaturized ATPE were first collected after full partition of the proteins in the cell supernatant. In the miniaturized approach, a three-outlet rather than a two-outlet structure [27, 29] was used to collect each phase simultaneously with negligible inter-phase contamination, as shown in Figure II-5. Furthermore, it was observed that the interface position was stable for 75 minutes during which 20 µL of each ATPS phase were collected. Although this technique works with volumes of the order of µL, which is a great advantage when discussing integration in analytical systems, this poses as a drawback at the preparative scale as it is necessary to maintain a stable interface for a considerable length of channel (of the order of cm, which corresponds to a transit time in the order of minutes) in a diffusion-limited system in order to extract an appropriate volume for analysis ≈ 100 µL. Furthermore, it is important to highlight that while a major disadvantage of this design is the pronounced loss of VLP-enriched PEG-rich phase through the middle outlet, the purpose of this experiment was to evaluate the purity of the top phase against the purity of the bottom phase, and not to optimize the recovery yields. Recovery yields are expected to be significantly improved with a more sophisticated design of the microfluidic system.

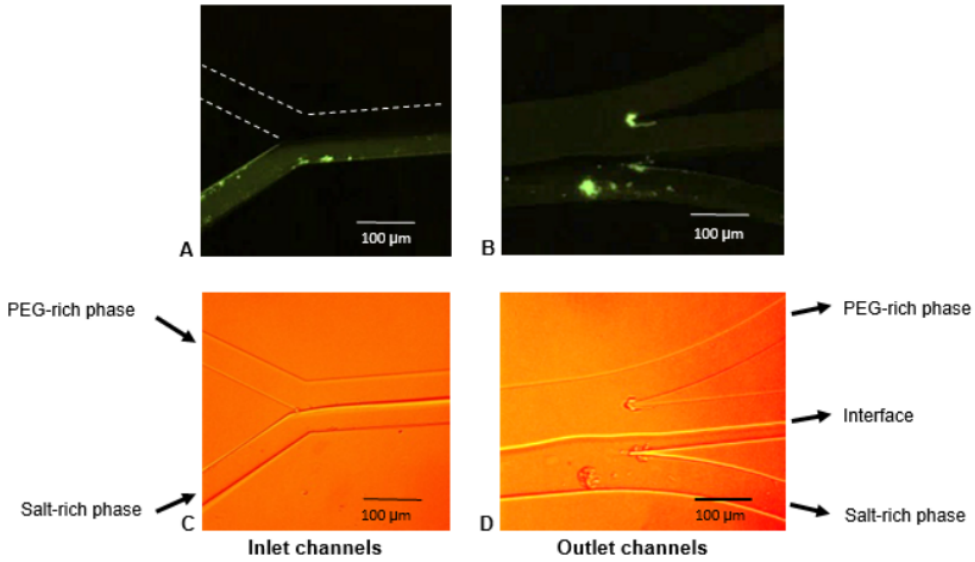

Figure II-5 - ***Miniaturized HIV-GFP VLP partition in a PEG-ammonium sulfate system****. The salt-rich phase containing HIV-GFP VLP was introduced through the bottom inlet with a volumetric pumping rate of 1 µL/min and the PEG-rich phase was introduced through the top inlets with a volumetric pumping rate of 0.3 µL/min. A) Image acquired near the entrance of the separation channel under the blue excitation fluorescence filter; B) Image acquired near the end of the separation channel under the blue excitation fluorescence filter; C) Image acquired near the entrance of the separation channel under bright field illumination; D) Image acquired near the end of the separation channel under bright field illumination. The microchannel boundaries are indicated with a dashed white line.*

After collecting both top PEG-rich and bottom salt-rich phases in the batch and miniaturized approaches to ATPE, a SDS-PAGE was performed in order to evaluate the degree of protein purity (Figure II-6).

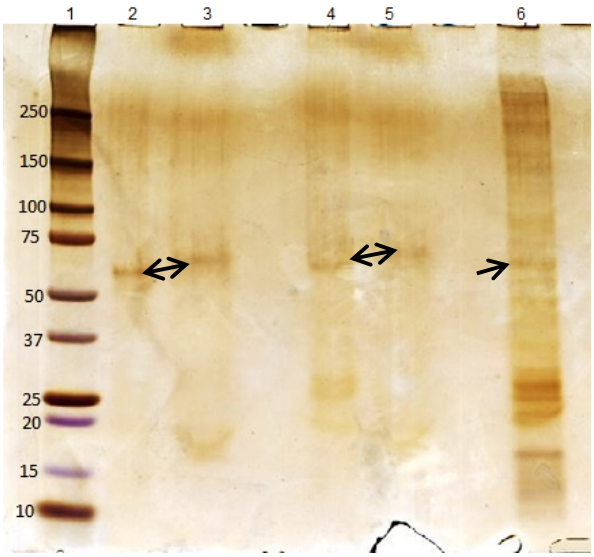

Figure II-6 - ***Silver stained SDS-PAGE of top and bottom phases of the PEG-ammonium sulfate systems in mL scale and miniaturized conditions****. Lanes ID: 1: Precision Plus ProteinTM Dual Color Standards (kDa); 2: PEG-ammonium sulfate PEG-rich phase collected from the microfluidic ATPE; 3: PEG-ammonium sulfate salt-rich phase collected from the microfluidic ATPE; 4: PEG-ammonium sulfate PEG-rich phase collected from a batch ATPE; 5: PEG-ammonium sulfate salt-rich phase collected from a batch ATPE; 6: CHO culture medium expressing HIV-GFP VLP. HIV Gag protein: 55.6 kDa (indicated by the solid black arrow)*

It can be observed in Figure II-6 that in both batch and continuous miniaturized approaches, similar protein profiles were obtained, thus validating the latter methodology as an effective purification methodology. Interestingly, when the ATPE is performed in batch conditions, the PEG-rich phase seems to have more putative impurities, located mainly in the 20-30 kDa range, than the miniaturized approach, wherein these particular impurities do not appear in any of the SDS-PAGE lanes. This observation may be justified by the loss of impurities by adsorption to the hydrophobic PDMS walls as an increased loss of proteins due to precipitation at the interface in the microfluidic approach is not likely to occur due to the relatively lower TLL. Nevertheless, although a full partition of HIV-GFP VLPs to the PEG-rich phase was not obtained, inherent to the partition coefficient of ≈ 4 obtained with this system, overall, a similar partition coefficients and pronounced removal of impurities can be observed when comparing both PEG-rich phases and the initial cell culture supernatant. It is still important to highlight that since Icosagen® use retroviral HIV Gag protein for formation of VLPs, this protein was used as indication of the VLP partition (Figure II-6, black arrows). The Gag protein is an important polyprotein precursor for HIV structural proteins and in this work recombinant HIV VLPs were produced with Gag protein of covalently attached to GFP to follow its partition in each ATPS. It is also important to refer that the SDS-PAGE analysis might lead to some unfounded conclusions based only on the identification of the Gag55 protein band since the presence of some putative free Gag-GFP doesn't necessarily reflect the HIV VLP partition. Still, since the partition coefficient obtained were also reflected in the structural integrity preservation checked by nanoparticle tracking analysis, it might be concluded that free Gag-GFP isn't a significant effect that would mislead the partition results.

II.4. Conclusions

This work described for the first time the optimization of a batch scale ATPE for HIV-GFP VLP primary partial purification directly from a CHO cell supernatant. The miniaturization of the optimized systems was also demonstrated by flowing the immiscible phases in parallel through a microfluidic channel and performing a continuous extraction. The continuous microfluidic ATPE was validated for preparative sample purification by obtaining comparable results of K and purity to classical batch extraction studies.

Good purities and partition coefficients (K = 4.4) were obtained using a PEG-ammonium sulfate system for direct processing of a CHO cell supernatant. This primary processing can then be integrated with further HIV-GFP VLP concentration and purification steps such as an ATPE multi-stage extraction [36], ATPE back extraction or other methodologies such as PEG precipitation [37] or anion exchange chromatography [38]. These results highlight ATPE in general as a promising technique to improve the effectiveness of VLP downstream processing, potentially providing a response to the increasing demand for high product titers. Furthermore, the results obtained in the miniaturized system highlight a good correlation between batch and continuous modes of operation in terms of K values and purity. Such conclusion validates the system towards scale out in a preparative scale and highlights a potential application in miniaturized analytical systems [39].

II.5. Supplementary information

a. Evaluation of HIV-GFP VLP dilution effect on fluorescence intensity

In order to evaluate the dilution effect on the HIV-GFP VLP fluorescence measures, it was measured the fluorescence intensity for different HIV-GFP VLP supernatant percentages (Figure SII-1). It was confirmed that on the tested concentration range the fluorescence intensity is directly proportional to the concentration of the VLP, and thus, it is a good assumption that the partition coefficient (*K)* values can be calculated as the ratio of the absolute fluorescence intensities between each of the immiscible phases.

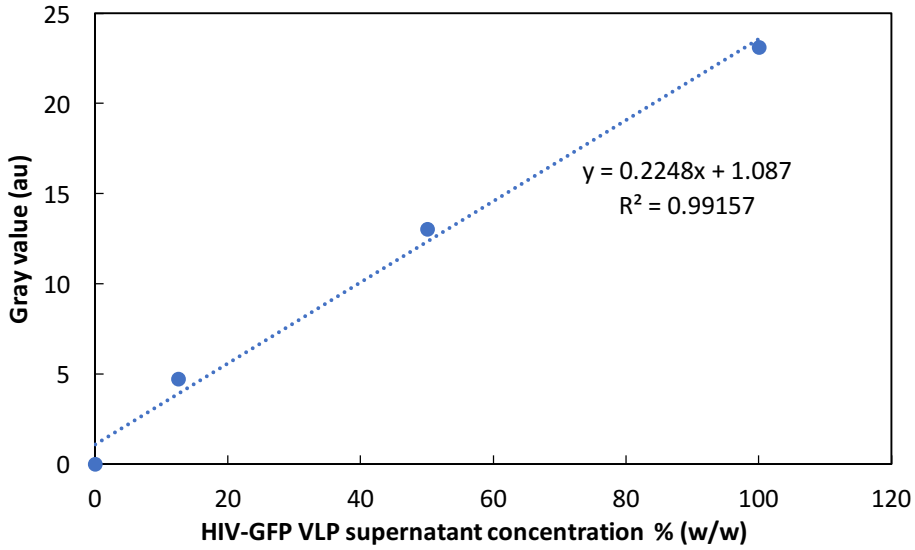

Figure SII-1 - HIV-GFP VLP supernatant dilution effect on fluorescence intensity. Tendency line described as: Fluorescence intensity = 0.2248 x Sample concentration + 1.087 (r2 = 0.9916)

b. HIV-GFP VLP partition evaluation in macroscale ATPE

In order to perform the optimization of ATPE in batch conditions for the partition of HIV-GFP VLPs, an initial system composition was selected and the influence of each parameter over the K was evaluated by fixing all system conditions except each one of the parameters under analysis [40]. The parameters under analysis were the pH, polymer molecular weight (MW), the TLL, loading concentration and neutral salt concentration.

For the purpose of simplifying the optimization procedure, as most binodal curves of the systems under study were not already published in the literature, the TLL values were approximated as “distance to the origin % (w/w)” values, which reasonably reflect the effect of increasing the TLL without the need to quantify the exact composition of each phase since the slope of the tie line (STL) is often within a range of 1 to 3 units.

i. PEG-potassium phosphate

The starting conditions were 20% PEG, 14% potassium phosphate pH 8, 20% sample loading. The parameters were tested in the following order: PEG MW, TLL, pH, sample load and the addition of sodium chloride (Figure SII-2). PEG 3 350 was first selected. Then, multiple TLL values were tested by using the following compositions: 15% PEG, 10% potassium phosphate (18.03% distance to the origin), 16% PEG, 11% potassium phosphate (19.4%), 18.5% PEG, 13% potassium phosphate (22.6%) and 20% PEG, 14% potassium phosphate (24.4%). A composition of 20% PEG and 14% potassium phosphate showed the best result, with the K being directly proportional to the TLL increase. The pH showed a similar trend, in which pH 8 provided the best result. The mass fraction of sample (loading) applied to the system showed a maximum at 25% (w/w) and precipitation was observed for higher sample load values. Likewise, the addition of sodium chloride promoted precipitation in the PEG-rich phase and it was not considered. The performed analysis lead to a final selected system with PEG 3 350 20% - 14% potassium phosphate pH 8 – 25% loading.

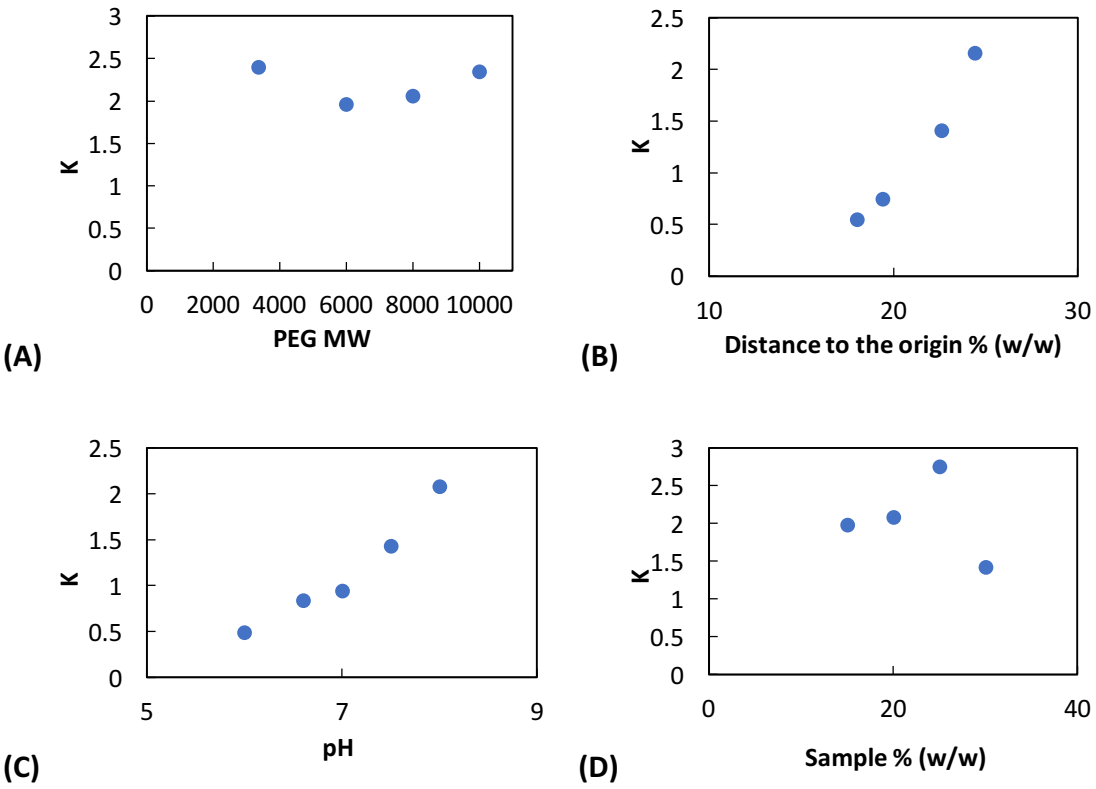

*Figure SII-2 - **PEG- potassium phosphate system optimization**: PEG MW (A), TLL (B), pH (C) and sample load in the system.*

ii. PEG-dextran

A composition of 9% PEG, 12% dextran 40 000, 20% sample loading was first selected. The parameters were tested in the following order: PEG MW, dextran MW, TLL, sample load and the addition of sodium chloride (Figure SII-3). For PEG MWs higher than 3 350 precipitation was found to occur in the PEG-rich phase; since PEG 1 500 and PEG 2 000 presented the same K value, PEG 1 500 was chosen due to its lower MW and viscosity. Dextran MWs of 40 000, 100 000, 162 000, 298 000 and 500 000 were tested. Dextran 100 000 was selected due to the very high viscosity of higher molecular weights, making it unpractical to handle using syringe needles. Multiple TLL values were tested by using the following compositions: 8% PEG, 14% dextran (distance to the origin 16.1%); 9% PEG, 15% dextran (17.5%); 9.5% PEG, 16 dextran (18.6%); and 10% PEG, 16.5% dextran (19.3%). 9% PEG 1500 and 15% dextran 100 000 resulted in the best K value. On sample load analysis, 20% was chosen as it was the higher concentration without observable precipitation effects. NaCl addition didn't lead to an increase on partition coefficient, thus, the final selected ATPS composition was 9% PEG 1 500 – 15% Dextran 100 000 – 20% Loading.

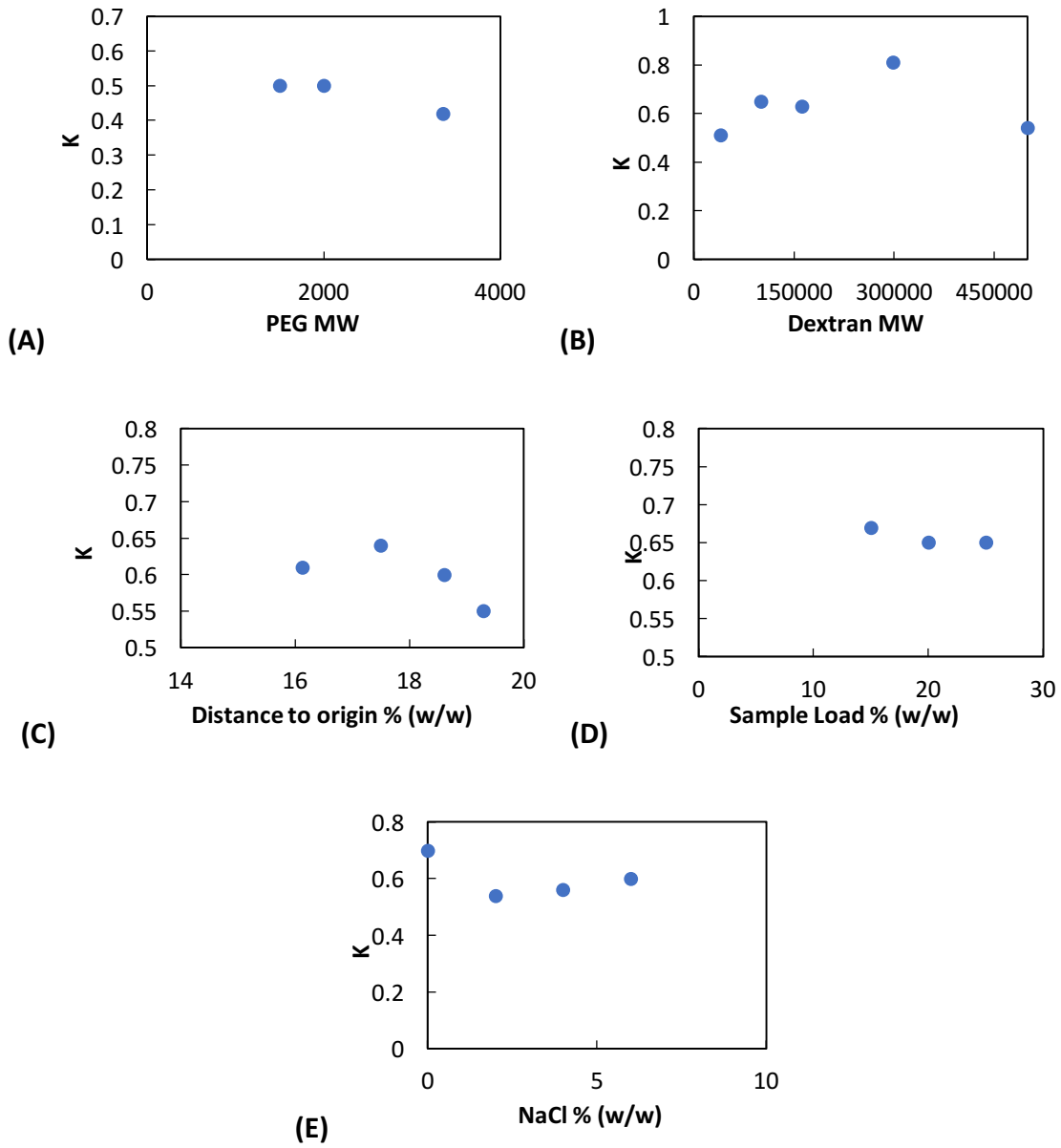

*Figure SII-3 - **PEG-dextran system optimization**: PEG MW (A), dextran MW (B), TLL (C), sample loading (D) and sodium chloride load in the system (E)*

iii. PEG-trisodium citrate

A composition of 22% PEG, 12% trisodium citrate pH 8 and 20% loading was first selected. The parameters were tested in the following order: PEG MW, TLL, pH and addition of sodium chloride (Figure SII-4). This system promoted undesired precipitation for higher sample loading percentages than 20%, and thus the influence of higher sample loading were not analyzed on a fluorescence partition coefficient basis. PEG molecular weights of 1 500, 3 350, 6 000, 8 000 and 10 000 Da were tested and PEG 1 500 was chosen for providing a higher K. Multiple TLL values were tested by using the following compositions: 22% PEG, 12% trisodium citrate (25.06% (w/w) distance to the origin), 24% PEG, 13% trisodium citrate (27.29%), 26% PEG, 14% trisodium citrate (29.53%) and 27.5% PEG, 15% trisodium citrate (31.32%). After optimizing the TLL, which also was also shown to provide a direct proportionality with the K, and the pH, the final selected system composition was 27.5% PEG 1 500, 15% trisodium citrate pH 7.5 and 20% loading.

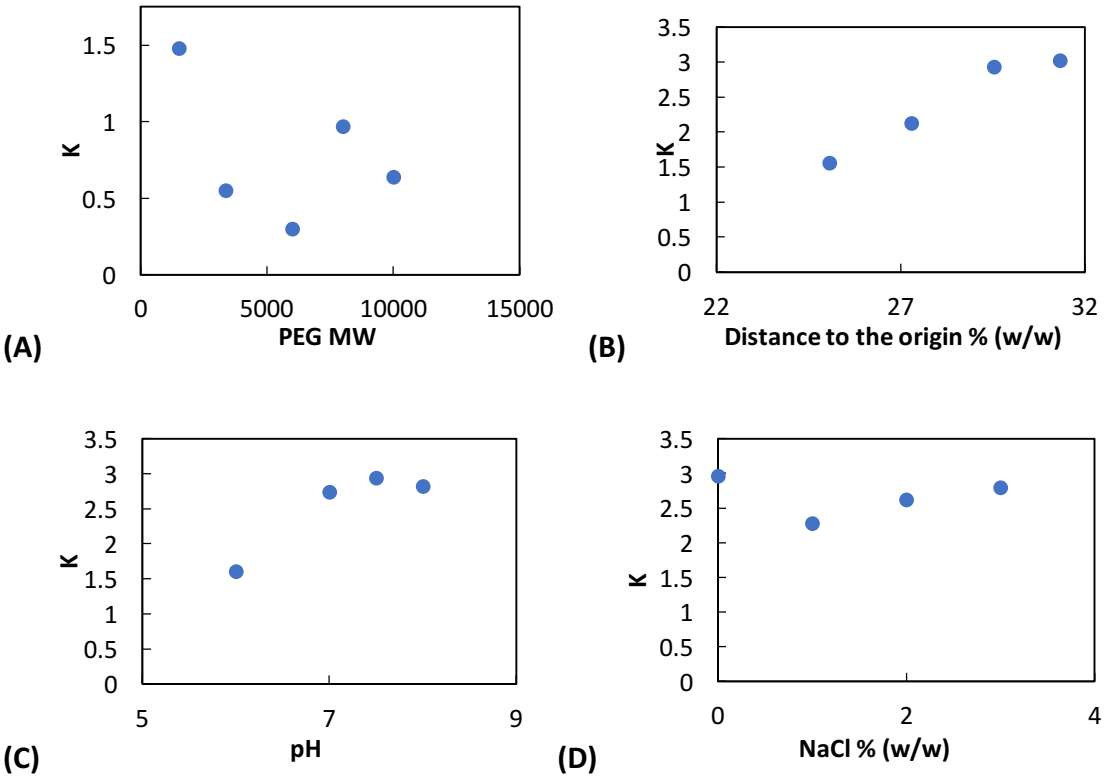

*Figure SII-4 - **PEG- trisodium citrate system optimization**: PEG MW (A), TLL (B), pH (C), sodium chloride load in the system (D)*

iv. PEG-ammonium sulfate

A composition of 25% PEG, 12.5% ammonium sulfate, 10 mM phosphate pH8 and 20% loading was first selected. The parameters were tested in the following order: PEG MW, TLL, pH, sample loading and addition of sodium chloride (Figure SII-5). It was studied PEG MW between 1 500 and 10 000, in which PEG 1 500 revealed to achieve higher partition coefficient. Multiple TLL values were tested by using the following compositions: 25% PEG 1 500, 12.5% ammonium sulfate (distance to the origin 27.5% (w/w)); 26% PEG 1500, 13% ammonium sulfate (29.97%); 28% PEG 1500, 14% ammonium sulfate (31.30%); and 29% PEG 1500 and 14.5% ammonium sulfate (32.42%). After optimizing all the parameters according to the procedures previously described, a composition of 29% PEG 1 500, 14.5% ammonium sulfate, 10 mM phosphate pH 8 and 15% loading was selected.

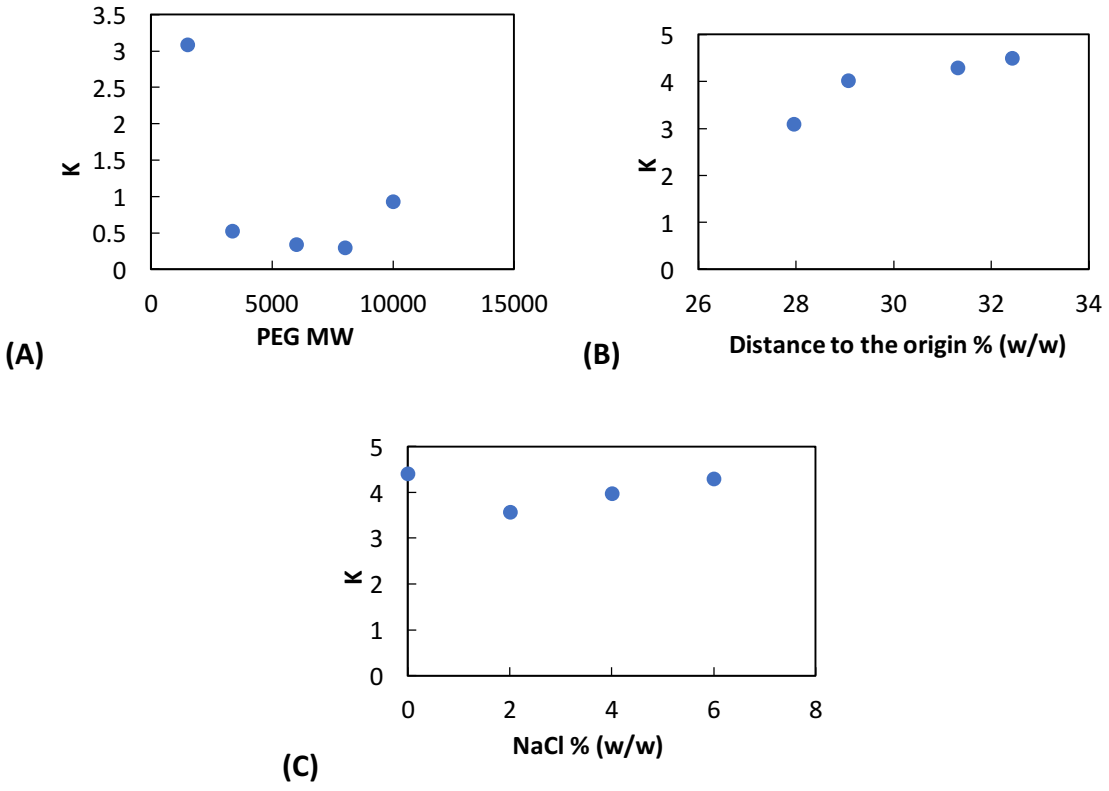

*Figure SII-5 - **PEG- ammonium sulfate system optimization**: PEG MW (A), TLL (B), and sodium chloride load in the system (C)*

II.6. References

1. Aucoin, M.G., et al., *Virus-like particle and viral vector production using the baculovirus expression vector system/insect cell system: adeno-associated virus-based products.* Methods Mol Biol, 2007. **388**: p. 281-96.
2. Bachmann, M.F. and G.T. Jennings, *Virus-Like Particles: Combining Innate and Adaptive Immunity for Effective Vaccination*, in *Novel Vaccination Strategies*, M.-P.-I.f.I. Biology, Editor. 2004, Wiley-VCH Verlag GmbH & Co. KGaA.
3. Garcea, R.L. and L. Gissmann, *Virus-like particles as vaccines and vessels for the delivery of small molecules.* Curr Opin Biotechnol, 2004. **15**(6): p. 513-7.
4. Wolf, M.W. and U. Reichl, *Downstream processing of cell culture-derived virus particles.* Expert Rev Vaccines, 2011. **10**(10): p. 1451-75.
5. Morenweiser, R., *Downstream processing of viral vectors and vaccines.* Gene Ther, 2005. **12 Suppl 1**: p. S103-10.
6. Huhti, L., et al., *A comparison of methods for purification and concentration of norovirus GII-4 capsid virus-like particles.* Arch Virol, 2010. **155**(11): p. 1855-8.
7. Liu, C.C., et al., *Purification and characterization of enterovirus 71 viral particles produced from vero cells grown in a serum-free microcarrier bioreactor system.* PLoS One, 2011. **6**(5): p. e20005.
8. Branston, S., et al., *Precipitation of filamentous bacteriophages for their selective recovery in primary purification.* Biotechnol Prog, 2012. **28**(1): p. 129-36.
9. Hu, J., et al., *Purification of porcine reproductive and respiratory syndrome virus from cell culture using ultrafiltration and heparin affinity chromatography.* J Chromatogr A, 2010. **1217**(21): p. 3489-93.
10. Asenjo, J.A. and B.A. Andrews, *Aqueous two-phase systems for protein separation: phase separation and applications.* J Chromatogr A, 2012. **1238**: p. 1-10.
11. Rosa, P.A., et al., *Aqueous two-phase systems: A viable platform in the manufacturing of biopharmaceuticals.* J Chromatogr A, 2010. **1217**(16): p. 2296-305.
12. Azevedo, A.M., et al., *Optimisation of aqueous two-phase extraction of human antibodies.* J Biotechnol, 2007. **132**(2): p. 209-17.
13. Negrete, A., T.C. Ling, and A. Lyddiatt, *Aqueous two-phase recovery of bio-nanoparticles: a miniaturization study for the recovery of bacteriophage T4.* J Chromatogr B Analyt Technol Biomed Life Sci, 2007. **854**(1-2): p. 13-9.
14. García-Pérez, A.I., P. Sancho, and M. Pinilla, *Surface and metabolic properties of microcytic and macrocytic human anaemic red blood cells detected in polymer aqueous two-phase systems.* J Chromatogr B Biomed Sci Appl, 1998. **711**(1-2): p. 301-7.
15. Benavides, J., et al., *Rotavirus-like particles primary recovery from insect cells in aqueous two-phase systems.* J Chromatogr B Analyt Technol Biomed Life Sci, 2006. **842**(1): p. 48-57.
16. Luechau, F., T.C. Ling, and A. Lyddiatt, *Recovery of B19 virus-like particles by aqueous two-phase systems.* Food and Bioproducts Processing, 2011. **89**(4): p. 322-327.

17. Walker, S.G. and A. Lyddiatt, *Processing of nanoparticulate bioproducts: application and optimisation of aqueous two-phase systems.* Journal of Chemical Technology and Biotechnology, 1999. **74**(3): p. 250-255.
18. Trindade, I.P., et al., *Purification of plasmid DNA vectors by aqueous two-phase extraction and hydrophobic interaction chromatography.* J Chromatogr A, 2005. **1082**(2): p. 176-84.
19. Zaslavsky, B.Y., *Aqueous two-phase partitioning : physical chemistry and bioanalytical applications*. 1995, New York: M. Dekker.
20. Hatti-Kaul, R., *Aqueous two-phase systems. A general overview.* Mol Biotechnol, 2001. **19**(3): p. 269-77.
21. Hammar, L., et al., *Concentration and purification of feline leukaemia virus (FeLV) and its outer envelope protein gp70 by aqueous two-phase systems.* J Virol Methods, 1989. **24**(1-2): p. 91-101.
22. Hammar, L., et al., *The use of aqueous two-phase systems to concentrate and purify bovine leukemia virus outer envelope protein gp51.* Biotechnol Appl Biochem, 1989. **11**(3): p. 296-306.
23. Hammar, L. and G. Gilljam, *Extraction of HIV-1 in aqueous two-phase systems to obtain a high yield of gp120.* AIDS Res Hum Retroviruses, 1990. **6**(12): p. 1379-88.
24. Rito-Palomares, M. and A.P.J. Middelberg, *Aqueous two-phase systems for the recovery of a recombinant viral coat protein from Escherichia coli.* Journal of Chemical Technology and Biotechnology, 2002. **77**(9): p. 1025-1029.
25. Hardt, S. and T. Hahn, *Microfluidics with aqueous two-phase systems.* Lab Chip, 2012. **12**(3): p. 434-42.
26. Silva, D.F., et al., *Design of a microfluidic platform for monoclonal antibody extraction using an aqueous two-phase system.* J Chromatogr A, 2012. **1249**: p. 1-7.
27. Novak, U., et al., *Ionic liquid-based aqueous two-phase extraction within a microchannel system.* Separation and Purification Technology, 2012. **97**: p. 172-178.
28. Hu, R., et al., *Rapid, highly efficient extraction and purification of membrane proteins using a microfluidic continuous-flow based aqueous two-phase system.* J Chromatogr A, 2011. **1218**(1): p. 171-7.
29. Meagher, R.J., Y.K. Light, and A.K. Singh, *Rapid, continuous purification of proteins in a microfluidic device using genetically-engineered partition tags.* Lab Chip, 2008. **8**(4): p. 527-32.
30. Johansson, H.-O., et al., *Separation and partitioning of Green Fluorescent Protein from Escherichia coli homogenate in poly(ethylene glycol)/sodium-poly(acrylate) aqueous two-phase systems.* Separation and Purification Technology, 2008. **62**(1): p. 166–174.
31. Fexby, S., et al., *Partitioning and characterization of tyrosine-tagged green fluorescent proteins in aqueous two-phase systems.* Biotechnol Prog, 2004. **20**(3): p. 793-8.
32. Johansson, H.O., et al., *Driving forces for phase separation and partitioning in aqueous two-phase systems.* J Chromatogr B Biomed Sci Appl, 1998. **711**(1-2): p. 3-17.

33. Choi-Miura, N.H., et al., *Purification and characterization of a novel glycoprotein which has significant homology to heavy chains of inter-alpha-trypsin inhibitor family from human plasma.* J Biochem, 1995. **117**(2): p. 400-7.
34. Filipe, V., A. Hawe, and W. Jiskoot, *Critical evaluation of Nanoparticle Tracking Analysis (NTA) by NanoSight for the measurement of nanoparticles and protein aggregates.* Pharm Res, 2010. **27**(5): p. 796-810.
35. Gentile, M., et al., *Determination of the size of HIV using adenovirus type 2 as an internal length marker.* J Virol Methods, 1994. **48**(1): p. 43-52.
36. Ladd Effio, C., et al., *Downstream processing of virus-like particles: single-stage and multi-stage aqueous two-phase extraction.* J Chromatogr A, 2015. **1383**: p. 35-46.
37. Kutner, R.H., X.Y. Zhang, and J. Reiser, *Production, concentration and titration of pseudotyped HIV-1-based lentiviral vectors.* Nat Protoc, 2009. **4**(4): p. 495-505.
38. Richieri, S.P., et al., *Characterization of highly purified, inactivated HIV-1 particles isolated by anion exchange chromatography.* Vaccine, 1998. **16**(2-3): p. 119-29.
39. Soares, R.R., et al., *On-chip sample preparation and analyte quantification using a microfluidic aqueous two-phase extraction coupled with an immunoassay.* Lab Chip, 2014. **14**(21): p. 4284-94.
40. Benavides, J. and M. Rito-Palomares, *Practical experiences from the development of aqueous two-phase processes for the recovery of high value biological products.* Journal of Chemical Technology and Biotechnology, 2008. **83**(2): p. 133-142.

CHAPTER III – Viral purification case study II: Polymeric ionic liquids as alternative separation matrices

Abstract Bacteriophage M13 is a filamentous, non-lytic bacteriophage that infects *E. coli* via the F pilus. The outer layer is occupied by negatively charged N-terminal region of the major coat protein pVIII, which has a low isoelectric point. Currently, M13 is widely used in phage display technology and bio-nanotechnology, and is considered a possible antibacterial therapeutic agent, among other applications.

Conventional phage purification employs gradient ultracentrifugation or a combination of precipitation, centrifugation and microfiltration, leading to long process times, high operational costs, and significant product loss (approximately 60%). Thus, there is a need to design new large-scale processes to achieve high yield and purity and minimize operating cost.

In this work, hydrophobic polymeric ionic liquids with a positive polymeric backbone were used as novel anion-exchange chromatographic matrices for negatively-charged M13 phages at neutral pH. A variety of system parameters were studied, including cation, anion and crosslinker nature and concentration, either in batch adsorption/elution or chromatographic operation mode. PIL separation was found to be a rapid and simple method for the recovery of phages from clarified bacterial culture, reaching over 70% M13 recovery in a single chromatography step. To our knowledge, this is the first time that PILs have been used as separation agents for biological products.

Keywords: Polymeric ionic liquids, Bacteriophage M13, Downstream processing, Anion-exchange, Batch adsorption, Chromatography

---

Part of this chapter has been published as: Jacinto, M.J., Patinha, D.J.S., Marrucho, I.M., Gonçalves, J., Willson, R.C., Azevedo, A.M. and Aires-Barros, M.R., M13 bacteriophage purification using poly(ionic liquids) as alternative separation matrices, *Journal of Chromatography A*, 2018, 1532, 246-250

Part of this chapter has been submitted for publication in Biotechnology Journal as: Jacinto, M.J., Wagner, A., Sá, I. M., Patinha, D.J.S., Marrucho, I.M., Gonçalves, J., Willson, R.C., Azevedo, A.M. and Aires-Barros, M.R., Screening of different polymeric ionic liquids for chromatography-based purification of bacteriophage M13.

III.1. Introduction

M13 is a filamentous, non-lytic bacteriophage (phage) that infects *Escherichia coli* via the F pilus [1]. The phage particle is approximately 1 µm in length and 7 nm in diameter [2, 3]. The major coat protein of M13, pVIII, is responsible for 98% of the viral protein mass [1]. The outermost layer of M13 is occupied by the negatively charged N-terminal region of pVIII, which is rich in acidic amino acid residues that interact with solvent and give the phage a low isoelectric point (pI) of approximately 4.5 [3-5]. Currently, bacteriophage M13 is the basis of most phage display technologies [6, 7] and is considered a possible antimicrobial agent for the treatment of bacterial infections [8-11]. Also, M13 phage is used in high-sensitivity lateral-flow immunoassays [12] and, on a large scale, for food safety applications [13].

Despite the rapid progress in phage technology, the purification of phages has not been extensively studied, until recently. Conventionally, purification of phages is performed by cesium chloride density gradient centrifugation or through successive rounds of high-speed ultracentrifugation, both time consuming, laborious, and lacking scalability [14]. Another downstream alternative consists of combining precipitation, centrifugation, and microfiltration, which often results in a long processing time, high operational and maintenance costs, and significant product loss due to degradation [14]. Thus, there is a vast need to design and develop large-scale cost effective processes for the purification of phages, while maintaining high yield and purity.

Ion exchange chromatography is a popular technique for the purification of peptides, proteins, oligonucleotides, nucleic acids, and other charged molecules. Although this method has been used to purify some viral particles [15, 16], the purification of M13 with anion exchange chromatography has only been reported twice and involved the use of two different resins: DEAE and Q [14, 17]. Ionic liquids (ILs) are salts composed of ions (organic cations and either organic or inorganic anions) with melting points below a conventional temperature of 100°C [18]. ILs have attracted great attention in the field of chromatography due to their easy chemical tunability via the judicious choice of either the cation or the anion - there are theoretically as many as 10^{18} possible cation-anion combinations [19]. Thus, the diversity of available ILs is very broad since there are many known and potentially new cation and anion combinations [20, 21]. Recently, M13

bacteriophage primary recovery and partial purification using ionic liquid-based aqueous two-phase systems was reported [22]. Poly(ionic liquids) (PILs) are a subclass of polyelectrolytes that comprises IL species connected through a polymeric backbone to form a macromolecular framework [23]. The advantage of using PILs instead of ILs lays on the combination of the distinctive physical and chemical properties of ILs with the mechanical and thermal properties of a polymer. Presently, PILs are being studied for their affinity properties, and new applications are under development [23]. In particular, PILs are being explored as new separation and absorption phases in gas separation membranes, gas chromatography, capillary electrophoresis, and solid-phase microextraction to extract a specific component, such as a gas, metal ions and pharmaceuticals inorganic pollutants, from complex systems [23, 24]. To the best of our knowledge, the use of PILs as separation matrices for biological products has never been proposed before.

In this work, different PILs were studied and analyzed for its performance for a selective separation of M13 bacteriophage from *E. coli* supernatant. A hydrophobic PIL, bearing a polycation based on imidazolium cation combined with bis(trifluoromethylsulfonyl)imide anion, poly (1–vinyl-3-ethyl imidazolium bis(trifluoromethylsulfonyl) imide) — poly(VEIM-TFSI) — was selected from several PILs studied as the most promising anion exchange separation matrix for negatively charged M13 phages at neutral pH. The imidazolium cation was chosen as a study option since it is the most common cation of chemical ionic liquids tool box, while the selection of the TFSI anion was due to its delocalized charge which grants a low cation-anion binding energy, thus facilitating anion exchange schemes [25]. The use of poly(VEIM-TFSI) as anion exchanger enabled the development of a rapid and simple method for the recovery of phage M13 from *E. coli* supernatant, with over 70% recovery and 4 as purification factor after only one purification step, either in adsorption/elution assay or chromatographic operation mode.

III.2. Material and methods

a. Poly(ionic liquid) synthesis

For the preparation of imidazolium-based ionic liquids, the monomers 1-vinyl-3-ethylimidazolium bromide and 1-vinyl-3-tetradecylimidazolium bromide was

synthesized as previously described [26]. Briefly, 1-vinylimidazole was mixed with an equimolar amount of bromoethane or bromotetradecane at 40°C for 24 h at 800 rpm. The product was precipitated in ethyl acetate and thoroughly washed to remove any unreacted reagent. After filtration and drying under nitrogen flow, the monomer was dissolved in methanol and subjected to anion metathesis (for TFSI anion PILs) by mixing it with an equimolar amount of LiTFSI, during 24 h at 500 rpm, to obtain the hydrophobic monomer 1-vinyl-3-ethyl imidazolium bis (trifluoromethanesulfonyl)imide (VEIM-TFSI) and 1-vinyl-3-tetradecylimidazolium bis (trifluoromethanesulfonyl)imide, after drying under nitrogen atmosphere.

For the cross-linked polymer synthesis, the monomers were mixed with divinylbenzene (DVB) or ethyleneglycol dimethacrylate (EGDMA) as the cross-linker (x % (w/w) to the monomer) and 2-hydroxy-2-methylpropiophenone as the photo initiator (5% (w/w) to the monomer). The mixture was transferred to a silicon mold (2 $\times$ 4 cm) and placed under UV light until complete polymerization. The resulting material was washed with acetone to remove any unreacted precursors. After filtration, the obtained solid was dried in an oven at 60°C during 8 h. Finally, the dried material was ground, using a small blade coffee grinder, and stored at room temperature.

In order to synthesize the 2-(dimethylethylamino)ethyl methacrylate bromide, equimolar quantities of 2-(dimethylamino)ethyl methacrylate and bromoethane were mixed, at room temperature for 15 h at 800 rpm, in the absence of light. Then, the obtained product was submitted to three washing steps with ethyl acetate and, since the monomer is highly reactive, it was not possible to filter the compound, being only able to later dry under vaccum (1 Pa) and subject it to vigorous stirring at room temperature for at least two days, in the absence of light.

With the purpose of exchanging the counter ion of the formerly obtained monomers, equimolar portions of the compound and LiTFSI were mixed and incubated at room temperature for 15 h at 500 rpm. The resulting monomer was washed with distilled water for at least 3 times. The monomers were further dried under vaccum (1 Pa) with vigorous stirring for, at least, two days.

The monomer 2-(dimethylethylamino)ethyl methacrylate bis(trifluoromethylsulfonyl), was mixed with 30% of DVB crosslinker and with 5% of a photoinitiator (2-hydroxy-2-

methylpropiophenone). The resulting solutions were polymerized under UV light until complete polymerization and the obtained polymer ground with a coffee grinder. The PILs were then washed with acetone to remove any unreacted precursors and subsequently stored at 4°C.

All synthesized structures were analyzed by ^{1}H NMR on a Bruker 400 MHz Ultra-Shield-Plus Magnet NMR instrument using d_6 – DMSO as deuterated solvent.

b. M13 bacteriophage production

Bacteriophage M13 KE was propagated in *E. coli* strain XL1-Blue grown in Super Optimal both (SOB) medium (20 g/L tryptone, 5 g/L yeast extract, 0.5 g/L NaCl, 2.5 mM KCl, 10 mM $MgCl_2$, 10 µg/mL tetracycline). The culture was separated at 4°C by centrifugation for 30 min at 2021 *g*. The supernatant containing phage particles was filtered using a 0.22-µm filter (just to assure that no bacteria would be present in the supernatant) and used as feedstock for the subsequent PIL-based purification process.

For optimization studies, the supernatant was precipitated with 3% NaCl and 4% PEG-8000 for 10 min at 37°C 220 rpm, and cooled on ice for 45 min. After a 20-minute centrifugation at 4ºC and 8085 g, the pellet was resuspended in 1% BSA and 15% glycerol in PBS 1×, and centrifuged for 5 min at 4°C and 8085 *g*.

c. Phage titration

The concentration of M13 phage particles was determined by phage titration as plaque forming units per milliliter (#/mL). Ten-fold serial dilutions of each fraction containing M13 were prepared until a final dilution of 10^8 was reached. Ten microliters of each phage dilution sample were dispensed into a sterile microcentrifuge tube containing 200 µL mid-log phase *E. coli* XL1-Blue (resistant to tetracycline) culture (OD 0.3 to 0.6) with no agitation at room temperature for 20 min. A vortex was used to mix each mixture with ~3 mL LB top agar (Nzytech LB liquid medium, 7 g/L agar), which was previously equilibrated at 55°C in a dry bath incubator. The mixture was poured onto an LB agar plate (Nzytech LB solid medium) containing 10 µg/mL tetracycline, covering all the plate surface. The plates were cooled to room temperature and incubated inverted overnight at 37°C. Plaques formed were counted, and the concentration of phage was determined as #/mL. The amount of phage particles was calculated by counting the plaques on plates that had between 10 to 100 plaques. Multiplying each number by the dilution factor for

that plate provided the phage titer in plaque forming units per volume (#/mL), equation 1. All assays were performed in triplicates.

$$\#/\mathrm{mL} = \left(\frac{\#\,\mathrm{plaques}}{10\mu L} \times 10^{(\mathrm{dilution})} \right) \times \frac{1000\mu L}{\mathrm{mL}} \qquad (1)$$

d. Adsorption/Elution studies

Adsorption and elution runs were performed using a 96-well MultiScreen-HV Filter Plate (0.45 µm; Millipore) connected to a MultiScreen® HTS Vacuum Manifold (Millipore) and filtered in a DirectStack™ mode. To recover the non-contaminated process fractions (waste, adsorption, and elution), three different 96-well plates (Greiner UV-Star® 96-well plates) were used to collect each fraction in the correspondent operation step.

For optimization tests, 20 mg of tested PIL was weighted and dispersed into each well. The PIL was equilibrated twice for 15 min with 200 µL adsorption buffer (50 mM Tris-HCl pH 7.5; or 50 mM citrate buffer pH 4) using a Shaker-Incubator Stat Fax-2200 at velocity 7 (1500 rpm) at room temperature, and then the liquid was filtered to waste. For the adsorption step, 50 µL of 3.73×10^{10} #/mL purified M13 bacteriophage solution were diluted with 150 µL of adsorption buffer and incubated with the PIL on the plate for 30 minutes with 1500 rpm agitation and room temperature. Longer incubation times did not provide higher adsorption yields (data not shown). After incubation, the flow-through liquid was filtered to a collection plate and kept for further analysis. Finally, 200 µL elution buffer (1.5 M NaCl in 50 mM citrate buffer pH 4; 50 mM citrate buffer pH 4; or 1.5 M NaCl in 50 mM Tris-HCl pH 7.5) were applied for 30 min with 1500 rpm agitation at room temperature to elute the bound phage particles. The elution liquid was filtered to a collection plate and kept for further analysis. The adsorption and elution buffer volumes used were based on the M13 adsorption kinetics (Figure SIII-1, supplementary information) and on previous works performed at iBB [27].

This adsorption/elution studies format was also used for M13 recovery directly from 0.22 µm filtered *E. coli* supernatant.

Adsorption efficiency is considered as the percentage of bound phage during the adsorption step; Elution efficiency is determined as the percentage of recovered phage

particles in the elution step from the previously adsorbed phage; Total recovery yield is the percentage of the initial phage feedstock applied measured in the elution step.

e. PIL chromatography column preparation

To prepare the PIL column, 100 mg of poly(VEIM-TFSI) reticulated with 30% DVB as reticulant agent were weighted and then added to a column with inner diameter of 5 mm (Tricorn 5/20, GE Healthcare). The PIL present in the column was washed with 1 mL of MQ water for 3 times to reduce the amount of small PIL particles that could pass through the column filter and be detected by absorbance at 280 nm during the chromatographic runs. After adding the PIL, the column was closed with the top adjustable cap and connected to an ÄKTApurifier10 system (GE Healthcare).

f. PIL-based chromatography

PIL-based chromatography was performed using the column prepared as described in the previous section, and connected to an ÄKTApurifier10 system (GE Healthcare) under the control of UNICORN 5.11 software (GE Healthcare). The column was washed with MilliQ water until a conductivity inferior to 0.054 mS/cm was reached and no variation on controlled parameters was observed. It was used buffer A (50 mM Tris-HCl pH 7.5) for equilibrium and adsorption and buffer B (1.5 M NaCl in 50 mM citrate buffer pH 4) for elution. The absorbance of the eluate was continuously measured at 280 nm by a UV detector positioned after the column outlet.

The column was equilibrated at 0.1 mL/min with buffer A for 10 CV. Then, 250 µL of filtered *E. coli* supernatant diluted with 750 µL of buffer A was injected into the column by washing the 1 mL loop with 3 mL of buffer A. All unbound sample was washed out of the column in 10 CV of buffer A. The bound material was eluted with an elution step of buffer B during 40 CV. The flow-through and eluate were collected during the course of the chromatographic run in 0.5 mL and 0.1 mL fractions, respectively, in a 1.5 mL microtubes positioned on a Frac-950 collector (GE Healthcare). The collected fractions were analyzed by acrylamide gel electrophoresis, total protein amount and phage titration.

g. Analytical Methods

i. Protein Gel Electrophoresis, SDS-PAGE

Samples were diluted in Bio-Rad (Hercules, CA, USA) 4× loading buffer (277.8 mM Tris-HCl, pH 6.8, 4.4% LDS, 44.4% (w/v) glycerol, 0.02% bromophenol blue) and denatured in reducing conditions with 100 mM dithiothreitol at 100°C for 5-10 min. Samples were applied in a 15% acrylamide gel and run at 90 mV for 1.5 hours using a running buffer containing 192 mM glycine, 25 mM Tris and 0.1% SDS, pH 8.3. Each gel was loaded with a Precision Plus Protein Dual-color standard from Bio-Rad. Gels were stained with Coomassie Brilliant Blue R-250 (Pharmacia, Uppsala, Sweden) for 1 hour. Gels were then destained by immersion in 30% (v/v) ethanol and 10% (v/v) acetic acid for 1.5 h. Silver staining was performed whenever higher sensitivity was required using a Bio-Rad silver staining kit. Images were acquired with a GS-800 calibrated densitometer from Bio-Rad.

ii. Total protein concentration

Total protein concentration was determined by BCA protein assay (23225, ThermoFisher). The analysis was performed according to the manufacturer's instructions using the SpectraMax 384Plus microplate reader (Molecular devices, Sunnyvale, CA, USA). BSA was used as a standard curve with concentration between 2000-0 µg/mL.

III.3. Results and discussion

a. Poly(VEIM-TFSI) characterization

Poly(VEIM-TFSI) was chosen as a proof-of-concept PIL for bioseparations since the imidazolium cation is the most common cation of chemical ionic liquids tool box, and TFSI anion presents delocalized charge which grants a low cation-anion binding energy, thus facilitating anion exchange schemes [25]. The synthesis of the ionic liquid monomer 1-vinyl-3-ethylimidazolium bromide was performed by nitrogen quaternization using commercially available 1-vinylimidazole, with yields higher than 90%. ^{1}H NMR in D_2O confirmed the purity of the monomer by showing -CH_3- resonances around δ=1.5 ppm and -CH_2- around δ=4.2 ppm. The poly(VEIM-TFSI) (Figure III-1) was successfully synthesized and cross-linked with 30% DVB under UV light without the use of any solvent, in less than 60 seconds. Given its cross-linked nature, the polymer was not

soluble in water or in any other common solvent, such as acetone, ethanol, or dimethylsulfoxide, thereby allowing its use as a novel adsorption matrix for biological products. The imidazolium groups present in polymer backbone structure confers a strong positive and localized charge to the backbone, while the flexible anion exhibiting highly delocalized charge, facilitates the anion exchange reaction.

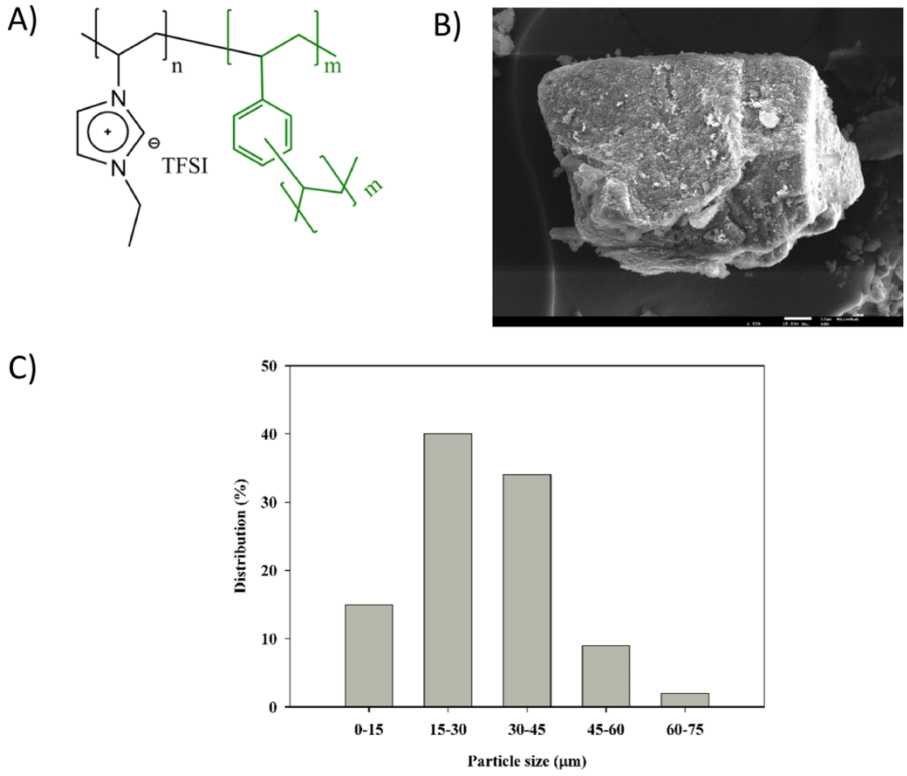

Figure III-1 - A) Chemical structure of Poly(VEIM-TFSI) and divinylbenzene crosslinker (DVB in green) used to obtain a 3D network. B) Representative SEM image of the overall 3D particle prepared in this work. C) Particle size distribution of the poly(VEIM-TFSI) used in the M13 bacteriophage

In Figure III-1B, a SEM image representative of the overall shape and size of the individual polymeric particles obtained after careful milling using a regular coffee grinder, is shown. In terms of size distribution, it can be observed in Figure III-1C that more than 70% of the particles have diameters between 15 µm and 45 µm.

The surface charge of the poly(VEIM-TFSI) particles was assessed by zeta potential measurements performed in Milli-Q purified water, using a Zetasizer Nanoseries equipment from Malvern Instruments. The surface charge of the polymeric ionic liquid particles in water was positive, with zeta potential values of 13.90 ± 3.15 mV, which was expected since a polycation, positively charged polymer backbone, was used. This opens

a wide perspective for the use of this material as a novel anion-exchanger for biological products, including bacteriophages.

b. Poly(VEIM-TFSI)-based anion-exchange proof of concept using M13 as a model

Poly(vinylethylimidazolium)-based PILs have been used for several applications, ranging from water purification [28], to optoelectronic devices [29], analytical chemistry [30], gas separation [24], among others. The use of DVB as a crosslinker in the synthesis of PILs has also been recently published for analytical chemistry [31]. To the best of our knowledge, the specific poly(vinylethylimidazolium) TFSI/DVB (or any other polymeric ionic liquid) has never been used for biological separations.

Despite the hydrophobic character of the PIL, the main interaction between the PIL and the M13 bacteriophage was thought to be electrostatic due to the high density of positive charge on the PIL backbone. To test this hypothesis, the interaction between the M13 bacteriophage and the PIL was studied at two different adsorption pH conditions (50 mM Tris-HCl, pH 7.5 and 50 mM citrate buffer, pH 4) in order to change the M13 surface charge (Figure III-2), considering that the M13 bacteriophage pI is approximately 4.5 [4, 5]. For both adsorption conditions, the elution buffer used was 1.5 M NaCl in 50 mM citrate, pH 4.

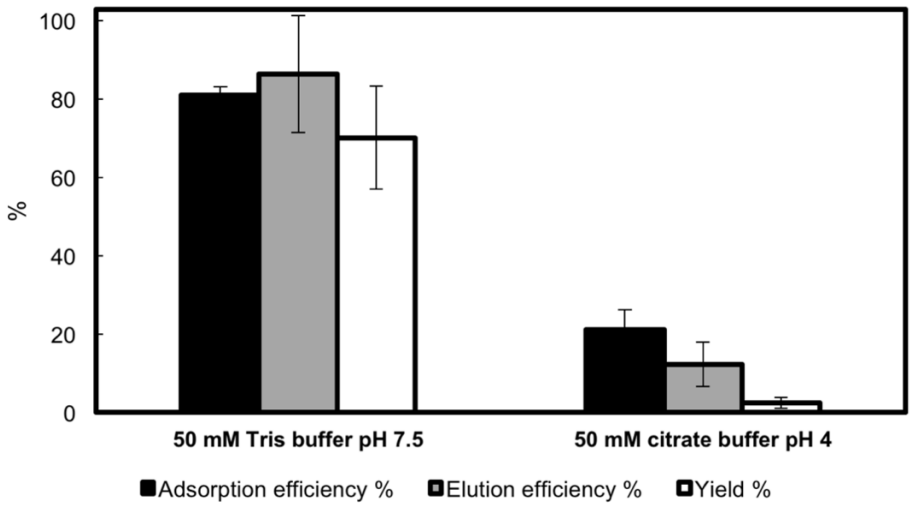

Figure III-2 - ***Separation of M13 bacteriophage particles using different adsorption buffers and poly(VEIM-TFSI) reticulated with 30% DVB as the separation matrix****. The assay was performed in a MultiScreen-HV Filter Plate (0.45 µm), 96-well plate with two different adsorption buffers (50 mM Tris-HCl pH 7.5 and 50 mM citrate buffer pH 4) and 1.5 M NaCl in 50 mM citrate buffer pH 4 as the elution buffer. Adsorption, elution, and total recovery yield percentages for the recovery of M13 phage particles in the elution fraction are shown. (n=3, mean ± standard deviation)*

The results presented in Figure III-2 show that when the adsorption buffer has a pH higher than the pI of the viral particle, the M13 particles are negatively charged and thus, interact with the positively charged polymeric backbone of the poly(VEIM-TFSI). On the other hand, using an adsorption buffer with a pH lower than the pI, the M13 bacteriophage is positively charged and the separation performance becomes much more limited, with an overall recovery yield of only 2.5 ± 1.3%. This clearly shows that anion exchange plays a major role in M13 bacteriophage interaction process with the positively charged, polymeric backbone structure of poly(VEIM-TFSI).

For M13 phage recovery using poly(VEIM-TFSI) as the anion exchanger, 50 mM Tris-HCl pH 7.5 as the adsorption buffer, and 1.5 M NaCl in 50 mM citrate buffer pH 4 as the elution buffer, a total recovery yield of 70.2 ± 13.2% was achieved in a single step, with 81.0 ± 2.2% adsorption and 86.4 ± 14.9% elution efficiencies (Figure III-2).

Also, the reuse of the chromatographic PIL was possible after washing with 0.1 M NaOH for 30 minutes; and comparable results in adsorption, elution, and total yield to the first-time batch assays were achieved (Figure III-3).

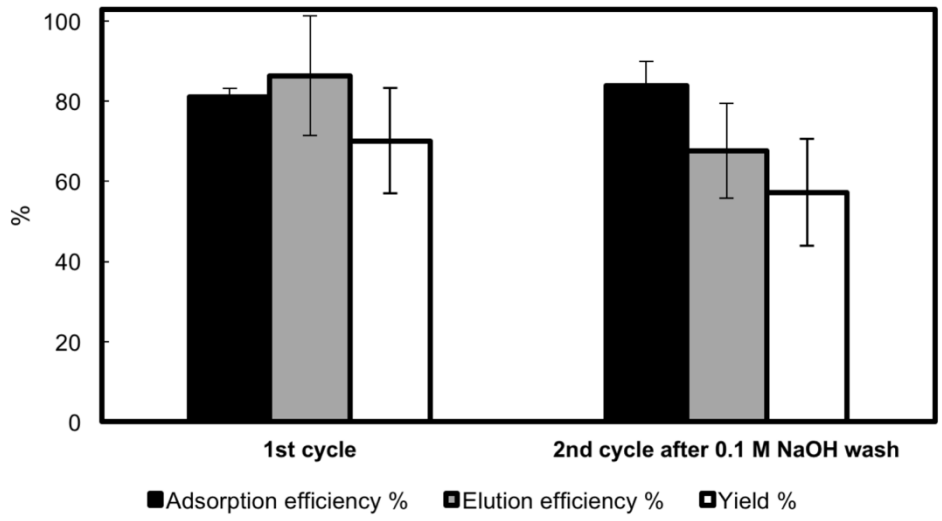

Figure III-3 - ***Reuse of poly(VEIM-TFSI) reticulated with 30% DVB as separation matrix for the recovery of M13 bacteriophage particles****. The assay was performed in MultiScreen-HV Filter Plate (0.45 µm), 96-well plates with 50 mM Tris-HCl pH 7.5 as the adsorption buffer and 1.5 M NaCl in 50 mM citrate buffer pH 4 as the elution buffer. Adsorption, elution, and total yield percentages for the recovery of M13 phage particles in the elution fraction are shown. (n=3, mean ± standard deviation)*

Although the adsorption step was mainly conditioned by electrostatic interactions, for the elution step, different conditions were considered. These included: (i) decrease to

pH=4 to individually assess the effect of charge repulsion between the positively M13 bacteriophage and the positively charged backbone; (ii) increase of the ionic strength through the addition of 1.5 M of NaCl in the adsorption buffer to increase the competition between the chloride anion and the M13 bacteriophage for the anion exchanger; and (iii) combination of bacteriophage charge change and high ionic strength (Figure III-4).

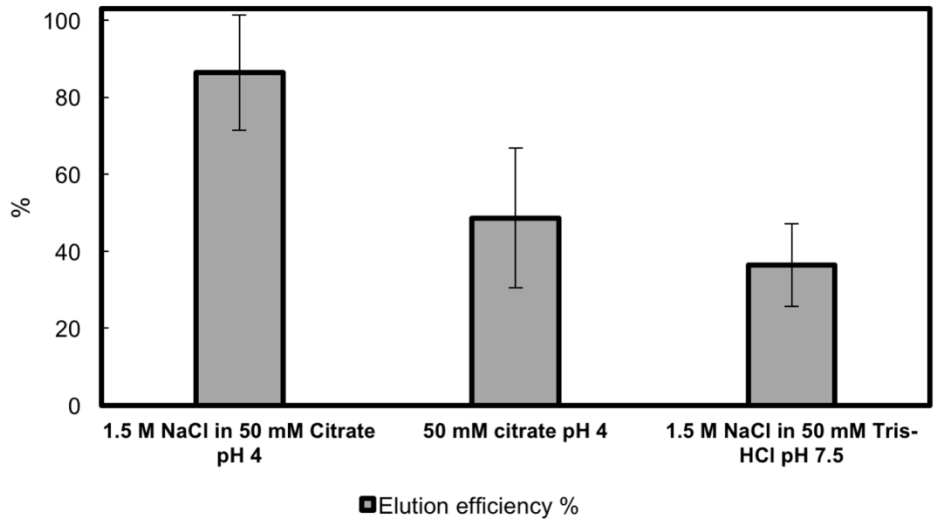

Figure III-4 - ***Elution efficiency of M13 bacteriophage particles using poly(VEIM-TFSI) reticulated with 30% DVB as separation matrix with different elution buffers****. The assay was performed in MultiScreen-HV Filter Plate (0.45 µm), 96-well plates with 50 mM Tris-HCl pH 7.5 as the adsorption buffer and different elution buffers (1.5 M NaCl in 50 mM citrate pH 4, 50 mM citrate pH 4, and 1.5 M NaCl in 50 mM Tris-HCl pH 7.5). Elution efficiency percentage is shown. (n=3, mean ± standard deviation)*

According to the results presented in Figure III-4 the use of 50 mM citrate buffer pH=4 in the presence of a high salt concentration was the most effective approach for phage elution (86.4 ± 14.9% elution efficiency). The use of a low pH buffer to switch the phage charge from negative to positive, with no salt addition, was not completely effective (48.6 ± 18.1% elution efficiency). Moreover, the increase of chloride anion concentration without a pH decrease was not enough to fully disrupt the ionic interactions (established between the positive PIL structure and the negative bacteriophage particles) and thus, to perform a complete anion exchange process to elute the viral particles (36.4 ± 10.6% elution efficiency). These results suggest that, even for a positively charged bacteriophage, a complete elution process is only achieved in the presence of salt. As the salt concentration is increased, the charge shielding effect increases, which promotes competition between the salt anion and the M13

bacteriophage, thus decreasing the binding affinity between the M13 and the PIL [32]. This phenomenon helps to release the adsorbed bacteriophages, decreasing the interactions between the adsorbent and the bound biomolecules. In conclusion, only the combination of positively charged phage particles and the presence of salt can accomplish a practical anion exchange process.

c. System parameters influence

Different system parameters were further explored in order to better understand their influence in the biological separation under study, since anion exchange plays a major role in M13 bacteriophage interaction process with the positively charged, polymeric backbone structure of poly(VEIM-TFSI), as shown in the previous section 'III.3.b.'. Therefore, the type and percentage of the crosslinker agent, the type of cation and anion were considered and further investigated.

i. Crosslinker agent type

The effect of two different crosslinker agents, DVB and EGDMA (Figure III-5), with different hydrophobicity profiles, on the M13 bacteriophage purification, was studied and compared to understand its influence in the separation of a hydrophilic bioproduct. Different assays using poly(VEIM-TFSI) with 30% of each crosslinker agent were performed.

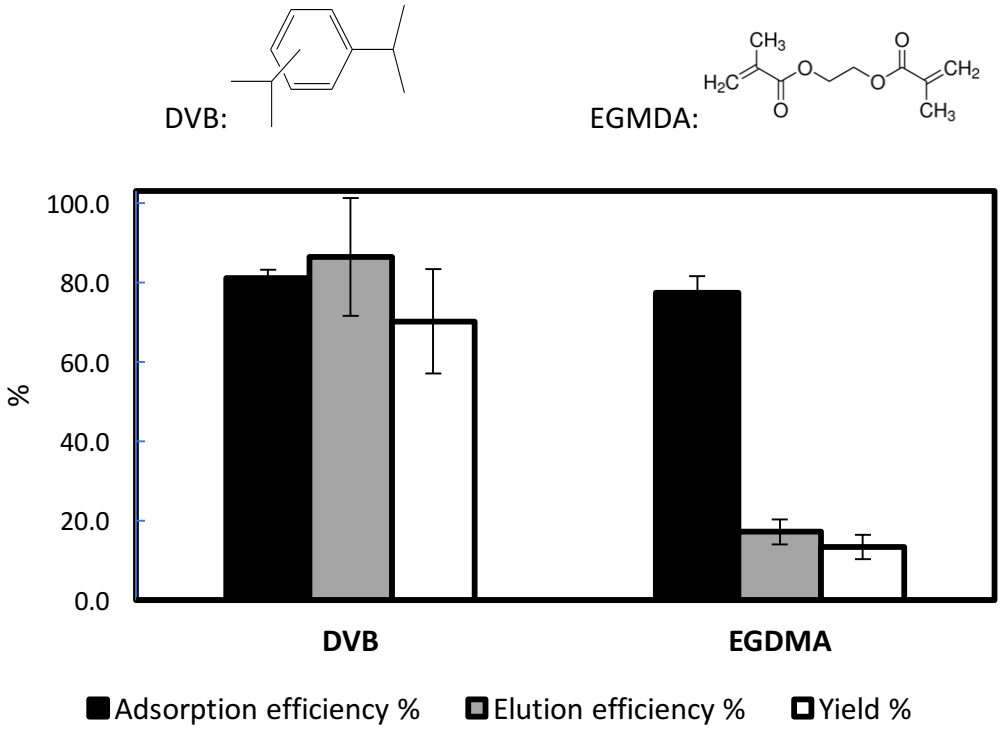

Figure III-5 - **Separation of M13 bacteriophage particles using 30% of different crosslinker agents (divinylbenzene – DVB -, or ethyleneglycol dimethylacrylate – EGDMA -) in poly(VEIM-TFSI) as the separation matrix**. The assay was performed in a MultiScreen-HV Filter Plate (0.45 µm), 96-well plate with 50 mM Tris-HCl pH 7.5 as adsorption buffer and 1.5 M NaCl in 50 mM citrate buffer pH 4 as the elution buffer. Adsorption, elution, and total recovery yield percentages for the recovery of M13 phage particles in the elution fraction are shown. (n=3, mean ± standard deviation)

According to Figure III-5, the EGMDA's more hydrophilic profile, when compared to the DVB's, didn't revealed to be advantageous for M13 bacteriophage adsorption efficiency, with 81.0 ± 2.2% for DVB and 77.4 ± 4.2% for EGDMA. Furthermore, when using the same elution buffer, the PIL synthetized with EGDMA led to a much lower elution efficiency when compared to the PIL synthetized with DVB as crosslinker, and the elution efficiency decreased from 86.4 ± 14.9 % to 17.2 ± 3.1 %, respectively. This is probably due to the more hydrophilic environment which prevent phage elution. A pore size measurement would be interesting approach to check potential differences in PIL structure related to the crosslinker agent used.

ii. Crosslinker agent %

The percentage of the crosslinker agent used in the PIL synthesis was also studied and different assays using poly(VEIM-TFSI) with different percentages of DVB as crosslinker agent were performed (Figure III-6). It is important to refer that the different values used reflect the percentage of the crosslinker agent offered to the ionic liquid monomer,

which leads to lower amounts of ionic liquid at higher percentages of crosslinker agent, and vice-versa. Besides, higher crosslinker agent percentages reflect a tighter polymer net, with smaller pore sizes. Thus, smaller pore sizes and lower charge density are expected with the increase of the crosslinker agent percentage.

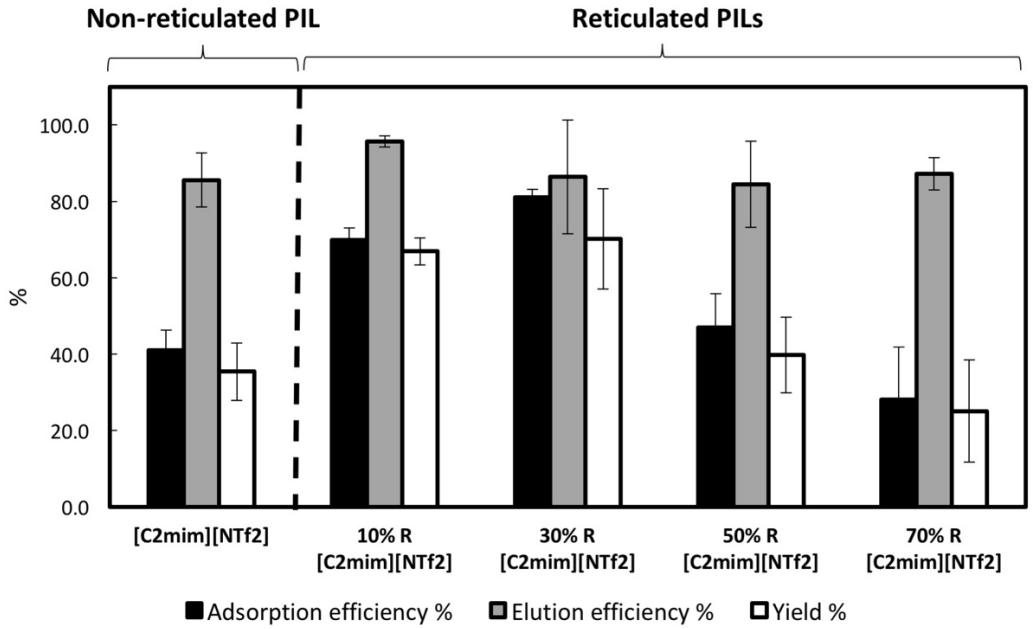

Figure III-6 – **Separation of M13 bacteriophage particles using different DVB crosslinker agent percentages (0, 10, 30, 50 and 70%) in poly(VEIM-TFSI) as the separation matrix.** The assay was performed in a MultiScreen-HV Filter Plate (0.45 µm), 96-well plate with 50 mM Tris-HCl pH 7.5 as adsorption buffer and 1.5 M NaCl in 50 mM citrate buffer pH 4 as the elution buffer. Adsorption, elution, and total recovery yield percentages for the recovery of M13 phage particles in the elution fraction are shown. (n=3, mean ± standard deviation)

Although the absence of the crosslinker agent provides to the polymer a higher charge density and higher pore sizes, when comparing to the same polymer with 10 and 30% DVB as crosslinker agent, the non-reticulated PIL wasn't the most effective for the M13 separation. In fact, with the increase of crosslinker percentage in the synthesized PIL there is a clear increase on the adsorption efficiency (40.9 ± 5.4% for non-reticulated PIL, 69.9 ± 3.2% for 10% DVB and 81.0 ± 2.2% for 30% DVB). Regarding the elution efficiency, it is possible to observe that it remains mostly constant for all the PILS in study. Also, the increase of crosslinker agent percentages from 50 to 70% led to lower adsorption efficiencies, 47.0 ± 8.8% and 28.1 ± 13.8%, respectively, and consequent lower M13 recovery yields. These results suggest that the optimum separation condition is a balance between the polymer charge density and its pore size for this kind of large biological product as the M13 phage, where the use of a crosslinker agent (< 30%) enhances the adsorption efficiency. Again, a pore size measurement would be very

useful technique to use to check the effective porosity differences in PIL structure that lead to significant M13 recovery differences related to the crosslinker agent percentage used.

iii. PIL Cation

The effect of the cation polymerazible group on the phage purification was also analyzed, since the anion exchange was the predominant effect in the M13 separation. Thus, the performance of a sequence of cation with increasing hydrophobicity profile was compared: 2-(dimethylethylamino)ethyl, 1-vinyl-3-ethyl imidazolium, and 1-vinyl-3-tetradecyl imidazolium, respectively, conjugated with TFSI as anion and crosslinked with 30% DVB (Figure III-7).

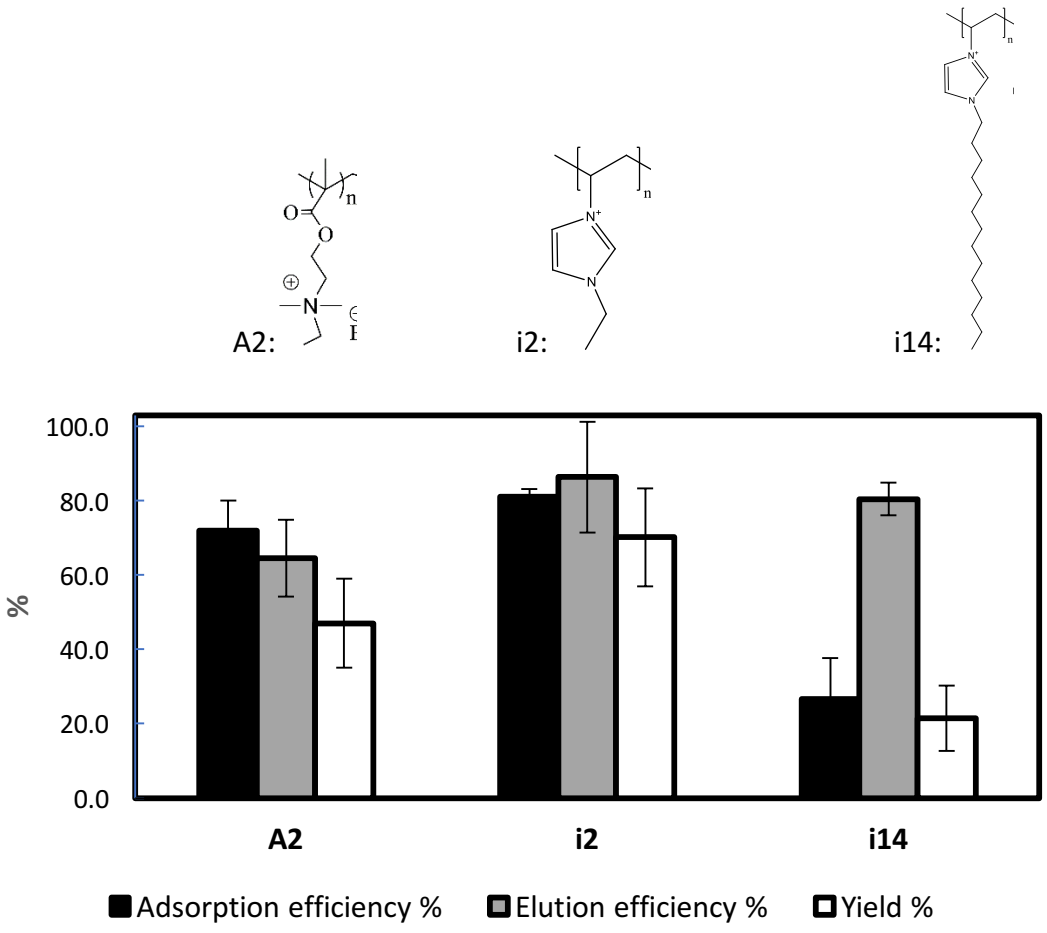

Figure III-7 - **Separation of M13 bacteriophage particles using different cations (2-(dimethylethylamino)ethyl methacrylate – A2 -, 1-vinyl-3-ethyl imidazolium – i2 -, 1-vinyl-3-tetradecyl imidazolium - i14 -) in poly(-TFSI) crosslinked with 30% DVB as the separation matrix**. The assay was performed in a MultiScreen-HV Filter Plate (0.45 µm), 96-well plate with 50 mM Tris-HCl pH 7.5 as adsorption buffer and 1.5 M NaCl in 50 mM citrate buffer pH 4 as the elution buffer. Adsorption, elution, and total recovery yield percentages for the recovery of M13 phage particles in the elution fraction are shown. (n=3, mean ± standard deviation)

It was observed that the cation hydrophobicity decreases the adsorption efficiency to some extent; although 2-(dimethylethylamino)ethyl is a more hydrophilic cation compared to 1-vinyl-3-ethyl imidazolium, it wasn't observed a significant difference in the M13 phage adsorption efficiency, 72.0 ± 8.0% and 81.0 ± 2.2 %, respectively. However, the more hydrophilic environment provides a lower elution efficiency, leading to a lower total recovery yield, 47.0 ± 12.0% and 70.2 ± 13.2%, respectively. On another hand, 1-vinyl-3-tetradecyl imidazolium showed to be a too hydrophobic cation for the separation in study, leading to a M13 adsorption yield of 26.6 ± 11%.

iv. PIL Anion

Finally, the influence of the anion coupled to the polymerizable cation group was analyzed and bis(trifluoromethylsulfonyl) imide – TFSI - and bromide conjugated with 1-vinyl-3-ethyl imidazolium as cation and crosslinked with 30% DVB was considered (Figure III-8).

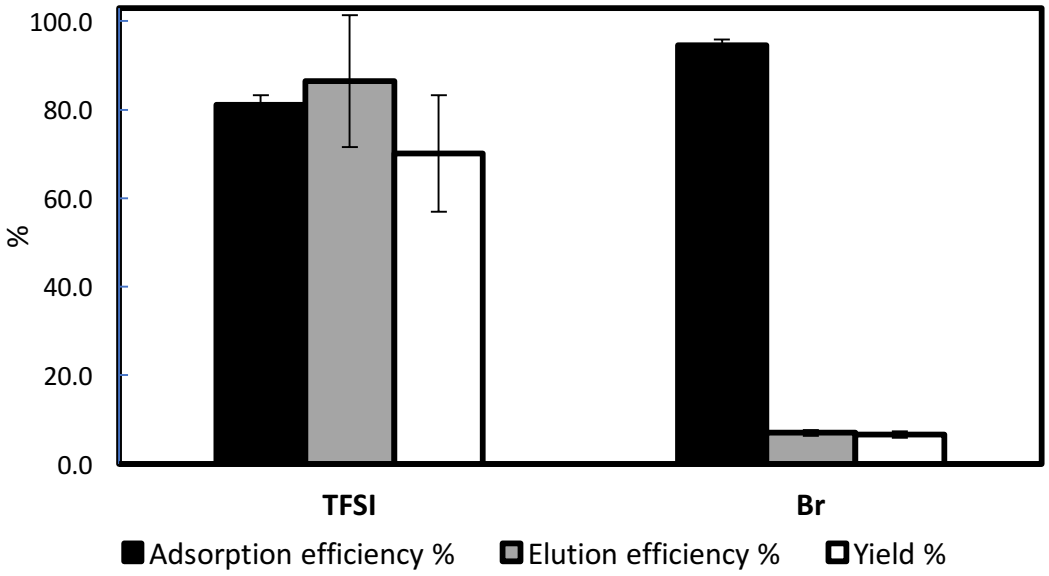

Figure III-8 – **Separation of M13 bacteriophage particles using different anions (TFSI or bromide) in poly(VEIM) crosslinked with 30% DVB as the separation matrix**. The assay was performed in a MultiScreen-HV Filter Plate (0.45 µm), 96-well plate with 50 mM Tris-HCl pH 7.5 as adsorption buffer and 1.5 M NaCl in 50 mM citrate buffer pH 4 as the elution buffer. Adsorption, elution, and total recovery yield percentages for the recovery of M13 phage particles in the elution fraction are shown. (n=3, mean ± standard deviation)

As expected, a smaller anion enhances the adsorption process (81.0 ± 2.2 % for TFSI and 94.6 ± 1.2% for bromide) since it makes it easier to switch position with the negatively charged M13 phage. However, this effect probably lead to a higher quantity of cation-M13 charge interactions that compromised the phage elution efficiency with 86.4 ± 14.9 % for TFSI and 7.0 ± 0.6 % for bromide. Higher amounts of salt, 2 M NaCl, were also

tested to elute the M13 phage from poly(VEIM) bromide, but a significant recovery enhancement was not observed (data not shown).

Although the study of the influence of the system parameters was limited due to the narrow number of possible alternatives evaluated for each parameter, it was a valuable analysis to better understand the M13 bacteriophage interaction with the PIL matrix. Still, the most effective PIL for the separation in study, among all the PILs tested, was the poly(VEIM-TFSI) crosslinked with 30% DVB, the same PIL used in the initial separation proof of concept, which presented 81.0 ± 2.2% adsorption yield, 86.4 ± 14.9% elution yield and 70.2 ± 13.2% total recovery yield.

d. M13 direct purification from *E. coli* supernatant

The performance of the poly(VEIM-TFSI) crosslinked with 30% DVB was then evaluated for the recovery of the M13 bacteriophage directly from the *E. coli* supernatant using batch adsorption, in order to study the influence of the supernatant impurities in the PIL-phage interaction. The same adsorption/elution studies conditions as described before were used with a 0.22 µm filtered *E. coli* supernatant.

The results observed revealed a good agreement with the previous optimization studies, where 81.0 ± 2.2% and 77.3 ± 6.6% adsorption efficiency, 86.4 ± 14.9% and 97.9 ± 10.2% elution efficiency, and 70.2 ± 13.2% and 76.1 ± 13.2% total recovery yield were achieved from pre-purified M13 studies and filtered *E. coli* supernatant, respectively. A purification factor of 4.2 ± 0.7 was calculated as the ratio between the amount of M13 phage per total amount of protein in the elution fraction and the amount of M13 phage per total amount of protein in the initial *E. coli* filtered supernatant feedstock. The results obtained shown a considerable increase on the purification performance, since 4.2 times more M13 particles per total amount of protein was observed when compared with the initial supernatant feedstock.

A SDS-PAGE analysis was performed in order to evaluate the degree of protein purity in the initial *E. coli* filtered supernatant and in the flow-through and elution fractions (Figure III-9). Since the M13 bacteriophage is composed by different proteins (pIX – 3.5 kDa -, pVII – 3.6 kDa -, pVIII – 5 kDa -, pVI – 13 kDa -, and pIII – 42.6 kDa that appear at

the 60 kDa level [33]), it was considered fractions with high amount of M13 when all phage proteins bands are identified in that same lane.

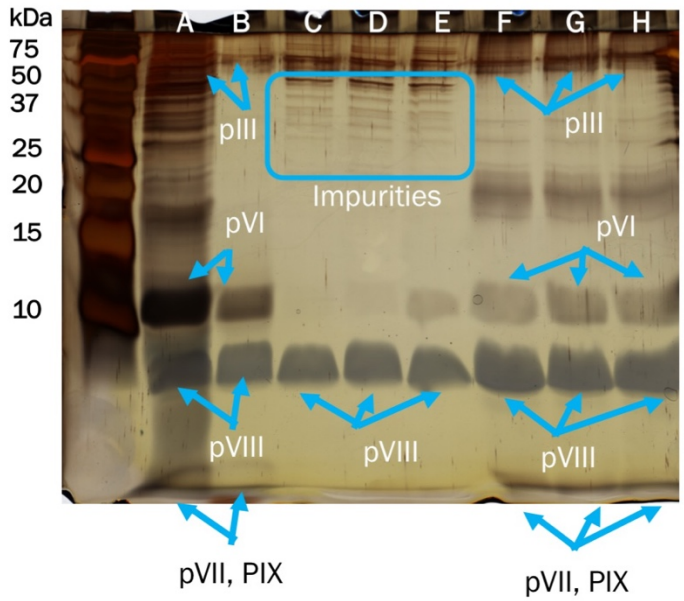

Figure III-9 ***- Silver stained SDS-PAGE of M13 purification from E. coli supernatant using poly(VEIM-TFSI) crosslinked with 30% DVB as separation matrix****. Lanes ID: A: E. coli culture medium supernatant infected by M13; B: Pre-purified M13; C to E: flowthrough triplicate fractions; F to H: elution triplicate fractions. M13 pVII, pIX, pVIII, pVI and pIII are indicated by solid blue arrows. Main supernatant impurities separated in flowthrough fraction are also identified by a blue border. Precision Plus Protein™ Dual Color Standards is represented in the first left lane (kDa).*

As show in Figure III-9, the four main protein bands can be easily identified in the initial feedstock (lane A) and in the pre-purified M13 used in the previous batch optimization studies (lane B), as expected. Considering the differences between the flow-through and elution triplicate fractions, a series of impurities, between 25 and 50 kDa (identified in a blue box), that are mainly identified in the flow-through fractions can be observed. On another hand, the pVI and pVII, pIX protein bands are much more visible in the feedstock and elution fractions lanes, indicating a higher concentration of the M13 bacteriophage in these samples. Therefore, M13 bacteriophage could be recovered directly from the *E. coli* supernatant in batch operation mode using poly(VEIM-TFSI) crosslinked with 30% DVB.

e. Poly(VEIM-TFSI) as an alternative chromatographic support

Since poly(VEIM-TFSI) crosslinked with 30% DVB has been proven to work as a novel separation matrix for the recovery of the M13 bacteriophage directly from the *E. coli*

supernatant in adsorption/elution batch operation mode, as shown in the previous section, the possibility to use this polymer as a chromatographic support was explored. In order to explore the use of poly(VEIM-TFSI) crosslinked with 30% DVB as a chromatographic matrix, 100 mg of this PIL were weighted and then added to a column with inner diameter of 5 mm and connected to an ÄKTA Purifier 10 system. This approach would lead to the use of this separation support in a more conventional and well-established platform, with online monitoring of the system performance, for future biological separation applications. The chromatogram obtained is represented in Figure III-10.

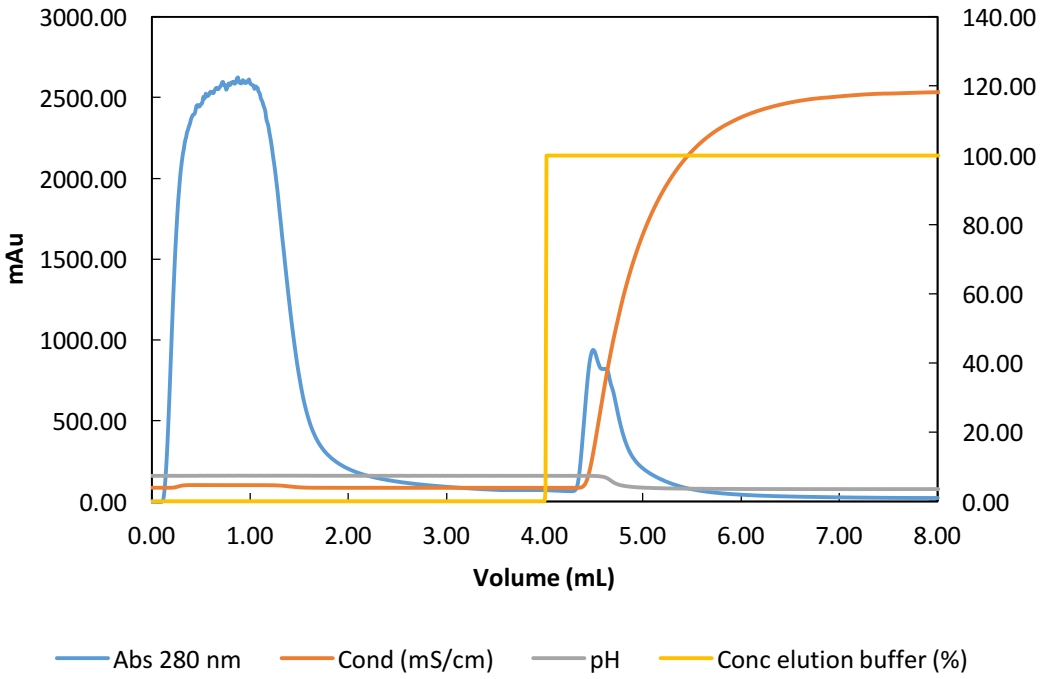

Figure III-10 – ***Chromatogram illustrative of M13 bacteriophage purification from a filtered E. coli supernatant using poly(VEIM-TFSI) crosslinked with 30% DVB as chromatographic separation matrix.*** *250 µL of filtered supernatant diluted in 750 µL of buffer A (50 mM Tris-HCl pH 7.5) was injected into a pre-packed poly(VEIM-TFSI) column, pre-equilibrated with buffer A. Unbound material was washed with 10 CV of buffer A and step elution was performed with 40 CV of buffer B (1.5 M NaCl in 50 mM citrate buffer pH 4). The absorbance at 280 nm, conductivity (mS/cm), pH and concentration of elution buffer B detected after the column outlet are represented by blue, orange, grey and yellow continuous lines, respectively.*

It was observed an increase in the absorbance during the flow-through reflecting unbounded impurities that didn't adsorb to the polymer and thus flowed through the column unretained. Also, a high amount of M13 bacteriophage bound to the separation matrix since 76.5 ± 1.3% M13 adsorption yield was achieved. When buffer B (1.5M NaCl in 50 mM citrate buffer pH 4) was applied, the decrease in the pH and the increase of conductivity caused the elution of 95.0 ± 2.8% of the bound M13 bacteriophages.

Overall, a 72.7 ± 3.4 % total recovery yield and 4.6 ± 0.5 purification factor were achieved.

A new SDS-PAGE gel was performed in order to check the M13 purity in the eluted fractions (Figure III-11). Again, it was considered fractions with high amount of M13 when all phage proteins bands (pIX and pVII, pVIII, pVI, and pIII) are identified in that same lane.

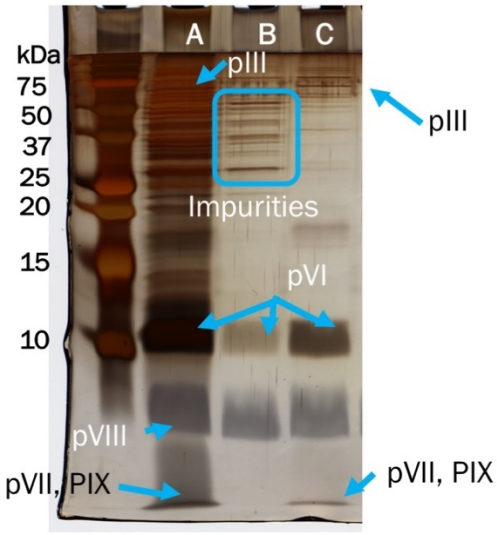

Figure III-11 - ***Silver stained SDS-PAGE of M13 purification from E. coli supernatant using poly(VEIM-TFSI) crosslinked with 30% DVB as chromatographic support****. Lanes ID: A: E. coli culture medium supernatant infected by M13; B: chromatographic flow-through fraction; C: chromatographic elution fraction. M13 pVII, pIX, pVIII, pVI and pIII are indicated by solid blue arrows. Main supernatant impurities separated in flow-through fraction are also identified by a blue border. Precision Plus Protein™ Dual Color Standards is represented in the first left lane (kDa).*

The four main protein bands can be easily identified in the initial feedstock (lane A), as in the batch adsorption/elution studies performed in the previous section, and it can be observed a clear series of impurities between 25 and 50 kDa (identified in a blue box) that are mainly identified in the flowthrough fraction. On another hand, the pVII, pIX protein bands are only visible in the feedstock and elution fractions lanes, indicating a much more significant presence of the M13 bacteriophage in these samples.

A comparative table with adsorption, elution, recovery yields and purification factors of the three study stages are represented in Table III-1.

As observed in Table III-1, the three operation modes presented similar adsorption, elution and recovery efficiencies. Also, chromatographic operation mode, an automatic, conventional and well-established platform, with online monitoring of the system performance, revealed to be a suitable separation process for M13 from directly filtered *E. coli* supernatant.

Table III-1 – ***Adsorption, elution and recovery yield (%) and purification factor in adsorption/elution and chromatographic separations of M13 bacteriophage in pre-purified and filtered E. coli supernatant samples using poly(VEIM-TFSI) crosslinked with 30% DVB as separation matrix***

Loading sample & operation mode	Adsorption yield (%)	Elution yield (%)	Recovery yield (%)	Purification factor
Pre-purified – batch adsorption/elution	81.0 ± 2.2	86.4 ± 14.9	70.2 ± 13.2	-
Supernatant – batch adsorption/elution	77.3 ± 6.6	97.9 ± 10.2	76.1 ± 13.2	4.2 ± 0.7
Supernatant – chromatography	76.5 ± 1.3	95.0 ± 2.8	72.7 ± 3.4	4.6 ± 0.5

This polymeric ionic liquid based separation revealed to be much more efficient than the conventional purification processes, which only recovers up to 36% of the viral particles by precipitation and centrifugation [14], and comparable to other published anion exchange chromatographies, as 82.9% in an expanded bed or 74% using a pre-packed SepFast™ Super Q column [14, 17].

However, it is also important to refer that the PIL packing is a current topic of optimization that can mainly affect the elution profile. To show that, it was performed two consecutive chromatographic runs using the same *E. coli* filtered supernatant batch with two parallel PIL packings (Figure III-12).

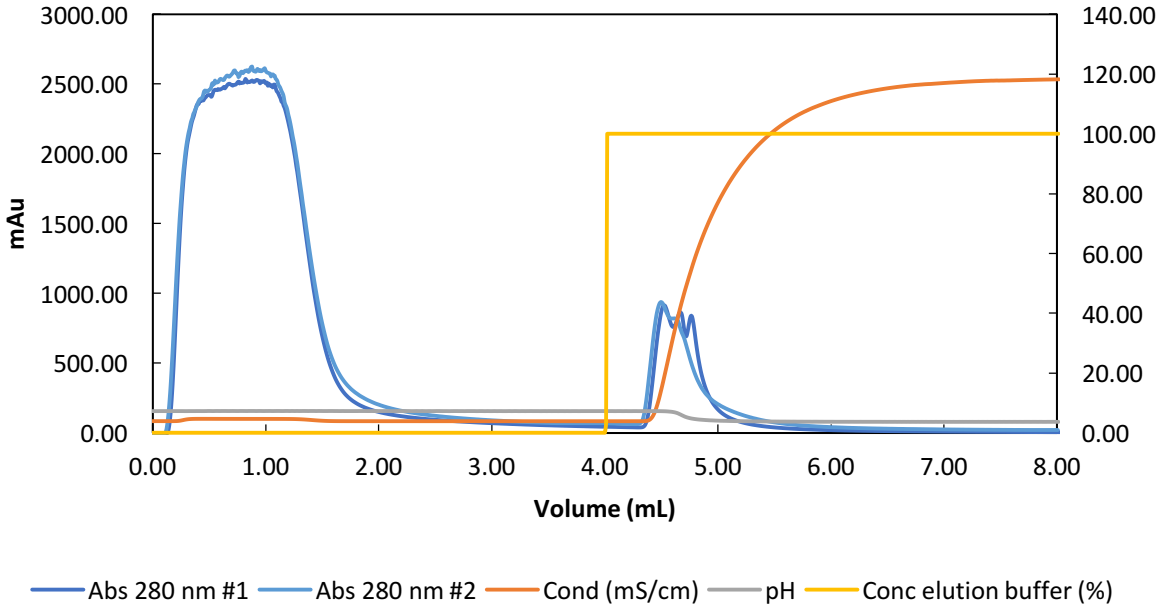

*Figure III-12 – **Two consecutive chromatograms using the same filtered E. coli supernatant with two parallel poly(VEIM-TFSI) crosslinked with 30% DVB chromatographic support packing**. 250 µL of filtered supernatant diluted in 750 µL of buffer A (50 mM Tris-HCl pH 7.5) was injected into a pre-packed poly(VEIM-TFSI) column, pre-equilibrated with buffer A. Unbound material was washed with 10 CV of buffer A and step elution was performed with 40 CV of buffer B (1.5 M NaCl in 50 mM citrate buffer pH 4). The absorbance at 280 nm (run #1 and #2), conductivity (mS/cm), pH and concentration of elution buffer B detected after the column outlet are represented by blue (light and dark blue), orange, grey and yellow continuous lines, respectively.*

As it can be seen in Figure III-12, although the flow-through profile is really similar between the two runs, the elution profile transformed from two to three 'bump' elution peak. Since these 'bumps' are not well separated elution peaks, it was studied different elution conditions, as gradient, two- and three-step elution, but it only led to wider peaks with lower total protein concentration (data not shown). Although the individual peaks could lead to an even more pure M13 fraction, it was concluded that the PIL packing affected the elution profile, at least for large biological products separation. This is probably due to the non-uniform grounding, which was performed by using a small blade coffee grinder in this work. This is a future work topic to be explored in future assays.

III.4. Conclusions

Separation of M13 bacteriophages based on an anion exchange process was successfully developed using a poly(ionic liquid) as a novel separation matrix for the purification of biological products. Using cross-linked poly(VEIM-TFSI) as the anion exchanger for M13 phage recovery it was achieved an excellent agreement between optimization assays and direct use of filtered *E. coli* supernatant, either in batch adsorption-elution mode or chromatographic operation mode. A total recovery yield of 72.7 ± 3.4% and 4.6 ± 0.5 purification factor were achieved in a single chromatographic process. Therefore, polymeric ionic liquid-based separation is an efficient method that can compete with conventional purification processes, which only recover up to 36% of the viral particles by precipitation and centrifugation [14]. Traditional chromatography processes, such as anion exchange chromatography, present comparable results with the presented technology, with recoveries of 82.9% in an expanded bed or 74% using a pre-packed SepFast^{TM} Super Q column [14, 17]. Also, when compared to reported ionic liquid-based aqueous two-phase systems recovery techniques, the use of a poly(ionic liquid) as a novel adsorption matrix improved the extraction process since the bacteriophage was collected in a single fraction, with no need for further treatment to extract the desired product, unlike with PEG or ionic liquid phases [22]. To the best of our knowledge, PILs have never been used as separation matrices for biological products before and this successful demonstration, together with the large number of cations and anions available to prepare PILs, provides some encouragement for future design and use of PILs as customizable separation matrixes for biological products.

III.5. Supplementary information

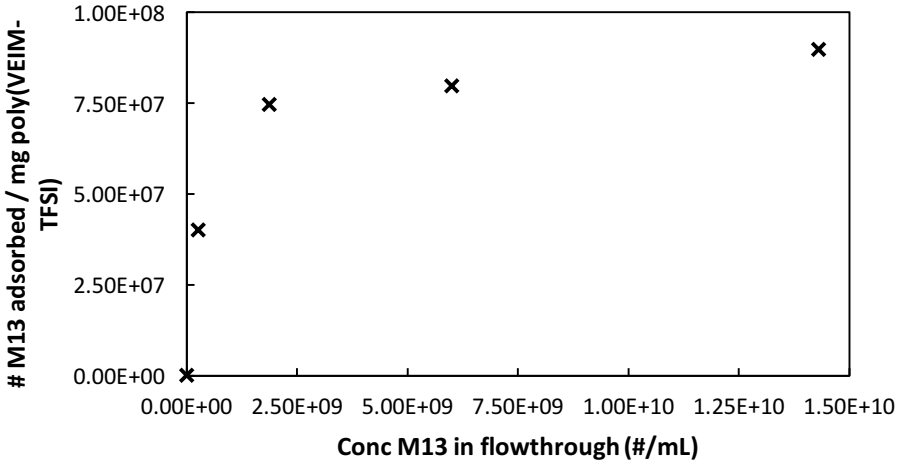

Figure SIII-1 - ***M13 adsorptive thermodynamics in poly(VEIM-TFSI).*** *The M13 adsorption kinetics reflects a Langmuir adsorption behavior* $q = q_{max}\frac{C}{K_d+C}$*, where C is the M13 concentration in the flow-through, which is in equilibrium with the adsorbed M13 to the poly(VEIM-TFSI) (q, amount of M13 particles adsorbed per mg of poly(VEIM-TFSI),* q_{max} *is the amount of M13 particles adsorbed at surface saturation when all the binding sites are filled, and* K_d *is the adsorption equilibrium constant for the Langmuir adsorption process. Correlating the data with the model, it was extrapolated a saturation value* q_{max} *of* 8.77×10^7 *M13 particles per mg of poly(VEIM-TFSI) and* K_d *equal to* 3.16×10^8 *#/mL.*

III.6. References

1. Rasched, I. and E. Oberer, *Ff coliphages: structural and functional relationships.* Microbiol Rev, 1986. **50**(4): p. 401-27.
2. Glucksman, M.J., S. Bhattacharjee, and L. Makowski, *Three-dimensional structure of a cloning vector. X-ray diffraction studies of filamentous bacteriophage M13 at 7 A resolution.* J Mol Biol, 1992. **226**(2): p. 455-70.
3. Marvin, D.A., et al., *Molecular models and structural comparisons of native and mutant class I filamentous bacteriophages Ff (fd, f1, M13), If1 and IKe.* J Mol Biol, 1994. **235**(1): p. 260-86.
4. Zimmermann, K., et al., *The ionic properties of the filamentous bacteriophages Pf1 and fd.* J Biol Chem, 1986. **261**(4): p. 1653-5.
5. Branston, S., et al., *Precipitation of filamentous bacteriophages for their selective recovery in primary purification.* Biotechnol Prog, 2012. **28**(1): p. 129-36.
6. Sidhu, S.S.e. and C.R.e. Geyer, *Phage display in biotechnology and drug discovery*. 2nd edition / edited by Sachdev S. Sidhu, Clarence Ronald Geyer. ed.
7. Sidhu, S.S., *Engineering M13 for phage display.* Biomol Eng, 2001. **18**(2): p. 57-63.
8. Chan, B.K., S.T. Abedon, and C. Loc-Carrillo, *Phage cocktails and the future of phage therapy.* Future Microbiol, 2013. **8**(6): p. 769-83.
9. Lu, T.K. and J.J. Collins, *Engineered bacteriophage targeting gene networks as adjuvants for antibiotic therapy.* Proc Natl Acad Sci U S A, 2009. **106**(12): p. 4629-34.
10. Cao, J., et al., *Helicobacter pylori-antigen-binding fragments expressed on the filamentous M13 phage prevent bacterial growth.* Biochim Biophys Acta, 2000. **1474**(1): p. 107-13.
11. Westwater, C., et al., *Use of genetically engineered phage to deliver antimicrobial agents to bacteria: an alternative therapy for treatment of bacterial infections.* Antimicrob Agents Chemother, 2003. **47**(4): p. 1301-7.
12. Adhikari, M., et al., *Functionalized viral nanoparticles as ultrasensitive reporters in lateral-flow assays.* Analyst, 2013. **138**(19): p. 5584-7.
13. Petsong, K. and K. Vongkamjan, *Applications of Salmonella bacteriophages in the food production chain*, in *The Battle Against Microbial Pathogens: Basic Science, Technological Advances and Educational Programs*, A. Méndez-Vilas, Editor. 2015, Formatex Research Center. p. 275-283.
14. Ling, T.C., et al., *Purification of filamentous bacteriophage M13 by expanded bed anion exchange chromatography.* J Microbiol, 2004. **42**(3): p. 228-32.
15. Morenweiser, R., *Downstream processing of viral vectors and vaccines.* Gene Ther, 2005. **12 Suppl 1**: p. S103-10.
16. Brorson, K., et al., *Characterization and purification of bacteriophages using chromatofocusing.* J Chromatogr A, 2008. **1207**(1-2): p. 110-21.
17. Monjezi, R., et al., *Purification of bacteriophage M13 by anion exchange chromatography.* J Chromatogr B Analyt Technol Biomed Life Sci, 2010. **878**(21): p. 1855-9.
18. Plechkova, N.V. and K.R. Seddon, *Ionic liquids: "Designer" solvents for green chemistry*, in *Methods and reagents for green chemistry: an introduction*, P. Tundo, A. Perosa, and F. Zecchini, Editors. 2007, John Wiley & Sons: Hoboken, NJ, USA. p. 103 - 130.

19. Carmichael, A.J. and Seddon, *Polarity study of some 1-alkyl-3-methylimidazolium ambient-temperature ionic liquids with the solvatochromic dye, Nile Red.* Journal of Physical Organic Chemistry, 2000. **13**: p. 591-595
20. Plechkova, N.V. and K.R. Seddon, *Applications of ionic liquids in the chemical industry.* Chem Soc Rev, 2008. **37**(1): p. 123-50.
21. Patinha, D.J.S., et al., *New Low-Toxicity Cholinium-Based Ionic Liquids with Perfluoroalkanoate Anions for Aqueous Biphasic System Implementation.* ACS Sustainable Chemistry & Engineering, 2016. **4**: p. 2670-2679.
22. González-Mora, A., et al., *Recovery and Primary purification of Bacteriophage M13 Using Aqueous Two-Phase Systems.* Journal of ChemicalTechnology and Biotechnology, 2017.
23. Yuan, J., D. Mecerreyes, and M. Antonietti, *Poly(ionic liquid)s: An update.* Progress in Polymer Science, 2013. **38**: p. 1009–1036.
24. Tomé, L.C. and I.M. Marrucho, *Ionic liquid-based materials: a platform to design engineered CO2 separation membranes.* Chem Soc Rev, 2016. **45**(10): p. 2785-824.
25. Fernandes, A.M., et al., *Evaluation of cation-anion interaction strength in ionic liquids.* J Phys Chem B, 2011. **115**(14): p. 4033-41.
26. Tomé, L.C., et al., *Polymeric ionic liquid-based membranes: Influence of polycation variation on gas transport and CO_2 selectivity properties.* Journal of Membrane Science, 2015. **486**: p. 40-48.
27. Pires, V.M., et al., *Stability and Ligand Promiscuity of Type A Carbohydrate-binding Modules Are Illustrated by the Structure of Spirochaeta thermophila StCBM64C.* J Biol Chem, 2017. **292**(12): p. 4847-4860.
28. Isik, M., et al., *Preparation of poly(ionic liquid) nanoparticles and their novel application as flocculants for water purification.* Polymer Chemistry, 2016. **7**(8): p. 1668-1674
29. Pozo-Gonzalo, C., et al., *PEDOT:Poly(1-vinyl-3-ethylimidazolium) dispersions as alternative materials for optoelectronic devices.* Journal of Polymer Science: Part A: Polymer Chemistry, 2008. **46**(9): p. 3150-3154
30. Wu, M., et al., *Ionic liquid polymer functionalized carbon nanotubes-doped poly(3,4-ethylenedioxythiophene) for highly-efficient solid-phase microextraction of carbamate pesticides.* J Chromatogr A, 2016. **1444**: p. 42-9.
31. Patinha, D.J.S., et al., *Expanding the Applicability of Poly(Ionic Liquids) in Solid Phase Microextraction: Pyrrolidinium Coatings.* Materials (Basel), 2017. **10**(9).
32. Tsumoto, K., et al., *Effects of salts on protein-surface interactions: applications for column chromatography.* J Pharm Sci, 2007. **96**(7): p. 1677-90.
33. Steiner, D., et al., *Signal sequences directing cotranslational translocation expand the range of proteins amenable to phage display.* Nat Biotechnol, 2006. **24**(7): p. 823-31.

CHAPTER IV – Viral detection case study I: Magnetic particles as lateral flow assay reporters for Norwalk detection

Abstract Noroviruses are the major source of foodborne illness (58%), causing around 19-21 million disease cases, up to 71 000 hospitalizations and 800 deaths per year in the United States. They are easily-spread pathogens, with a 50% human infectious dose near 103 virions.

The most common norovirus diagnostic techniques are electron microscopy, RT-PCR and ELISA. However, these techniques require sophisticated and expensive laboratory materials and equipment, and also are time-consuming. Lateral flow assays (LFAs) are fast, inexpensive and simple point-of-care diagnostic tools which have been used in the detection of a variety of targets such as proteins, pathogens, drugs, and hormones.

Here we present an investigation of the mechanisms of magnetic LFA enhancement sensitivity. By optimizing electromagnet pulse duration, operation mode, and location, we test specific hypothetical mechanisms of LFA enhancement by magnetic fields, including increased time of transit of reporter particles through capture zones, and relocation of particles to shallower, more-visible depths in the LFA strip. We find that in the system tested, particle relocation to more visible depths plays an important, previously-unsuspected role in magnetic enhancement of LFA sensitivity.

It was also explored the labeling of magnetic nanoparticles with HRP and the use of the magnetic properties of magnetic beads to develop a more sensitive LFA assay for Norwalk detection. We have also explored the potential of magnetic particles as pre-concentration and reporter tools for the detection of Norwalk VLPs in human stool samples. Using magnetic beads labeled with HRP in a pre-concentration step followed by a LFA assay, we were able to achieve a reproducible and lower LoD test for Norwalk GI.4 VLPs compared to previously-reported studies.

Keywords: Norovirus, Lateral flow assays, Detection, Magnetic particles, Particle relocation, Pre-concentration

Part of this chapter has been published as: Jacinto, M.J., Trabuco, J.R.C., Vu, B.V., Garvey, G., Khodadady, M., Azevedo, A.M., Aires-Barros, M.R., Chang, L., Kourentzi, K., Litvinov, D., and Willson, R.C., Enhancement of lateral flow assay performance by electromagnetic relocation of reporter particles, *PLoS ONE*, 2018, 13 (1)

IV.1. Introduction

Norovirus are currently the major source of foodborne illness (58%), causing around 19-21 million disease cases, between 56 000-71 000 hospitalizations and 570-800 deaths per year in the United States [1, 2]. The common symptoms are nausea, vomiting, abdominal cramps and watery diarrhea [3, 4]. Common sites of infection include crowded, closed spaces like cruiser and military ships, long-term care facilities, restaurants, schools and hospitals [4-7]. The most common transmission routes are person-to-person (fecal-oral mode or inhalation of airborne droplets of vomitus) and food-borne outbreaks [4, 7]. It is a highly infectious pathogen, where the 50% human infectious dose is around 10^3 virions [3, 8]. The symptoms usually start 10–51 hours after exposure and illness lasts between 12 and 60 hours [4, 9], and the virus can still be present in patient stool after 3 weeks [10].

The most common norovirus diagnostic techniques are electron microscopy, qPCR and ELISA (examples [11-15]). However, these techniques require sophisticated and expensive laboratory materials and equipment, and also are time-consuming. LFAs are rapid, simple, and inexpensive point-of-care diagnostic tools which have been used in the detection of a variety of targets such as toxins, pathogens, drugs, and hormones. The home pregnancy test for human chorionic gonadotropin (hCG) is the best-known application of the LFA technology [16]. In a sandwich LFA, a sample wicks by capillary action along a porous chromatographic membrane in which immobilized analyte-specific recognition elements, e.g. antibodies or DNA/RNA probes, form analyte capture test lines. Reporter particles bearing their own recognition elements are analyte-bridged to the membrane at the test line to produce a visible line indicating a positive result. Excess reporter particles are captured in an analyte-independent way at a control line to confirm the proper flow of the liquid along the membrane [16, 17]. A variety of particles such as colloidal gold, colored latex particles, carbon nanoparticles [18], phosphors [19], virus particles [20-22] or magnetic particles [23-33] can be used as reporters.

There have been reported some immunochromatographic norovirus LFA detection kits using gold nanoparticles [34-41], coloured latex [42] or phage [21] as reporters. The most studied test is the lab-commercial RIDA QUICK (R-Biopharm, Germany) which

provides a yes/no response for genogroups 1 (GI) and 2 (GII) in stool samples with high sensitivity (64-83% in published works, or 92% according to the manufacturer) and 97-100% specificity [34, 35, 37, 39, 40]. However, it is only reported the limit of detection LoD for genogroup GII.17 ($6.54x10^6$ copies/g of stool [37]). The test uses biotinylated anti-norovirus antibodies and gold-labeled anti-norovirus antibodies; when target noroviruses are present in the sample, it is formed a complex with both kinds of antibodies and start flowing through the strip. A streptavidin test line captures the gold-labeled migrating complexes via the biotinylated anti-norovirus antibodies. Unbound gold-labeled antibodies are bound later at the control line, assuring that the test was performed correctly. S. Takanashi *et al.* also reported a LFA test using color latex with a LoD of $3.5x10^7$ copies/g of stool for GII.3 and $4.6x10^6$ copies/g of stool for GII.4 (69.8% sensitivity and 93.7% specificity) [42]. It has also been reported a LoD for the commercial SD BIOLINE norovirus of $1.7x10^7$ and $9.5x10^7$ copies/g of feces for GII.3 and GII.4, respectively [36], and $4.48x10^6$ copies/mL in stool samples [41]. However, the main drawback of traditional LFAs using colour latex or gold nanoparticles is the high LoD, which reveals as an opportunity for new reporters and approaches.

Magnetic particle reporters may be detected visually by the naked eye [23-25], or by their magnetic properties using magnetic sensors [25-33, 43]. Detection of magnetic particles by their magnetic properties allows for quantitation, although a specialized reader is required. For example, Xu *et al.* described a highly-sensitive lateral flow assay using 111 nm superparamagnetic nanoparticles and a magnetic assay reader, with a detection limit of 0.01 ng/mL cardiac troponin I, compared to 10 ng/mL detectable by enzyme-linked immunosorbent assay (ELISA) [29]. Orlov *et al.* reported that the limit of detection for prostate-specific antigen using their magnetic LFA-based detection platform was four times better than for a conventional ELISA, using the same antibody pair [43].

Another important possibility for LFA reporters is its labeling with the enzyme horseradish peroxidase (HRP). An enzyme-substrate reaction might increase the detection capacity of point-of-care detections compared to conventional immunochromatographic assays using colloidal gold as reporters [44]. There are prior reports of signal amplification on gold nanoparticles labeled with HRP for DNA [45, 46] and human IgG detection [47], as well as phage particles as reporters [20-22]. Cho and

Irudayaraj reported the detection of *Listeria monocytogenes* using magnetic beads labeled with HRP as a pre-concentration and LFA reporter tool [44]. Magnetic particles provide not only the opportunity to be used as an enzymatically-labeled reporter but their magnetic properties also allow to pre-concentration of the target from the sample and then be applied in a simple LFA test.

Magnetic particle-based assays also have been proposed in which magnetic particles are used not as reporters, but as capture agents for target/reporter complexes. A magnetic field is applied to concentrate the magnetic particle/target/reporter complexes at the desired location for detection [48, 49]. Although not in LFAs, the application of an external magnetic field also has been shown to modulate magnetic particle movement in a microfluidic channel [50] and to enhance particle binding efficiency and thus assay sensitivity [51-55].

Recently, Ren *et al*. (2016) demonstrated that the LoD of an LFA using magnetic particle reporters could be improved by positioning a permanent magnet under the test line, and suggested that this was because of a longer target-capture line interaction time, leading to increased reporter capture at the detection zone [56]. It also has previously been shown that delaying the sample flow in gold particle LFAs using strips with incorporated hydrophobic barriers [57] or focusing target-gold reporter complexes into a thin band and transporting them to the test line using isotachophoresis [58] can improve the LoD of gold particle LFAs.

Here we present an investigation of the mechanisms of magnetic LFA enhancement sensitivity. By optimizing electromagnet pulse duration, operation synchrony, and location, we test specific hypothesized mechanisms of LFA enhancement by magnetic fields, including increased time of transit of reporter particles through capture zones, and relocation of particles to shallower, more-visible depths in the LFA strip. We find that in the system tested, particle relocation to more visible depths plays an important, previously-unsuspected role in magnetic enhancement of LFA sensitivity. Also, HRP labeling and the use of magnetic properties of magnetic beads were also explored to develop a more sensitive LFA assay for Norwalk detection. We have explored the magnetic particles potential as pre-concentration and reporter tools for the detection of Norwalk VLPs in human stool samples. Using magnetic beads labeled with HRP in a pre-concentration step followed by a LFA assay, we were able to achieve

a reproducible and lower LoD test for Norwalk GI.4 VLPs compared to previously-reported studies.

IV.2. Materials and methods

a. Chemicals and Biologicals

Tween-20, bovine serum albumin (BSA), human chorionic gonadotropin (hCG; 1 µg = 9.28 IU according to the 3rd International Standard), sodium (meta) periodate ($NaIO_4$) and hydroxylamine hydrochloride were purchased from Sigma-Aldrich (St Louis, Missouri, USA). Phosphate-buffered saline (PBS) tablets were purchased from Takara Bio Inc. (Shiga, Japan). Sodium cyanoborohydride was obtained from Thermo Fisher (Waltham, Massachusetts, USA). Buffers were prepared using sodium acetate (Mallinckrodt, St Louis, Missouri, USA), sodium carbonate (EM Science, Gibbstown, New Jersey, USA), sodium bicarbonate (EM Science), and pH was adjusted with 1 M sodium hydroxide (Macron, Nashville, Tennessee, USA) and 99.7% min acetic acid (Macron) stock solutions. All buffers were prepared with deionized water (Millipore Milli-Q). Mouse monoclonal anti-β hCG antibody (#ABBCG-0402), polyclonal anti-α hCG antibody (#ABACG-0500) and anti-mouse antibody (#ABGAM-0500) were purchased from Arista Biologicals (Allentown, PA, USA). Anti-norovirus antibodies (10–1510 and 10–1511, called F1 and F2 respectively, below) were purchased from Fitzgerald (Acton, Massachusetts, USA). 1-step ultra TMB-Blotting solution was purchased from Thermo Scientific (Rockford, Illinois, USA). Frozen stool sample (1 donor x 20 g from ascending colon) was purchased from Analytical Biological Services Inc (Wilmington, Delaware, USA).

b. Norwalk VLP production

Norwalk VLPs were expressed, purified and kindly provided by Dr. Robert L. Atmar's group at Baylor College of Medicine. Briefly, the major capsid proteins (VP1 and VP2) were expressed, from a baculovirus vector, in Sf9 insect cells. The VLPs were purified using a cesium chloride gradient, and the structure was confirmed by electron microscopy. VLPs were stored in PBS at 4°C.

c. Functionalization of magnetic particles with anti-hCG and anti-norovirus antibodies

Fc-directed immobilization of the mouse monoclonal anti-β hCG antibodies onto magnetic particles was carried out using periodate-based oxidation of the glycosylated Fc residues [59]. Anti-hCG antibodies (0.9 mL, 0.1 mg/mL in 100 mM sodium acetate buffer, pH 5.4) were reacted with 90 µL of 0.1 M $NaIO_4$ for 30 minutes at room temperature with gentle mixing, while protected from light. The oxidized antibodies were immediately purified using 100 kDa Amicon Ultra centrifugal filter units (Millipore, Billerica, MA, USA), and stored in 200 mM sodium carbonate buffer, pH 9.6 ('activation buffer'), at 30 µg/mL for further conjugation steps.

Streptavidin-coated magnetic particles (#0321, Ademtech, Pessac, France; 120 nm diameter: 25 µl, ~$2x10^{10}$ particles) were washed in activation buffer, resuspended in 100 µL of activation buffer and incubated with oxidized antibodies for 2 hours at room temperature with gentle mixing. Sodium cyanoborohydride ($NaCNBH_3$) solution (5 M $NaCNBH_3$ in 1 M NaOH, 15 µL), was then added to the reaction solution and incubated for 30 minutes at room temperature with gentle mixing. Unreacted aldehydes were quenched with 1 M hydroxylamine in activation buffer (75 µL) for 30 minutes at room temperature with gentle mixing. The antibody-functionalized magnetic particles were separated by magnetic separation, washed thrice in PBS and stored at 4˚C (~$2x10^8$ particles/µL). The same protocol was used for monoclonal anti-norovirus (Fitzgerald 10–1510, F1) antibody.

For biotinylated antibody binding with streptavidin-coated magnetic particles, monoclonal anti-norovirus antibody (Fitzgerald 10–1510, F1) were biotinylated using EZ-Link Sulfo-NHS-LC-Biotin reagent (Thermo Fisher Scientific) using a 20-fold molar excess of biotin reagent according to the manufacturer's instructions. Streptavidin-coated magnetic particles were incubated with a 2500-fold molar excess of biotinylated antibody for 1 hour at room temperature, before uncoupled antibodies were removed by magnetic separation. The antibody-magnetic particles-conjugate was washed and resuspended in PBS, and thereafter stored in PBS at 4°C (~$8x10^8$ particles/µL).

d. Labeling magnetic particles functionalized with anti-norovirus antibodies with HRP

Periodate functionalized magnetic particles with anti-norovirus antibody (Fitzgerald 10–1510, F1), as described above, were labeled with HRP by adding 10 molecules of biotinylated HRP per functionalized magnetic bead, for 30 minutes at room temperature with gentle mixing. The particles were then magnetically separated, washed and resuspended in PBS to a final concentration of ~$8x10^8$ particles/µL, and stored at 4˚C until further use.

e. LFA strip preparation

Whatman FF80HP nitrocellulose membrane (GE Healthcare) was cut into 6 cm by 29.7 cm pieces. The test and control lines were dispensed using a lateral flow reagent dispenser (Claremont BioSolutions, Upland, CA) powered by a programmable DC power supply (BK Precision 9130) and equipped with an external Fusion 200 syringe pump (Chemyx, Stafford, TX). Antibody solutions (1 mg/mL polyclonal anti-α hCG antibody and 1 mg/mL of anti-mouse antibody solutions in 1x PBS, pH 7.4) were dispensed at a rate of 0.22 mL/min with a head speed of 4 cm/s, providing a dispensed protein quantity of 1 µg/cm. The lines were spotted 1.7 cm apart from each other, and the test line was spotted at 1.3 cm from the sample pad end (Figure IV-1). The membranes were assembled on adhesive cards from DCN Diagnostics with Fusion 5 sample pads and Whatman CF5 absorbent pads. The membrane assembly was then cut using a standard paper guillotine, to create individual strips 4 mm wide and 7 cm long. The strips were then allowed to dry overnight at room temperature and stored desiccated until use.

For Norwalk detection, it was used the same apparatus and system conditions with 1 mg/mL of Fitzgerald 10-1511 (F2) as capture antibody for test line and 0.5 mg/mL anti-mouse for control line, both diluted in 1x PBS, pH 7.4.

f. Lateral flow assays

hCG test protein was diluted in PBS and 50 µL of each sample was dispensed onto the sample pad of strips with anti-hCG antibodies on the test line and anti-mouse antibodies on the control line. The strips were washed with 20 µL LFA buffer (1% Tween-20, 0.5% BSA, in PBS, pH 7.4) before applying 5 µL of the conjugated magnetic beads (~10^9 particles). The strips were washed again with 200 µL LFA buffer and immediately imaged

using a flatbed color scanner (Perfection V600, Epson, Long Beach, CA). The scanned images were analyzed with the Gel Analysis Tool of ImageJ (National Institutes of Health, Bethesda, MD, USA) [60] by plotting the line intensity profile and numerically integrating the area under each peak. Ratios of the test line (T) intensity to the control line (C) intensity, T/C, were calculated for each strip and replicates (n=3) were averaged.

For conventional LFA test for Norwalk VLP detection, the VLPs were diluted in PBS until the desired concentration onto the sample pad of strips with anti-norovirus antibodies on the test line and anti-mouse antibodies on the control line. It was used the same procedure as described above with magnetic functionalized with anti-norovirus with and without HRP label. For HRP labeled particles, after running the LFA test, the strips were let dry for 10 minutes and spotted 7.5 µL of TMB blotting solution on test and control line locations. Line intensity profiles were scanned and measured before and after 15 minutes of TMB application. The limit of detection was determined as the lowest concentration measured to be above the mean plus 3 times the standard deviation of the no-analyte control.

g. Determination of hCG LoD

To evaluate the analytical sensitivity of the assay, “half-strip” dipstick LFAs (3 mm wide, consisting only of membrane and absorbent pad, with use of sample and conjugate pads avoided for maximal reproducibility) were performed. 50 µl of hCG test protein in PBS ranging from 1.25 ng/mL down to 0.03 ng/mL (serial two-fold dilutions), were incubated with 1 µL of the conjugated magnetic beads (~10^9 particles) for 5 min. The sample was then concentrated to 10 µL using a magnet. The half-strip was dipped into the sample for 10 min. The strips were then washed with 50 µL LFA buffer (1% Tween-20, 0.5% BSA, in PBS, pH 7.4). The strips were dried for 2 hours, then scanned, and images were processed as described in IV.5 Supporting Information. The limit of detection was determined as the lowest concentration measured to be above the mean plus 3 times the standard deviation of the no-analyte control.

h. Electromagnet apparatus and programming

For magnetically enhanced LFA, two cylindrical electromagnets, 1.75” diameter X 1.25” height, (EM175-12-222, APW Company, Rockaway, NJ) were fitted with a pointed 2.5 cm length, 5 mm steel core to increase the field gradient and to concentrate the

magnetic force on a specific area. A custom LabView user interface was used to modulate the operating duration and timing of the electromagnets. The system can operate the two electromagnets independently (in unsynchronized mode) or in concert (synchronized mode). In synchronized mode, the electromagnets can be switched on or off simultaneously (synchronous mode) or alternatively (anti-synchronous mode).

To ensure reproducibility, a 3D-printed structure was used to fix the location of the electromagnets along the strip. The electromagnets were placed 5 mm above or below the strip, providing 0.03 Tesla magnetic field (measured using a Cole-Palmer 5170 Gaussmeter) to the strip at that location. Electromagnets could be placed between the sample pad and test line, at the test line, between the test and control lines, or at the control line (Figure IV-1).

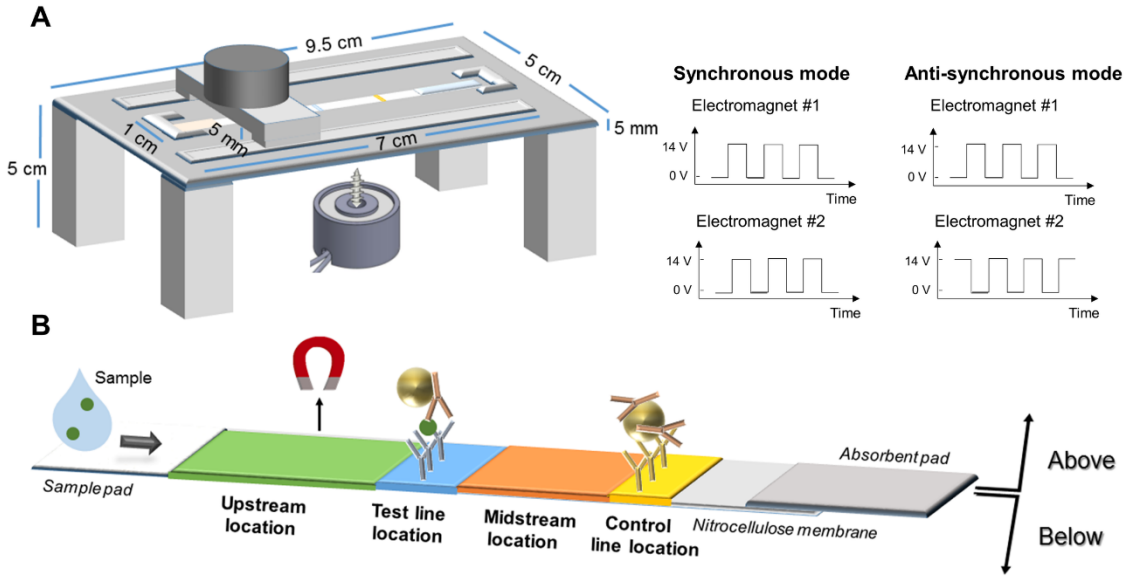

Figure IV-1 - A) ***3D-printed assay apparatus****. The apparatus holds an electromagnet over the strip's top surface and also enables the optional placement of another electromagnet below the strip. B)* ***Electromagnet-enhanced LFA for hCG detection****. Magnetic particles were functionalized with mouse monoclonal anti-β hCG antibodies. The test line contains goat polyclonal anti-α hCG antibodies, and the control line contains goat anti-mouse antibodies. In this schematic, one electromagnet is shown positioned above the "upstream" location, which is 2.5 cm upstream of the control line and 0.8 cm upstream of the test line. The test line is 1.7 cm upstream of the control line, and the "midstream" location is 1 cm upstream of the control line, between the test and control lines.*

A modified 3D-printed structure compatible with the half-strip dipsticks was also designed for LoD tests (Figure SIV-1). The apparatus holds the electromagnets over the half-strip's top and bottom surfaces and the positions can be adjusted and locked by a nut and bolt system. Two glass slides are glued perpendicular to the magnets to sandwich the membrane between them. An opening in the bottom part of the apparatus

fits a liquid container, made by cutting a 2 mL microcentrifuge tube at the 0.5-mL line. The apparatus is used in a "vertical" orientation with the TOP side of the membrane on the left and the BOTTOM side on the right. Fluids in the liquid container are exchanged either by replacing the container with a new one or by manual pipetting.

i. Magnetic Particle Counting by Alternating Gradient Field Magnetometer (AGFM)

A magnetometer was used to estimate the total number of magnetic material accumulated on the control and test lines. The control and test lines were cut out using a guillotine. An extra margin of 1 mm upstream and downstream of the position of each line was cut to ensure that the entire line was included in the resulting 3 mm x 3 mm cut out square. Each individual square was placed in a previously calibrated quartz AGFM probe, and a set of gradient coils were used to generate an alternating magnetic field that caused the probe to vibrate. The amplitude of such vibration (measured as electric signal generated by a piezo electric device) is proportional to the magnetic moment of the sample. The number of particles ($n_{particles}$) was determined from the measured magnetic signal (magnetization) with AGFM:

$$n_{particles} = \frac{M_T}{M_s \times \rho \times V}$$

Where M_T is the total magnetization measured by AGFM, M_s is magnetization at saturation of particles (40 emu/g), ρ is particle density (2 g/cm^3), and V is particle volume (4.2×10^{-12} mm^3).

j. Norwalk VLP pre-concentration and LFA test

For pre-concentration tests, 1 mL of Norwalk VLP diluted in PBS at the desired concentration was incubated with ~8×10^9 conjugated magnetic beads with anti-norovirus antibody (Fitzgerald 10–1510, F1) and labeled with HRP for 30 min with gentle rotation at room temperature. The magnetic beads were then magnetically separated by magnetic separation for 30 min. The beads were then washed (500 µL) and resuspended in 50 µL PBS. The final 50 µL solution was then applied to the LFA strip and washed with 200 µL LFA buffer. After running the LFA test, the strips were let dry for 10 minutes and spotted 7.5 µL of TMB blotting solution on test and control line locations. Line intensity profiles were scanned and measured before and after 15 minutes of TMB application.

The same test was also performed with human stool sample. 100 ± 10 mg of stool was weighted and spiked with the calculated amount of VLP to obtain the desired final concentration (VLP #/g). The sample was then diluted 1:10 with PBS and the pre-concentration and LFA assays were performed as described above.

The limit of detection was determined as the lowest concentration measured to be above the mean plus 3 times the standard deviation of the no-analyte control.

IV.3. Results and discussion

In this work, we investigated two mechanisms of enhancement of magnetic lateral flow assays: (1) the mechanism of particle retardation, where a magnetic field is used to slow down the passage of the reporters through the test line and increase the specific binding, and (2) the mechanism of particle relocation, where a magnetic field is used to alter the location of magnetic particles in the lateral flow membrane towards the upper, more visible, depths of the membrane. Using two electromagnets, we determined the optimal operating mode (timing and magnet position) with a model LFA using anti-mouse antibody test lines and magnetic particles modified with mouse antibodies. Furthermore, we demonstrated an increase in sensitivity of an hCG lateral flow assay.

a. Particle retardation

To confirm the effect of magnetic forces on retarding the movement of particles along the membrane, the particle transit time in a 6-cm unmodified Whatman FF80HP membrane (from sample application to visually-observed arrival of particles at the absorbent pad) was measured in the presence and absence of the magnetic field. Without the magnetic field, the transit took 22 ± 2 minutes (n=3); When the electromagnets were applied (10-second on/10-second off pulses at 14 V, 0.03 Tesla field strength, electromagnets at top upstream and bottom midstream positions in unsynchronized mode) the transit time increased from 22 to 28 ± 2 minutes (n=3), confirming that electromagnets can retard the movement of the particles, as previously suggested [56].

b. Pulse duration effect on test performance

On/off pulses of varied durations were applied while holding the fraction of time that the magnets were active ("duty cycle") constant at 50%. In these experiments, the electromagnetic apparatus was operated in the unsynchronized mode with two electromagnets above the upstream (0.8 cm before the test line; 2.5 cm before the control line) and below the midstream position (1 cm upstream of the control line) as illustrated in Figure IV-2. We observed that the assay performance was significantly affected by varying the magnetic pulse duration while keeping duty cycle unchanged (50%).

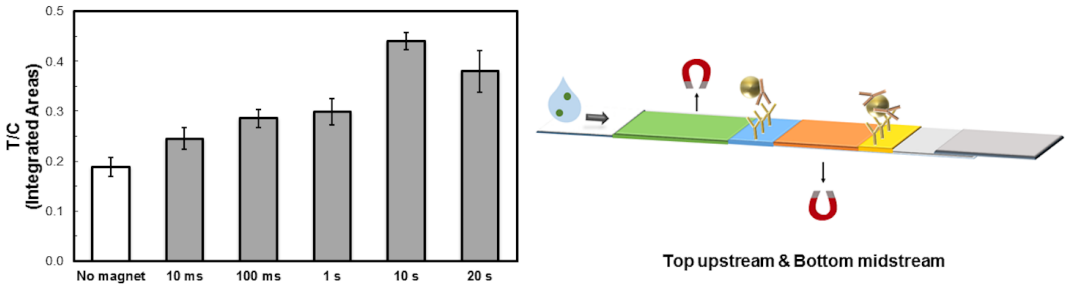

*Figure IV-2 - **Effect of pulse duration at a constant 50% duty cycle on electromagnetically controlled LFA performance factor**. 13.5 ng/mL hCG was detected using anti-hCG antibodies at the test line and mouse monoclonal anti-β hCG antibodies-functionalized magnetic particles. Control line consisted of anti-mouse antibodies. Two electromagnets were applied in top upstream and bottom midstream positions with different pulse durations at 14 V, in unsynchronized mode. For example, 10 ms represents 10-millisecond on/ 10-millisecond off pulses, unsynchronized. Line intensity profiles were evaluated by ImageJ density analysis [60]. The area under each peak was numerically integrated using the ImageJ Gel Analysis Toolbox, and the ratio of the test line intensity (T) divided by the intensity of the control line (C) for each strip was calculated, then averaged (n=3, mean ± SD).*

As the magnetic pulse duration increased from 10 ms to 10 s, the T/C ratio of test line signal to control line signal steadily increased, from 30% improvement at 10 ms to 234% improvement at 10 s, when compared to control test with no magnet. We observed that a 20-s pulse duration was less effective compared to a 10-s pulse duration. We speculate that there is a tradeoff between relocation to the surface with greater visibility, and spreading the particles among the available antibody binding sites (as opposed to over-saturating the antibody sites at the very top). The total transit time for the particles to travel the length of the LFA strip was not significantly affected by pulse duration, at constant 50% duty cycle. This suggests that simple magnetic force retardation (slower passage of magnetic reporter particles through test lines increases capture efficiency) is

not the sole mechanism of magnetic LFA enhancement as indicated by prior published work [56].

c. Particle relocation to more-visible depths

We hypothesized that magnetic forces can relocate particles closer to the surface of the translucent membrane, increasing their visibility and the resulting LFA signal strength. The apparatus design and opaque backing of the nitrocellulose membranes used precluded imaging the particles when applying an electromagnet above the strip. An electromagnet was therefore positioned 5 mm below a particle-impregnated nitrocellulose membrane (Figure IV-3), and the gradual "whitening" of the surface of the strip was observed as a measure of particle mobility and relocation.

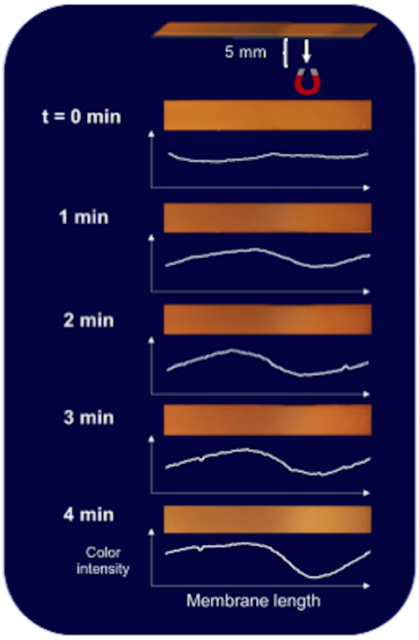

*Figure IV-3 - **Vertical magnetic particle movement under the influence of an electromagnet**. Images at 1 min intervals from above a particle-impregnated LFA membrane with an electromagnet applied 5 mm below the strip at the midstream position (10-second on/10-second off pulses at 14 V, 0.03 Tesla). Image intensity profiles using the same ImageJ image analysis settings and axes for each image. The electromagnet position is indicated in the top schematic.*

As shown in Figure IV-3, when an electromagnet was applied below the strip the particles gradually moved deeper into the translucent strip where they became less visible, leaving a lighter color on the top surface. This suggests that an electromagnet above a typical 100-µm thick LFA membrane can influence the vertical flow of particles throughout the thickness of the strip, by dragging the particles towards the more-visible top of the membrane, and thus enhancing optical detection. In a related experiment,

magnetic particles were applied to the sample pad and allowed to wick across the width of the strip with an electromagnet placed at the side of the LFA strip (Figure SIV-2). We observed the movement of the majority of the particles across the width of the membrane, and the darkening of the side of the strip nearest to the electromagnet. This confirmed that the electromagnet can magnetophoretically move particles even when located 5 mm from the edge of the strip.

d. Electromagnetic modulation of capture line intensity

In order to investigate the effect of the electromagnet on signal intensity, ~10^9 magnetic particles, modified with mouse monoclonal anti-β hCG antibodies, were applied to strips with a single capture line of goat anti-mouse antibodies and an electromagnet was applied on the right side of the strip at the midstream position (10 s pulse duration at 50% duty cycle, 0.03 Tesla) (Figure IV-4).

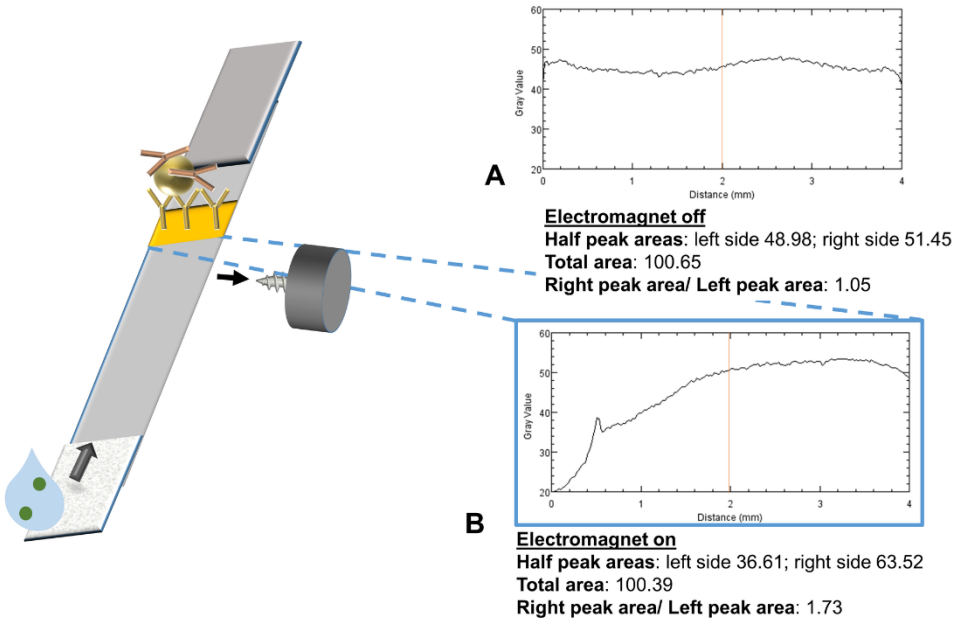

Figure IV-4 - Control line intensity profile in the absence (A) or presence (B, 10 s pulse duration at 50% duty cycle, 0.03 Tesla) of an electromagnet at the right midstream position.

The resulting capture line intensity profile had the same integrated total intensity but was strongly shifted toward the magnet, as compared to that of an identical strip run without an electromagnet. This result further supports the idea that magnetic forces can induce significant repositioning of magnetic particles within LFA strips.

e. Redistribution after magnetic relocation

To examine the time-dependence of magnetic repositioning of reporter particles during an LFA, the effect of electromagnet location on capture line intensity was studied using particles modified with mouse monoclonal anti-β hCG antibodies binding to an anti-mouse antibody capture line. All experiments used 10 s pulse duration at 50% duty cycle with 0.03 Tesla field strength. All possible positions of a single electromagnet along the strip (upstream, test line, midstream, control line, and 1 cm after the control line) both above and below the LFA strip were tested (Figure IV-5).

While prior work addressed the hypothesis that slower passage of magnetic reporter particles through test lines could increase capture efficiency, our results suggest that particle relocation from the deeper and less-visible regions of the membrane also plays an important role in magnetically-enhanced LFA signals. As seen in Figure IV-5, we observed that applying magnetic forces away from the test and control lines can affect LFA signal intensity even more strongly than magnetic forces applied directly on top of the lines, suggesting an additional mechanism independent of particle retardation in capture zones.

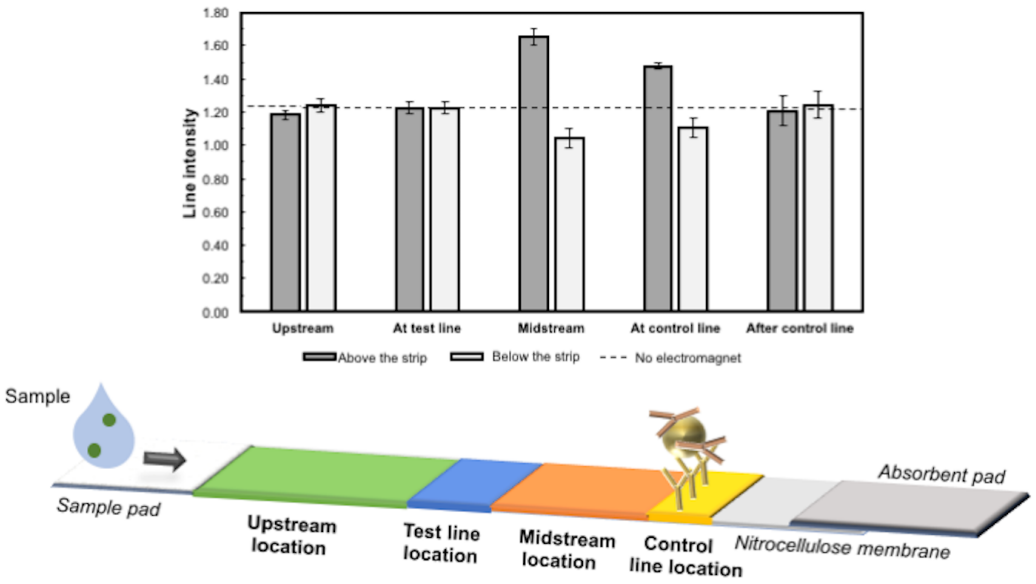

Figure IV-5 - ***Average control line intensity in magnetic LFA for different positions of a single electromagnet****. Magnetic particles modified with mouse monoclonal anti-β hCG antibodies were tested for binding to an anti-mouse antibody control line located in the same position as a typical control line. A single electromagnet was applied at different positions with 10 s pulse duration at 50% duty cycle and 0.03 Tesla field strength. "Above/below the strip" corresponds to the electromagnet positioned 5 mm above or below the LFA strip. Line intensity profiles were evaluated by ImageJ density analysis. The area under each peak was numerically integrated using the ImageJ Gel Analysis Toolbox and replicates averaged. The horizontal dashed line shows the intensity of the line in the absence of the electromagnet (n=3, mean ± SD; line intensity for no magnet control: 1.23 ± 0.02).*

We observed that placing a single electromagnet upstream of or directly on top of the test line location did not affect the intensity of the control line (I_{CL} =1.18±0.03. vs. I_{CL} =1.22±0.04, respectively) compared to the no-electromagnet condition (I_{CL}=1.23 ± 0.02). We believe that this is because of the relatively large distance between these positions and the control line (2.5 and 1.7 cm) - even if the magnetic particles were initially drawn to the top, they could redistribute throughout the membrane thickness before reaching the control line. On the other hand, placing a single electromagnet above the midstream location, 1 cm before the control line, increased its intensity (I_{CL} =1.65 ± 0.05) compared to the no-electromagnet test (I_{CL} =1.23 ± 0.02), suggesting that the magnetic particles were pulled by the electromagnet to flow (and bind) closer to the upper surface of the strip, where they are more visible. When applying one electromagnet directly above the control line position, the control line intensity also increased (I_{CL} =1.48 ± 0.02) but not as much as with a magnet 1 cm upstream. This suggests that the particles need time to magnetophorese towards the surface and become visible. This hypothesis is also supported by the data in Figure IV-3, which suggest a time scale of several minutes for vertical transport of the particles in the LFA membrane. Magnets placed below the strip were also tested; generally, the results were the inverse of those observed with a magnet above the strip. Finally, an electromagnet placed above or below the strip at 1 cm downstream of the control line produced no significant effect, as expected (I_{CL} =1.21 ± 0.09 and I_{CL} =1.24 ± 0.08, respectively). These results together provide further evidence against a retardation-only mechanism of magnetic LFA enhancement.

f. Demonstration of enhanced analytical performance of the magnetic LFA

We used “half-strip” dipsticks (to maximize throughput and reproducibility), to determine the analytical sensitivity of the magnetically-enhanced LFA when using the optimized magnet setup. The magnetic particles, widely used in sample cleanup and concentration, were also used here to pre-concentrate (by 5-fold) the target assemblies and thus maximize the benefits of magnetic particles before being added to the dipstick. Two-fold serial dilutions of hCG protein ranging from 0.08 to 2.5 ng/mL, were tested using half-strip LFAs in the presence and absence of the magnetic field (10 s pulse duration at 50% duty cycle, 0.03 Tesla, unsynchronous mode, above upstream and

below midstream positions, in three replicates (Figure SIV-5)). As expected, the T/C ratio increased as the concentration of the hCG protein increased for both groups. Moreover, the LoD, defined as the lowest concentration measured to be above the mean plus 3 times the standard deviation of the no-analyte control, was 0.31 ng/mL in the presence of the magnetic field, compared to 1.25 ng/mL when no magnetic field applied (Figure IV-6).

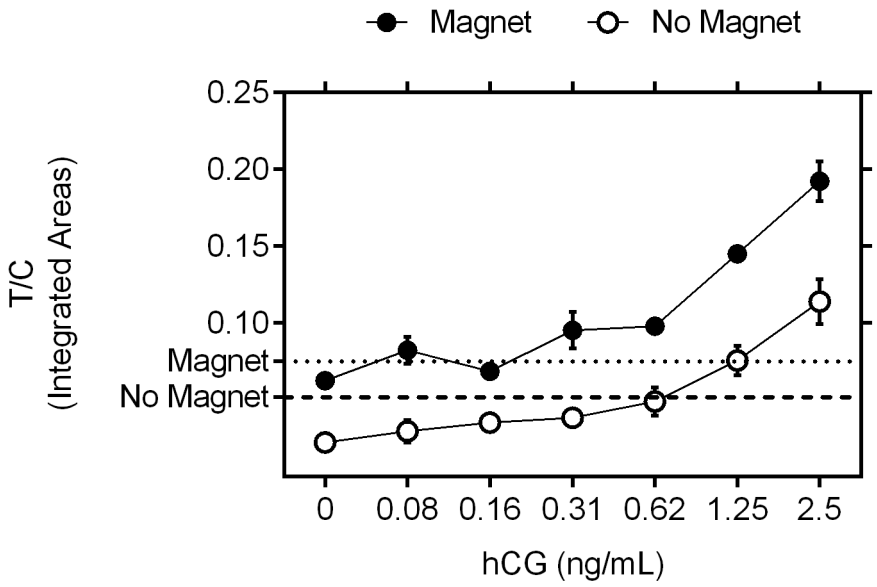

*Figure IV-6 - **Limit of Detection (LoD) of hCG LFA in the presence or absence of the magnetic field**. Two-fold hCG dilutions in PBS ranging from 2.5 ng/mL to 0.08 ng/mL were tested in half-strip dipsticks with anti-hCG antibodies as a test line and anti-mouse as a control line in the presence (full dots, 10 s pulse duration at 50% duty cycle, 0.03 Tesla, unsynchronous mode, above upstream and below midstream positions) and absence of a magnetic field (open dots). The strips were imaged and the T/C ratios of integrated areas of respective peaks were calculated (n=3). Limit of detection was considered to be the lowest tested concentration above the zero value plus three times its standard deviation (background + 3SD; dotted line denotes signal for the series with magnetic field present and dashed line denotes signal for the series without magnetic field).*

g. Magnetometric quantitation of bound particles

The magnetic measurement with AGFM allowed the estimation of the number of magnetic particles captured on the test and control lines. As expected, as analyte concentration increased, the number of particles captured was increased. Additionally, more particles were captured when the magnetic field was present (Figure SIV-7). The specific contrast, defined as the ratio of the visual signal to the magnetic signal (number of particles) measured by AGFM, was also calculated. As shown in Figure IV-7, the specific contrast for the test line increases with analyte concentration and the presence of a magnetic field.

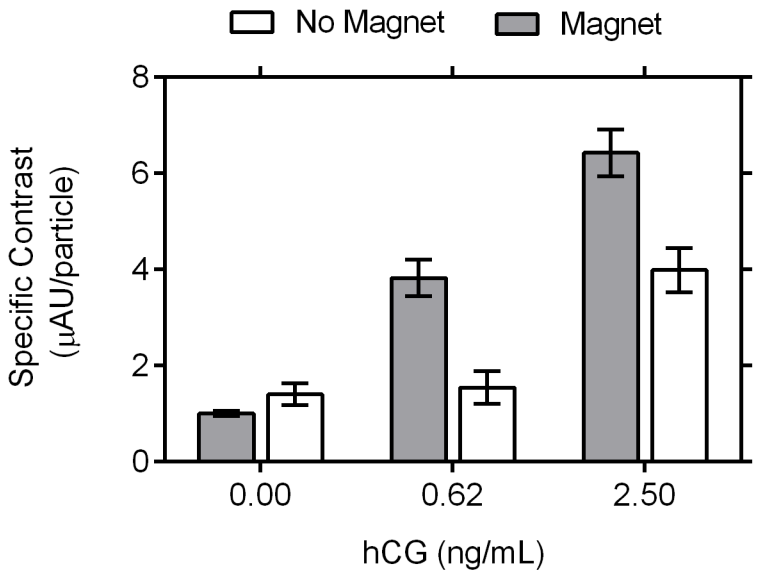

Figure IV-7 - ***Specific contrast of LFA test line (peak area divided by the total number of particles) in the presence or absence of magnetic field****. Specific contrast, the ratio of integrated area of the imaged test line peak to the number of particles measured by AGFM, was calculated for 0, 0.62 and 2.50 ng/mL hCG in assays run with (10 s pulse duration at 50% duty cycle, 0.03 Tesla, unsynchronous mode, above upstream and below midstream positions) and without a magnetic field, mean and standard error are represented (n=3). Two-way ANOVA was performed and statistically significant (95%) variance caused by concentration (p<0.0001), magnet (p=0.0003), and interaction between concentration and magnet (p=0.028) was found.*

The presence of the electromagnet increased the visual signal per particle. Reporters exposed to higher amounts of hCG yield a higher amount of hCG-reporter conjugates captured at the test line, enhancing the capacity to produce a visible line (Figure SIV-7). Moreover, the presence of the magnetic field, allows the formation of a better contrasting test line. Particle relocation initiated in the region immediately before the test line, allows a greater number of conjugates to be captured by the test line. Relocation generates a local concentration effect that is responsible for better particle binding in the visible regions (at the top) of the strip and when combined with the observed particle retardation this results in the observed enhancement of the limit of detection and the visual contrast of test line on the hCG lateral flow assay.

h. Magnetic particles as LFA reporters for Norwalk LFA detection

In this section it will be used T/T+C as test performance ratio for easier comparison with other Norwalk LFA detection works.

In any detection test, it is important to keep the recognition element function active to maintain its affinity in order to perform the target identification. Thus, it was evaluated two distinct binding protocols for anti-norovirus antibodies immobilization onto magnetic particles reporters by its LoD (Figure IV-8). On one hand, periodate oxidation provides Fc-directed immobilization of the mouse monoclonal anti-norovirus antibodies onto the magnetic particles using periodate-based oxidation of the glycosylated Fc residues. On another hand, biotinylation protocol 'attacks' amine groups independently of its location.

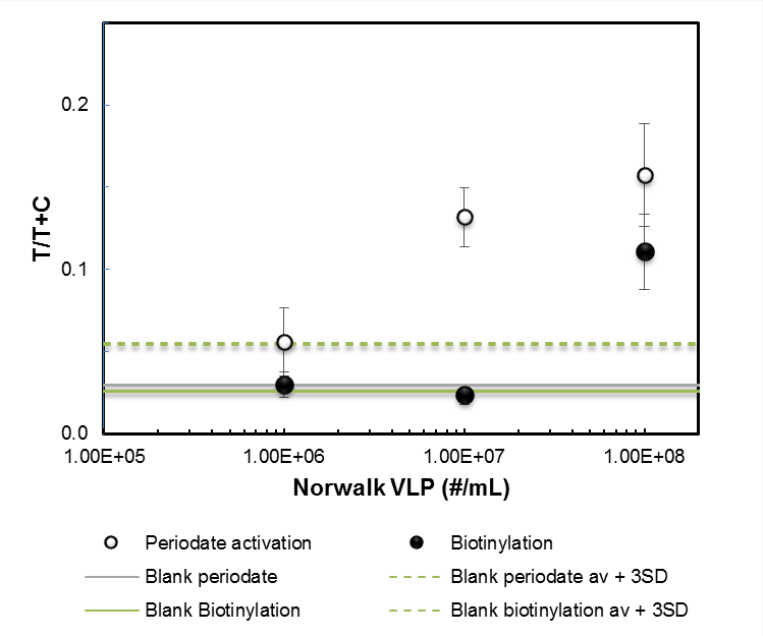

*Figure IV-8 - **Antibody binding protocol evaluation**. Average LFA test performance factor T/T+C at different Norwalk VLP concentrations using streptavidin magnetic particles as reporters, functionalized with monoclonal anti-norovirus (Fitzgerald 10–1510, F1) antibody using periodate oxidation protocol (white circles) and antibody biotinylation (black circles). No VLP LFA test for each binding protocol is also represented and its average plus 3 times its standard deviation. (n=3, mean ± SD)*

As observed in Figure IV-8, the periodate oxidation of the glycosylated Fc residues achieves a better LoD comparing to the biotinylation binding protocol. This might be due to the possible biotinylation action in the antibody epitopes, which would reduce its affinity performance. Thus, oriented binding by periodate oxidation was preferred and used in all further norovirus detection tests. This information is in agreement with previous studies, as when P. Peluso *et al.* studied the impact of oriented vs random immobilization strategies for protein microarrays, and concluded that specifically oriented attachment was 33% better than randomly oriented on average [61].

The enhancement of LFA performance by magnetic control of reporter particles, as described above, was also used in its optimized conditions for Norwalk detection (Figure IV-9).

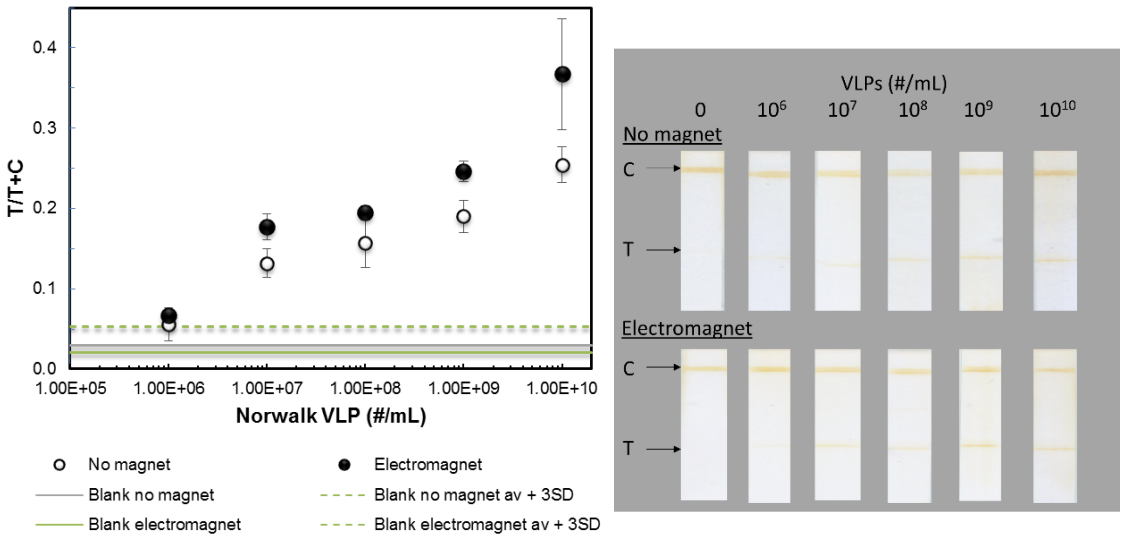

Figure IV-9 - ***Detection of Norwalk VLPs in lateral-flow assay (LFA) using streptavidin magnetic nanobeads functionalized with monoclonal anti-norovirus (Fitzgerald 10–1510, F1) antibody****. Average LFA test performance factor T/T+C at different Norwalk VLP concentrations using magnetic particles as reporters, with (black circles) and without (white circles) electromagnetic enhancement; for electromagnetic enhancement optimized conditions were: 10-second on/ 10-second off pulses at 14 V, above upstream and below midstream positions in unsynchronized operation mode. No VLP LFA test for each operation is also represented and its average plus 3 times its standard deviation. (n=3, mean ± SD). Norwalk VLPs in 50 µL are detected using anti-Norwalk antibodies in the test line (T); Control line (C) consists of anti-mouse antibodies. Nitrocellulose FF80HP was used as test membrane, Fusion 5 as sample pad and CF5 as absorbent pad.*

Although the electromagnetically enhanced LFA had a positive effect on test performance (increase between 19 and 44%), it didn't achieve a more sensitive LoD. This result is not in agreement with the former findings for hCG LoD described in the previously. This might be due to the targets' dimensional differences, where large targets as viral particles are probably easier detected by the recognition agents due to its higher surface area. Thus, the reporter particles might not need an "extra help" to spend more time near incubation sites to promote a similar result as in a standard LFA.

Still, another possible LFA enhancement for Norwalk detection was considered, HRP labelling to promote a higher visual contrast signal by its enzymatic reaction and consequently increase the test sensitivity (Figure IV-11).

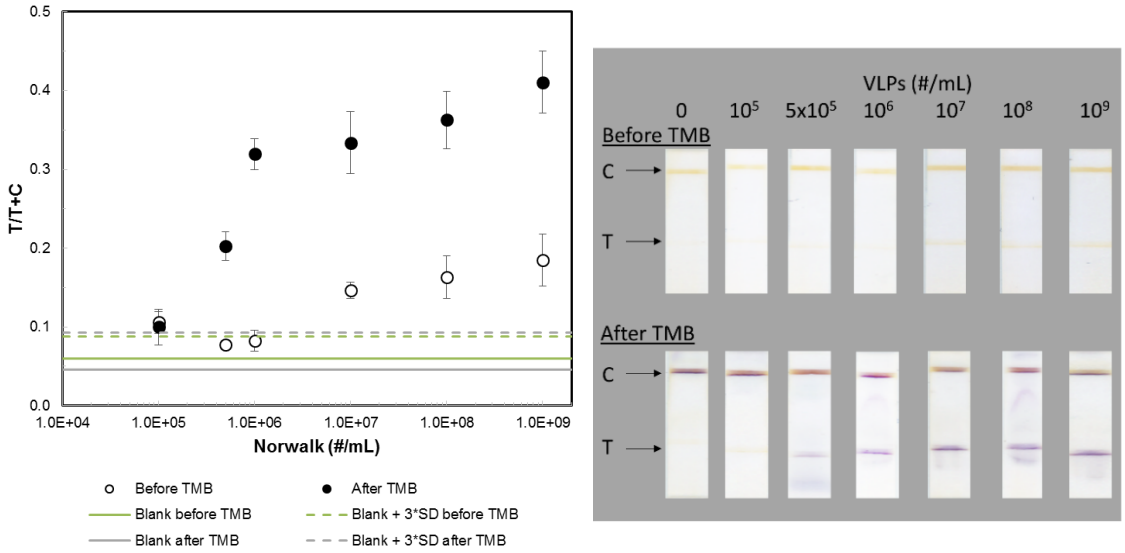

Figure IV-10 - ***Detection of Norwalk VLPs in lateral-flow assay (LFA) using streptavidin magnetic nanobeads functionalized with monoclonal anti-norovirus (Fitzgerald 10–1510, F1) antibody and labeled with HRP****. Average LFA test performance factor T/T+C at different Norwalk VLP concentrations using magnetic particles as reporters, with (black circles) and without (white circles) TMB application. No VLP LFA test for each case is also represented and its average plus 3 times its standard deviation. (n=3, mean ± SD). Norwalk VLPs in 50 µL are detected using anti-Norwalk antibodies in the test line (T); Control line (C) consists of anti-mouse antibodies. Nitrocellulose FF80HP was used as test membrane, Fusion 5 as sample pad and CF5 as absorbent pad.*

The LoD was enhanced from 10^7 Norwalk VLP/mL to $5x10^5$ Norwalk VLP/mL when comparing the results before and after TMB application. The 'before TMB' results match with results when using magnetic beads functionalized with mouse monoclonal anti-norovirus antibody without HRP labeling, which implies that HRP addition is not compromising antibody function. Electromagnet enhancement and TMB application didn't promote any significant difference: there is a slight increase of the visual effect of the magnetic particles (before TMB), as reported previously, but after the addition of TMB the results match with the same test performance as without electromagnet (data not shown).

In a previous work where phage nanoparticles were used as reporters and detected using anti-M13 HRP complex, an LoD of 10^7 Norwalk VLP/mL (also using ImageJ image analysis to calculate T/T+C performance ratio) [21] was achieved. This suggests that magnetic particles labeled with HRP could serve as a good and more sensitive alternative reporter compared to phage nanoparticles. However, it is also important to note that the reported results were achieved by using periodate oxidation as binding method instead of biotinylation, which has already been described as disadvantageous.

Another possible enhancement for the Norwalk detection test is the use of the magnetic properties of the reporter particles to easily increase assay sensitivity by sample pre-concentration (Figure IV-11).

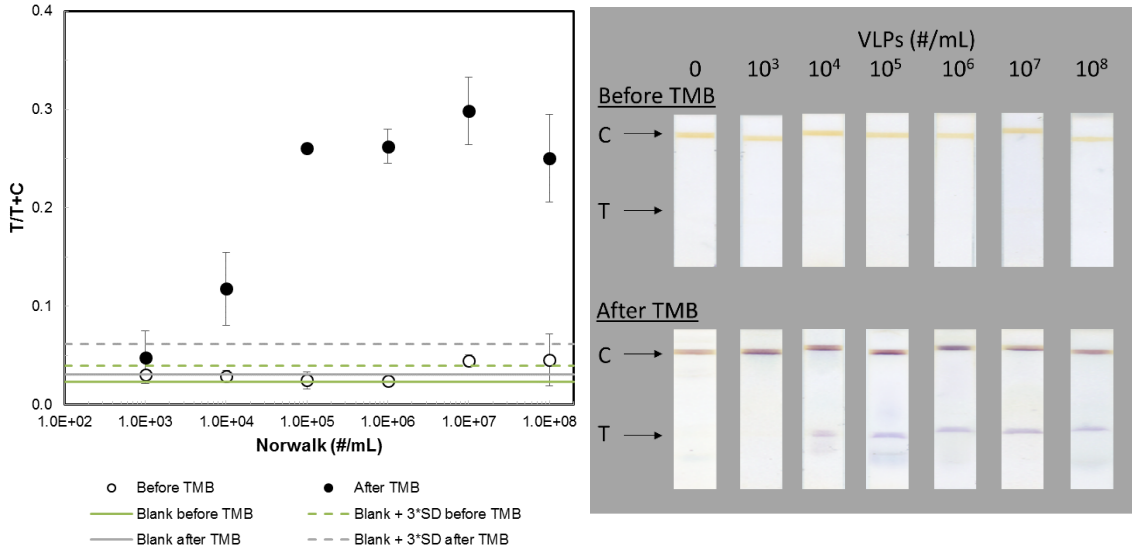

Figure IV-11 - ***Detection of Norwalk VLPs in lateral-flow assay (LFA) using streptavidin magnetic nanobeads functionalized with monoclonal anti-norovirus (Fitzgerald 10–1510, F1) antibody and labeled with HRP with and without 20x sample pre-concentration****. Average LFA test performance factor T/T+C at different Norwalk VLP concentrations using magnetic particles as reporters, with (black circles) and without (white circles) TMB application. No VLP LFA test for each case is also represented and its average plus 3 times its standard deviation. (n=3, mean ± SD). Norwalk VLPs pre-concentrated in 50 µL are detected using anti-Norwalk antibodies in the test line (T); Control line (C) consists of anti-mouse antibodies. Nitrocellulose FF80HP was used as test membrane, Fusion 5 as sample pad and CF5 as absorbent pad.*

One interesting result observed in Figure IV-11 in the lack of signal on test line before TMB for all Norwalk VLP concentrations used. This might be due to the fact that in the 20x pre-concentration step, the Norwalk VLP might get highly covered with reporters in this step and doesn't let a lot of free space for antibodies on test line to capture it. This leads to fewer particles bound to the test line, which is reflected by a weaker visual signal (compare test line colour intensity in Figure IV-10 and Figure IV-11). Still, enzymatic reaction overcomes that limitation and enhances the test LoD to 10^4 Norwalk VLP/mL.

These findings were then used in a final test, with human stool samples to better mimic real applications (Figure IV-12).

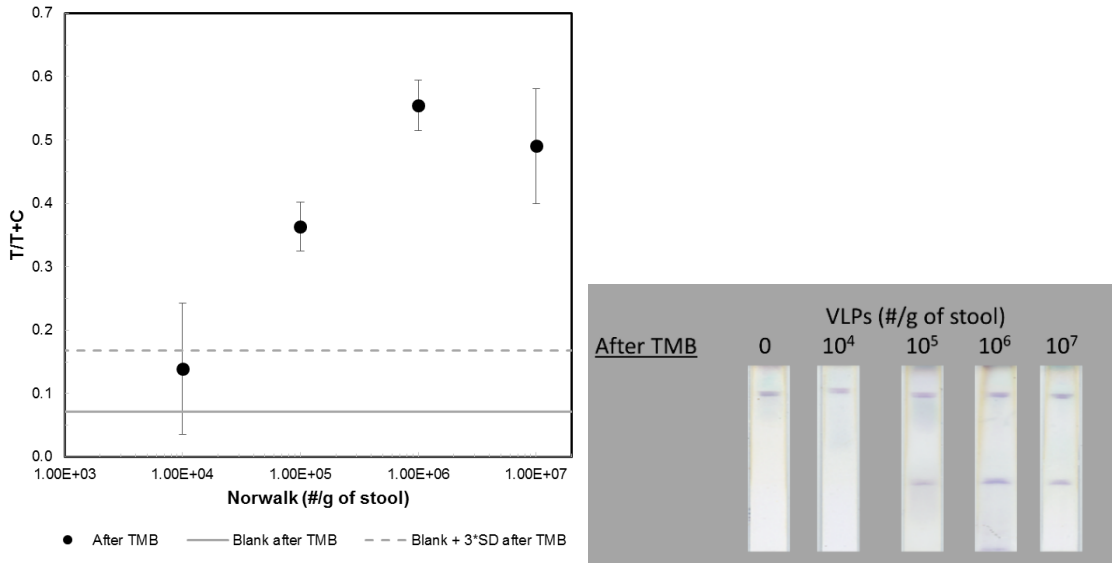

Figure IV-12 - ***Detection of Norwalk VLPs spiked in human stool samples in lateral-flow assay (LFA) using streptavidin magnetic nanobeads functionalized with monoclonal anti-norovirus (Fitzgerald 10–1510, F1) antibody and labeled with HRP****. Average LFA test performance factor T/T+C at different Norwalk VLP concentrations using magnetic particles as reporters, with (black circles) TMB application. No VLP LFA test is also represented and its average plus 3 times its standard deviation. (n=3, mean ± SD). Norwalk VLPs spiked in human stool sample pre-concentrated in 50 µL are detected using anti-Norwalk antibodies in the test line (T); Control line (C) consists of anti-mouse antibodies. Nitrocellulose FF80HP was used as test membrane, Fusion 5 as sample pad and CF5 as absorbent pad.*

The LoD obtained (10^5 Norwalk VLPs/g of stool) matched with the previously described pre-concentration tests when using Norwalk VLPs diluted in PBS (considering that in these pre-concentration tests, the human stool samples were spiked with the calculated amount of VLP to obtain the desired final concentration (VLP #/g), and then diluted 1:10 with PBS).

This result revealed to be better than other commercial kits or published detection systems, as RIDA®QUICK ($6.54x10^6$ copies/g of stool LoD for genogroup GII.17 [37]); SD BIOLINE norovirus ($1.7x10^7$ and $9.5x10^7$ copies/g of feces for GII.3 and GII.4 LoD, respectively,[36] and $4.48x10^6$ copies/mL LoD in stool samples[41]) and S. Takanashi *et al.* work with a LFA test using color latex with a LoD of $3.5x10^7$ copies/g of stool for GII.3 and $4.6x10^6$ copies/g of stool for GII.4 [42].

Although extremely low LoD isn't necessary for patient diagnosis (the average patient presents ~10^8 – 10^9 #/g of sample), the developed Norwalk detection test might be a useful approach for complex matrices or early days of infection or environmental contamination (example: public bathrooms).

IV.4. Conclusions

The application of magnetic field pulses in an LFA test conducted with magnetic particles has been suggested to delay the passage of reporter particles through capture zones, increasing their specific capture. We tested this effect, and confirmed an improvement in LoD from 1.25 ng/mL to 0.31 ng/mL for hCG detection. Electromagnets retard the movement of particles through the capture lines, leading to increased capture in that region. We also adduced evidence supporting an alternative mechanism, where magnetic forces bring particles to or near the more-visible top surface of the LFA strip, increasing their specific contrast. We showed that the upstream positioning (1 cm before a capture line) of a magnet is more effective than positioning the magnet at the line and may increase the transport of the particles vertically into the more-visible parts of the LFA membrane.

Magnetic particles were also used as LFA reporters for Norwalk detection. The addition of enzymatic labelling was revealed to be a more sensitive approach compared to the visual effect of plain magnetic particles. Also, the use of an extra step (pre-concentration) also increased the test sensitivity and gave better LoD values in human stool samples compared to other commercial and published detection platforms.

IV.5. Supporting Information

c. 3D-printed structure for the LOD determination tests

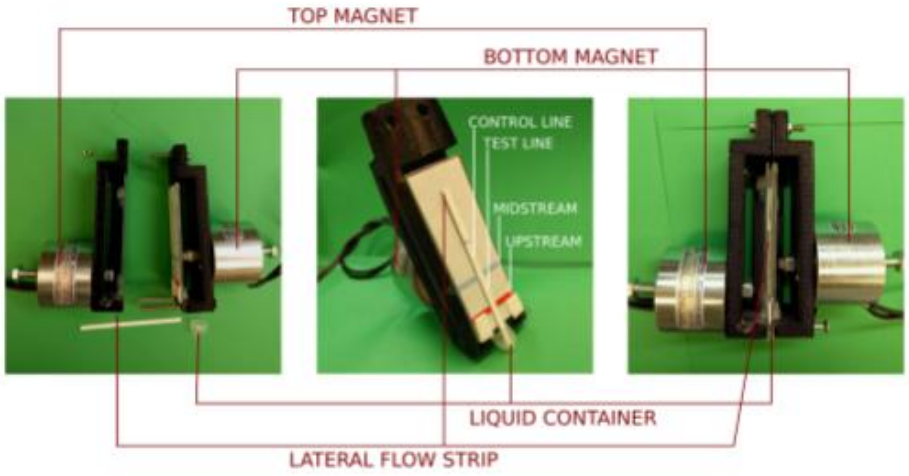

*Figure SIV-1 - **3D-printed structure for the LOD determination tests**. The apparatus holds the electromagnets over the half-strip's top and bottom surfaces, and the positions can be adjusted and locked by a nut and bolt system. Two glass slides are glued perpendicular to the magnets allowing to sandwich the membrane in between them. An opening in the bottom part of the apparatus fits a liquid container, made by cutting a 2 mL microcentrifuge tube at the 0.5-mL line. The apparatus is used in a "vertical" orientation with the TOP side of the membrane on the left and the BOTTOM side on the right. Fluids in the liquid container are exchanged either by replacing the container by a new one or by pipetting on the front of the apparatus.*

d. Lateral diversion of flowing particles by electromagnet

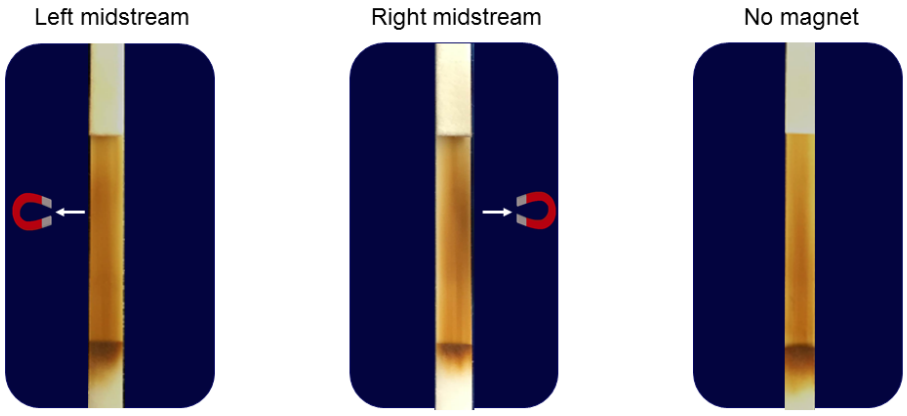

*Figure SIV-2 - **Lateral diversion of flowing particles by electromagnet action**. Magnetic particles move across the LFA membrane when an electromagnet is positioned on the left or the right midstream location, confirming that the magnet affects the particles even at a significant distance. In the absence of the electromagnet, the majority of the particles flow within the central region of the strip; the particles were applied onto the center of the sample pad. White arrows indicate the magnetic force direction (10-second on/ 10-second off pulses at 14 V, 0.03 T).*

e. Combined action of two electromagnets

After investigating the effect of a single electromagnet, the combined application of two electromagnets was studied. Magnetic particles modified with mouse monoclonal anti-β hCG antibodies were tested for binding to anti-mouse antibody control lines, one located in the position of a typical LFA test line (CL#1) and another in the position of a typical LFA control line (CL#2) (Figure SIV-3). All tests were performed using 10-second on/10-second off unsynchronized pulses at 14 V for the entire assay duration. When no electromagnets were applied, the intensities of the two lines were similar: ICL#1 = 1.34±0.03 and the second-encountered line ICL#2 = 1.27±0.06. Applying one electromagnet at the upstream position above the strip (0.8 cm before the first line and 2.5 cm before the second line) and the other electromagnet at the midstream position (between the two capture lines) below the strip led to an increase of the intensity of the first anti-mouse line (ICL#1 = 1.63±0.05) and a decrease in the intensity of the second (ICL#2 = 0.88±0.07). As we previously hypothesized, an electromagnet applied to a surface of a strip may pull the particles towards the upper surface where they bind and are more visible or down to where they cannot be seen. On the other hand, when the two electromagnets are applied in an opposing arrangement, below upstream (0.8 cm before the first line and 2.5 cm before the second line), and above midstream (1 cm upstream of the first line), the first anti-mouse line intensity decreases (ICL#1 = 0.96±0.03 vs. 1.34±0.03 when no electromagnet is applied) and the second one shows a higher intensity than the first line but lower than its previous no-magnet value (ICL#2 = 1.16±0.02 vs. no-magnet 1.27±0.06). Although the dwell time at the first line increases and more particles could bind at CL#1, they bind towards the bottom part of the strip where they are less visible. This could lead to fewer particles being available and still in a lower strip depth to flow to CL#2 and thus we could not observe the expected (because of the presence of the second electromagnet) increase in the second anti-mouse line.

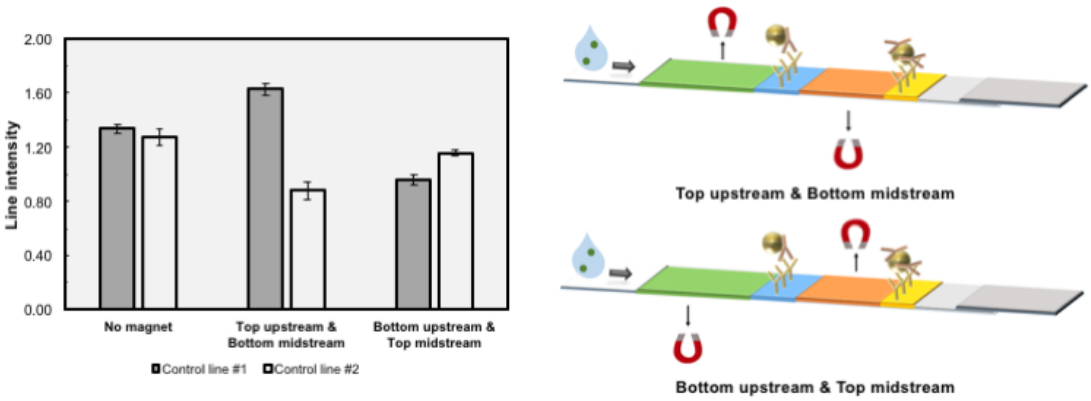

*Figure SIV-3 - **Average control line intensity for different arrangements of two electromagnets**. Magnetic particles modified with mouse monoclonal anti-β hCG antibodies were tested for binding to two anti-mouse antibody control lines; control line #1 (CL#1) is located in the position of a typical LFA test line and control line #2 (CL#2) is located in the position of a typical LFA control line. Electromagnets were applied in different arrangements with 10-second on/ 10-second off unsynchronized pulses at 14 V, for the entire assay duration. Line intensity profiles were evaluated by ImageJ density analysis. The area under each peak was numerically integrated using the ImageJ Gel Analysis Toolbox and replicate strips were averaged; (n=3, mean ± SD).*

f. Electromagnet operation mode

The combined application of two electromagnets allows three possible modes of operation. As previously described, the electromagnets can be switched on or off at the same time (synchronous mode) or in an alternating fashion, when one electromagnet is on, the other is off (anti-synchronous mode), or randomly in an unsynchronized manner. Two electromagnets were applied in top upstream and bottom midstream positions with 10-second on/ 10-second off pulses at 14 V, in different operation modes (synchronous, anti-synchronous or unsynchronized). The unsynchronized mode showed a 134% increase in the T/C ratio compared to a test with no electromagnets applied, and the anti-synchronous mode resulted in a 90% increase in the T/C ratio (Figure SIV-4). For both cases, as compared to the no-magnet control, the intensity of the TL increased whereas the intensity of the CL decreased but to a different extent. Despite the observations for a single electromagnet case in Figure IV-5 (main text), the synchronous mode resulted in no significant increase in the raw intensities of the test and control lines and the T/C performance factor. This was probably due to the fact that the combined and synchronized action from the top upstream and bottom midstream electromagnets created an overlap in the magnetic fields, regions in which the particles are stationary and are moved neither to the top nor to the bottom of the membrane.

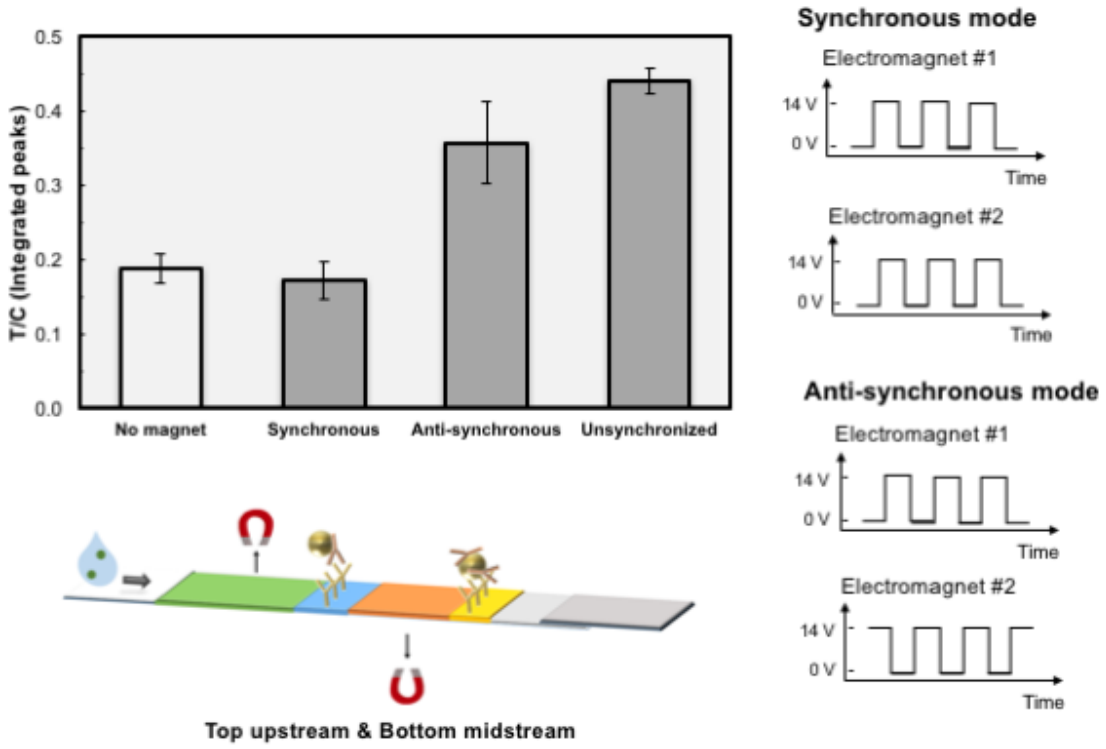

Figure SIV-4 - ***Effect of electromagnet operation mode on electromagnetically controlled LFA performance factor****. 13.5 ng/mL hCG was detected using anti-hCG antibodies at the test line and mouse monoclonal anti-β hCG antibodies-functionalized magnetic particles. Control line consisted of anti-mouse antibodies. Two electromagnets were applied in top upstream and bottom midstream positions with 10-second on/ 10-second off pulses at 14 V, in different operation modes (synchronous, anti-synchronous or unsynchronized). Line intensity profiles were evaluated by ImageJ density analysis. The area under each peak was numerically integrated using the ImageJ Gel Analysis Toolbox and the ratio of the intensity of the test line (T) divided by the intensity of the control line (C) for each strip was calculated and then averaged for replicate strips (n=3, mean ± SD).*

g. Effect of electromagnetically controlled LFA performance in hCG dilution series

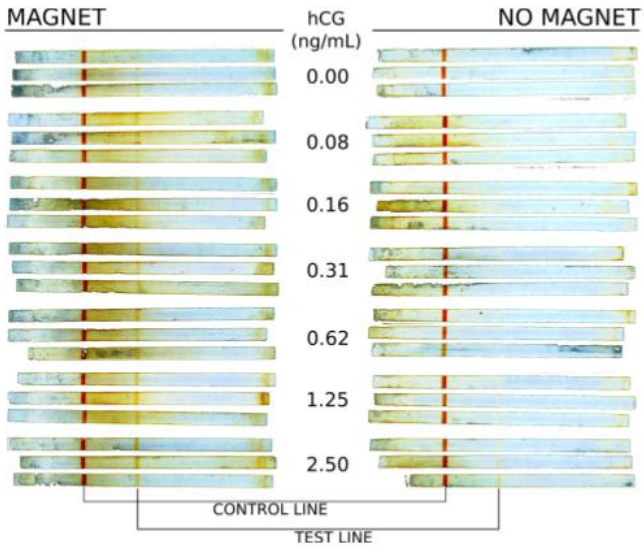

*Figure SIV-5 - **Effect of electromagnetically controlled LFA performance in hCG dilution series**. Two-fold dilutions of hCG ranging from 0.08 to 2.50 ng/mL were tested simultaneously with and without the presence of the magnetic field (10s interval, anti-synchronous mode, 0.03T). In three replicates resulting from three independent dilutions of hCG from a stock, with the same batch of magnetic particles, and the same batch of LFA "half strips". After drying for more than two hours at room temperature, the strips were placed in the flatbed scanner and imaged in the same scan. The resulting image was then histogram corrected to better identify the presence or absence of test and control lines.*

h. Image processing for T/C determination and histogram correction

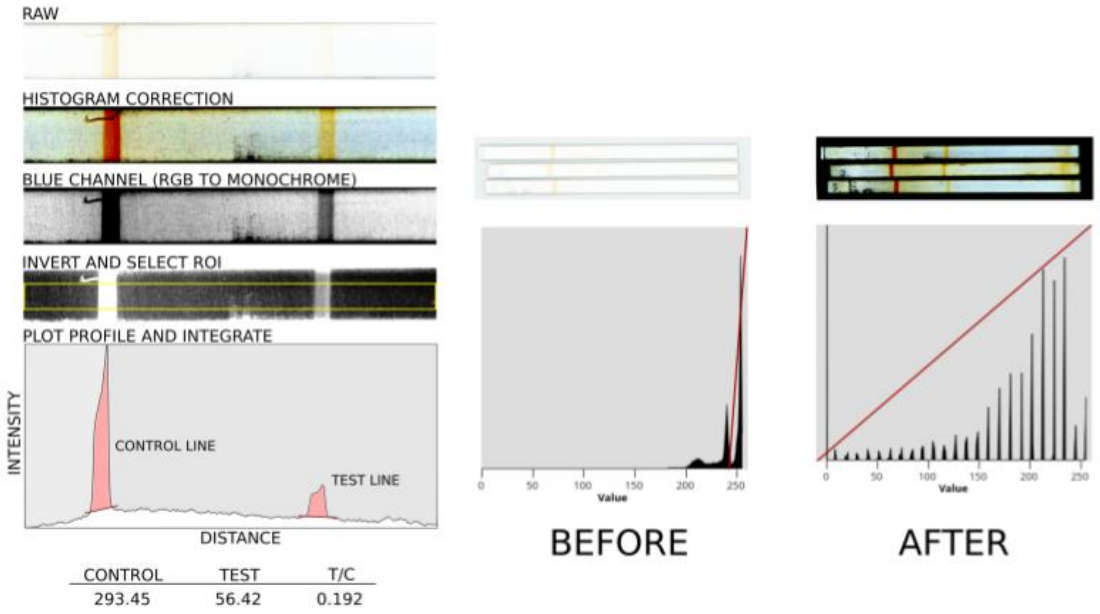

*Figure SIV-6 - **Image processing for T/C determination and histogram correction**. Images were obtained by scanning fully dried strips with a flatbed color scanner (Perfection V600, EPSON, Long Beach, CA) in reflective mode with a 1200 dpi spatial resolution and 48 bit RGB color depth. Images were simplified by a semi-destructive method of histogram correction and color channel separation, to visually enhance the presence of the test and control line and to facilitate graphical integration using ImageJ (NIH, Bethesda, MD, USA). Histogram corrected image is split in its three channels R,G and B resulting in three 16 bit black grayscale images, the blue channel is used for analysis because it shows the biggest contrast of the three channels and it does not seem to introduce any bias when compared to regular RGB to black and white conversion (data not shown). The image is inverted to display bright white bands in a black background and a region of Interest (ROI) is selected. ROI selection is done manually and aims to remove artifacts such as dust particles, scratches on the membranes, and edge caused by reflections on the edges of membranes. The intensity Vs Distance profile is plotted and the peaks are integrated taking into account the local baseline. Contrast of raw scanned images is enhanced in a semi-destructive histogram correction of the Value distribution in the Hue, Saturation, Value (HSV) color space. The pixels with value smaller than the background are converted to pure black and the new dynamic range of the image is calculated without interpolation of the new dynamic range. This results in a higher-contrast image that preserves all the features in the original picture (color, dynamic range, noise) but makes the features more visible. The red line represents the same range pixels before and after the transformation.*

i. Number of particles and visual peak area at the test line for hCG dilution series in the presence and absence of the magnetic field.

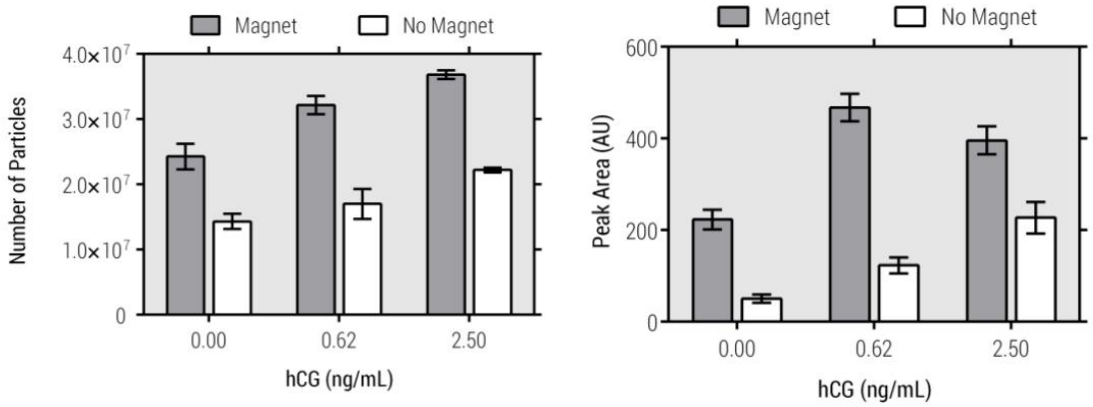

Figure SIV-7 - ***Number of particles and visual peak area at the test line for hCG dilution series in the presence and absence of the magnetic field****. Number of particles determined by AGFM. The magnetic properties of cut test lines were measured and the number of magnetic particles was determined for the concentrations of 0, 0.62 and 2.5 ng/mL hCG. (n=3). Mean and standard error are represented. Peak visual intensity determined in the 3x3mm cut out test line peak for the 0, 0.62 and 2.5 ng/mL hCG. Mean and Standard error are shown.*

IV.6. References

1. Scallan, E., et al., *Foodborne illness acquired in the United States--major pathogens.* Emerg Infect Dis, 2011. **17**(1): p. 7-15.
2. Hall, A.J., et al., *Norovirus disease in the United States.* Emerg Infect Dis, 2013. **19**(8): p. 1198-205.
3. Atmar, R.L., et al., *Determination of the 50% human infectious dose for Norwalk virus.* J Infect Dis, 2014. **209**(7): p. 1016-22.
4. Glass, R.I., U.D. Parashar, and M.K. Estes, *Norovirus gastroenteritis.* N Engl J Med, 2009. **361**(18): p. 1776-85.
5. Rhinehart, E., et al., *Frequency of outbreak investigations in US hospitals: results of a national survey of infection preventionists.* Am J Infect Control, 2012. **40**(1): p. 2-8.
6. Riddle, M.S., et al., *Epidemic infectious gastrointestinal illness aboard U.S. Navy ships deployed to the Middle East during peacetime operations--2000-2001.* BMC Gastroenterol, 2006. **6**: p. 9.
7. Vega, E., et al., *Genotypic and epidemiologic trends of norovirus outbreaks in the United States, 2009 to 2013.* J Clin Microbiol, 2014. **52**(1): p. 147-55.
8. Teunis, P.F., et al., *Norwalk virus: how infectious is it?* J Med Virol, 2008. **80**(8): p. 1468-76.
9. Hutson, A.M., R.L. Atmar, and M.K. Estes, *Norovirus disease: changing epidemiology and host susceptibility factors.* Trends Microbiol, 2004. **12**(6): p. 279-87.
10. Rockx, B., et al., *Natural history of human calicivirus infection: a prospective cohort study.* Clin Infect Dis, 2002. **35**(3): p. 246-53.

11. Bally, M., et al., *A virus biosensor with single virus-particle sensitivity based on fluorescent vesicle labels and equilibrium fluctuation analysis.* Biointerphases, 2013. **8**(1): p. 4.
12. Connelly, J.T., et al., *Micro-total analysis system for virus detection: microfluidic pre-concentration coupled to liposome-based detection.* Anal Bioanal Chem, 2012. **402**(1): p. 315-23.
13. Gilpatrick, S.G., et al., *Development of an immunomagnetic capture reverse transcription-PCR assay for the detection of Norwalk virus.* J Virol Methods, 2000. **90**(1): p. 69-78.
14. Lee, H.M., et al., *Rapid detection of norovirus from fresh lettuce using immunomagnetic separation and a quantum dots assay.* J Food Prot, 2013. **76**(4): p. 707-11.
15. Dimitriadis, A., L.D. Bruggink, and J.A. Marshall, *Evaluation of the Dako IDEIA norovirus EIA assay for detection of norovirus using faecal specimens from Australian gastroenteritis outbreaks.* Pathology, 2006. **38**(2): p. 157-65.
16. Posthuma-Trumpie, G.A., J. Korf, and A. van Amerongen, *Lateral flow (immuno)assay: its strengths, weaknesses, opportunities and threats. A literature survey.* Anal Bioanal Chem, 2009. **393**(2): p. 569-82.
17. O'Farrell, B., *Evolution in lateral flow-based immunoassay systems*, in *Lateral Flow Immunoassay*, R. Wong and H. Tse, Editors. 2009, Humana Press: New York. p. 1-33.
18. Posthuma-Trumpie, G.A., et al., *Amorphous carbon nanoparticles: a versatile label for rapid diagnostic (immuno)assays.* Anal Bioanal Chem, 2012. **402**(2): p. 593-600.
19. Paterson, A.S., et al., *Persistent luminescence strontium aluminate nanoparticles as reporters in lateral flow assays.* Anal Chem, 2014. **86**(19): p. 9481-8.
20. Adhikari, M., et al., *Functionalized viral nanoparticles as ultrasensitive reporters in lateral-flow assays.* Analyst, 2013. **138**(19): p. 5584-7.
21. Hagström, A.E., et al., *Sensitive detection of norovirus using phage nanoparticle reporters in lateral-flow assay.* PLoS One, 2015. **10**(5): p. e0126571.
22. Adhikari, M., et al., *Aptamer-Phage Reporters for Ultrasensitive Lateral Flow Assays.* Anal Chem, 2015. **87**(23): p. 11660-5.
23. Liu, C., et al., *Lateral flow immunochromatographic assay for sensitive pesticide detection by using Fe3O4 nanoparticle aggregates as color reagents.* Anal Chem, 2011. **83**(17): p. 6778-84.
24. Tang, D., et al., *Magnetic nanogold microspheres-based lateral-flow immuno dipstick for rapid detection of aflatoxin B2 in food.* Biosens Bioelectron, 2009. **25**(2): p. 514-8.
25. Wang, D.B., et al., *Detection of Bacillus anthracis spores by super-paramagnetic lateral-flow immunoassays based on "Road Closure".* Biosens Bioelectron, 2015. **67**: p. 608-14.
26. Granade, T.C., et al., *Rapid detection and differentiation of antibodies to HIV-1 and HIV-2 using multivalent antigens and magnetic immunochromatography testing.* Clin Vaccine Immunol, 2010. **17**(6): p. 1034-9.
27. Workman, S., et al., *Rapid detection of HIV-1 p24 antigen using magnetic immuno-chromatography (MICT).* J Virol Methods, 2009. **160**(1-2): p. 14-21.

28. Handali, S., et al., *Development and evaluation of a magnetic immunochromatographic test to detect Taenia solium, which causes taeniasis and neurocysticercosis in humans.* Clin Vaccine Immunol, 2010. **17**(4): p. 631-7.
29. Xu, Q., et al., *Development of lateral flow immunoassay system based on superparamagnetic nanobeads as labels for rapid quantitative detection of cardiac troponin I.* Materials Science and Engineering C, 2009. **29**: p. 702-707.
30. Taton, K., et al., *Lateral flow immunoassay using magnetoresistive sensors.* Journal of Magnetism and Magnetic Materials, 2009. **321**: p. 1679-1682.
31. Wang, D.B., et al., *Rapid detection of Bacillus anthracis spores using a super-paramagnetic lateral-flow immunological detection system.* Biosens Bioelectron, 2013. **42**: p. 661-7.
32. Wang, Y., et al., *Study of superparamagnetic nanoparticles as labels in the quantitative lateral flow immunoassay.* Materials Science and Engineering C, 2009. **29**: p. 714-718.
33. Marquina, C., et al., *GMR sensors and magnetic nanoparticles for immuno-chromatographic assays.* Journal of Magnetism and Magnetic Materials, 2012. **324**: p. 3495-3498.
34. Geginat, G., D. Kaiser, and S. Schrempf, *Evaluation of third-generation ELISA and a rapid immunochromatographic assay for the detection of norovirus infection in fecal samples from inpatients of a German tertiary care hospital.* Eur J Clin Microbiol Infect Dis, 2012. **31**(5): p. 733-7.
35. Ambert-Balay, K. and P. Pothier, *Evaluation of 4 immunochromatographic tests for rapid detection of norovirus in faecal samples.* J Clin Virol, 2013. **56**(3): p. 194-8.
36. Park, K.S., et al., *Evaluation of a new immunochromatographic assay kit for the rapid detection of norovirus in fecal specimens.* Ann Lab Med, 2012. **32**(1): p. 79-81.
37. Théry, L., et al., *Evaluation of immunochromatographic tests for the rapid detection of the emerging GII.17 norovirus in stool samples, January 2016.* Euro Surveill, 2016. **21**(4).
38. Bruggink, L.D., M.G. Catton, and J.A. Marshall, *Evaluation of the Bioline Standard Diagnostics SD immunochromatographic norovirus detection kit using fecal specimens from Australian gastroenteritis incidents.* Diagn Microbiol Infect Dis, 2013. **76**(2): p. 147-52.
39. Bruggink, L.D., et al., *Evaluation of the RIDA(®)QUICK immunochromatographic norovirus detection assay using specimens from Australian gastroenteritis incidents.* J Virol Methods, 2011. **173**(1): p. 121-6.
40. Battaglioli, G., et al., *Evaluation of the RIDAQuick norovirus immunochromatographic test kit.* J Clin Virol, 2012. **53**(3): p. 262-4.
41. Kim, H.S., et al., *Evaluation of the SD Bioline Norovirus rapid immunochromatography test using fecal specimens from Korean gastroenteritis patients.* J Virol Methods, 2012. **186**(1-2): p. 94-8.
42. Takanashi, S., et al., *Development of a rapid immunochromatographic test for noroviruses genogroups I and II.* J Virol Methods, 2008. **148**(1-2): p. 1-8.
43. Orlov, A.V., et al., *Rapid dry-reagent immunomagnetic biosensing platform based on volumetric detection of nanoparticles on 3D structures.* Biosens Bioelectron, 2016. **79**: p. 423-9.

44. Cho, I.H. and J. Irudayaraj, *Lateral-flow enzyme immunoconcentration for rapid detection of Listeria monocytogenes.* Anal Bioanal Chem, 2013. **405**(10): p. 3313-9.
45. Mao, X., et al., *Disposable nucleic acid biosensors based on gold nanoparticle probes and lateral flow strip.* Anal Chem, 2009. **81**(4): p. 1660-8.
46. He, Y., et al., *Ultrasensitive nucleic acid biosensor based on enzyme-gold nanoparticle dual label and lateral flow strip biosensor.* Biosens Bioelectron, 2011. **26**(5): p. 2018-24.
47. Parolo, C., A. de la Escosura-Muñiz, and A. Merkoçi, *Enhanced lateral flow immunoassay using gold nanoparticles loaded with enzymes.* Biosens Bioelectron, 2013. **40**(1): p. 412-6.
48. Carpenter, C.R., et al., *Lateral flow assay and device using magnetic particles*. 2007, IDEXX Laboratories, Inc. (Westbrook, ME, US): United States of America.
49. Feistel, C., *Systems and methods for performing magnetic chromatography assays*. 2006, Wavesesense, LLC (Irvine, CA, US): United States of America
50. Pamme, N. and A. Manz, *On-chip free-flow magnetophoresis: continuous flow separation of magnetic particles and agglomerates.* Anal Chem, 2004. **76**(24): p. 7250-6.
51. Dittmer, W.U., et al., *Rapid, high sensitivity, point-of-care test for cardiac troponin based on optomagnetic biosensor.* Clin Chim Acta, 2010. **411**(11-12): p. 868-73.
52. Dittmer, W.U., et al., *Sensitive and rapid immunoassay for parathyroid hormone using magnetic particle labels and magnetic actuation.* J Immunol Methods, 2008. **338**(1-2): p. 40-6.
53. Morozov, V.N. and T.Y. Morozova, *Active bead-linked immunoassay on protein microarrays.* Anal Chim Acta, 2006. **564**(1): p. 40-52.
54. Bruls, D.M., et al., *Rapid integrated biosensor for multiplexed immunoassays based on actuated magnetic nanoparticles.* Lab Chip, 2009. **9**(24): p. 3504-10.
55. Peyman, S.A., A. Iles, and N. Pamme, *Mobile magnetic particles as solid-supports for rapid surface-based bioanalysis in continuous flow.* Lab Chip, 2009. **9**(21): p. 3110-7.
56. Ren, W., et al., *Ultrasensitive detection of microbial cells using magnetic focus enhanced lateral flow sensors.* Chem Commun (Camb), 2016. **52**(27): p. 4930-3.
57. Rivas, L., et al., *Improving sensitivity of gold nanoparticle-based lateral flow assays by using wax-printed pillars as delay barriers of microfluidics.* Lab Chip, 2014. **14**(22): p. 4406-14.
58. Moghadam, B.Y., K.T. Connelly, and J.D. Posner, *Two orders of magnitude improvement in detection limit of lateral flow assays using isotachophoresis.* Anal Chem, 2015. **87**(2): p. 1009-17.
59. Wolfe, C.A. and D.S. Hage, *Studies on the rate and control of antibody oxidation by periodate.* Anal Biochem, 1995. **231**(1): p. 123-30.
60. Schneider, C.A., W.S. Rasband, and K.W. Eliceiri, *NIH Image to ImageJ: 25 years of image analysis.* Nat Methods, 2012. **9**(7): p. 671-5.
61. Peluso, P., et al., *Optimizing antibody immobilization strategies for the construction of protein microarrays.* Anal Biochem, 2003. **312**(2): p. 113-24.

CHAPTER V – Viral detection case study II:
Aqueous two-phase systems as a one-step viral detection platform

Abstract In this work an all-in-one detection platform based on aqueous two-phase systems (ATPS) was developed. Acknowledging the ATPS intrinsic properties combined with the versatility, low costs and ease to use and prepare, which can even be scalable by parallel processing by automatic liquid handling machines, it was explored an ATPS that would promote an opposite partition of a model target viral particle, M13 bacteriophage, and the labelled affinity reporter. The goal was to validate if, in the presence of the viral target, the labelled reporter would reflect a fluorescence shift from its ATPS rich-phase to the other where the viral particle is more abundant. As far as the authors knowledge, this is the first time where ATPS, a conventional purification platform, is applied in a different final application as a detection technique.

Keywords: Bacteriophage M13, Aqueous two-phase systems, Detection, One-step platform

V.1. Introduction

Aqueous two-phase systems (ATPSs) are formed when two immiscible compounds, such as two polymers or a polymer and a salt are mixed in an aqueous solution above a certain critical concentration, and spontaneously separate into two immiscible phases. These systems provide a biocompatible environment since they have a high water content, low interfacial tensions and some polymers also have a protein stabilizing effect [1], resulting in an efficient separation without denaturation or loss of biological activity. These systems have already been successfully applied to the separation of proteins from cell debris or to the purification of a target bioproduct from a crude feedstock [2, 3], including antibodies [3], viruses [4], intact cells [5], VLPs [6, 7], inclusion bodies [8], and plasmid DNA (pDNA) [9].

Although ATPS is a widely known and studied exclusively as purification method, there are also some efforts to applied it prior to a detection technique in order to concentrate the target analyte and/or avoid non-specific cross-reactions. Doctor Takayama's group has been working in the development minimized cross-reactivity multiplexing of ELISAs using ATPSs to restrict detection antibodies at specific locations [10, 11]. In these works, the detection antibodies are co-localized to corresponding capture antibody spots by denser dextran droplets in a PEG solution, in which detection antibodies are retained in the dextran phase due to partitioning effects. The assay not only achieves a cross-reactivity free ELISA, but also requires less antibody and sample than conventional ELISAs [10]. However, it can promote an increase number of false positive results. In a different approach, Kamei Laboratory at UCLA focused in ATPS as a pre-concentration step to enhance in 10 to 100-fold the LFA detection limit for protein [12-15] and viral particles [16, 17]. The same group has also demonstrated that target biomarkers can be simultaneously concentrate as the ATPS solution flows through a 3D paper well precast in the LFA strip sample pad, leading to shorter operation times and a simple and portable all-in-one diagnostic device [14, 15].

Acknowledging the ATPS intrinsic properties combined with the versatility, low costs and easiness of use and preparation, which can even be scalable by parallel processing by automatic liquid handling machines, in this work an all-in-one detection platform was developed by exploring an opposite partition of a model target viral particle, M13

bacteriophage, and the labelled affinity reporter. The goal was to validate if, in the presence of the viral target, the labelled reporter would reflect a partition shift from its ATPS rich-phase to the other where the viral particle is more abundant. As far as the authors knowledge, this is the first time where ATPS, a conventional purification platform, is applied in a different final application as a detection technique.

V.2. Materials and methods

a. Chemicals and biologicals

PEG with molecular weights of 1 500 and 8 000 Da, potassium phosphate monobasic anhydrous, potassium phosphate dibasic anhydrous, sodium phosphate monobasic anhydrous, phosphate buffered saline (PBS), tetracycline, BSA and sodium chloride (NaCl) were purchased from Sigma-Aldrich. Anti-M13 antibody (#NB100-1633) were purchased from Novus biologicals (Colorado, USA). BODIPY™ FL hydrazide was purchased from Lumiprobe. Human immunoglobulin G, with the commercial name of Gammanorm®, was obtained from Octapharma (Lachen, Switzerland), with a concentration of 165 mg/mL and 95% IgG (59% IgG1; 36% IgG2; 4.9% IgG3; 0.5% IgG4 and at maximum 82.5 µg/mL of IgA). Sodium-metaperiodate, sodium acetate, potassium chloride, and sodium cyanoborohydride were purchased from Merck; hydroxylamine hydrochloride was purchased from Fluka. Yeast extract was purchased from Liofilchem diagnostic. Bacto™ tryptone was purchased from Becton, Dickinson and Co. Glycerol was purchased from VWR Chemicals. Magnesium chloride heaxahydrated was purchased to Fagron Iberica.

b. M13 bacteriophage production and purification

Bacteriophage M13 KE was propagated in *E. coli* strain XL1-Blue grown in Super Optimal both (SOB) medium (20 g/L tryptone, 5 g/L yeast extract, 0.5 g/L NaCl, 2.5 mM KCl, 10 mM $MgCl_2$, 10 µg/mL tetracycline). The culture was separated at 4°C by centrifugation for 30 min at 2021 *g*. The supernatant was precipitated with 3% NaCl and 4% PEG-8000 for 10 min at 37°C 220 rpm, and cooled on ice for 45 min. After a 20-minute centrifugation at 4°C and 8085 *g*, the pellet was resuspended in 1% BSA and 15% glycerol in PBS 1×, and centrifuged for 5 min at 4°C and 8085 *g*.

c. Gammanorm® and anti-M13 labelling

Gammanorm® was dissolved in 20 mM sodium acetate, 150 mM sodium chloride at pH 3.5 in order to obtain a final concentration of 5 mg/mL; 100 µL of purchased anti-M13 (4.3 mg/mL) was diluted in 900 µL of 20 mM sodium acetate, 150 mM sodium chloride at pH 3.5 and concentrated in a Vivaspin 2 ultrafiltration device with 30,000 MWCO PES (GE Healthcare) for 10 min at 3000 *g*, and resuspended with 20 mM sodium acetate, 150 mM sodium chloride at pH 3.5 up to 100 µL. Sodium periodate ($NaIO_4$) was dissolved in the same buffer to a final concentration of 0.05 M and covered with aluminium foil to protect from light. 10 µL of $NaIO_4$ were added to 100 µL of each antibody solution and let to react in the dark for 30 min at 37°C. 390 µL of 100 mM sodium phosphate, 150 mM NaCl, pH 6.5 were then added to the solution and the entire volume was used in a 500 µL Amicon 10 kDa (Merck Millipore) for 10 minutes at 14000 *g* to remove the $NaIO_4$. The concentrated volume was diluted in 500 µL of 100 mM sodium phosphate, 150 mM NaCl, pH 6.5.

BODIPY™ FL hydrazide dye was added in 10-fold molar excess over the amount of antibody present (11.4 µL from 1 mg/mL BODIPY™ FL hydrazide stock) and let it to react for 2h at room temperature, protected from light. In a fume hood, 10 µL of 0.25 M sodium cyanoborohydride ($NaCNBH_3$), dissolved in 1 M NaOH, was added to the reaction mixture and react for 30 min at room temperature. To block unreacted aldehyde sites, 5 µL of 0.5 M hydroxylamine hydrochloride ($NH_2OH.HCl$), dissolved in carbonate buffer pH 9.6, were added and let it react for 30 min at room temperature.

In order to purify the labelled antibody from the free BODIPY™ FL hydrazide present in the reactional mixture, a PD-10 desalting column (GE Healthcare) was used using PBS as final solvent. Between 24 and 30 fractions of 1 mL were collected and analyzed in 96 well-plate in a SpectraMax 385 Plus at 280 nm and 503 nm to measure the IgG and BODIPY™ FL hydrazide concentration, respectively, in each fraction. 0.15 to 0.2 mg/mL of labelled antibody fractions were obtained and used in the ATPS formation.

d. ATPS formation

Stock solutions of PEG 50% (w/w) and potassium phosphate pH 7.4 40% (w/w) were prepared using ultrapure water, obtained from a MilliQ purification system from Millipore (Billerica, MA, USA). 15% PEG 1500, 15% potassium phosphate pH 7.4 ATPS

was prepared by weighting the appropriated mass amounts of the phase forming components (PEG and potassium phosphate stock solutions), sample (labelled Gammanorm®; pure M13 bacteriophage; labelled anti-M13; or pre-incubated anti-M13 with pure M13 at different concentrations) and MilliQ water to a total final system mass of 3 g, in order to achieve the desired final mass fractions of PEG, potassium phosphate (% w/w) and sample.

All system components were thoroughly mixed in a vortex mixer (Ika, Staufen, Germany) and let to settle for at least 30 minutes at room temperature to assure total phase separation. The volumes of top and bottom phases were measured and samples from both phases were taken for further analysis.

e. Analytical Methods

i. Total M13 particles determination

The total amount of M13 bacteriophages particles in each ATPS phase was determined by spectrophotometry [18]. This technique developed by George Smith is based on the 6 times more protein amount than DNA in filamentous phage; the protein therefore contributes substantially to the absorption spectrum, accounting for a broad plateau at 260–280 nm, with a shallow maximum at 269 nm [18]. At 320 nm there is little light absorption from phage chromophores and this value is thus used to correct for light scattering from phage particles and non-phage particulate contaminants [18].

The concentration of phage in virions/mL was calculated from the difference between A_{269} and A_{320} as follows:

$$\text{virions/ml} = \frac{(A_{269} - A_{320}) \cdot 6 \times 10^{16}}{\text{number of bases/virion}}$$

M13 presents approximately 9312 bases/virion.

ii. Fluorescence measures

For the quantification of the labelled Gammanorm® and anti-M13 present in both phases in the ATPS formed, the BODIPY™ FL hydrazide corrected fluorescence was recorded with a Horiba Jobin Yvon Fluorolog spectrophotometer. Based on the BODIPY™ FL hydrazide features, an excitation wavelength of 503 nm and emission between 507 and 525 were used, with excitation and emission slits set at 2 nm. The readings were performed using a glass cuvette.

V.3. Results and Discussion

a. Pre-studies: Gammanorm® and purified M13 independent ATPS partition

Gammanorm® was first labelled with BODIPY™ FL hydrazide (Figure V-1) in order to follow its partition in the selected ATPS, as a pre-test for the further used anti-M13 antibody reporter for the viral detection test. The Gammanorm® and BODIPY™ FL hydrazide concentration in each 1 mL PD-10 desalting resulting fraction (Figure V-1) was determined by its absorbance at 280 nm and 503 nm, respectively.

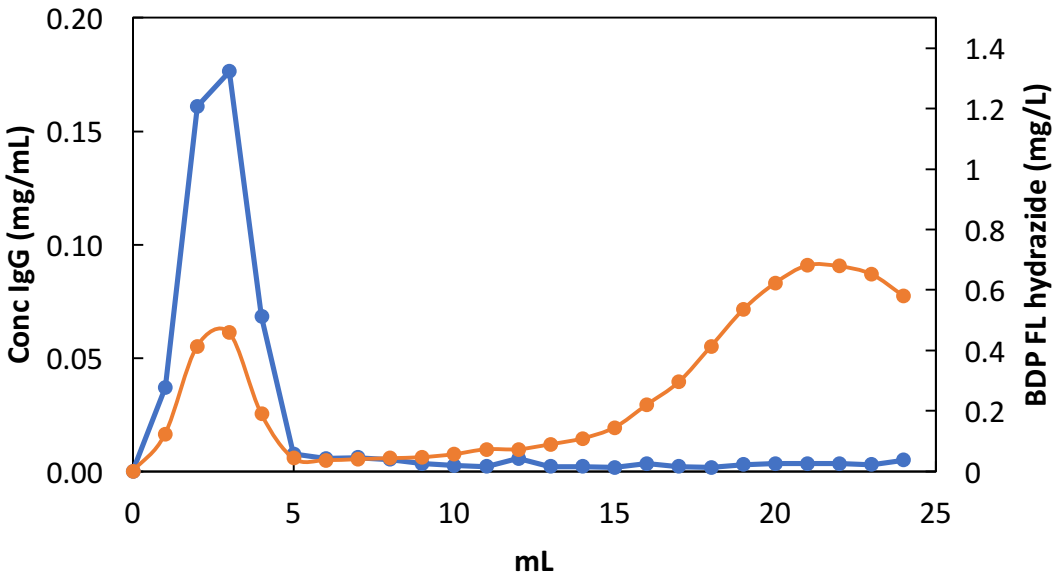

*Figure V-1 – **Gammanorm® labelling purification profile**. Gammanorm® and BODIPY™ FL hydrazide concentration in each 1 mL PD-10 desalting column resulting fractions is represented by blue and orange dots, respectively. Considering the molecules molecular weight, it was achieved a degree of labelling of 1.2 ± 0.1 for the most concentrated Gammanorm® fractions.*

It is easily observed a unique Gammanorm® 'peak' in the first fractions, and two BODIPY™ FL hydrazide 'peaks': one matching with IgG fraction, revealing the bounded fluorophore to the Gammanorm®, and a later one revealing unbounded fluorescence dye.

The concept explored in this chapter is based on the use of an ATPS where the labelled affinity reporter (i.e. the antibody) and the target viral particle exhibit an opposite partition behavior . The goal was to validate if, in the presence of the viral target, the labelled reporter would reflect a partition shift from its ATPS rich-phase to the other

where the viral particle is more abundant. It is reported that low PEG MW, as 1500 Da, promote lower exclusion effects in the top phase and the partition of proteins, as antibodies, increases [19]. Thus, and since antibody is a much smaller biomolecule (6 to 10 nm hydrodynamic diameter [20]) compared to a viral particle as M13 bacteriophage (filamentous phage with 7 nm in diameter and 1 µm long [21, 22]), it was explored a 15% PEG 1500 15% potassium phosphate pH 7.4 ATPS for antibody partition to the system top phase and M13 partition to the system bottom phase.

The total amount of M13 bacteriophages particles in each ATPS phase was determined by spectrophotometry. In a 15% PEG 1500 15% potassium phosphate pH 7.4 ATPS with 10^{12} total M13 particles in the system, 37 ± 4% of M13 particles were identified in the system top phase and 60 ± 11% in the system bottom phase.

On another hand, 'small' biomolecules, as proteins like antibodies, are expected to partition to the system top phase with such low MW PEG. Thus, it was studied the partition of 10^{13} labelled Gammanorm® IgG with BODIPY™ FL hydrazide in a 15% PEG 1500 15% potassium phosphate pH 7.4 ATPS, with and without the addition of 10^{12} total M13 particles in the system (Figure V-2).

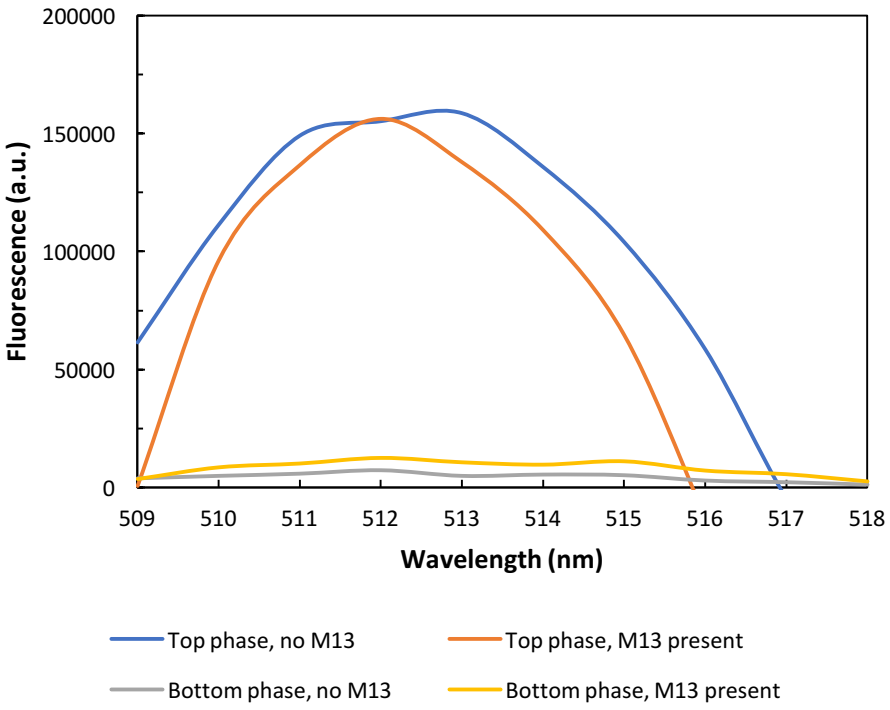

*Figure V-2 – **10^{13} #Labelled Gammanorm® fluorescence in 15% PEG 1500 15% potassium phosphate pH 7.4 ATPS top and bottom phases, with and without presence of 10^{12} # M13 in the system**. The fluorescence was measured with an excitation wavelength of 503 nm and emission between 507 and 525 nm.*

As expected, the great majority of fluorescence is detected in the system top phase, reflecting much more labelled Gammanorm® in the system top phase comparing to the bottom phase. Also, comparing the maximum fluorescence measures in systems top phase with and without M13 bacteriophage particles present, it is noticeable that M13 presence doesn't affect labelled Gammanorm® partition. Therefore, in order to minimize reagents, sample and labelled reporter consumption, and to perform fluorescence emission measures away from low-value/noise region, for the further assays it was only performed ATPS top phase measurements.

b. M13 ATPS-based detection test

Anti-M13 was labelled with BODIPY™ FL hydrazide (Figure V-3) to work as a reporter for the model viral detection test. Again, anti-M13 and BODIPY™ FL hydrazide concentration in each 1 mL PD-10 desalting resulting fraction (Figure V-3) was determined by its absorbance at 280 nm and 503 nm, respectively.

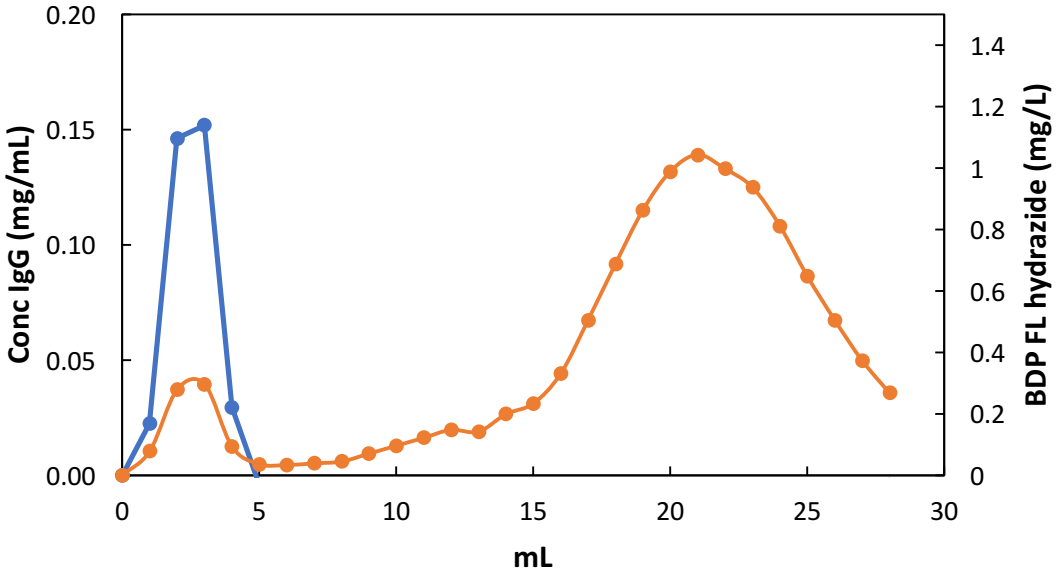

*Figure V-3 – **Anti-M13 labelling purification profile**. Anti-M13 and BODIPY™ FL hydrazide concentration in each 1 mL PD-10 desalting column resulting fractions is represented by blue and orange dots, respectively. Considering the molecules molecular weight, it was achieved a degree of labelling of 0.84 ± 0.01 for the most concentrated anti-M13 fractions.*

As expected, most anti-M13 amount was identified and collected in the first fractions, and BODIPY™ FL hydrazide was measured with anti-M13 fractions, revealing the bounded fluorophore to anti-M13, and unbounded fluorescence dye revealed in the later fractions.

10^{13} labelled anti-M13 were then applied in 15% PEG 1500 15% potassium phosphate pH 7.4 ATPS with different amounts of M13 bacteriophages added to the system, and the fluorescence in the system top phase was measured with an excitation wavelength of 503 nm and emission between 507 and 525 nm (Figure V- 4).

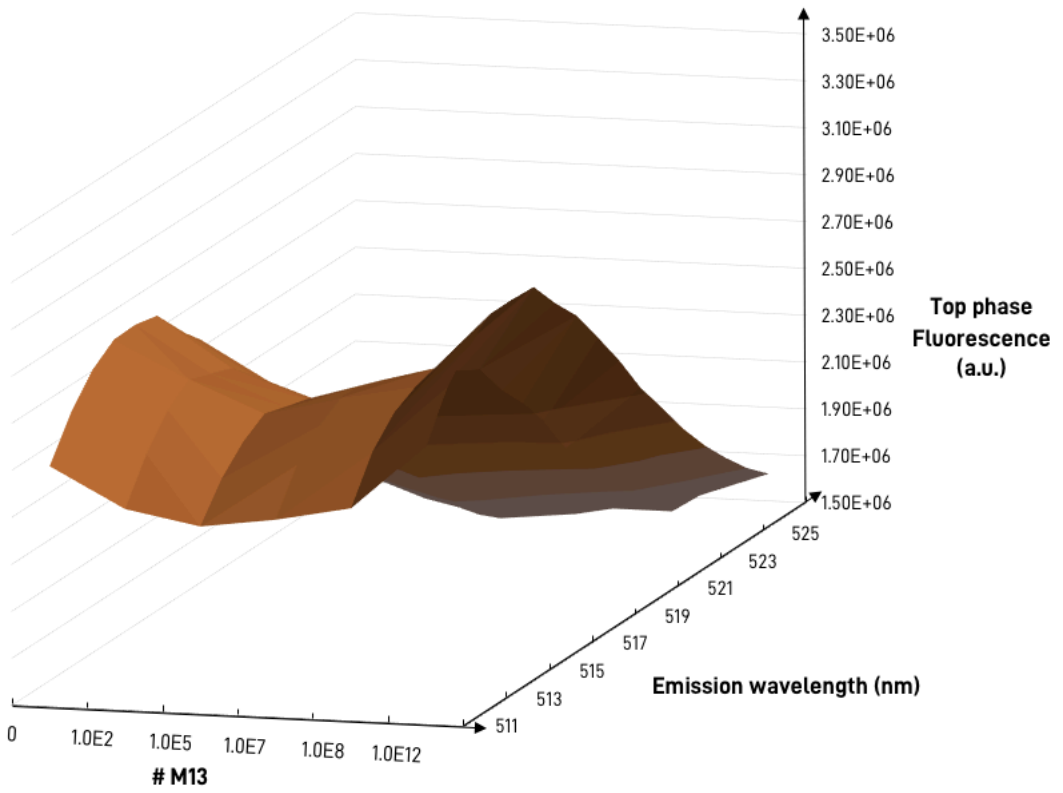

*Figure V- 4 – **ATPS-based M13 detection system response**. 10^{13} labelled anti-M13 were applied in 15% PEG 1500 15% potassium phosphate pH 7.4 ATPS with different amounts of M13 bacteriophages added to the system The fluorescence in the system top phase was measured with an excitation wavelength of 503 nm and emission between 507 and 525 nm.*

As the amount of M13 applied to the ATPS increases, there is a first fluorescence decrease since less and less labelled anti-M13 are present in the system top phase due to target-specific binding which pull the antibody to the ATPS bottom phase where the M13 partition preferentially. Also, the low molecular exclusion in the system bottom phase promoted by the low M13 particles presence, enhances the consequent pull of bounded anti-M13 to M13 bacteriophage particles to the viral particle rich bottom phase. As the M13 bacteriophage amount applied to the system continues to increase,

the first fluorescence decrease is a followed by fluorescence increase up to the 'no phage' control fluorescence; the increasing amount of M13 bacteriophage present in the system bottom phase promotes a higher molecular exclusion in the system bottom phase, leading to more anti-M13 re-excluded to the system top phase. The presence of above 10^{12} total M13 particles in the system promotes a higher fluorescence measurements compared to the control (no M13 bacteriophages applied to the ATPS), revealing a saturated system bottom phase due to the presumed highly concentrated M13 bacteriophage ATPS bottom phase.

This 'V' shape behavior between 10^{1} and 10^{11} M13 particles present in the system, provides not only a qualitative response (target presence or absence by fluorescence decrease or preservation in the system top phase, respectively) but also a quantitative opportunity. By doing a 10-fold dilution of a sample, the increase or decrease of fluorescence intensity in the top phase between the two analysis reflect if the sample is in the decrease or increase phase of the 'V' curve. This indication can thus provide at least an identification of the M13 concentration range present in the sample.

V.4. Conclusions

In this chapter, a simple and easy to use detection platform was developed based on a traditional separation technique. This detection model proof-of-concept explores not only the 'out of the box' application of a widely known and studied purification method, but also a one-step detection tool that can be expanded to other clinical and environmental applications, as bacterial or highly contagious viral pathogens. Since the developed platform concept is based on a simple sequence as basic as 'add sample – close the tube cap - vortex – read the result', this detection tool presents a significant potential to be applied to 'hard to handle' samples, such as saliva, vomit or stool, that usually difficult the performance of most detection kits.

Considering the brief period of time spent in the development of this work, it is acknowledged that some extra experiments are missing to achieve a complete proof-of-concept. Not only selectivity tests against other viral particles are missing, but also the concept application to more urgent detection samples with true infectious targets (for example, *E. coli* in water samples) in real sample matrixes would be advantageous to reinforce the work developed so far.

V.5. References

1. Asenjo, J.A. and B.A. Andrews, *Aqueous two-phase systems for protein separation: phase separation and applications.* J Chromatogr A, 2012. **1238**: p. 1-10.
2. Rosa, P.A., et al., *Aqueous two-phase systems: A viable platform in the manufacturing of biopharmaceuticals.* J Chromatogr A, 2010. **1217**(16): p. 2296-305.
3. Azevedo, A.M., et al., *Optimisation of aqueous two-phase extraction of human antibodies.* J Biotechnol, 2007. **132**(2): p. 209-17.
4. Negrete, A., T.C. Ling, and A. Lyddiatt, *Aqueous two-phase recovery of bio-nanoparticles: a miniaturization study for the recovery of bacteriophage T4.* J Chromatogr B Analyt Technol Biomed Life Sci, 2007. **854**(1-2): p. 13-9.
5. García-Pérez, A.I., P. Sancho, and M. Pinilla, *Surface and metabolic properties of microcytic and macrocytic human anaemic red blood cells detected in polymer aqueous two-phase systems.* J Chromatogr B Biomed Sci Appl, 1998. **711**(1-2): p. 301-7.
6. Benavides, J., et al., *Rotavirus-like particles primary recovery from insect cells in aqueous two-phase systems.* J Chromatogr B Analyt Technol Biomed Life Sci, 2006. **842**(1): p. 48-57.
7. Luechau, F., T.C. Ling, and A. Lyddiatt, *Recovery of B19 virus-like particles by aqueous two-phase systems.* Food and Bioproducts Processing, 2011. **89**(4): p. 322-327.
8. Walker, S.G. and A. Lyddiatt, *Processing of nanoparticulate bioproducts: application and optimisation of aqueous two-phase systems.* Journal of Chemical Technology and Biotechnology, 1999. **74**(3): p. 250-255.
9. Trindade, I.P., et al., *Purification of plasmid DNA vectors by aqueous two-phase extraction and hydrophobic interaction chromatography.* J Chromatogr A, 2005. **1082**(2): p. 176-84.
10. Frampton, J.P., et al., *Aqueous two-phase system patterning of detection antibody solutions for cross-reaction-free multiplex ELISA.* Sci Rep, 2014. **4**: p. 4878.
11. Simon, A.B., et al., *Aqueous two-phase systems enable multiplexing of homogeneous immunoassays.* Technology (Singap World Sci), 2014. **2**(2): p. 176.
12. Mashayekhi, F., et al., *Enhancing the lateral-flow immunoassay for detection of proteins using an aqueous two-phase micellar system.* Anal Bioanal Chem, 2012. **404**(6-7): p. 2057-66.
13. Chiu, R.Y., et al., *An Aqueous Two-Phase System for the Concentration and Extraction of Proteins from the Interface for Detection Using the Lateral-Flow Immunoassay.* PLoS One, 2015. **10**(11): p. e0142654.
14. Pereira, D.Y., et al., *Single-step, paper-based concentration and detection of a malaria biomarker.* Anal Chim Acta, 2015. **882**: p. 83-9.
15. Chiu, R.Y., et al., *Simultaneous concentration and detection of biomarkers on paper.* Lab Chip, 2014. **14**(16): p. 3021-8.
16. Mashayekhi, F., et al., *Enhancing the lateral-flow immunoassay for viral detection using an aqueous two-phase micellar system.* Anal Bioanal Chem, 2010. **398**(7-8): p. 2955-61.

17. Jue, E., et al., *Using an aqueous two-phase polymer-salt system to rapidly concentrate viruses for improving the detection limit of the lateral-flow immunoassay.* Biotechnol Bioeng, 2014. **111**(12): p. 2499-507.
18. Labs, A.D. *Quantification of Bacteriophage by Spectrophotometry*. 2013 [cited 2018 11/10/2018].
19. Azevedo, A.M., et al., *Chromatography-free recovery of biopharmaceuticals through aqueous two-phase processing.* Trends Biotechnol, 2009. **27**(4): p. 240-7.
20. Rosa, S.A.S.L., et al., *Thermodynamics of the adsorption of monoclonal antibodies in phenylboronate chromatography: Affinity versus multimodal interactions.* J Chromatogr A, 2018. **1569**: p. 118-127.
21. Glucksman, M.J., S. Bhattacharjee, and L. Makowski, *Three-dimensional structure of a cloning vector. X-ray diffraction studies of filamentous bacteriophage M13 at 7 A resolution.* J Mol Biol, 1992. **226**(2): p. 455-70.
22. Marvin, D.A., et al., *Molecular models and structural comparisons of native and mutant class I filamentous bacteriophages Ff (fd, f1, M13), If1 and IKe.* J Mol Biol, 1994. **235**(1): p. 260-86.

CHAPTER VI – Conclusions and future challenges

Viruses are the most abundant biological forms on Earth. These biological products are mainly known by its viral pathogenesis, which is the process where a biological virus infects its target host, leading to molecular and cellular level consequences. However, viral particles can also be regarded as biomedical, namely VLPs - biological nanoparticles with the most direct application as their use as vaccines against the virus from which they were derived, providing a high immunogenic response – and bacteriophages – virus that only infect bacteria, and thus faced as potential antibacterial agents for direct application to living tissues, without damaging the surrounding environment but only its target host.

When viral particles are used as biomedical agents, the downstream processing of their production procedure, where the recovery and purification of the target biological product from impurities is achieved, is becoming an important factor in the seeking for an overall high productivity and lower process cost.

The ATPS performance, both in batch mL scale and in continuous microscale, for the recovery of recombinant HIV VLP from CHO cell supernatant, is compared as an alternative for first capture and primary purification. Indeed, a continuous microfluidic ATPE was successfully validated for preparative sample purification by obtaining comparable results of K and purity to classical batch extraction studies. PEG-ammonium sulfate revealed to be the most promising system with good purities and partition coefficients (K = 4.4) for direct processing of a CHO cell supernatant. This primary processing can be integrated with further concentration and purification steps, such as an ATPE multi-stage extraction, ATPE back extraction, or PEG precipitation and ion exchange chromatography. These results highlight ATPE in general as a promising technique to improve the effectiveness of VLP downstream processing, potentially providing a response to the increasing demand for high product titers. Furthermore, the results obtained in the miniaturized system highlight a good correlation between batch and continuous modes of operation, and validate the system towards scale out in a preparative scale and highlights a potential application in miniaturized analytical systems.

In a different approach, PILs were studied either in batch adsorption/elution studies or in chromatographic operation mode as a novel approach for biological products

purification, namely M13 bacteriophage, which was used as a viral model. Using cross-linked poly(VEIM-TFSI) as the anion exchanger for M13 phage recovery it was achieved an excellent agreement between optimization assays and direct use of filtered *E. coli* supernatant, either in batch binding-elution mode or chromatographic operation mode. A total recovery yield of 72.7 ± 3.4% and 4.6 ± 0.5 purification factor were achieved in a single chromatographic process. This simple downstream operation revealed to be much more efficient for the recovery of M13 phage than conventional purification processes, such as combined precipitation and centrifugation, which only recovers 36% of the applied viral particles, and revealed to be comparable to published methods that used conventional anion exchange chromatography operations (82.9% recovery for expanded bed anion exchange adsorption, and 74% yield for a pre-packed SepFast^{TM} Super Q column). Also, the use of a PIL as a novel adsorption matrix improves the extraction process compared to ionic liquid-based ATPS since the bacteriophage was collected in a single fraction, with no need for further treatment to extract the desired product, unlike with PEG- or ionic liquid-rich phases. This is the first time that PILs were successfully demonstrated as separation matrices for biological products and, together with the large number of cations and anions available to prepare PILs, provides some encouragement for future design and use of PILs as customizable separation matrixes for biological products.

Although both purification case studies were already developed using producing culture supernatant, it was only studied the first capture and primary recovery of each target viral biological product. It is essential to design and develop a complete downstream process in order to achieve a complete downstream processing, with acceptable recovery and purification yields comparable or improved to the traditional purification processes of each bioprocess. A complete economic analysis of the explored alternative downstream techniques should also be performed in order to have, not only purification performance factors, but also economic standings to be compared to other established processes. Also, for PIL-based separations, it is important to recall that PIL packing affected the elution profile when using this separation matrix as a chromatographic support. This topic, namely the PIL grounding method, should be further developed in future studies.

Traditional viral detection methods, as electron microscopy, ELISA and PCR, present some important disadvantages as the need of highly-trained personnel, requires expensive instrumentation, and it is time and lab equipment consuming. Thus, the conception of diagnostic tools with the same performance and quality assurance characteristics as in laboratory-based methods but in a more patient/final user friendly format has increased.

Magnetic nanoparticles were explored as multi-tasking tools (target capture and concentration, and test reporter) for low LoD of a LFA for Norwalk detection. The application of magnetic field pulses in an LFA test conducted with magnetic particles has been suggested to delay the passage of reporter particles through capture zones, increasing their specific capture. We also adduced evidence supporting an alternative mechanism, where magnetic forces bring particles to or near the more-visible top surface of the LFA strip, increasing their specific contrast. We tested these effects, and confirmed an improvement in LoD from 1.25 ng/mL to 0.31 ng/mL for hCG detection. Magnetic particles were also explored and used as versatile LFA reporters for Norwalk detection through enzymatic labelling, sample pre-concentration and target capture to increase the test sensitivity to better LoD values in human stool samples, which achieved better results to other commercial and published detection platforms.

Also, by acknowledging the ATPS intrinsic properties combined with the versatility, environmentally-friendliness, low costs and ease to use and prepare which can even be scalable by parallel processing, it was developed the first biosensor in which the ATPS plays a primary role, by exploring its ability to switch the partition of an affinity reporter when the target viral particle is present. A first draft of a simple and easy to use detection platform was developed based on a traditional separation technique, for a semi-quantitative detection between 10^1 and 10^{11} M13 bacteriophage particles, the chosen viral model, present in the sample. This one-step detection tool can be expanded to other clinical and environmental applications, as bacterial or highly contagious viral pathogens. Since the developed platform concept is based on a simple sequence as basic as ‘add sample – close the tube cap - vortex – read the result’, this detection tool presents a significant potential to be applied to ‘hard to handle’ samples, such as saliva, vomit or stool, that usually difficult the performance of most detection kits. However,

not only selectivity tests against other viral particles are missing, but also the concept application to more urgent detection samples with true infectious targets (for example, *E. coli* in water samples) in real sample matrixes would be advantageous to reinforce the work developed so far.

Although the LFA Norwalk detection was tested and validated with human stool samples, the ATPS-based detection platform needs not only selectivity tests but also the application of real samples. Still, in both cases, the platforms application to more urgent detection samples with true infectious targets (real infectious Norwalk or other animal or human contagious virus) in real sample matrixes would be mandatory to validate both approaches.